Differential Roles of PRDM16 Isoforms in Normal and Malignant Hematopoiesis

David J. Corrigan

Submitted in partial fulfillment of the requirements
for the degree of Doctor of Philosophy
in the Graduate School of Arts and Sciences

COLUMBIA UNIVERSITY

2018

ABSTRACT

Differential Roles of PRDM16 Isoforms in Normal and Malignant Hematopoiesis

David J. Corrigan

PRDM16 is a transcriptional co-regulator that is highly expressed in HSCs and required for their maintenance. It is also involved in translocations in acute myeloid leukemia (AML), myelodysplastic syndromes (MDS) and T-cell acute lymphoblastic leukemia. *Prdm16* is expressed as both full-length (*f-Prdm16)* and short-length (*s-Prdm16)* isoforms, the latter lacking an N-terminal PR domain homologous to SET methyltransferase domains. The roles of both isoforms in normal and malignant hematopoiesis are unclear. In chromosomal rearrangements involving *PRDM16*, the PR domain is deleted. Furthermore, overexpression of *s-Prdm16,* but not *f-Prdm16*, can cause leukemia in a $p53^{-/-}$ background predisposed to malignancy. Based on this, *s-Prdm16* has been proposed as an oncogene whereas *f-Prdm16* has been suggested to possess tumor suppressor activity.

The aim of this thesis was to more clearly elucidate the role of each *Prdm16* isoform in normal and malignant hematopoiesis. We first showed that *Prdm16* is essential for adult HSC maintenance using a conditional deletion mouse model specific for hematopoietic cells, as previous findings using an embryonic-lethal global $Prdm16^{-/-}$ mouse demonstrated this only in fetal liver. We then found, using a specific $f\text{-}Prdm16^{-/-}$ mouse model, that full-length *Prdm16* is essential for HSC maintenance and induces multiple genes involved in GTPase signaling and represses inflammation. Based on a comparison of $Prdm16^{-/-}$ HSCs lacking both isoforms, and $f\text{-}Prdm16^{-/-}$ HSCs which express *s-Prdm16*, we were able to infer some hematopoietic properties of *s-Prdm16* – namely that this isoform induces inflammatory gene expression and supports development of a $Lineage^{-}Sca1^{+}cKit^{-}$ lymphoid progenitor distinct from CLPs which predominantly differentiates into marginal zone B-cells. *s-Prdm16* expression alone, however, was not sufficient to maintain HSCs.

We used a mouse model of human MLL-AF9 leukemia and found that leukemia derived from *Prdm16*-deficient HSCs had extended latency, although expression of *Prdm16* decreases during MLL-AF9 transformation and is undetectable in *ex vivo* leukemic cells. Forced expression of *f-Prdm16* in these cells further extended leukemic latency, while forced expression of *s-Prdm16* shortened latency. Gene expression profiling using RNAseq indicated that forced expression of *f-Prdm16* resulted in altered respiratory metabolism of MLL-AF9 cells, whereas expression of *s-Prdm16* induced a strong inflammatory gene signature, comparable to that seen in HSCs expressing only *s-Prdm16*. Several inflammatory cytokines and chemokines induced by *s-Prdm16* are associated with MDS and with a worse prognosis in human AML. Furthermore, leukemia expressing *s-Prdm16* had an elevated number of cells with abnormal nuclei, characteristic of dysplasia.

Finally, we performed an analysis of *PRDM16* in human AML from the publically-available Cancer Genome Atlas dataset, containing clinical and gene expression data for 179 cases of AML. *PRDM16* expression negatively correlated with overall survival, both in the entire dataset and in the NPM1-mutated and MLL-rearranged subsets, and *s-PRDM16* exhibited a stronger correlation than *f-PRDM16*. *HOX* gene expression correlated with *PRDM16* expression, suggesting that HOX genes may positively regulate *PRDM16* expression in AML. In NPM1-mutant and MLL-rearranged subsets of AML, we also found that high *PRDM16* expression correlated with an inflammatory gene signature, thus corroborating our findings in mouse MLL-AF9.

Our findings demonstrate distinct roles for *Prdm16* isoforms in both normal hematopoiesis and AML, and identify *s-Prdm16* as one of the drivers of prognostically-adverse inflammatory gene expression in leukemia.

Table of Contents

List of Figures

List of Tables

Acknowledgements

The journey to obtaining a PhD is a difficult one fraught with long hours, detours that sometimes last for months but do not yield fruitful results, public presentations, and the stress of manuscript preparation and submission. When I have hit those rough patches in this journey, it has been wonderful to know there are people to lean on, and occasionally just to take a break with and remember how great life still is outside the confines of the lab!

Firstly, to the members of my lab – Mariana, Linda, Ya-Wen, Alex, Ana, Corey, Jessie, Anna, Mavis, Davide, Melanie, Kenjiro, Rafa, and Bryn – you've been great partners to work with and I have loved spending time with you in and out of the lab. Particularly, I have to thank Dr. Larry Luchsinger who has been an excellent lab mentor and friend, who taught me nearly everything I know about hematopoiesis, and who always knows some trick to make lab or computer work less difficult. Thank you for rescuing me from more than one panicked and dire situation!

To Dr. Hans Snoeck, my mentor, thank you for all the guidance throughout these six years. It would be disingenuous to call your style anything other than "tough love," but I do believe that working in a lab with high expectations produces strong scientists, and I am grateful for that! You've also taught me a great deal about how to think about science and plan a project. Thank you for getting me through the tough times of manuscript and thesis preparation with (most of) my sanity intact!

To my thesis chair, Dr. Christian Schindler, and to my committee Dr. Mark Heaney, Dr. Steven Emerson, and Dr. Ulf Klein, thank you for attending my TRAC meetings and providing guidance along the way. I have received some great advice and insight from you and I'm so glad to have chosen the members that I did. And thank you in advance to Dr. Ulrich Steidl for agreeing to serve as my outside defense committee member, I am extremely grateful. Thank you also to Dr. Valeria Culotta, my first PI while I was getting my masters in Johns Hopkins, who inspired me to pursue a career in science.

To my friends that I have made here in grad school, I'm so glad to have taken this journey with all of you, your friendship has been invaluable. To Melanie, Joe, Mariana, Lyla, and Ben, the time we've spent together has been great. I've loved the many lunches spent with Melanie and Mariana, going out for drinks and dinner with Joe and Lyla, and having some fun to look forward to after a long day or week at work! I wish all of you the best of luck going forward, you're all amazing and I hope we can continue to stay in touch wherever each of us ends up next.

To my amazing partner Bill, I'm so glad to have met you halfway through this crazy grad school adventure. There is nothing better than knowing I have a loving (and clean!) place to spend a weekend and recuperate. You've been an amazing partner to lean on and relax with in some of the most stressful times, as I've worked on writing my manuscript and now my thesis. I'm inspired by you, love you dearly, and I'm looking forward to the future by your side!

To my sister Andrea, you're amazing, thank you so much for being there for me when I really needed it! When I started grad school, you were still in college. Now you've got a bachelor's degree, a master's degree, an inspiring career doing such good for people, a great husband, and a beautiful, wonderful daughter. And all I got was this lousy PhD! You're the best sister I could ask for, thank you for being you!

To Mom and Dad, I thank you most of all, as I always will for any success that I may find in life. For reading to me when I was little, for making sure I did my homework when I absolutely did not want to, for helping to keep my disorganized mind organized, I certainly would not be where I am today without you! Thank you for being there during the tough times – Dad with your pragmatic, thoughtful advice, and Mom with your offers to "give Hans a call" when things would get tough. Your love and support mean everything to me, I love you and can never thank you enough.

Dedication

I would like to dedicate this thesis to my grandfather, James A. Corrigan, who passed away while I was in graduate school.

He loved learning, probably more than anyone I know. The people, places and things that make up the world around us were fascinating to him. More than once, he would give me books, newspaper articles, or magazines to read because he had read something he found interesting, and he was usually right.

He was so proud and thrilled to have a grandson going all the way and studying for a P H D. Grandpa, this one's for you!

Chapter 1 – Introduction – Hematopoietic Stem Cell Biology

Section 1.1 – Hematopoiesis

1.1.1 Overview of hematopoiesis

Hematopoiesis is the process by which the body generates all of the mature component cells of the blood. Mature cells have limited lifespans and therefore exhibit a continuous cycle of death and replacement. For this reason, hematopoiesis must be tightly regulated to maintain a proper balance of blood cells, particularly in cases of infection or stress. Hematopoietic Stem Cells (HSCs) are the parent cells that ultimately give rise to all the downstream cellular components of blood[1]. In mammals, they primarily reside within the bone marrow, and even there, they are extremely rare, found in a frequency of only 1 in 10^5 nucleated cells[2].

The three broad cell types that comprise the cellular component of blood are erythrocytes, platelets, and white blood cells. Red blood cells, or erythrocytes, are responsible for oxygen delivery from the lungs to all tissues of the body, and depletion or loss-of-function of these cells leads to anemia. Platelets, or thrombocytes, are important protective cells that work with non-cellular coagulation factors to form clots and stop blood loss after injury. Finally, white blood cells, or leukocytes, are a heterogeneous population of cells which together form the largest component of the immune system, with a broad range of functions including immune surveillance, generation of antibodies to fight infection, and destruction of pathogens. White blood cell deficiency results in increased susceptibility to infection and disease. All of these cells are ultimately derived from HSCs, illustrating why proper HSC function is critical for survival.

The HSC serves as a model for stem cell biology, and was in fact the first stem cell to be discovered[1]. Stem cells have two essential properties that define and distinguish them from other cells. These are their ability to self-renew and to differentiate into specialized mature cells. The self-renewal aspect of stem cell

biology is critical because in most tissues cells must be constantly replenished. Maintenance of a stem cell pool is therefore necessary throughout the lifetime of an individual. The importance of differentiation is self-evident, as differentiated cells perform the necessary cellular functions that sustain life. The balance between stem cell renewal and differentiation maintains homeostasis in an organism. Stem cell dysregulation is often one of the underlying causes of malignancy, as will be introduced in Chapter 2. HSCs give rise to a series of progenitors as they differentiate. These progenitors progressively lose self-renewal capacity and multipotency, gradually becoming committed to a more limited number of possible cell fates, Finally, they become fully committed progenitors, directly upstream of terminally-differentiated mature cells. Differentiation of erythrocytes, platelets, and most white blood cells including myeloid cells and B-cells occurs in the bone marrow, whereas T-cells differentiate and mature in the thymus.

1.1.2 Developmental biology of the hematopoietic system

Hematopoiesis begins in the embryo, progressing through multiple sites during fetal development, and does not take place exclusively in the bone marrow until shortly after birth. A complete understanding of HSC development from pluripotent stem cells may allow for the *in vitro* generation of HSCs for clinical applications, lending significant impact to the field of HSC developmental biology. The earliest murine blood cell development can be found in the yolk sac by embryonic day (E)7 in what are termed blood islands[3]. Blood islands develop from $Flk1^+$ mesodermal progenitors, which differentiate into cells termed "hemangioblasts" with the ability to further differentiate into either blood or endothelial cells[4]. This early period is termed "primitive hematopoiesis," a stage in which only primitive erythrocytes and certain myeloid cells are produced. This is an early, transient stage of hematopoiesis with no multipotent or self-renewing HSCs present, and yolk sac progenitors are likely not the source of later definitive hematopoiesis[5]. Recent evidence suggests that there may be other early embryonic sites of hematopoiesis, including in the head, cardiac tissue and placenta. However, these sites, like the yolk sac, have not been shown to contain definitive HSCs[6-8].

The first “definitive HSCs” with long-term self-renewal and multipotent differentiation potential are found in the aorta, gonads, and mesonephros (AGM) region at day (E)10.5[9]. Within the AGM, HSCs specifically localize within the dorsal aorta, particularly along the ventral wall[10-12]. The HSCs found in the AGM have a higher self-renewal potential compared to adult HSCs, although their long-term reconstitution ability is somewhat lower[11,13,14]. The first definitive HSCs develop from endothelial precursors[15]. Because of the localization of the earliest HSCs along the aortal wall, this was long hypothesized to be the case[16]. The developmental process as currently understood is that mesodermally-derived hemangioblasts differentiate into “hemogenic endothelial” cells, which serve as direct precursors of both definitive HSCs and endothelial cells[17]. Various factors, including SCL, RUNX1, and GATA2, are required in the early stages of embryonic HSC development. SCL (Tal1) is essential for embryonic blood development[18,19] and is required for differentiation of hemangioblasts into hemogenic endothelium. RUNX1 is then required for differentiation of hemogenic endothelium into early HSCs[20,21], but not required after this stage or for adult hematopoiesis[22]. Hemogenic endothelial differentiation into hematopoietic cells is known as the endothelial-to-hematopoietic transition (EHT) and RUNX1 is considered the key regulator of this process[23]. GATA2 is highly expressed in early definitive HSCs in the AGM and maintains their immaturity, preventing differentiation and thereby maintaining the HSC pool[24]. GATA2 retains this role in adult HSCs and is therefore required for HSC maintenance throughout life[24].

Within the next few days of murine development, HSCs migrate to the fetal liver and greatly expand. The fetal liver is considered the first site of major HSC expansion[25]. Fetal liver HSCs in mice express similar surface markers as adult HSCs, except for Mac-1 which is expressed on fetal liver but not adult HSCs[26]. Fetal liver HSCs are capable of long-term multilineage reconstitution and have an increased reconstitution potential compared to adult HSCs. In contrast to adult HSCs, they are highly proliferative and the majority are found in cell cycle[25]. Differences in repopulation capacity between fetal and adult HSCs may be explained by a number of differentially expressed genes, including Lin28b/Hmga2/Let-7, whose

overexpression in adult HSCs can increase their repopulation and self-renewal capacity and has been proposed as one of the drivers of HSC potential[27]. Fetal liver HSCs also have a different metabolism, using more oxidative phosphorylation than glycolysis for ATP production. They have higher expression of tricarboxylic acid cycle (TCA) genes and higher levels of reactive oxygen species (ROS) production[28]. Functional differences between fetal liver and adult HSCs may result from microenvironmental differences between fetal liver and bone marrow. This microenvironment, termed the "niche", is described in Section 1.3.2. Fetal liver stromal cells are different from those in the bone marrow – they are more proliferative and express different cell surface markers, notably SCF, DLK, and regulators of the Wnt signaling pathway[29,30]. Fetal liver HSCs lack CEBP/α, and deletion of this gene from adult HSCs causes an increase in cell number and proliferation[31]. Fetal liver HSCs also retain some endothelial markers, including VE-cadherin, which are not present in bone marrow HSCs and support the hypothesis of endothelial origins of embryonic HSCs[15,32]. The frequency of HSCs in murine fetal liver begins to diminish after day (E)15.5, at which point HSCs begin populating nascent bone marrow[25,33]. Fetal liver hematopoiesis is largely eliminated within a few days after birth.

In humans, hematopoiesis occurs in nearly all bones in newborns, with red marrow (responsible for hematopoiesis) found throughout the bones and very little yellow (fatty) marrow present. As we age, however, yellow marrow begins to spread, beginning from the ends of long bones (the epiphyseal region)[34]. Eventually, hematopoietic output from red marrow decreases and centralizes, with nearly all hematopoietic activity found in central skeleton, femurs, and humeri later in life[35].

Aging also causes physiological changes within the HSC compartment, resulting in reduced hematopoietic output and a weakened immune system. Somewhat surprisingly, the frequency of murine HSCs increases in aged bone marrow. However, the competitive efficiency of these HSCs compared to young controls decreases significantly, to an estimated 25%[36]. HSCs from old mice are also significantly myeloid biased relative to young HSCs[37]. This may be because the HSC compartment loses heterogeneity, tending to

become dominated by the clonal expansion of a limited number of myeloid-biased HSCs, which are slowly conferred a competitive advantage through somatic mutations over the years, resulting in the higher HSC frequency but lowered competitive efficiency seen in aged blood[38,39].

Section 1.2 – Applications, techniques, and assays of HSCs

1.2.1 Clinical HSC transplantation

HSC research has led to significant medical advances, most notably in the field of transplantation. Bone marrow transplantation (BMT), now often referred to as HSC transplantation (HSCT), is an important and still-evolving medical procedure whose purpose is to transplant healthy HSCs into a patient with defective or malignant HSC activity. The technique was first reported in humans in 1957[40]. It has predominantly been used in malignancy, to reestablish healthy HSC function in patients whose bone marrow has been ablated by strong chemotherapy or radiation, and in patients with life-threatening genetic immune deficiencies or subtypes of anemia, to reestablish a healthy hematopoietic system using transplanted donor HSCs. Over the past 50 years, this procedure has evolved significantly. Early breakthroughs included the refinement of donor/recipient pairing and improvement of immunosuppressive conditioning. Bone marrow transplants are at risk for both rejection and graft-versus-host disease (GVHD), where donor lymphocytes mount an immune response and attack recipient tissues[41,42]. The risks of mortality from infection and GVHD remain high, which in the past rendered total BMT applicable only for life-threatening disorders. More recent developments, however, have included depletion of mature cells[43] or purification of $CD34^+$ hematopoietic progenitors from bone marrow to reduce the risk of GVHD from mature donor cells. This is not applicable for many cases of leukemia however, where donor lymphocytes exhibit important anti-tumor effects. Adult peripheral blood and umbilical cord blood have also become established as a source of donor HSCs that are easier to collect and bank, providing more options for donor/recipient pairing. Lastly, autologous HSCT, in which a patient's own HSCs are removed and transplanted back after chemotherapy, has become a widely-used technique, accounting for more than half of HSCT procedures. Today, more than 50,000 HSCT are performed annually and the specific procedures are decided on a case-by-case basis, often determined by the age and overall health of the patient, and the disease being treated[44,45].

1.2.2 HSC expansion and de novo generation

The extremely limited number of HSCs *in vivo* provides a significant obstacle for their clinical use. A complete understanding of HSC biology would theoretically allow for the expansion of these cells *ex vivo*, generating a potentially unlimited pool of HSCs which could be used for transplantation[46]. This could have extraordinary benefits in treating both malignancies and blood disorders, particularly for autologous transplants where a patient's HSCs could be manipulated or "repaired," expanded and transplanted back with few side effects[47]. HSC expansion would also benefit scientific research, with many more cells available for experimentation. As will be described in Section 1.3, HSCs are typically quiescent. HSC expansion would therefore require the means to bring HSCs out of quiescence and to mimic signals from the niche which promote symmetric cell division, in which HSCs divide evenly into two daughter HSCs, rather than asymmetric cell division, where one daughter cell begins to differentiate.

Many small signaling proteins, termed cytokines, are produced in the bone marrow and regulate HSCs. Early attempts to expand HSCs *in vitro* focused on combinations of cytokines, with limited success. Numbers of functional HSCs rapidly begin to decrease *in vitro* once isolated, and the best cytokine combinations could only essentially maintain the existing HSC pool[48]. It was later shown that forced expression of the transcription factor HOXB4, which is normally expressed in HSCs, can generate immortalized HSC lines capable of self-renewal and with multilineage engraftment potential[49]. However, the abnormal proliferation of these cells, and a low but statistically significant increase in their leukemic potential, led to the conclusion that genetic manipulation is not an ideal method for HSC expansion[50]. More recently, large chemical library screens have been performed, yielding promising results. One such screen revealed that the compound StemRegenin1 (SR1), an antagonist of the aryl hydrocarbon receptor (AHR), can expand human $CD34^+$ cells and increase the number of long-term reconstituting HSCs in culture[51]. The pyrimidoindole derivative UM171 was also found to induce *in vitro* expansion of long-term

reconstituting HSCs, in an AHR-independent manner[52]. Of note, these compounds showed efficacy in human but not mouse HSC maintenance, and investigators have not yet demonstrated their clinical use.

Alternatively, HSCs could be generated *de novo* from pluripotent stem cells. This would also provide a means of unlimited HSC generation as pluripotent stem cells are immortalized, expandable cell lines. An HSC differentiation protocol could therefore be used to produce any quantity of HSCs. Furthermore, the ability to transform adult fibroblasts into pluripotent stem cells (iPSCs) was a landmark achievement that has provided new opportunities for stem cell therapy using adult cells[53]. Two broad strategies have been followed in the "directed differentiation" of iPSCs into HSCs. The first was to use signaling molecules to mimic embryonic signals specifying HSC commitment within the AGM[54,55]. These methods have generated progenitors with restricted hematopoietic potential, providing further insight into HSC development. Other recent efforts have focused on bypassing this process through direct expression of combinations of HSC transcription factors[56-58]. These efforts also have yielded hematopoietic progenitors with limited potential, providing optimism that efforts in the near future may produce functional HSCs.

1.2.3 Overview of the hematopoietic progenitor compartment

A number of methods are available to study hematopoietic output. Before describing these assays, however, a brief description of the hematopoietic progenitor compartment is warranted. An abridged illustration is provided in (**Figure 1-1**). "HSC" is most often used to describe the long-term hematopoietic stem cell (LT-HSC) and throughout the literature the two are often used interchangeably. LT-HSCs can reconstitute the entire hematopoietic compartment and persist and self-renew over a long period of time, potentially through a lifetime in humans and for multiple lifetimes in mice. The short-term HSC (ST-HSC) is another multipotent progenitor with some self-renewal capacity, but in contrast to LT-HSCs, only for a limited time, typically less than 8 weeks in mice. It cannot reconstitute the hematopoietic system long-term. ST-HSCs are less likely than LT-HSCs to be quiescent and have more potent *in vitro* proliferative

capacity in the short-term[59]. Lastly, the multipotent progenitor (MPP) represents the third multipotent cell type within the hematopoietic system. The MPP has little or no self-renewal capacity but can still differentiate into any mature blood cell. Recent studies, however, have shown that the MPP population is more heterogeneous than originally thought[59-61]. HSCs are also heterogeneous, which has a significant impact on aging and disease and will be further discussed in Section 1.2.6. As a group, LT-HSCs, ST-HSCs, and MPPs are termed hematopoietic stem and progenitor cells (HSPCs), a classification used broadly in the literature to refer to multipotent blood progenitors. A common surface marker phenotype for these cells in the mouse is Lineage$^-$cKit$^+$Sca1$^+$ (LSK), and therefore LSK cells are often taken as the basis of HSPCs, despite the limitations of grouping such a heterogeneous cell population together[62]. Based on this wide variety of definitions, it is important to read the literature carefully and determine precisely which cells are defined as HSCs or HSPCs in any given publication.

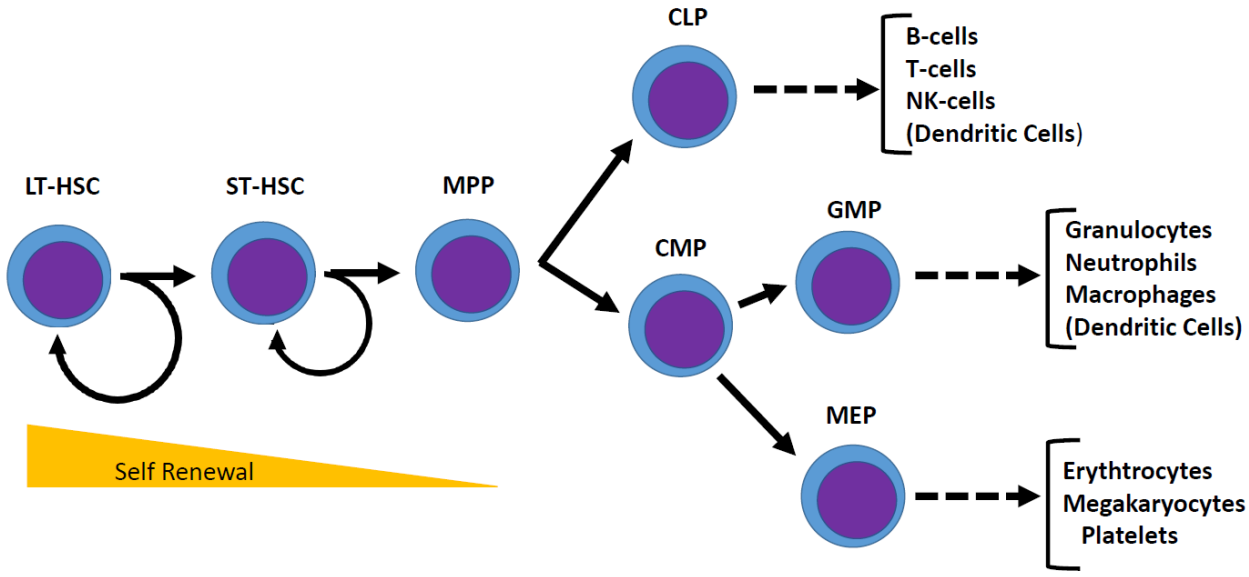

Figure 1-1: Simplified diagram of differentiation from LT-HSCs to mature cells. LT-HSCs have a high capacity for self-renewal and can also differentiate into ST-HSCs and then multipotent progenitors (MPPs). In these first steps, self-renewal capacity is lost but multipotency is retained. MPPs can then differentiate into progenitors with lymphoid potential (common lymphoid progenitors or CLPs, which later produce lymphocytes) or myeloid potential (common myeloid progenitors or CMPs, which differentiate into either granulocuyte-macrophage progenitors [GMPs] or megakaryocyte-erythrocyte progenitors [MEPs])

Beyond the MPP stage, progenitors lose multipotency, and start to become restricted to different mature lineages. This is a broad field of research with dozens of committed progenitors described in the literature[63]. This introduction will therefore focus on only a select group near the top of the hierarchy. Common lymphoid progenitors (CLPs) are lymphoid-restricted progenitors that further differentiate into committed progenitors of B-cells, T-cells, NK-cells, and likely dendritic cells[64]. The common myeloid progenitor (CMP) is the counterpart of the CLP, which can further differentiate into the granulocyte/macrophage progenitor (GMP) (the progenitor of mature myeloid cells including neutrophils, macrophages, and other granulocytes) and the megakaryocyte/erythrocyte progenitor (MEP) (the upstream progenitor of erythrocytes and megakaryocytes, which produce platelets)[65]. This a very simplified description, as current research suggests more plasticity to these cell fates[66], but broadly serves to introduce the main progenitors of the hematopoietic system. One additional progenitor relevant to this thesis was first described in our lab, termed the "LSK-" cell. LSK- cells are lymphoid progenitors distinct from CLPs. They are found in bone marrow, increase in frequency with age, and are Lineage$^-$cKit$^-$Sca1$^+$[67]. LSK- cells are biased toward B-cell production and generate a higher ratio of marginal zone/follicular B-cells within the spleen than CLPs. Their mature progeny also retain higher Sca1 levels than those derived from other progenitors[68]. LSK- cells have not been widely studied, but bear relevance to our Prdm16 genetic model, as will be discussed in Chapter 4.

1.2.4 In vitro hematopoietic assays

A number of *in vitro* methods exist to measure hematopoietic progenitor frequency. Perhaps the simplest are colony-forming assays[1], first pioneered as *in vivo* experiments measuring the formation of myeloerythroid colonies within the spleens of recipient mice. Today, colony assays are well-established *in vitro* experiments that measure the frequency of hematopoietic progenitors, but do not effectively measure HSCs. Combinations of cytokines, such as SCF, IL-6, and IL-3, provide signals required for colony formation[62]. The resulting cellular composition depends on the combination of cytokines and progenitors

present in the culture. Cells are plated in semi-solid methylcellulose media and colonies are counted and classified based on the cell types present in each colony[69]. This process essentially quantifies the frequency of short-term, lineage-restricted progenitors but not HSCs. To measure cells with long-term potential, *in vitro* assays have been developed that rely on extended co-culture with stromal cells, either from primary bone marrow or from immortalized cell lines[70]. Cobblestone assays use microscopy to visualize colonies (termed cobblestone area-forming cells or CAFCs) found within stromal cells after 5 weeks of culture[71]. Colonies formed within two weeks signify short-term restricted progenitors, while colonies found at 4-5 weeks are thought to represent more long-term multipotent stem cells. The best *in vitro* estimate of HSC frequency is determined by using a modified stromal-cell assay to measure "long-term culture initiating cells" (LTC-ICs). After 5 weeks in stromal culture, media is removed and replated with methylcellulose. Precursors in this assay persist for weeks on stromal culture and therefore represent long-term progenitors[72]. Though they can provide an estimate of HSC frequency, these experiments have limitations. They rely on stromal culture and cannot distinguish LT-HSCs. They also do not account for potential defects in bone marrow localization or homing. For these reasons, *in vivo* assays, described below, are the preferred method to detect and quantify LT-HSCs.

1.2.5 Competitive transplantation assays

LT-HSCs can persist throughout the lifetime of an individual, and therefore their functional assessment can only be reliably measured in a long-term *in vivo* experiment. Competitive repopulation experiments are the gold standard to measure LT-HSC function[73]. In this assay, equal numbers (or any preferred ratio) of experimental donor cells and competitor cell controls are injected into lethally irradiated recipient mice. Essential to the assay is that donor, competitor, and recipient cells can be distinguished, by using two alleles of the CD45 gene, CD45.1 and CD45.2, and heterozygous (double-positive) CD45.12 cells[74]. Differences in donor reconstitution between experimental groups and wild-type controls can indicate either a loss or gain of HSC function. Measurements at least 16 weeks post-transplant are considered an

adequate readout of true LT-HSC function, although serial transplant experiments may also be employed to measure HSC output over longer periods of time. Competitive transplant assays can be used to quantitatively determine the frequency of LT-HSCs in a given cell population through the use of limiting dilution assays[75]. These are competitive transplants with low numbers of donor cells, using a stochastic range of cell doses designed so that some fraction of recipients will not receive donor LT-HSCs. Poisson statistical analysis can then be performed to estimate LT-HSC frequency, defined as the inverse of the cell dose at which approximately 37% of recipients are non-responders[76].

One limitation to competitive transplantation is that this technique forces a LT-HSC to endure the stresses imposed by radiation and engraftment, to survive and proliferate rapidly upon transplantation to begin repopulating the mouse, and to function in a bone marrow environment that is temporarily remodeled as a result of irradiation. These conditions are not typically experienced by steady-state HSCs, making competitive transplants an imperfect representation of steady-state hematopoiesis. Recent studies have used advanced labeling techniques to study hematopoiesis in unperturbed conditions[77,78]. These studies have suggested that steady-state hematopoiesis is predominantly derived from a polyclonal population of ST-HSCs and MPPs, refreshed by occasional LT-HSC activity. This work has shed more light on the hematopoietic system and has illustrated the physiological importance of all progenitors within the HSPC hierarchy.

1.2.6 Single-cell transplantation and HSC heterogeneity

Recent evidence has revealed that HSCs are in fact a more heterogeneous population than previously assumed[79]. Single-cell competitive transplants have been essential for deepening our understanding of HSC heterogeneity[80]. These studies have demonstrated that a broad range of potential hematopoietic outputs is possible from individual HSCs[81]. All HSCs can self-renew and fully repopulate the hematopoietic system, but single-cell transplants have shown that individual HSCs can be biased toward different lineage

outputs[81,82]. Apart from lineage bias, HSCs can also be found in different cell-cycle states, existing in either active (division every 30 days) or dormant phases (50-190 days). HSCs have the ability to cycle between these two states, with the active HSCs contributing to the bulk of hematopoietic output[83,84].

At least four broad classes of HSC have been described (illustrated in **Figure 1-2**) – "balanced" HSCs which generate similar numbers of myeloid and lymphoid progenitors, "myeloid-biased" HSCs which produce mostly myeloid cells, "lymphoid-biased" HSCs that generate very few myeloid cells, and "platelet-biased" HSCs[85] which appear to be a myeloid-biased subset generating a high number of megakaryocytes and platelets[86]. Younger mice contain more balanced and lymphoid-biased HSCs, whereas older mice contain predominantly myeloid-biased HSCs[87]. Furthermore, myeloid-biased HSCs have a higher capacity for self-renewal and a longer functional lifespan than lymphoid-biased HSCs, with lymphoid-biased HSCs more closely resembling the ST-HSC compartment[88]. Some publications have given these HSCs a new nomenclature – α-HSCs (myeloid-biased), β-HSCs (balanced) and γ/δ-HSCs (lymphoid-biased)[14]. Myeloid-biased and balanced/lymphoid-biased HSCs can be separated to some extent based on surface expression of CD150[38]. $CD150^{high}$ HSCs are enriched for the myeloid-biased, long-term subtype, whereas $CD150^{low}$ HSCs are enriched for balanced and lymphoid-biased subsets. Furthermore, von Willibrand Factor (vWF), a megakaryocyte gene involved in platelet aggregation[89], has been shown to distinguish between myeloid and lymphoid-biased HSCs and specifically marks the platelet-biased HSC population that generates large numbers of megakaryocytes. Further studies have also demonstrated differences in TGFβ1-responsiveness[90], BMP activation[91], and lineage transcriptome, with balanced and lymphoid-biased HCSs expressing higher levels of lymphoid regulators including Il7r, Pax5, E2a, and Ikaros[14]. It remains unclear precisely how HSC heterogeneity is determined or established. Three possibilities have been proposed and under investigation. The first is that the niche, described in Section 1.3.2, provides different signals to each HSC, establishing their identity. A second possibility is that HSC lineages are programmed during development based on spatial positioning within the hemogenic endothelium or ventral wall of the dorsal

aorta. Finally, it is possible that there is a direct progression from one HSC subtype to another. Of note, recent data from our lab suggests that the mitofusin MFN2 may influence HSC lineage fate, either directly through mitochondrial remodeling or more likely through altered cellular metabolism and calcium buffering[92]. HSC heterogeneity remains an active field of investigation that has substantially altered older assumptions about HSC biology.

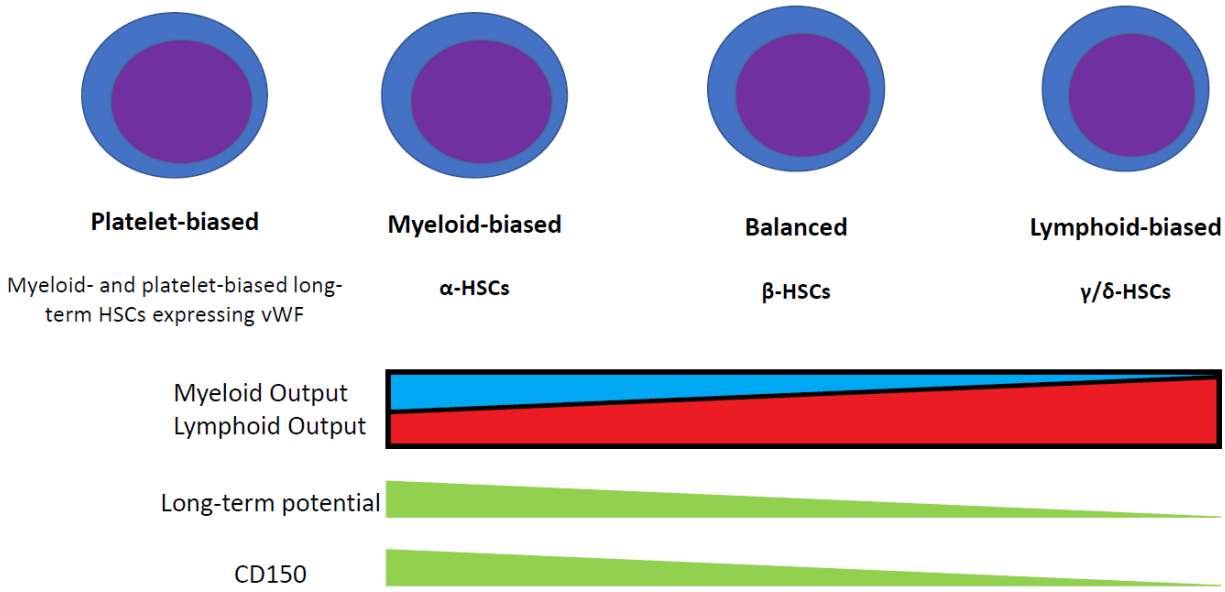

Figure 1-2: Overview of HSC heterogeneity. Depiction of four HSC subtypes that have been described in the literature. Generally, lymphoid-bias is associated with shorter-term reconstitution potential and lower expression of CD150. Myeloid-biased HSCs accumulate in frequency with age. Two distinct nomenclatures have been proposed for these subsets, based on roughly equivalent criteria, and are listed above. "Platelet-biased" HSCs were described recently, produce large numbers of megakaryocytes, and show a myeloid bias. They also may have the ability to differentiate into short-term lymphoid-biased HSCs. Of note – all HSC subtypes described have lymphoid capability. The criteria for "myeloid-biased" is a lymphoid to myeloid output ratio of less than 3. Lymphoid-biased HSCs, however, produce almost no mature myeloid cells. The criteria for distinction of delta HSCs is myeloid output of less than 1%.

Section 1.3 – HSC phenotype and biology

1.3.1 HSC surface marker phenotype

A significant amount of effort has been spent attempting to purify HSCs from the bone marrow or other tissues. This has important clinical and scientific implications, described earlier. Flow cytometry provides the means to achieve this, allowing for single cells to be sorted from a mixed population based on differences in surface antigen expression. HSCs were first enriched in mice using the combination of cell surface markers $Lin^{-}Sca1^{+}cKit^{+}CD90^{-}$[93]. This scheme allowed for enrichment of LT-HSCs to better than 1 in 30 sorted cells. Since then, additional markers have been discovered, demonstrating that murine LT-HSCs are $FLT3^{-}$, $CD34^{-}$, $CD150^{+}$, $CD48^{-}$, and $CD244^{-}$[94]. Combinations of these markers can enrich HSCs to roughly half of a sorted population of cells. Surface markers for human LT-HSCs are somewhat different, most notably in that they are $CD34^{+}$, that the Sca1 protein has no direct homolog in human, and that some additional markers (CD38 and CD49F) are found on human HSCs. Human HSCs are lineage negative, however, and a currently-accepted surface phenotype for human HSC isolation is $Lin^{-}CD34^{+}CD38^{-}CD45RA^{-}CD90^{+}CD49F^{+}$[95,96].

1.3.2 The HSC niche

After birth, nearly all HSC activity is found within the bone marrow. There, HSCs are maintained by a complex milieu of external signaling programs within the HSC microenvironment, which is termed the niche[97]. A better understanding of niche biology could improve *ex vivo* HSC expansion and reduce toxicity from conditioning regimens for HSC transplantation. Exactly which cells comprise the niche has been the subject of considerable debate. The earliest evidence pointed to osteoblasts as essential niche components[98], as ablation of osteoblasts lead to a significant alteration of hematopoietic output[99]. However, overall bone marrow composition was affected by osteoblast deficiency, raising the possibility that HSC effects were due to general bone marrow stress. Osteoblasts now appear to play a more specific

role in regulating early lymphocyte precursors, particularly of B-cells, through release of factors that promote B-cell development[100].

More recently, 3-D imaging and improved HSC staining techniques using either SLAM family markers ($CD150^{+}CD48^{-}CD41^{-}$) or a combination of α-catulin (Ctnnal1) and cKit have led investigators to conclude that nearly all HSCs in the bone marrow localize near sinusoidal blood vessels, in what is called the perivascular niche[94,101]. Recently HOXB5 has been identified as a highly specific marker for LT-HSCs, and fluorescently-labelled $HOXB5^{+}$ HSCs have been confirmed to associate with VE-$cadherin^{+}$ endothelial cells, supporting the notion of a perivascular niche for HSCs[102].

More recent studies have utilized both the CXCL12-CXCR4 pathway and the growth factor SCF to gain further insight into essential niche components. CXCR4 is expressed on HSCs[103] and both the receptor CXCR4 and its ligand CXCL12 are essential for HSC maintenance[104,105]. SCF and its receptor cKit are also essential for HSC maintenance and were among the first HSC factors to be discovered[106,107]. CXCL12 is highly expressed by perivascular stromal cells, with measurable though considerably lower expression on endothelial cells and osteoblasts. SCF has similar expression patterns. Deletion of CXCL12 from perivascular stromal cells using a Lepr-Cre conditional knockout mobilizes HSCs from the bone marrow into the spleen and peripheral blood, confirming the importance of the CXCL12-CXCR4 pathway and of perivascular stromal cells in the HSC niche[108]. The authors proposed osteoblasts as potential niche cells for lymphoid progenitors, as deletion of CXCL12 from osteoblasts reduced CLP levels and caused a reduction in lymphoid reconstitution ability[108]. A significant HSC depletion from a Prrx1-Cre CXCL12 conditional deletion, which recombines in a broader population of stromal cells, suggests that there may also be $Lepr^{-}$ stromal cells involved in HSC niche retention. Unanswered questions remain in the ongoing study of the HSC niche. There are nearly 100 times as many stromal $Lepr^{+}$ cells as HSCs, leading to the question of what other role these cells may serve and if HSC niche space is as limited as is hypothesized. Furthermore, other cells including macrophages, megakaryocytes, and Schwann cells, are suggested to be

a part of the functional HSC niche. Finally, the role of the niche in leukemogenesis is a promising topic of investigation, as certain leukemias remodel the bone marrow to promote oncogenesis, which will be addressed in Section 2.

1.3.3 HSC efflux capacity

HSCs and in fact many stem cell populations exhibit an unusual capacity to efflux small molecules. This is often proposed to be an evolutionary method to protect stem cells from genotoxic agents, as any mutations acquired within a stem cell at the top of a tissue hierarchy will propagate throughout the tissue upon differentiation. HSCs express several efflux transporters that confer this ability including the ATP binding cassette (ABC) transporter family members Bcrp1/Abcg2, Mdr1a, and Mdr1b[109,110]. Ablation of efflux capacity does not have overt effects on hematopoiesis but does render HSCs more susceptible to genotoxic compounds[111]. This phenomenon has allowed for the isolation of LT-HSCs from marrow by their low fluorescence when stained with the dyes Hoecsht 33342 or Rhodamine-123, where the dimly-stained population is referred to as the "side population" and contains most LT-HSCs[112,113].

The efflux capacity of HSCs also caused a long misevaluation of HSC mitochondrial content. Mitotracker Green (MTG) is a widely-used fluorescent dye for visualization and quantification of mitochondria that specifically labels these organelles. Mitochondrial staining of HSCs with MTG suggested that LT-HSCs were MTG^{low} and therefore had low mitochondrial content[114-116]. It has since been shown, however, that this is a result of MTG efflux from LT-HSCs – in fact, HSCs have a high quantity of mitochondria within the hematopoietic compartment[117], a finding which has a significant connection to much of the research undertaken in our lab.

1.3.4 Mitochondrial properties of HSCs

This work primarily focuses on the PRDM16 gene, and its role in normal and malignant hematopoiesis. Recent work from our lab has demonstrated that *Prdm16*-deficient HSCs have significantly impaired

reconstitution potential and drastically altered mitochondrial morphology[92,118]. As a result, Chapter 6 is an investigation of the potential role mitochondrial morphology may play in leukemogenesis. Mitochondria are dynamic organelles that can be found in either fragmented, "bean-shaped" structures typically seen in textbooks, or highly-fused, elongated networks. The proteins responsible for mitochondrial fusion are integral membrane GTPases known as mitofusins, and in mammals there are two – Mfn1 and Mfn2[119-121]. Another fusion protein, Opa1, is involved in fusion of the mitochondrial inner membrane[122]. The opposite process of mitochondrial fragmentation is mediated by Drp1 and Fis1[123,124]. LT-HSCs have elongated mitochondria compared to other HSPCs and progenitors[92]. However, *Prdm16*-deficient HSCs show a complete loss of this phenotype, with significantly fragmented HSCs. Indeed, *Prdm16*-deficient HSCs and mouse embryonic fibroblasts (MEFs) have similar mitochondrial morphology to that observed in a Mfn2 knockout, and Prdm16 binds to the Mfn2 promoter, which may explain the mitochondrial phenotypes of this knockout[92]. It is therefore an ongoing topic of investigation whether mitochondrial effects are responsible for the deficiencies seen in the Prdm16 knockout. It also raises questions regarding the roles of mitochondria and cell metabolism in HSC regulation, which will be described in the next section.

1.3.5. Metabolic and proliferative phenotypes of HSCs

HSCs exhibit unusual proliferative and metabolic phenotypes compared to most other mature cells. One of the most striking features of adult LT-HSCs is that they are highly quiescent[112]. Furthermore, the HSC niche has long been considered a hypoxic environment, with relatively low oxygen tension within the bone marrow. HSCs are reportedly highly sensitive to reactive oxygen species (ROS). Low environmental oxygen tension and energy derivation from glycolysis instead of oxidative phosphorylation would result in less ROS within the cell and could therefore be important for HSC maintenance[125]. Sorted LT-HSC populations have high levels of glycolysis, low levels of oxidative phosphorylation, and express the hypoxic master regulator HIF-1α[114]. Studies using the hypoxic marker pimonidazole and perfusion studies using Hoescht

dye also suggest that HSCs are hypoxic and not located in highly vascular regions[126,127], although this finding may be a result of pimonidazole serving as a marker of low oxidative phosphorylation. Two-photon microscopic imaging has demonstrated low oxygen tension in the peri-sinusoidal regions believed to comprise the HSC niche[128]. HSC express and stabilize HIF1-α, which promotes glycolysis instead of respiration, and has been implicated in maintaining HSC quiescence[129]. It remains unclear if HIF-1α expression in HSCs is due to hypoxic signaling or an intrinsic metabolic program within HSCs. Basal oxygen consumption and maximal respiration levels are far lower in HSCs compared to other HSPCs, even in normoxic conditions, further suggesting the unique metabolic properties of HSCs may be due to intrinsic signaling and not a response to low oxygen tension[117].

Our lab has also recently shown that HSCs have elongated mitochondria, a result of selective expression of the mitofusin Mfn2[92]. The importance of this phenotype for HSC maintenance is yet to be completely elucidated, but early results have shown that Mfn2 increases buffering of intracellular calcium (Ca^{2+}), leading to reduced NFAT transcription factor activity and promoting HSC maintenance, particularly of balanced and lymphoid-biased HSCs. These results highlight the fact that there likely remain many undiscovered metabolic factors with important roles in HSC maintenance.

Section 1.4 – Cytokine and external regulation of HSCs

1.4.1 Growth factor cytokine regulation of HSCs

There are several external factors that promote HSC maintenance or self-renewal. These include cytokine growth factors, ligands from classical signaling pathways including Notch, WNT, and BMP, and inflammatory cytokines. Some of the most well-studied and essential factors involved in HSC maintenance are growth factors. As described in Section 1.3.2, SCF is an essential regulator of HSC maintenance and a critical factor within the HSC niche, expressed by perivascular stromal cells and binding to the cKit ligand on HSCs[130]. The cytokine TPO, and its receptor MPL are also essential to maintain HSCs[131]. Adult HSCs from mice lacking TPO showed accelerated cell cycling resulting in a severe reduction of the quiescent HSC pool and in downstream hematopoiesis[132]. The source of TPO within the niche has yet to be elucidated[133]. Pleiotrophin (PTN) is another secreted growth factor, which functions non cell-autonomously and has been found to promote HSC expansion and regeneration. Deletion of PTN causes inhibition of hematopoietic development[134,135]. VEGFA and its receptor VEGFR are involved in both angiogenesis and hematopoiesis and are required for efficient hematopoiesis *in vivo*. Deletion of either gene results in an impairment of HSC function as measured by competitive repopulation ability[136,137]. VEGFA is induced by hypoxia, and its involvement with HSC function may relate to the proposed hypoxic HSC niche, described in 1.3.2. Finally, angiopoietin-1 (Ang-1) ligand interaction with its HSC receptor Tie2 is required for adult hematopoiesis and for the development of definitive hematopoiesis in the embryo[138,139]. As with many signaling factors, a loss of this signaling leads to a reduction of HSC quiescence and competitive reconstitution ability[140]. Tie-2/Ang-1 signaling is another important component of the adult HSC niche, illustrating the interplay between niche biology and external signaling pathways that are essential for HSC maintenance.

1.4.2 Role of classical signaling pathways in HSC maintenance

There are a number of well-characterized signaling pathways that play key roles in both embryonic development and in regeneration of adult tissues. Of these pathways, the BMP/TGF-β signaling pathway is important for HSC maintenance. Broadly, TGF-β signaling involves the binding of TGF-β superfamily ligands – which include TGF-β, bone morphogenic proteins (BMPs), and activin – to TGF-β receptors, resulting in downstream phosphorylation, dimerization, and nuclear translocation of SMAD proteins. TGF-β is one of the key factors involved in maintaining HSCs quiescence[141]. *TGF-β*-deficient HSCs also have defects in bone marrow homing[142,143]. However, there are multiple TGF-β superfamily ligands, and one of these ligands, TGF-β2, functions as a positive regulator of hematopoiesis and proliferation[144]. Thus, the example of TGF-β illustrates that regulatory dynamics of HSC maintenance are highly complex, and that different members of the same families may exert differential hematopoietic effects. Nonetheless, TGF-β signaling is essential for HSC maintenance, as deletion of the key downstream SMAD protein, SMAD4, from HSCs leads to significant reconstitution defects in competitive transplants[145].

The NOTCH signaling pathway also regulates both embryonic development and adult tissues. This pathway appears to play relevant but not necessarily essential roles in HSC maintenance. Deletion of Notch1 and its ligand Jagged1, which are expressed in HSCs and niche cells respectively, did not produce a competitive disadvantage in transplants or cause decreased survival after fluorouracil (5-FU) challenge[146], an *in vivo* survival experiment in which stress is applied to the bone marrow compartment through ablation of cycling progenitors, requiring efficient HSC activity to regenerate the hematopoietic compartment[147]. However, *in vitro* treatment with the Notch ligand Delta1 in combination with certain cytokines can maintain or partially expand reconstituting HSCs[148]. This role of the WNT pathway in HSC maintenance remains unclear – activation of WNT signaling using activated β-catenin, which propagates the WNT signal in the nucleus through transcription factor interactions, helps to maintain the HSC pool[149].

Non-canonical WNT signaling mediated through WNT-5A may expand or maintain HSCs by maintaining their quiescence *in vivo*[150,151].

1.4.3 Inflammatory regulation of HSCs

HSC may experience any number of stress conditions throughout the lifetime of an individual. These include irradiation and blood loss from injury, both of which reduce the hematopoietic compartment and require an activation of hematopoiesis to reestablish homeostasis. Furthermore, recent evidence suggests that HSCs can be affected directly by inducers of inflammation and innate immunity. The effect of specific pathogen infection on HSC maintenance in the mouse has also been studied. Induction of sepsis via cecal puncture or infection with *Staphylococcus aureus* induces expansion of both LT-HSCs and ST-HSCs[152]. Infection with *Mycobacterium avium* enhanced cycling of LT-HSCs leading to expansion with a corresponding impairment of long-term reconstitution capacity[153]. This study implicated interferons, particularly IFN-gamma, as mediators of HSC activation. These data are in accord with more direct studies of the effect of interferons on HSC maintenance. HSCs from mice treated with IFN-alpha exit G0 and enter active cell cycle[154]. These effects are mediated through Stat1, which is phosphorylated upon IFN-alpha stimulation, and through Sca1, which is upregulated by IFN-alpha and whose deletion renders HSCs insensitive to IFN-alpha stimulation. Similar to *M. avium* infection, IFN-alpha stimulation impairs HSC function and competitive repopulation capacity[154]. In steady-state, interferon regulatory factor-2 (IRF2) may protect HSCs from IFN-mediated exhaustion. *IRF2*$^{-/-}$ HSCs have enhanced cycling and impaired competitive repopulation capacity which is reversed if IFN signaling is disabled[155]. It is important to note that, in earlier *in vitro* studies, interferons and other proinflammatory molecules appeared to have suppressive effects on HSCs. This may be because HSCs begin cycling rapidly *in vitro*, illustrating the potential complications of *in vitro* experiments to study HSCs[156].

Other work has investigated the effect of stimulation with inflammatory antigens. Toll-like receptors (TLRs) are inflammatory mediators that recognize components of pathogens known as pattern-associated molecular patterns (PAMPs) which play a critical role in innate immunity by detecting invading pathogens[157]. TLR-4, the receptor for lipopolysaccharide (LPS), is expressed on HSCs and can induce HSC proliferation *in vitro*[158]. Upon LPS stimulation many progenitors, particularly ST-HSCs and MPPs, released cytokines including TNF-α, IL-6, IL-12, and TGF-β[159]. This stimulation occurred through the NF-kB pathway. TNF-α is a potent inflammatory mediator whose activity is frequently blocked by drugs to treat chronic inflammatory diseases[160]. Overexpression of TNF-α has been implicated in bone marrow failure associated with Fanconi Anemia[161]. Administration of TNF-α induces cycling, reduces HSC competitive reconstitution ability, and leads to a reduction in bone marrow cellularity[162].

As will be discussed in Section 2, there is growing evidence that inflammatory signaling can play a role in the progression of myelodysplasias and malignancy. Evidence presented in this thesis suggests that the short isoform of PRDM16 may induce an inflammatory signature in HSCs and leukemic cells, and therefore an understanding of the roles of inflammation in HSC maintenance may yield further insights into the role of PRDM16 in the hematopoietic system.

Section 1.5 – Transcriptional and epigenetic regulation of HSCs

1.5.1 Overview of intrinsic HSC regulation

This project focuses on the transcriptional regulator PRDM16, and its role in both normal and malignant hematopoiesis. The exact function of PRDM16 in HSCs is not fully understood, and what is currently known about PRDM16 function will be described in detail in Section 3. However, many proteins are known to intrinsically regulate HSCs in various ways. The key aspects of HSC regulation are balancing self-renewal and differentiation, and balancing proliferation and quiescence. Many regulators play important roles in the development or maintenance of HSCs. These include direct transcriptional regulators such as RUNX1, GATA2, SCL, MYB, EVI1, and E2A, and epigenetic regulators including MLL, TET2, DNMT3A, and ASXL1. Research into the roles of these genes has illuminated specific aspects of HSC biology, and provided insight into the key steps in HSC development and maintenance.

Because there are a limited number of transcriptional regulators, many of those involved in embryonic HSC development also play roles in regulating adult hematopoiesis. In some cases, developmental transcription factors later play roles in lineage specification, pushing the differentiation of HSPCs toward specific cell fates and inhibiting the expression of factors that promote self-renewal. A related concept is that in cases of malignancy, aberrant activity of the same transcriptional regulators often leads to leukemogenesis, illustrating the important point that malignancy is in many ways a disruption of normal hematopoiesis. An overview of the notable transcriptional and epigenetic regulators of HSC maintenance is provided below.

1.5.2 Transcription factor regulation of HSCs

Many transcriptional regulators are involved in HSC homeostasis. As described in Chapter 3, PRDM16 is one such factor. Another highly homologous transcriptional regulator of HSCs is PRDM3 or EVI-1[163]. As described in Chapters 2 and 3, this protein is the closest homolog of PRDM16 and has oncogenic

potential[163,164]. It is highly expressed in LT-HSCs and its expression within the HSC compartment correlates with cells with the most potent and long-term reconstitution capacity[165]. Conditional EVI-1 deletion models show lowered HSC frequency and an inability to maintain hematopoiesis or reconstitute irradiated mice[166].

SCL is highly expressed in LT-HSCs[167], and is often found in transcriptional complexes with different partners, some of which include GATA2, E2A, and the adaptor proteins LDB1 and LMO2[168,169]. The members of this complex are all involved in HSC maintenance. SCL is required for HSC maintenance, as heterogeneous mutants or SCL knockdown experiments cause impaired HSC function. SCL maintains HSCs in a G0 quiescent state and its deletion initiates HSC cycling[167]. *E2A*-deficient bone marrow exhibits a significant reduction in HSPC frequency, and defects in long-term reconstitution capacity[170]. Deletion of the LDB1 adaptor protein results in a loss of functional HSCs in both fetal and adult compartments[171]. LMO2-deleted ES cells in chimeric mice are completely unable to produce hematopoietic cells[172]. These studies illustrate the essential nature of members of the SCL transcriptional complex in HSC development and maintenance.

The HOX genes are another important set of transcription factors involved in HSC maintenance. Specifically, they regulate HSC self-renewal and differentiation into downstream progenitors. Loss of this regulation can lead to exhaustion of the HSC pool, and inadequate HSC availability later in life. The HOX genes are organized into four clusters (A, B, C, and D) based on their colocalization on four different chromosomes[173]. Members of the HOX A, B, and C clusters are expressed in HSCs and other immature progenitors, and their downregulation is important for HSC differentiation and lineage commitment[174]. The HOX genes interact with DNA-binding cofactors from the PBX or MEIS families to exert their effects[175,176]. In HSCs, the HOX genes, including HOXB3, HOXB4, HOXA9, and HOXA10, prevent the differentiation of HSCs, thereby maintaining the HSC pool[174]. HOX genes are frequently upregulated in

leukemia, causing a block in differentiation and accumulation of aberrant progenitor cells. This will be further described in Chapter 2.

1.5.3 Epigenetic regulation of HSCs

Epigenetic regulation has emerged in recent years as an absolutely essential process in which cells undergo phenotypic changes without any alteration in DNA sequence. Primary epigenetic modifications include modifications to chromatin structure, DNA methylation, and histone modification. The hematopoietic system is extensively regulated by epigenetics, and as with transcriptional regulators, epigenetic aberrations can lead to defective HSC activity or malignancy.

The first epigenetic regulators shown to affect hematopoiesis were histone modifiers. MLL1 is a lysine methyltransferase and member of the Trithorax group of epigenetic regulators. The Trithorax and Polycomb group of genes encode epigenetic factors that work in opposition to regulate gene expression, notably of the HOX gene cluster[177], with the Trithorax group serving as the positive regulator and the Polycomb group as the negative regulator. MLL1 was the first mammalian Trithorax protein discovered, notable for its chromosomal rearrangement in a substantial percentage of both childhood and adult leukemias[178]. Deletion of MLL1 is embryonic lethal, and even a heterozygous mutant has substantial abnormalities, including within the hematopoietic compartment[179]. In an inducible deletion model in hematopoietic cells of adult mice, death occurs within three weeks due to hematopoietic failure, illustrating the absolute requirement for MLL1 in HSC and progenitor maintenance[180]. Deletion of MLL1 from committed progenitors downstream of the HSPC compartment did not cause defects, showing the specificity of MLL1 requirement to the multipotent HSPC compartment. MLL1 positively regulates HOX genes as well as both EVI1 and PRDM16, illustrating the epigenetic network through which MLL1-mediated histone methylation maintains HSC function[181]. The repressive Polycomb family of protein complexes include the “initiating” PRC2 complex and the PRC1 complex which maintains repression.

These complexes function to repress cell cycle activators and lineage-specific genes[182]. Overexpression of the PRC complex member EZH2 enhances the long-term reconstitution ability of HSCs, and deletion of ASXL1 impairs normal hematopoiesis and self-renewal of HSCs, which can result in myelodysplasia[183,184]. Thus, both Trithorax and Polycomb histone modifiers play important roles in the maintenance of HSCs.

Recent findings have illustrated important roles for DNA methylation in HSC maintenance. DNA methylation occurs on cytosine residues, typically those found within CpG dinucleotides, which are often clustered in regions termed CpG islands. The methyltransferases DNMT3A and DNMT3B function as *de novo* cytosine methylases whereas DNMT1 serves as a maintenance methylase[185]. Conditional deletion of DNMT3A or DNMT3B in HSCs results in a loss of differentiation potential and a striking long-term buildup of HSCs which becomes more pronounced after serial transplantations[186,187]. Combined deletion shows an even more pronounced effect. DNMT3A mutations are common in hematopoietic malignancy, as will be described in Chapter 2. TET enzymes serve an opposing function to DNMTs, converting 5-methylcytosine into 5-hydroxymethylcytosine (5hMC). 5hMC serves as a distinct epigenetic marker and tends to result in demethylation[188]. TET2 is the only TET enzyme expressed in HSCs, and conditional deletion of TET2 leads to enhanced HSC self-renewal and competitive repopulation but also to extensive myeloproliferation and development of malignancy[189]. In principle, epigenetic modifications are more readily reversible than DNA mutations. Because of this, epigenetic disruptions have emerged as promising targets for therapies to reverse defective or malignant hematopoiesis.

Chapter 2 – Introduction – Leukemia and Hematopoietic Malignancy

Section 2.1 – Classification and overview of blood malignancies

2.1.1 Introduction

Stem cells are essential to the function of multicellular organisms, which exist as vast multicellular complexes with a constant balance of cellular generation and death. However, the essential stem cell properties of self-renewal and multipotency can be co-opted and manipulated when a cell undergoes changes due to genetic mutation or epigenetic dysregulation, which can lead to malignancy. Most often, stem or progenitor cells are the culprits underlying oncogenesis, typically through enhancement of self-renewal and a block in differentiation. As a result, many of the genes required for stem cell maintenance are also mutated in cancer. The hematopoietic system is no exception – most malignancies develop from oncogenic changes in either the HSPC compartment or the early committed progenitor pool.

Proper classification of hematological malignancies is essential in order to provide optimal treatment for leukemic patients. Many forms of leukemia appear clinically similar but nonetheless have vastly different molecular properties and optimal treatments. The number of leukemic classifications continues to expand as investigators uncover different genetic and molecular distinctions underpinning malignancy. A coordinated worldwide attempt to develop a classification system of hematologic malignancy resulted in the World Health Organization (WHO) classification system[190]. Broadly, the criteria used to provide these definitions include clinical features, genetic abnormalities, morphology, and immune or cell surface phenotype. Techniques frequently employed to classify a malignancy include stained peripheral blood smears, bone marrow core biopsy or aspirate, immune phenotyping, genetic sequencing, and single-nucleotide polymorphism (SNP) analysis. A brief introduction to the types of hematologic malignancies is presented in this section.

2.1.2 Myeloproliferative Neoplasms (MPN) and Chronic Myelogenous Leukemia (CML)

Myeloid neoplasms are broadly classified by the WHO as either acute myeloid leukemia (AML), myeloproliferative neoplasms (MPNs), myelodysplastic syndromes (MDS), or those falling in between, termed MDS/MPN or "overlap" syndromes[191]. A recent update to these definitions creates additional smaller subsets, but the overall structure remains intact[192].

MPNs are a group of proliferative neoplasms resulting primarily from transformations of the early HSPC compartment. These disorders cause an increase of myeloid cells in the blood, with various symptoms depending on which cells are hyperproliferative. The best studied of the MPNs is chronic myelogenous leukemia (CML), which is characterized by an accumulation of myeloid cells, predominantly granulocytes and their precursors, in the bone marrow and blood. CML is strongly associated with one genomic aberration – essentially all cases of CML are associated with a t(9;22)(q34;q11.2) translocation leading to a fusion of the BCR and ABL1 tyrosine kinase genes[193]. This was the first cancer-associated genetic abnormality to be discovered, in 1960, termed the Philadelphia (Ph) chromosome[194]. It most commonly afflicts adults, and the Ph rearrangement is believed to take place in a multipotent HSPC, because the aberration is found in nearly all mature blood cells[195]. The chromosomal breakpoint in BCR can occur at three distinct locations, yielding three chimeric protein variants – they include the most common $P210^{BCR\text{-}ABL1}$, classically associated with CML; a smaller $P190^{BCR\text{-}ABL1}$ variant, occurring in cases of acute leukocytic leukemia (ALL); and a rare, larger $P230^{BCR\text{-}ABL1}$ variant found in chronic neutrophilic leukemia[196,197]. CML begins in a chronic phase, characterized by an expansion of myeloid cells within the peripheral blood and a slight expansion of immature malignant progenitors (blast cells) in the bone marrow. The disease then progresses to an accelerated phase, in which myeloblasts begin to expand and symptoms worsen[198]. Lastly, CML progresses to blast crisis phase, which resembles acute leukemia with a high proportion of blast cells in the bone marrow and blood, and a rapid progression of symptoms and short period of survival. Treatment of CML has been dramatically improved by the development of

imatinib, a selective tyrosine kinase inhibitor targeting the BCR-ABL1 fusion gene[199]. With imatinib, patient survival has been significantly extended. Median survival prior was approximately 4 years[200]. Today, 90% of patients survive past 8 years, and often the cause of death is not leukemic progression[201].

Other MPN disorders do not express the BCR-ABL1 oncogene. The most common of these include essential thrombocyhemia (ET), polycythemia vera (PV), and primary myelofibrosis (MF). ET is a chronic disorder with excess platelet production. In cases of the slowly-developing disorder polycythemia vera, there is excess red blood cell production and hypercoagulability[202]. Primary myelofibrosis is a disorder in which signaling from platelets and megakaryocytes leads to overgrowth of fibrous tissue in the bone marrow, extramedullary hematopoiesis, and ultimately bone marrow failure[203].

Common characteristics are shared by ET, PV, MF, and CML. All originate from oncogenically-transformed HSPCs, are chronic in nature and exhibit clonal proliferation. Most notably, these diseases all feature hallmark mutations of tyrosine kinases. Most cases of ET, PV, or MF contain mutations to one of two proteins – the JAK2 non-receptor tyrosine kinase, or the TPO receptor MPL which is a JAK2-activating tyrosine kinase. BCR/ABL1 protein also enhances JAK2/STAT activation, suggesting that this pathway is critical in the pathogenesis of MPNs[204,205]. A subset of MF and ET cases show mutations in calreticulin, which may also relate to tyrosine kinase signaling through calreticulin-mediated stabilization of MPL[206]. The presence of aberrant tyrosine kinase activity in most cases of MPN suggests a common underlying mechanism and provides potential therapeutic targets for Ph^- MPNs.

2.1.3 Myelodysplastic syndromes (MDS) and MPN/MDS "overlap" syndromes

Myelodysplastic syndromes (MDS) differ from MPN in that they exhibit a decrease in one or more mature cell types (cytopenia) leading to ineffective hematopoiesis and symptoms arising from this deficiency. The most common symptom in MDS is anemia resulting from a lowered erythrocyte count. The term "refractory anemia" was used for many years to describe the disease, but WHO reclassification has

eliminated this nomenclature and renamed all cases in this family as MDS, with subsets distinguished based on the number of dysplastic cell types and blast cells present[192]. MDS typically develops in a multi-step process, a result of somatic mutations occurring over a long period of time, leading to clonal expansion of malignant progenitors and abnormalities in maturation and differentiation within these clones. Patients with MDS have an elevated risk (>30%) of developing acute leukemia[207]. MDS is therefore sometimes considered a "pre-leukemic" disorder, although this oversimplification minimizes some important distinctions between AML and MDS, described in Section 2.3. Because of the multi-hit pathogenic development of MDS, it is predominantly found in older patients. By the time of diagnosis, a number of somatic mutations are typically found. Furthermore, there are many chromosomal abnormalities that may be found in MDS, in contrast to MPN. Three specific abnormalities, however, are seen in a larger proportion of MDS patients (>10%) and are classified as specific genetic subsets. They include 5q- or 7q- syndromes – deletions of part of the long arms of chromosomes 5 or 7 – and trisomy 8[208]. In addition to chromosomal changes, somatic mutations are frequently found in MDS patients. The most commonly mutated genes include TET2, SFRB1, RUNX1, ASXL1, SRSF2, P53, U2AF1, RAS, and DMNT3A[208].

Lastly, there are malignancies that show proliferative phenotypes in certain blood lineages but dysplasia in other lineages and signs of ineffective hematopoiesis. These diseases are now classified separately as MDS/MPN or "overlap" neoplasms. The most common MDS/MPN is chronic myelomonocytic leukemia (CMML)[209]. CMML resembles an MPN, with high numbers of circulating monocytes, but also exhibits bone marrow dysplasia not seen in other monocytic MPNs. Genetically, CMML is closely related to MDS, with mutations in TET2, DNMT3A, ASXL1, SRSF2, and RUNX1 commonly found[209]. The possible oncogenic role of these genes will be discussed further in Section 2.3.

2.1.4 Acute Myelogenous Leukemia (AML) overview

AML is the primary focus of Chapter 5 of this thesis, with an investigation of the role of PRDM16 and its two isoforms in this disease. Therefore, a more detailed overview of AML is provided in Section 2.2. AML is distinguished from MDS by the presence of a large number of dysfunctional immature blast cells resembling myeloid precursors. WHO standards require that >20% of nucleated cells in the bone marrow or peripheral blood be blast cells for the diagnosis of AML[192]. Patients with MDS have fewer than 20% blasts, though both AML and MDS can show dysplasia and often cytopenias. Blast cell percentage is considered an indicator of malignant proliferation, higher in AML and lower in MDS. This does, however, illustrate the continuum existing between MDS and AML.

AML incidence increases with age, with a median diagnosis age of 70 years, as opposed to acute lymphoblastic leukemia (ALL), which peaks in younger people. There is a relatively even gender ratio, with males 1.2 times more likely to develop the disease[210].

AML is a genetically heterogeneous disease. Older classifications relied primarily on blast cell morphology, with some blasts resembling undifferentiated HSPCs and others resembling more committed progenitors such as CMPs. This was the French-American-British (FAB) classification first proposed in 1976[211]. Recent findings have suggested that AML can be more precisely defined based on the specific genetic abnormality present. There are several chromosomal abnormalities or karyotipically-normal mutations that can function as driver mutations in AML. These will be described in more detail in Section 2.3.

2.1.5 Lymphoid leukemia and lymphomas

Lymphoid cancers account for the majority of hematologic malignancies in the United States, with an estimated 140,000 cases in 2017 according to the American Cancer Society, compared to only 40,000 myeloid or other non-lymphoid cases. Lymphoid malignancies can be divided into three groups – lymphoma, myeloma, and lymphoid leukemia. Lymphomas are associated with mature lymphocytes,

most commonly B-cells, with a smaller number of T-cell and NK-cell lymphomas[212]. Lymphocytes proliferate and expand massively as part of the immune response, which is rare among mature cells. Furthermore, B-cells and T-cells induce DNA breaks and alter their somatic DNA sequences during maturation[213] as a part of their immune function. This combination of high proliferation and deliberate DNA mutation is unique to lymphocytes, rendering them particularly susceptible to malignancy. The most common tissue affected in lymphoma is the lymph node, where B-cells and T-cells proliferate and undergo somatic mutations. Other tissues often affected include spleen, thymus, and bone marrow.

Lymphoblastic leukemias resemble cases of AML. Acute lymphoblastic leukemia (ALL) manifests as a proliferation of blast cells in the bone marrow with the appearance of immature lymphoid precursors[214]. Blast cells in ALL are typically smaller than myeloblasts. Most cases of ALL are either B-cell or T-cell specific, identifiable by cell surface markers, generally CD19 for B-cells and CD3 for T-cells[215]. Like cases of AML, and in contrast to lymphoma, these disorders are generally caused by malignant transformations of HSPCs.

Section 2.2 – AML in-depth overview

2.2.1 Treatment of AML

AML is an aggressive malignancy, usually associated with a rapid progression of symptoms from the time of diagnosis, often within a few months. Research over the past 30 years has significantly improved outcome for patients under 60, but less so for older patients. For younger patients, the standard treatment procedure is induction chemotherapy, which involves a combination of two strong chemotherapeutic agents administered over seven days – cytarabine on all seven days and an anthracycline such as daunorubicin or idarubicin on only the first three days[216]. This treatment typically destroys most bone marrow and leukemic cells. Biopsies taken a month after treatment are considered successful if blast frequency is <5%. Then begins the consolidation phase of treatment consisting of high dose cytarabine therapy, with the intention of eliminating all blasts and leading to complete remission. For younger patients otherwise in good health with intermediate or high risk cases of AML, this therapy is typically followed by HSPC transplant[216].

Chemotherapy is highly intensive, destroying healthy cells and causing serious side effects. Older people are therefore not ideal candidates for this treatment. They instead receive milder drugs with fewer side effects, with periodical treatment rather than in intense induction and consolidation phases. The development of drugs that could specifically target leukemic cells without side effects would therefore be highly beneficial to older patients. This is currently an active area of research, with some drugs in early clinical trials. Alternately, the potential for targeted immunotherapies using the patient's own immune system to eliminate leukemia is being investigated in both leukemia and solid tumors[217].

2.2.2 Animal models of AML

Primary human AML cells are an invaluable resource for studying leukemia, but important research has also been conducted using mouse models of AML. There are two primary methods used in murine AML

models – introducing mutations or oncogenic genes into mice corresponding to those in human AML, or by directly transplanting human AML cells into recipient mice[218].

As discussed in Section 2.3, the WHO classification system categorizes AML based on the primary "driver mutations" underlying the disease. Some of these aberrations are fusion proteins formed by chromosomal translocation and others are mutations of certain genes in karyotypically-normal cells. Expression of oncogenic genes in mouse cells is possible using retroviral expression systems, which introduce permanent alterations to DNA. Examples of leukemic models developed using this system include BCR-ABL, MOZ-TIF2[219], PML/RARα[220], NUP98-HOXA9[221], and AML1-ETO (corresponding to human RUNX1-RUNX1T1)[222]. Importantly for this thesis, retroviral models also exist for MLL-rearranged leukemias, which comprise approximately 10% of AML. MLL-AF9 is the most common MLL fusion protein, and the MLL-AF9 mouse model is used extensively in leukemic research[223]. Retroviral transduction of HSCs with MLL-AF9 immortalizes the cells, allowing for expansion *in vitro* in the presence of SCF, IL-6, and IL-3. When transplanted into irradiated recipient mice, blasts accumulate in the bone marrow and spread to other hematopoietic tissues, leading to symptoms mirroring AML. Survival is approximately 60-70 days. MLL-AF9 transduction of MPPs or CMPs also leads to immortalization and leukemogenesis, though with an increased latency compared to HSC-transformed cells[224]. Certain oncogenic fusions, such as BCR-ABL, can only transduce HSCs, which may offer insight into malignant mechanisms of different driver oncogenes[225]. Murine models also exist for commonly mutated AML genes, including FLT3-ITD and NPM1[226]. Some of these models recapitulate AML differently than in the human disease. For example, mice transplanted with FLT3-ITD-expressing cells develop a malignancy more closely resembling MDS, although leukemic latency is similar to other AML models[227].

Xenotransplantation of primary human AML cells into immunodeficient mice is another technique used to model human AML. This has both benefits and limitations compared to retroviral oncogene models. The downside of this technique is that the leukemic phenotype is incomplete. Recipient mice typically

present some characteristics of AML, including organ infiltration and blast cell proliferation. However, they do not usually develop a lethal disease or show significant leukocytosis within the blood[228]. Furthermore, they require human cytokines (IL-3, SCF, GM-CSF) for survival, making experiments more challenging than retroviral models. However, these studies have yielded important insight into the nature of leukemic stem cells, a topic that will be discussed in the next section[229].

2.2.3 Leukemic stem cells

The existence of cancer stem cells was first demonstrated for human AML, and the currently accepted model is that leukemia organizes itself in a hierarchical manner akin to normal hematopoiesis, with a malignant version of an HSC termed a leukemic stem cell (LSC) which sustains the blast population through self-renewal and limited differentiation (diagram in **Figure 2-1**). LSCs have been defined similarly to HSCs – they are cells capable of completely reconstituting AML and generating downstream leukemic blasts[230]. The LSC model has significant clinical implications, suggesting that the destruction of LSCs would be necessary and sufficient to cure leukemia, and that elimination of only blasts will not cure the disease as any remaining LSCs will eventually regenerate leukemia in the patient.

Early xenotransplantation studies using human AML cells demonstrated that there were cells capable of LSC activity. Virtually all LSCs were found in the $CD34^+CD38^-$ population, with a much lower frequency in the double positive population[229]. One exception has been observed in karyotypically normal, NPM1-mutated AML where there is a significant subset of $CD34^-$ LSCs[231]. Further refinement of LSC experiments has elucidated two LSC subtypes that may exist in AML patients. One resembles a more primitive MPP ($Lin^-CD34^+CD38^-CD90^-CD45RA^+$) and another more closely resembles a committed myeloid precursor ($Lin^-CD34^+CD38^+CD123^+CD45RA^+$)[232]. Patients with a high frequency of $CD34^+CD38^-$ cells, or frequency of calculated LSCs in xenotransplantation experiments, have a worse prognosis and shorter overall survival, confirming the clinical significance of LSCs[233,234].

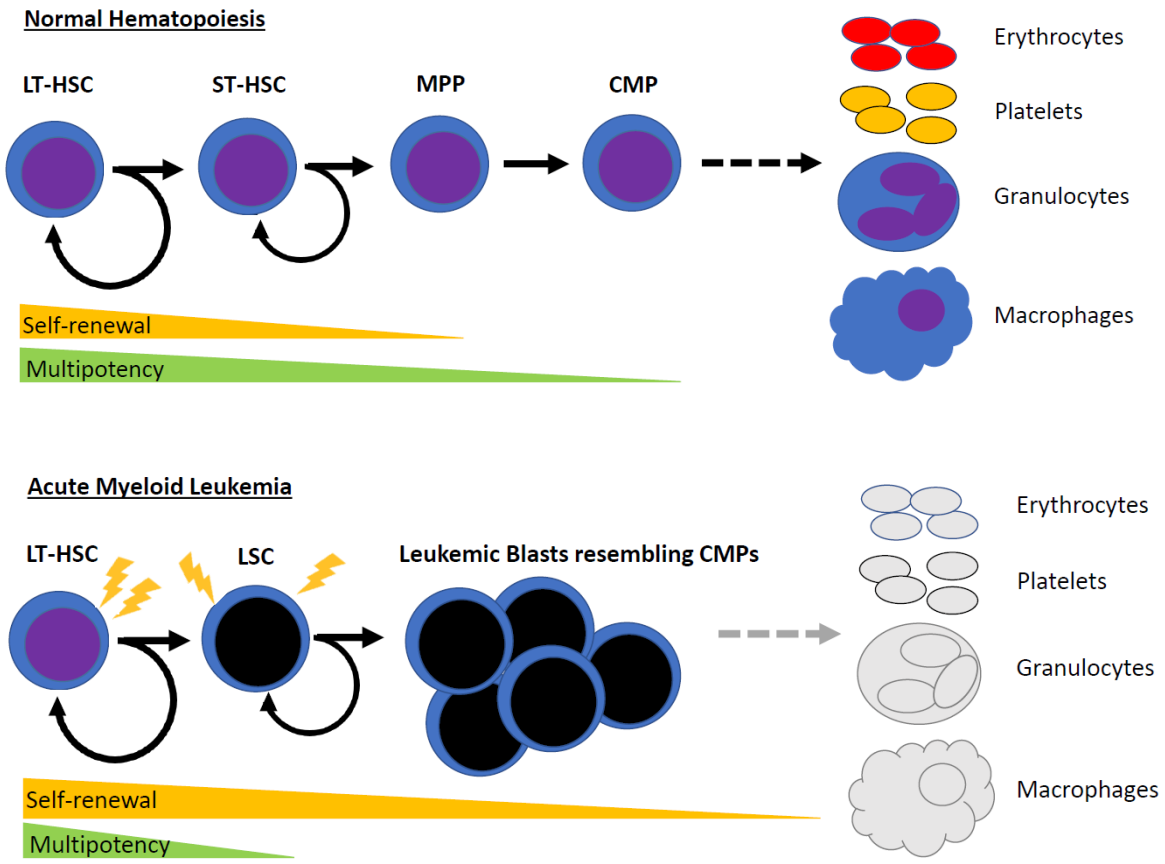

Figure 2-1: Leukemic stem cell model in AML. In normal hematopoiesis, HSCs differentiate into downstream progenitors with progressively lower self-renewal potential and multipotency, resulting in mature cell production. In acute myeloid leukemia, HSCs or other progenitors undergo mutations, epigenetic alterations, or chromosomal translocations which cause enhanced self-renewal capability and a block in differentiation resulting in a decrease in multipotency. The bone marrow compartment begins to fill with blast cells resembling myeloid progenitors (CMPs or GMPs) but with little or no capacity to differentiate into mature cells. This loss of mature cell production is responsible for the symptoms observed in AML.

Different methods have been proposed to specifically target and eliminate LSCs, which would represent a major step forward in AML treatment. LSCs could be targeted with cytotoxic antibodies if they exhibited a specific surface expression pattern. In humans, CD123[235], CD47[236,237], TIM3[238], and IL1RAP[239] are overexpressed in LSCs relative to healthy HSPCs and may serve as potential targets. LSCs also have a distinct biology from HSCs, and therefore targeting intracellular pathways inherent to LSCs could eliminate them, leaving healthy progenitors intact. The proinflammatory NF-kB pathway is upregulated in $CD34^+$

AML cells compared to $CD34^+$ HSCs and is important for their survival, as inhibition of NF-kB activity by preventing degradation of IkB inhibitors causes cell death in LSCs with no effect on HSCs[240]. LSCs also have significantly altered epigenetics, possibly a result of mutated epigenetic regulators including TET2, MLL, and DNMT3A, described in Section 2.3. These changes may induce leukemogenesis by blocking normal differentiation and enhancing self-renewal[241]. Inhibition of BRD4, a "reader" of modified histones, promotes terminal differentiation of AML cells and reduces leukemic burden in mouse models of AML[242]. Lastly, another aspect of LSC biology believed to be important for their survival is the maintenance of low reactive oxygen species (ROS) levels. LSCs have high expression of the anti-apoptotic BCL-2 protein and require its expression for their survival. Inhibition of BCL-2 elevates oxidative phosphorylation and ROS levels in LSCs, leading to cell death[243,244]. These pathways illustrate some of the important differences between LSCs and normal HSPCs which may serve as promising targets in future AML therapies.

Section 2.3 – Pathobiology of AML and MDS

2.3.1 Chromosomal rearrangements in AML

The current WHO classification of AML focuses on the underlying genetic abnormality. Approximately half of AML patients have gross chromosomal changes visible at the karyotypic level[245]. These include deletions or extra copies of chromosomes, translocations between two chromosomes, or inversions within one chromosome. A brief description of some of the most common chromosomal abnormalities, and their potential mechanism of action and prognosis, is described below.

Chromosomal rearrangements involving the mixed-lineage leukemia (MLL) gene at 11q23 are among the most common, occurring in 10% of AML patients and associated with a poor prognosis. MLL rearrangements are the most common subtype found in therapy-related AML (t-AML)[246]. The N-terminus of MLL contains a DNA-binding domain which normally controls expression of HOX genes and others important for HSC maintenance and differentiation. In MLL rearrangements, the C-terminus of MLL is replaced by the C-terminus of one of over 70 different binding partners, the most common of which are AF9, AF4, ENL, and AF10[245]. Most MLL binding partners comprise part of the super elongation complex, which interacts with the H3K79 methyltransferase DOT1L and alters the expression of MLL target genes[247]. Thus, MLL-rearrangements result in upregulation of HOX genes and blockage of differentiation while enhancing self-renewal. A small subset of AML cases contains a partial tandem duplication of MLL exons 5-12 (MLL-PTD), with a similar phenotype as MLL-rearranged AML[248]. MLL rearrangements are particularly important for this project as we employ the MLL-AF9 mouse model for our studies.

Another commonly occurring rearrangement in AML occurs within the RUNX1 gene. RUNX1 rearrangements also comprise approximately 10% of AML cases. The most common of these is the t(8;21) rearrangement, which generates a RUNX1-RUNX1T1 fusion protein, equivalently known as AML1-ETO. Less common C-terminal partners for RUNX1 include MGT16 and the PR proteins EVI1 and PRDM16[249].

These fusions alter the core binding factor (CBF) transcription factor complex, impacting its oligomerization and impairing interaction with the corepressors SMRT and N-CoR, which are important for hematopoietic differentiation[250]. A related leukemic rearrangement in another CBF complex gene is inv(16), which generates a CBFB-MYH11 fusion protein. This AML subset has similar mechanistic and prognostic characteristics to RUNX1, albeit with different blast cell morphology[251]. In comparison to MLL-rearranged leukemias, RUNX1 and CBFB fusions are associated with a relatively favorable outcome after high-dose cytarabine treatment regimens. Highly aggressive treatments such as HSCT are therefore not often recommended in these cases.

Rearrangements of the retinoic acid receptor genes comprise the third large subset of chromosomal AML aberrations, again accounting for approximately 10% of cases. Most commonly found as t(15;17) rearrangements with a PML-RARα fusion, this AML subtype causes a unique malignancy known as acute promyelocytic leukemia (APL)[252]. APL has a distinct treatment regimen, as cells are highly responsive to all-trans retinoic acid (ATRA). The PML-RARα fusion protein is a potent transcriptional repressor of differentiation and induces an accumulation of blasts resembling promyelocytic granulocyte precursors. In the presence of ATRA, however, this gene reverses function, becoming a transcriptional activator and causing differentiation, eliminating the leukemia.

There many other less common gene fusions with distinct oncogenic mechanisms. The NUP214 protein is a member of the nuclear pore complex which regulates nuclear transport. In approximately 1% of adult AML, its C-terminus is fused to the N-terminus of the DEK oncogene, leading to leukemia with poor prognosis[253]. Of interest to our project, the RPN1-EVI1 fusion, generated from a inv(3) rearrangement, translocates the enhancer of RPN1 upstream of EVI1, leading to EVI1 overexpression. It is found in approximately 3% of AML patients and causes a distinct hypermethylation signature[254]. Notably, this leukemia often presents with features of MDS and shows a unique bone marrow morphology with multilineage dysplasia and abnormal megakaryocytes[254,255].

2.3.2 Genes commonly mutated or aberrantly expressed in AML

Chromosomal rearrangements and their resulting fusion proteins account for approximately half of AML cases. The rest are classified as karyotypically normal. In these cases, the primary drivers of leukemogenesis are mutations or aberrant expression of oncogenes with no chromosomal abnormalities present. These leukemias are typically diagnosed with an "intermediate" prognosis. This subset is nonetheless highly heterogenous, with very different outcomes depending on the specific genes altered and number of mutations present. The typical AML patient has fewer than 20 somatic mutations within their AML cells, less than in many solid cancers[256]. Some of these are present in a much higher frequency than would be expected by chance and considered to be oncogenic mutations. These genes, and their possible mechanisms of action, are described in this section.

The most common mutation encountered in karyotypically-normal AML occurs in the nucleophosmin (NPM1) gene. Most often, the mutation observed is a 4bp frameshifting TCTG insertion within exon 12, although other frameshifts in exon 12 can occur and exhibit a similar phenotype[257]. NPM1 is a nuclear molecular chaperone involved in ribosome assembly and the prevention of nuclear protein aggregation. NPM1 mutations associated with AML result in a cytosolic form of the protein with altered function, termed NPM1c. Most cases of NPM1-mutated AML show similar phenotypes, namely downregulation of CD34, upregulation of HOX cluster genes, and morphological similarities[258]. Mouse models of mutated NPM1 expressed in HSPCs exhibit enhanced self-renewal, expanded myelopoiesis, and HOX upregulation, though recipient mice do not typically develop AML[259]. This, and the fact that most NPM1-mutated leukemias occur alongside other secondary mutations, suggests that NPM1 mutation primes cells for oncogenesis without directly inducing malignancy. Nonetheless, NPM1-mutated leukemias are the most common AML subset, representing approximately 30% of AML cases and having an intermediate prognosis.

FLT3 is the other mutation found with a very high frequency in leukemia, occurring in approximately 40% of AML patients. Often, the mutation present in FLT3 is an in-frame internal tandem duplication (FLT3-ITD) in the membrane-spanning region, although mutations within the tyrosine kinase domain (FLT3-TKD) also occur, with similar phenotypes. FLT3 mutations in the background of other oncogenic fusions generally cause a worse patient prognosis and higher relapse rate. Moreover, FLT3-ITD shows synergistic effects in mouse models of AML, decreasing latency of AML progression in recipient mice[260-264]. On its own, FLT3-ITD expressed in mice causes a myeloproliferative disease resembling ET[265]. Activation of STAT5 is one important mechanism by which FLT3-ITD promotes oncogenesis[266,267]. Other less commonly mutated signaling genes in AML include cKit (CD117) and RAS, either NRAS or KRAS, which are mutated in approximately 5% of AML.

2.3.3 Epigenetic contribution to AML pathogenesis

Genes involved in epigenetic regulation are also commonly mutated in AML. Of these genes, DNMT3A (mutated in 22% of AML patients), ASXL1 (20%), IDH1/2 (17%), and TET2 (in 14%) occur most often. Epigenetics are now understood to play important oncogenic roles. This has been proposed, as human cancers exhibit altered DNA methylation compared to normal cells[268]. DNMT3A mutations likely function as early events in the AML oncogenesis. In AML patients with concurrent NPM1 and DNMT3A mutations, the HSC population contains a subset of DNMT3A mutants with unmutated NPM1, with a repopulation advantage over normal HSCs. These cells were labeled “pre-leukemic” HSCs and implicated DNMT3A mutations in the early stages of leukemogenesis[269]. Advances in whole genome sequencing have revealed somatic mutations in leukemic cells, aged HSCs, and MDS and have illuminated some of the genes involved in the progression of HSCs into LSCs. These studies have reinforced the significance of epigenetics in AML progression and elucidated the relationship between MDS and AML. DNMT3A ablation causes an increase in self-renewal and myeloproliferation ultimately resulting in a lethal MDS/MPN[270]. DNMT3A therefore functions to limit self-renewal and prevent myeloid progenitor expansion. Another gene with a similar

phenotype is ASXL1, commonly mutated in AML and MDS. Hematopoietic deletion of ASXL1 causes an MDS-like disease with shortened latency upon serial transplantation[184]. ASXL1 mediates PRC2-mediated H3K27 trimethylation, again demonstrating the importance of epigenetics in self-renewal, differentiation and the prevention of malignant transformation[271].

An estimated 45% of AML patients have mutations in at least one gene related to DNA methylation, and in addition to DNMT3A another commonly mutated set of genes include isocitrate dehydrogenase 1 and 2 (IDH1/IDH2) and TET2[272]. IDH mutations in AML are gain-of-function mutations occurring at either R132 in IDH1 or R140/R172 in IDH2[273]. These mutants gain the ability to reduce α-ketoglutarate (α-KG) into 2-hydroxyglutarate (2HG), an α-KG inhibitor[274,275]. TET2 utilizes α-KG to hydroxylate 5-methylcytosine residues in DNA[276]. Loss-of-function TET2 mutations have a similar epigenetic signature and non-overlapping incidence with IDH mutations in AML, suggesting a common mechanism[277]. Because of this, hypomethylating agents are currently being considered for therapeutic potential, specifically in patients with mutations in these genes. Furthermore, inhibition of oncogenic mutant proteins may represent a targeted approach to reverse the epigenetic dysregulation found in myeloid malignancies, and potential drugs have been identified, primarily inhibitors of mutant IDH[278-281].

2.3.4 Role of inflammation in MDS/AML pathogenesis

Growing evidence points to the importance of inflammatory signaling in HSC progression into preleukemic stem cells and myeloid oncogenesis[282]. This is of particular importance to this thesis, as the short isoform of PRDM16 initiates inflammatory gene expression, as will be described in Chapter 5. Inflammation may involve external signals received from the microenvironment or internal signaling within HSPCs.

TNF-α is a potent inflammatory protein that activates the NF-kB pathway. Excessive TNF-α signaling is associated with worse prognosis in MDS, increased apoptosis and bone marrow failure[283], suggesting that TNF activity may impair normal hematopoiesis and promote leukemogenesis. Impairment of NF-kB

signaling suppresses MLL-dependent AML progression, lending further support to this hypothesis[284]. IL-1β is a proinflammatory cytokine with elevated expression in MPNs, CML, and certain subsets of AML, which is associated with poor prognosis[285-287]. Correlation of IL1 receptor accessory protein (IL1RAP), which mediates IL1 and IL33 responses, with poor prognosis in some AML subsets[288], as well as an inhibitory effect of IL1R antagonist (IL1Ra) on AML blast growth[289] lend further support to the notion that IL1-mediated inflammatory signaling can contribute to AML progression. Furthermore, a number of secreted cytokines are associated with worse prognosis in AML or MDS, including VEGF[290], HGF[291], and the alarmin proteins S100A8 and S100A9[272,292]. Though the role of inflammatory signaling in AML progression is still being investigated, recent work suggests that AML cells may use inflammatory signaling to remodel the bone marrow compartment to suppress normal hematopoiesis and make the environment more favorable for leukemic development[293].

Parallels may exist between inflammatory signaling in AML and aging. A chronic inflammatory state is associated with a number of aged tissues, and be involved in some age-related diseases[294]. Furthermore, aged individuals acquire an increasing number of somatic mutations in the HSPC compartment, leading to clonal hematopoiesis and myeloproliferation as described in 1.1.2. Many “first-hit” epigenetic modifiers associated with pre-leukemic cells, including TET2, DNMT3A, and ASXL1 are associated with cases of MDS[295]. Recent studies suggest that disruption of these proteins leads to increased inflammatory signaling through either IL-1β, IL-6, or inflammasome activation[296-298]. A link between some of the most commonly-mutated MDS and AML genes with inflammation underscores the potential significance of inflammatory signaling to both HSC aging and myeloid malignancy.

Chapter 3 – The Physiological and Malignant Roles of PRDM16

Section 3.1 – Introduction to PRDM16 and the PRDM family

3.1.1 The PRDM family

The PRDI-BF1 and RIZ1 homology domain containing (PRDM) family consists of a conserved set of 16 genes between mouse and human (PRDM 1-16) and an additional putative gene in humans, ZF408 or PRDM17[299]. All PRDM proteins share two common structural characteristics – C-terminal DNA-binding Zn-finger domains, and an N-terminal PR domain with high homology to the SET domain of histone methyltransferases found in *Drosophila* Trithorax and its mammalian homologs MLL, EZH, and EHMT[300]. A third characteristic common to the PRDM family is the existence of two protein isoforms – a full-length isoform and a short-length isoform lacking the N-terminal PR domain. Despite a significant similarity to the SET domain, only a few PRDM family proteins have been definitively shown to have catalytically-active histone methyltransferase activity – namely PRDM2, PRDM8, and PRDM9[301-303]. PRDM16 has been purported to possess either H3K9 or H3K4 methyltransferase ability, raising questions as to which of these is accurate. Instead, most PRDM family members exert their functions by recruiting other histone-modifying and transcription factors. The list of proteins known to be recruited by PRDM family members includes HMTs, histone deacetylases (HDACs), protein methyltransferases Prmt5, p300/CBP, and Lsd1, as well as co-repressors such as CtBP[304].

PRDM family members are extensively involved in development, and the role of PRDM proteins as stem cell regulators remains an active field of research. Nearly all PRDM family members are expressed in at least one site of embryonic development. PRDM proteins with prominent developmental roles include PRDM1, PRDM3, PRDM8, PRDM14 and PRDM16, which are expressed in multiple embryonic tissues and cause developmental defects when deleted. PRDM proteins play distinct and non-redundant developmental roles. PRDM1 is involved in retinal development and specification of B-cell and T-cell

lineages[305-307]. PRDM14 plays an essential role in development of pluripotent primordial germ cells (PGCs) which differentiate into oocytes and spermatozoa gamete cells[308]. PRDM9 marks hotspots of recombination during meiosis. Progression though meiotic prophase is disrupted in mice lacking PRDM9[309]. PRDM6 is a regulator of vascular smooth muscle differentiation[310]. PRDM3/EVI1 is essential for the maintenance of quiescent long-term HSCs[165], and PRDM16, as described in 3.1.3 and 3.2.2, plays critical roles in both brown fat differentiation and HSC maintenance, among other developmental roles.

Unsurprisingly, given that PRDM family members regulate stem cells and tissue development, many PRDM family members are associated with mutations or deletions in cancer. In multiple instances, oncogenic chromosomal rearrangements cause deletion of the PR domain, leading to the hypothesis that the two PRDM isoforms may play opposite roles in malignancy, with the full-length isoform suppressing oncogenesis and the short form functioning as an oncogene[311]. It is unclear what function of the PR domain may confer opposing oncogenic characteristics to full-length and short-length PRDM isoforms. It may plausibly be methyltransferase activity of the PR domain, but this appears unlikely as most PRDM proteins do not have proven methyltransferase activity. The PR domain lacks the most conserved H/RxxNHxC motif thought to be essential for enzymatic activity in the SET domain[312]. Alternatively, the PR domain may mediate specific protein-protein interactions which are therefore unavailable in short PRDM isoforms. Further investigation of this topic is warranted and provides one of the bases on which this project was undertaken.

3.1.2 Basic PRDM16 biology

PRDM16 is a member of the PRDM family of proteins, and the central focus of this research project. Like other members of the PRDM family it contains an N-terminal PR domain, suggested in conflicting reports to possess either H3K9me1 or H3K4 methyltransferase activity[313,314]. Human PRDM16 is found on chromosome 1p36, encoding a protein with 1257 amino acids across 17 exons. The 1073aa short isoform

of the protein (s-Prdm16) contains a translational start codon at ATG597 within exon 4. Mouse Prdm16 is located on the reverse strand of chromosome 4qE2, encoding a highly homologous protein to human PRDM16, with similar size, domain structure, and full/short isoform distinction[299]. Mouse/human and full/short sequences and domain structures are illustrated in **Figure 3-1**. Full and short PRDM16 isoforms in both mouse and human contain 10 zinc-finger DNA binding domains, localized in two clusters on opposite ends of the protein (ZF1 and ZF2), a proline-rich repressor domain, C-terminal acidic activation domain and two CtBP-binding domains. Among PRDM family proteins, PRDM16 is most closely related to PRDM3, also known as MECOM, sharing approximately 60% amino acid identity and a nearly identical domain structure[164]. The short isoform of PRDM3 is named separately from the MECOM/PRDM3 nomenclature, referred to as EVI1.

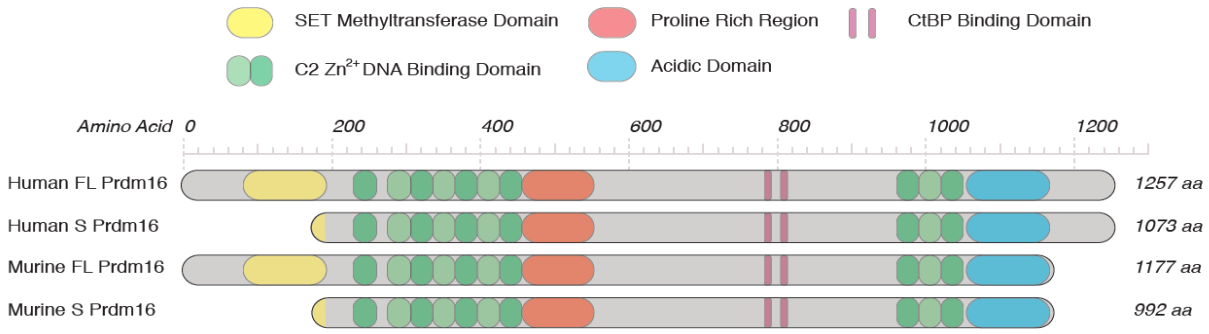


```
HsFPRDM16       MRSKARARKLAKSDGDVVNNMYEPNRDLLASHSAEDEAEDSAMSPIPVGPPSPFPTSEDFTPKEGSPYEAPVYIPEDIPIPADFELRESSIPGAGLGVWA 100
MsFPRDM16       MRSKARARKLAKSDGDVVNNMYEPDPDLLAGQSAEEETEDGILSPIPMGPPSPFPTSEDFTPKEGSPYEAPVYIPEDIPIPPDFELRESSIPGAGLGIWA 100
HsSPRDM16       ------------------------------------------------------------------------------------------------------ 0
MsSPRDM16       ------------------------------------------------------------------------------------------------------ 0

HsFPRDM16       KRKMEAGERLGPCVVVPRAAAKETDFGWEQILTDVEVSPQEGCITKI-SEDLGSEKFCVDANQAGAGSWLKYIRVACSCDDQNLTMCQISEQIYYKVIKD 199
MsFPRDM16       KRKMEIGERFGPYVVTPRAALKEADFGWEQMLTDTEVSSQESCIKKQISEDLGSEKFCVDANQAGSGSWLKYIRVACSCDDQNLAMCQINEQIYYKVIKD 200
HsSPRDM16       ----------------------------------------------------------------------------MCQISEQIYYKVIKD 15
MsSPRDM16       ----------------------------------------------------------------------------MCQINEQIYYKVIKD 15
                                                                                               ****.********** 

HsFPRDM16       IEPGEELLVHVKEGVYPLGTVPPGLDEEPTFRCDECDELFQSKLDLRRHKKYTCGSVGAALYEGLAEELKPEGLGGG-SGQAHECKDCERMFPNKYSLEQ 298
MsFPRDM16       IEPGEELLVHVKEGAYSLGVMAPSLDEDPTFRCDECDELFQCRLDLRRHKKYACSSAGAQLYEGLGEELKPEGLGVGSDGQAHECKDCERMFPNKYSLEQ 300
HsSPRDM16       IEPGEELLVHVKEGVYPLGTVPPGLDEEPTFRCDECDELFQSKLDLRRHKKYTCGSVGAALYEGLAEELKPEGLGGG-SGQAHECKDCERMFPNKYSLEQ 114
MsSPRDM16       IEPGEELLVHVKEGAYSLGVMAPSLDEDPTFRCDECDELFQCRLDLRRHKKYACSSAGAQLYEGLGEELKPEGLGVGSDGQAHECKDCERMFPNKYSLEQ 115
                ************.*.**.:.*.***:***********.:*********:*.*.** *****.******** * .********************* 

HsFPRDM16       HMVIHTEEREYKCDQCPKAFNWKSNLIRHQMSHDSGKRFECENCVKVFTDPSNLQRHIRSQHVGARAHACPDCGKTFATSSGLKQHKHIHSTVKPFICEV 398
MsFPRDM16       HMIVHTEEREYKCDQCPKAFNWKSNLIRHQMSHDSGKRFECENCVKVFTDPSNLQRHIRSQHVGARAHACPDCGKTFATSSGLKQHKHIHSTVKPFICEV 400
HsSPRDM16       HMVIHTEEREYKCDQCPKAFNWKSNLIRHQMSHDSGKRFECENCVKVFTDPSNLQRHIRSQHVGARAHACPDCGKTFATSSGLKQHKHIHSTVKPFICEV 214
MsSPRDM16       HMIVHTEEREYKCDQCPKAFNWKSNLIRHQMSHDSGKRFECENCVKVFTDPSNLQRHIRSQHVGARAHACPDCGKTFATSSGLKQHKHIHSTVKPFICEV 215
                **::********************************************************************************************** 

HsFPRDM16       CHKSYTQFSNLCRHKRMHADCRTQIKCKDCGQMFSTTSSLNKHRRFCEGKNHYTPGGIFAPGLPLTPSPMMDKAKPSPSLNHASLGFNEYFPSRPHPGSL 498
MsFPRDM16       CHKSYTQFSNLCRHKRMHADCRTQIKCKDCGQMFSTTSSLNKHRRFCEGKNHYTPGSIFTPGLPLTPSPMMDKTKPSPTLNHGGLGFSEYFPSRPHPGSL 500
HsSPRDM16       CHKSYTQFSNLCRHKRMHADCRTQIKCKDCGQMFSTTSSLNKHRRFCEGKNHYTPGGIFAPGLPLTPSPMMDKAKPSPSLNHASLGFNEYFPSRPHPGSL 314
MsSPRDM16       CHKSYTQFSNLCRHKRMHADCRTQIKCKDCGQMFSTTSSLNKHRRFCEGKNHYTPGSIFTPGLPLTPSPMMDKTKPSPTLNHGGLGFSEYFPSRPHPGSL 315
                ************************************************.**:*************:****:***..***.************ 

HsFPRDM16       PFSTAPPTFPALTPGFPGIFPPSLYPRPPLLPPTSLLKSPLNHTQDAKLPSPLGNPALPLVSAVSNSSQGTTAAAGPEEKFESRLEDSCVEKLKTRSSDM 598
MsFPRDM16       PFSAAPPAFPALTPGFPGIFPPSLYPRPPLLPPTPLLKSPLNHAQDAKLPSPLGNPALPLVSAVSNSSQGATAATGSEEKFDGRLEDAYAEKVKNRSPDM 600
HsSPRDM16       PFSTAPPTFPALTPGFPGIFPPSLYPRPPLLPPTSLLKSPLNHTQDAKLPSPLGNPALPLVSAVSNSSQGTTAAAGPEEKFESRLEDSCVEKLKTRSSDM 414
MsSPRDM16       PFSAAPPAFPALTPGFPGIFPPSLYPRPPLLPPTPLLKSPLNHAQDAKLPSPLGNPALPLVSAVSNSSQGATAATGSEEKFDGRLEDAYAEKVKNRSPDM 415
                ***:***:************************.********:************************:***:*.****:.****: .**:*.**.** 

HsFPRDM16       SDGSDFEDVNTTTGTDLDTTTGTGSDLDSDVDSDPDKDKGKGKSAEGQPKFGGGLAPPGAPNSVAEVPVFYSQHSFFPPPDEQLLTATGAAGDSIKAIAS 698
MsFPRDM16       SDGSDFEDINTTTGTDLDTTTGTGSDLDSDLDSDRDKGKDKGKPVESKPEFGGASVPPGAMNSVAEVPAFYSQHSFFPPPEEQLLTASGAAGDSIKAIAS 700
HsSPRDM16       SDGSDFEDVNTTTGTDLDTTTGTGSDLDSDVDSDPDKDKGKGKSAEGQPKFGGGLAPPGAPNSVAEVPVFYSQHSFFPPPDEQLLTATGAAGDSIKAIAS 514
MsSPRDM16       SDGSDFEDINTTTGTDLDTTTGTGSDLDSDLDSDRDKGKDKGKPVESKPEFGGASVPPGAMNSVAEVPAFYSQHSFFPPPEEQLLTASGAAGDSIKAIAS 515
                ********:********************:*** **.*.***..*.:*:***. .**** *******.**********:******:*********** 

HsFPRDM16       IAEKYFGPGFMGMQEKKLGSLPYHSAFPFQFLPNFPHSLYPFTDRALAHNLLVKAEPKSPRDALKVGGPSAECPFDLTTKPKDVKPILPMPKGPSAPASG 798
MsFPRDM16       IAEKYFGPGFMSMQEKKLGSLPYHSVFPFQFLPNFPHSLYPFTDRALAHNLLVKAEPKSPRDALKVGGPSAECPFDLTTKPKEAKPALLAPKVPLIPSSG 800
HsSPRDM16       IAEKYFGPGFMGMQEKKLGSLPYHSAFPFQFLPNFPHSLYPFTDRALAHNLLVKAEPKSPRDALKVGGPSAECPFDLTTKPKDVKPILPMPKGPSAPASG 614
MsSPRDM16       IAEKYFGPGFMSMQEKKLGSLPYHSVFPFQFLPNFPHSLYPFTDRALAHNLLVKAEPKSPRDALKVGGPSAECPFDLTTKPKEAKPALLAPKVPLIPSSG 615
                **********.*************.************************************************************:.** *  ** *  *:** 

HsFPRDM16       EEQPLDLSIGSRARASQNGGGREPRKNHVYGERKLGAGEGLPQVCPARMPQQPPLHYAKPSPFFMDPIYSRVEKRKVTDPVGALKEKYLRPSPLLFHPQM 898
MsFPRDM16       EEQPLDLSIGSRARASQNGGGREPRKNHVYGERKPGVSEGLPKVCPAQLPQQPSLHYAKPSPFFMDPIY-RVEKRKVADPVGVLKEKYLRPSPLLFHPQM 899
HsSPRDM16       EEQPLDLSIGSRARASQNGGGREPRKNHVYGERKLGAGEGLPQVCPARMPQQPPLHYAKPSPFFMDPIYSRVEKRKVTDPVGALKEKYLRPSPLLFHPQM 714
MsSPRDM16       EEQPLDLSIGSRARASQNGGGREPRKNHVYGERKPGVSEGLPKVCPAQLPQQPSLHYAKPSPFFMDPIY-RVEKRKVADPVGVLKEKYLRPSPLLFHPQM 714
                ********************************* *..****:****::****.************** *******:****.**************** 

HsFPRDM16       SAIETMTEKLESFAAMKADSGSSLQPLPHHPFNFRSPPPTLSDPILRKGKERYTCRYCGKIFPRSANLTRHLRTHTGEQPYRCKYCDRSFSISSNLQRHV 998
MsFPRDM16       SAIETMTEKLESFAAMKADSGSSLQPLPHHPFNFRSPPPTLSDPILRKGKERYTCRYCGKIFPRSANLTRHLRTHTGEQPYRCKYCDRSFSISSNLQRHV 999
HsSPRDM16       SAIETMTEKLESFAAMKADSGSSLQPLPHHPFNFRSPPPTLSDPILRKGKERYTCRYCGKIFPRSANLTRHLRTHTGEQPYRCKYCDRSFSISSNLQRHV 814
MsSPRDM16       SAIETMTEKLESFAAMKADSGSSLQPLPHHPFNFRSPPPTLSDPILRKGKERYTCRYCGKIFPRSANLTRHLRTHTGEQPYRCKYCDRSFSISSNLQRHV 814
                ********************************************************************************************** 

HsFPRDM16       RNIHNKEKPFKCHLCNRCFGQQTNLDRHLKKHEHENAPVSQHPGVLTNHLGTSASSPTSESDNHALLDEKEDSYFSEIRNFIANSEMNQASTRTEKRADM 1098
MsFPRDM16       RNIHNKEKPFKCHLCNRCFGQQTNLDRHLKKHEHEGAPVSQHSGVLTNHLGTSASSPTSESDNHALLDEKEDSYFSEIRNFIANSEMNQASTRMDKRPEI 1099
HsSPRDM16       RNIHNKEKPFKCHLCNRCFGQQTNLDRHLKKHEHENAPVSQHPGVLTNHLGTSASSPTSESDNHALLDEKEDSYFSEIRNFIANSEMNQASTRTEKRADM 914
MsSPRDM16       RNIHNKEKPFKCHLCNRCFGQQTNLDRHLKKHEHEGAPVSQHSGVLTNHLGTSASSPTSESDNHALLDEKEDSYFSEIRNFIANSEMNQASTRMDKRPEI 914
                ***********************************.******.************************************************ :**.::: 

HsFPRDM16       QIVDGSAQCPGLASEKQEDVEEEDDDDLEEDDEDSLAGKSQDDTVSPAPEPQAAYEDEEDEEPAASLAVGFDHTRRCAEDHEGGLLALEPMPTFGKGLDL 1198
MsFPRDM16       QDLDSNPPCPGSASAKPEDVEEEEEEELEEEDDDSLAGKSQEDTVSPTPEPQGVYEDEEDEEPPS-LTMGFDHTRRHMQ---------------------- 1177
HsSPRDM16       QIVDGSAQCPGLASEKQEDVEEEDDDDLEEDDEDSLAGKSQDDTVSPAPEPQAAYEDEEDEEPAASLAVGFDHTRRCAEDHEGGLLALEPMPTFGKGLDL 1014
MsSPRDM16       QDLDSNPPCPGSASAKPEDVEEEEEEELEEEDDDSLAGKSQEDTVSPTPEPQGVYEDEEDEEPPS-LTMGFDHTRRHMQ---------------------- 992
                * :*... *** ** * ******::::***:*:********:*****:****..*********.: *::******* :

HsFPRDM16       RRAAEEAFEVKDVLNSTLDSEALKHTLCRQAKNQGSLDAWLKVTGATSESGAFHPINHL 1257
MsFPRDM16       ------------------------------------------------------------ 1177
HsSPRDM16       RRAAEEAFEVKDVLNSTLDSEALKHTLCRQAKNQGSLDAWLKVTGATSESGAFHPINHL 1073
MsSPRDM16       ------------------------------------------------------------ 992
```

Figure 3-1: PRDM16 domain structure in full and short isoforms from human and mouse. Schematic illustration (top) of distinct PRDM16 domains, including the SET methyltransferase domain, zinc-finger DNA binding domains, proline-rich region, acidic domain, and CtBP-binding motifs. Amino acid sequences (bottom) for each isoform from both mouse and human with domains highlighted in corresponding colors. Asterisks (*) represent identical amino acid residues, whereas periods (.) and colons (:) represent residues with limited homology.

Prdm16 can directly bind DNA and thereby regulate gene expression through its two zinc-finger domains[164], but most of its regulatory effects are thought to be mediated through binding and interaction with other co-regulators. PRDM16 physically interacts with many known transcription factors including PPARγ and the PPARγ-coactivator proteins PGC-1α and PCG-1β, the CtBP complex genes CtBP-1 and CtBP-2[315], C/EBP-β[316], and the histone methyltransferase EHMT1[317]. Furthermore, it binds directly to sites in immediate proximity to Sp1 binding sites, though a physical interaction with Sp1 has not been demonstrated[92]. Through interaction with these various factors, Prdm16 can either activate or repress gene expression indirectly.

Prdm16 is expressed in several tissues in mice, with high mRNA expression detected in brown adipose tissue and HSCs, and low but detectable expression in brain, kidney, lung and heart[118,318]. Prdm16 is also expressed in neuronal stem cells, and is widely expressed in developing embryonic tissues, specifically in the brain, lung, kidney, and GI tract[319]. Protein regulators of Prdm16 expression are not currently described, but several microRNAs (miRNAs) regulate Prdm16, including miR-133, miR-27, and miR-150[320-322]. These studies have occurred in the context of brown fat differentiation. Prdm16 regulation by miRNAs occurs in the 3'UTR region of the gene[323].

3.1.3 Non-hematopoietic roles of PRDM16

PRDM16 has physiological roles apart from its role in the hematopoietic system. Notably, PRDM16 is most commonly known as the "master regulator" of brown adipose tissue (BAT) differentiation. Brown fat is a distinct form of adipose tissue that can dissipate heat and is important for thermal regulation in animals. It also inhibits the establishment and progression of obesity. White adipose tissue (WAT), in contrast, is the more classically-known fatty tissue which stores chemical energy in the form of triacylglycerols[324]. Both forms of adipose tissue require the "master adipose regulator" PPARγ for their differentiation and maintenance[325]. PRDM16, however, serves as the specific master regulator of brown fat. It is absolutely required for BAT differentiation and maintenance[318]. Forced expression of PRDM16 in WAT induces a brown thermogenic program in these cells, and mice that overexpress PRDM16 in all fat cells have large clusters of brown-like cells embedded within white fat tissue and increased overall energy expenditure[326]. Mechanistically, PRDM16 initiates the BAT gene expression network by forming a transcriptional complex with C/EBPβ, which induces the downstream regulators PPARγ (to initiate general adipogenesis) and PGC1a, which specifically activates brown fat genes[316]. PRDM16 binding to the histone methyltransferase EHMT1 also promotes BAT differentiation by forming a repressive complex to suppress expression of white adipose genes[317,327]. Notably, brown adipogenesis is partially inducible through cold exposure, presumably to help animals adapt to cold through by increasing internal thermogenesis. Cold exposure suppresses expression of miR-133 and miR-27, abrogating their repression of PRDM16 and therefore inducing brown adipogenesis[322].

PRDM16 plays additional roles in stem cell maintenance and tissue development. PRDM16 is expressed in neuronal stem cells and is required for their maintenance[328]. A particular PRDM16 SNP is one of only three known susceptibility loci for common migraine, with an odds ratio of 1.11, supporting the notion of PRDM16 involvement in healthy neurogenesis[329]. PRDM16 is also required for development of the pancreas, specifically the differentiation of islet α-cells and β-cells[330,331]. Finally, PRDM16 is required for

proper palatogenesis in mice, with some evidence to suggest this is due to co-regulation of TGFβ[332]. PRDM16 is expressed in developing orofacial tissue[333], and was among a short list of facial feature determinants in a survey of European participants[334]. These roles suggest involvement of PRDM16 in a multitude of developing tissues, and also raise the question of whether PRDM16 and PRDM family proteins may promote a general “stemness” mechanism, worthy of future investigation.

Section 3.2 – The role of PRDM16 in the hematopoietic system

3.2.1 The role of PRDM16 in leukemia

PRDM16 was initially discovered from its overexpression in a subset of leukemias characterized by t(1;3)(p36;q21) chromosomal rearrangements[164]. This rearrangement translocates the enhancer of the constitutively expressed housekeeping gene ribophorin 1 (RPN1) upstream of the coding region of PRDM16, resulting in overexpression. A later study found that s-PRDM16 was the predominant isoform translated in these leukemias and was the first to discover the existence of this isoform[335]. A highly similar disease occurs in the 3q21q26 translocation, in which the RPN1 enhancer is repositioned upstream of EVI1, the short isoform of PRDM3[336]. As mentioned earlier, PRDM3 is the closest homolog to PRDM16. One notable distinction between PRDM3 and PRDM16 is that the N-terminal portion of the PRDM3 locus has been observed as a unique transcript, with its own nomenclature (MDS1), and can also exist with EVI1 as a full-length protein (MDS1-EVI1 or MECOM) homologous to full length PRDM16 (f-PRDM16)[337].

PRDM16 is also found in other AML-associated chromosomal rearrangements. These include the t(1;21)(p36;q22) abnormality often associated with therapy-related AML (tAML) in which the N-terminus of RUNX1 fuses to the C-terminal portion of PRDM16, removing the PR domain[338]. Again there is a parallel between PRDM16 and EVI1, as the RUNX1-EVI1 transcript is a relatively common rearrangement (3% of cases) in AML[339]. The N-termini of both ETV6 and IKZF1 are also found, though rarely, as oncogenic fusions with the C-terminus of PRDM16[340]. A PRDM16-SKI fusion has also been observed in at least one patient with AML, though the resulting protein was out of frame and reversed from the typical arrangement and therefore may be associated with a different mechanism than other cases[341].

PRDM16 is also expressed in the majority of human adult T-cell leukemia (ATL) cell lines, a relatively rare T-cell leukemia etiologically associated with the human T-cell leukemia virus (HTLV-I)[342]. In these cell lines PRDM16 is hypomethylated and quantitative PCR using primers bridging exon 1/2 (specific for f-PRDM16)

showed no amplification, leading to the conclusion that only s-PRDM16 was expressed. RACE experiments showed potential alternate transcriptional start sites (TSS) in intron 3, and shorter transcripts resulting from later TSS in intron 5, while also acknowledging that s-PRDM16 may be co-transcribed with f-PRDM16 in other cell types[343].

AML with a normal karyotype accounts for approximately half of all AML cases, and is associated with an intermediate prognosis. NPM1 mutations underlie half of karyotypically-normal AMLs and therefore represent a sizable proportion (nearly 30%) of all AML cases. PRDM16 is expressed in most AML cases within this subset, and both *PRDM16* transcripts are detectable in the vast majority of those[344]. Because NPM1-mutated AML has elevated expression of HOXA and HOXB genes, it is possible that HOX induction is responsible for upregulation of PRDM16 in NPM1-mutated AML.

In mice, forced expression of either PRDM16 isoform in HSPCs (in this particular study defined as a transduced population of Lin^- cells) does not lead to malignancy. However, the authors did show that of 8 mice transplanted with *s-Prdm16*-overexpressing Lin^- cells, 2 of the mice did develop leukemia classified as "AML with maturation," whereas mice transplanted with empty vector or *f-Prdm16*-overexpressing cells did not develop leukemia. It was concluded that overexpression of s-Prdm16 may induce AML in murine HSCs, but with a low penetrance[344]. To investigate this more completely, the authors performed the same experiments in a $p53^{-/-}$ background, which is a common mutation in leukemia that shortens latency and causes a worse prognosis[345]. In $p53^{-/-}$ HSPCs, *s-Prdm16* overexpression led to AML with complete penetrance when transplanted into recipient mice. Those receiving empty vector or *f-Prdm16*-expressing cells did not develop AML and had a significantly longer overall survival than the *s-Prdm16* cohort, although many did eventually succumb to hematological malignancies at later time points as a result of p53 deletion[344,345].

The preponderance of evidence from human studies suggests a potential oncogenic role for s-PRDM16, and studies on HSPC immortalization in mice provide support for this hypothesis. Retroviral transduction has the potential to immortalize hematopoietic cells by causing overexpression of PRDM16 or its homolog EVI1. When bone marrow cultures are retrovirally transduced, there is insertion of retroviral DNA into the genomes of transduced cells. In experiments using murine stem cell virus (MSCV), where bone marrow cultures are transduced and placed in serial liquid culture, a fraction of cultures developed into immortalized cell lines. Nearly all of these had MSCV insertions in intron 1 or 2 of either *Prdm16* or, less commonly, *Evi1*[346]. This insertion caused overexpression of truncated Prdm16 or Evi1 resembling the short PRDM isoform. In serial bone marrow transplantations, hematopoietic cells with retroviral insertions in *Prdm16* or *Evi1* eventually induced leukemia in recipient mice[347]. Evidence for the oncogenic potential of s-Prdm16 has also been demonstrated in the opposite way – downregulation of s-Prdm16 prevents leukemogenesis in HOXB4-mediated transformation. Forced expression of HOXB4 immortalizes HSCs and maintains self-renewal potential without developing leukemia. HOXB4 represses *Prdm16* expression during transformation. Forced expression of both HOXB4 and *s-Prdm16* leads instead to enhanced self-renewal, myeloid expansion, and dysplasia with blast cells when transplanted into recipient mice[50]. This study also demonstrated that while HOXB4 repressed *Prdm16* expression, HOXA9 and HOXA10 induced *Prdm16*.

Based on available evidence, it has been proposed that in contrast to the short isoform, full-length PRDM proteins, including f-PRDM16, may function as tumor suppressors. Limited data currently exists to support this hypothesis for PRDM16. A recent study has suggested that forced expression of *f-Prdm16* inhibits leukemogenesis in a mouse model of MLL-AF9-mediated AML and that H3K4 methyltransferase activity in the PR domain was responsible for this inhibition[314]. This study, however, did not include an analysis of the short isoform and performed overexpression experiments in a WT background, which could confound interpretation of the results. They did use a full-length mutant with no histone methyltransferase activity

and found no oncogenic role for this protein, but this did not serve as an adequate model for s-Prdm16 as a mutated PR domain was still present.

Taken together, these findings seem to strongly suggest a leukemic role for the short isoform of PRDM16, but many unanswered questions remain. Firstly, no study to date has compared leukemogenesis in *Prdm16*-deleted HSPCs to WT in a mouse model of AML. Furthermore, the effect of forced expression of each PRDM16 isoform on AML progression has not been characterized in a *Prdm16*$^{-/-}$ background, which is the only way to determine the role of each individual Prdm16 isoform without the possibility of expression of the opposite isoform. Finally, the effect of total *Prdm16* deletion compared to specific *f-Prdm16* deletion on AML progression has not been investigated and would provide important insight into the individual leukemic role of each PRDM16 isoform. These questions are explored in Chapter 5 of this thesis.

3.2.2 The role of PRDM16 in normal hematopoiesis

While PRDM16 was first discovered in the context of leukemia, our lab and others have since shown that PRDM16 plays an essential role in normal hematopoiesis[118,328]. These studies were performed using mice with a global *Prdm16* deletion. These mice die perinatally or immediately at birth, and therefore experiments were performed using fetal liver cells. *Prdm16*$^{-/-}$ mice had a lower frequency of phenotypic fetal liver HSCs, and competitive transplants of LSK cells with competitor bone marrow showed a substantial multilineage reconstitution defect compared to WT LSKs. Secondary transplants showed an even more severe phenotype, suggesting an essential role for PRDM16 in both the short-term and long-term maintenance of HSCs. Expression of *Prdm16* in the hematopoietic system was specific to HSPCs, with the highest expression in HSCs and approximately 20% of that level in MPPs and CLPs. Prdm16 was low or undetectable in CMPs and Lineage^{+} cells[118,328]. Gene expression studies suggested that Prdm16 may positively regulate a number of targets, including its binding partner in brown fat, *PPARγ*, and *BMI1*, which

is involved in HSC maintenance through regulation of HSC proliferative capacity[348]. Conversely, a number of genes were upregulated in *Prdm16*$^{-/-}$ HSCs, including *p53*, *Puma*, and *Tmbim4*, which may explain increased levels of apoptosis observed in these cells, and the cell cycle regulators *Cdkn1a* and *Cdkn1b*. Prdm16 therefore plays a role in HSC maintenance through both the induction and repression of downstream targets.

One potential mechanism by which Prdm16 promotes HSC maintenance may be through transcriptional regulation of *PPARγ*, which must be present and activate to positively regulate hematopoiesis by induction of TGF-β2-mediated FLT3 signaling[144]. Another mechanism may be through regulation of *Gpx3*. HSCs overexpressing *Gpx3* have a significant competitive advantage relative to WT controls, and conversely, shRNA knockdown of *Gpx3* causes competitive defects. *Gpx3* expression also correlates with adverse outcome in AML. Overexpression of *Prdm16* in HSCs results in an increase in *Gpx3* expression, providing another potential mechanism of action for Prdm16 in HSC maintenance[349]. Lastly, in HSCs s-Prdm16 induces the expression of *Mfn2*, whose function is described in 1.3.4. Mfn2 plays a role in maintaining HSCs, particularly those with lymphoid potential, and may exert its effects directly through mitochondrial remodeling, or indirectly through its ability to buffer intracellular Ca^{2+}, which Mfn2 accomplishes by functioning as a tether between the endoplasmic reticulum and the mitochondria[92].

Several unanswered questions remain regarding the role of Prdm16 in HSC maintenance. Firstly, the two studies to show the essential role for Prdm16 in maintaining HSCs both used an embryonic lethal, global deletion of *Prdm16*. Because of this, fetal liver HSCs were the only cells available to study. It is an important question whether Prdm16 has the same function in adult bone marrow HSCs. Secondly, no study has yet compared the relative roles of f-Prdm16 and s-Prdm16 in HSC maintenance. Finally, genome-wide expression analysis, which may yield additional insights into mechanisms of Prdm16 in HSC maintenance, has not been performed. These questions are each investigated in this thesis project, and results are reported in Chapter 4.

Chapter 4 – The Role of PRDM16 Isoforms in Normal Hematopoiesis

Section 4.0 – Introduction

Our lab has previously shown that fetal liver HSCs from a global murine *Prdm16*$^{-/-}$ deletion have severe defects in competitive repopulation efficiency and a lower HSC frequency[118]. These findings suggest that Prdm16 is essential for HSC maintenance, but this has not yet been demonstrated in adult HSCs. Section 4.1 is therefore a study of the effects of Prdm16 deficiency in a non-lethal conditional deletion of *Prdm16* in the hematopoietic system. Some of the work performed in Section 4.1 was a collaborative effort in conjunction with Dr. Larry Luchsinger, Linda Williams, and Mariana Justino de Almeida. Section 4.2 describes an in-depth gene expression analysis of these HSCs using RNAseq, and related mechanistic experiments derived from this data.

We then shift our focus to a specific analysis of the individual isoforms of Prdm16. We were able to generate a specific global mouse deletion of the full-length Prdm16 isoform. Like the global *Prdm16*$^{-/-}$ strain, the *f-Prdm16*$^{-/-}$ strain is also embryonic lethal, which required us to focus our analysis on fetal liver HSCs. We were not able to specifically delete *s-Prdm16*, as the entire coding region of the short isoform is contained within *f-Prdm16*. Nonetheless, the data gleaned from the *f-Prdm16*$^{-/-}$ deletion revealed interesting findings which are presented in Section 4.3, and certain properties of s-Prdm16 were able to be inferred by comparing differences between the complete and full-length deletion. A more detailed examination of the hematopoietic compartments found in *f-Prdm16*$^{-/-}$ mice are presented in Section 4.4, and finally, gene expression analysis of *f-Prdm16*$^{-/-}$ HSCs is presented in Section 4.5.

Section 4.1 – Prdm16 is required for effective HSC maintenance in adult HSCs

4.1.1 Generation and phenotypic profile of conditionally-deleted *Prdm16*$^{-/-}$ mice

As germline-deleted *Prdm16*$^{-/-}$ mice die at or shortly before birth, we generated a mouse line with a conditional deletion of Prdm16 within the hematopoietic system. The *Vav* gene is expressed in all hematopoietic cells and in a small subset of endothelial cells[350]. Mice expressing Bacteriophage P1 iCre under the *Vav* promoter induce recombination of *LoxP* sites throughout the hematopoietic system[351]. To use this system to conditionally delete *Prdm16*, we inserted *LoxP* sites into flanking positions around exons 6 and 7 of C57NL/6 mice. This is illustrated schematically in (**Figure 4-1A**). *Prdm16*$^{fl/fl}$ mice were generated by Ingenious Targeted Laboratory, Inc. (Ronkonkoma, NY). A neomycin resistance cassette flanked by *FRT* and a 3'*LoxP* site were inserted upstream of exon 6 and a second *LoxP* site was inserted downstream of exon 7 in a 10.2 Kb fragment from a C57NL/6 BAC clone, extending from intron 5 through exon 9. The modified BAC clone was electroporated into mouse ES cells, and neomycin resistant clones were expanded, screened for retention of the *Neo* cassette and second *LoxP* site, and injected into C57NL/6 blastocysts to generate chimeric mice. Removal of the *Neo* cassette was accomplished by crossing to *FLP* heterozygous mice, yielding mutant, *Prdm16*$^{fl/fl}$ mice with *LoxP* sites flanking exon 6 and 7. *Prdm16*$^{fl/fl}$ mice were then crossed with *Vav-Cre*$^{+/-}$ mice to generate a *Prdm16*$^{fl/fl}$*.Vav-Cre* strain. In contrast to what was observed in the global *Prdm16* knockout mouse, *Prdm16*$^{fl/fl}$*.Vav-Cre* mice are born in Mendelian ratios and survive to adulthood (**Figure 4-1B**). Excision in hematopoietic cells of *Prdm16*$^{fl/fl}$*.Vav-Cre*$^{+}$ mice was verified by PCR amplification of DNA extracted from peripheral blood (**Figure 4-1C**).

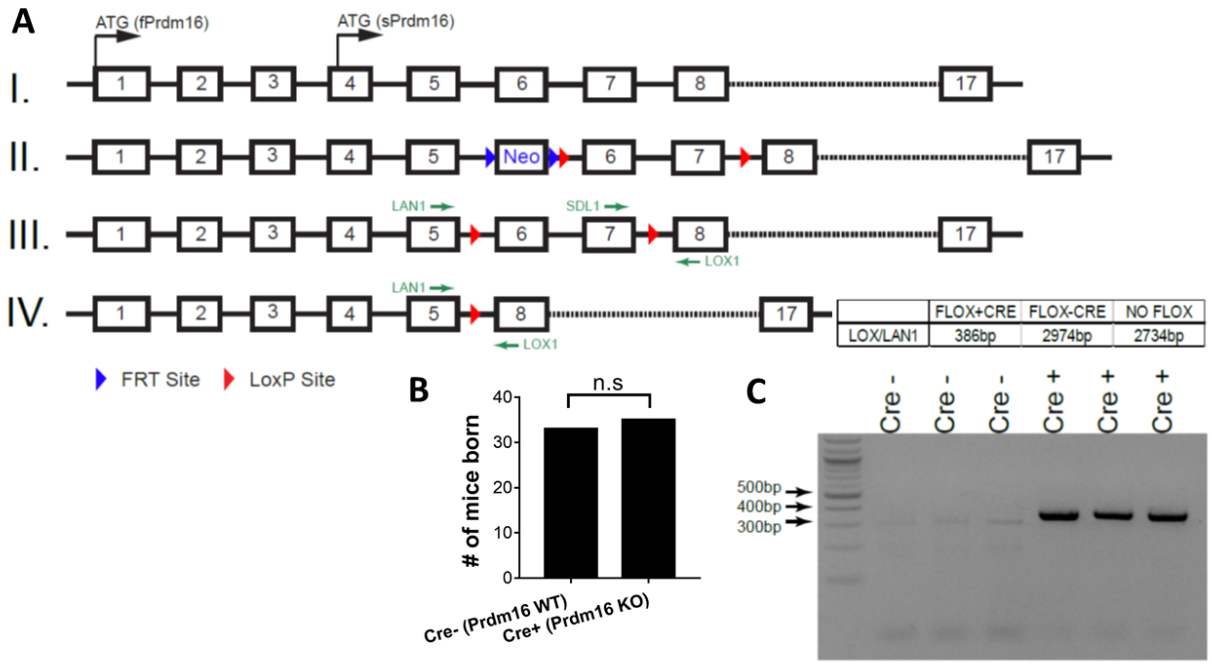

Figure 4-1: Generation of *Prdm16$^{fl/fl}$.Vav-Cre* mice. (**A**) Schematic representation of the generation of *Prdm16$^{fl/fl}$* mice – I. Map of *Prdm16* exons and introns, including the two start codons for *f-Prdm16* and *s-Prdm16*, respectively. II. Insertion of a Neomycin-resistance cassette flanked by *FRT* sites, and of *LoxP* sites around exons 6 and 7. III. Map of the *Prdm16$^{fl/fl}$* genomic structure after removal of the Neo cassette by crossing to a FLP-recombinase$^{+/-}$ mouse, with the highlighting (in green) of LAN1, SDL1, and LOX1 primers for use in genotyping. IV. Deletion of *Prdm16* exon 6 and 7 in the presence of Cre recombinase, with LAN1/LOX1 locations and a table illustrating differences in LOX1/LAN1 amplicon length with or without genomic excision. (**B**) Cre$^{+/-}$ and Cre$^{-/-}$ mice are born in Mendelian ratios. (*n* = 65 mice, *P* = 0.92, Chi-square test). (**C**) LOX1/LAN1 PCR of hematopoietic peripheral blood cells from three Cre^{-} and three Cre^{+} mice showing the presence of a 380bp amplicon in the excised mice.

We then analyzed the *Prdm16$^{fl/fl}$.Vav-Cre* mice to determine the effect of *Prdm16* deletion on the hematopoietic compartment. We assayed the bone marrow of adult *Prdm16$^{fl/fl}$.Vav-Cre* mice and observed that HSC frequency (defined as Lin^{-}cKit^{+}Sca1^{+}CD48^{-}Flt3^{-}CD150^{+}) was lower in these mice compared to WT littermate controls (**Figure 4-2A**). The frequency of LSK cells, encompassing the total HSPC compartment, and Lin- cells, which encompass the broader population of progenitor cells, was unchanged between WT and *Prdm16*-deficient mice, suggesting that *Prdm16* deletion specifically affected the HSC pool. Bone marrow cellularity was similar, and as a result the absolute HSC number in

Prdm16$^{fl/fl}$*.Vav-Cre*$^{+}$ mice was reduced as well, with no change in absolute LSK or Lin- cell numbers. A representative FACS plot for HSC and LSK specification is presented in **Figure 4-2B**.

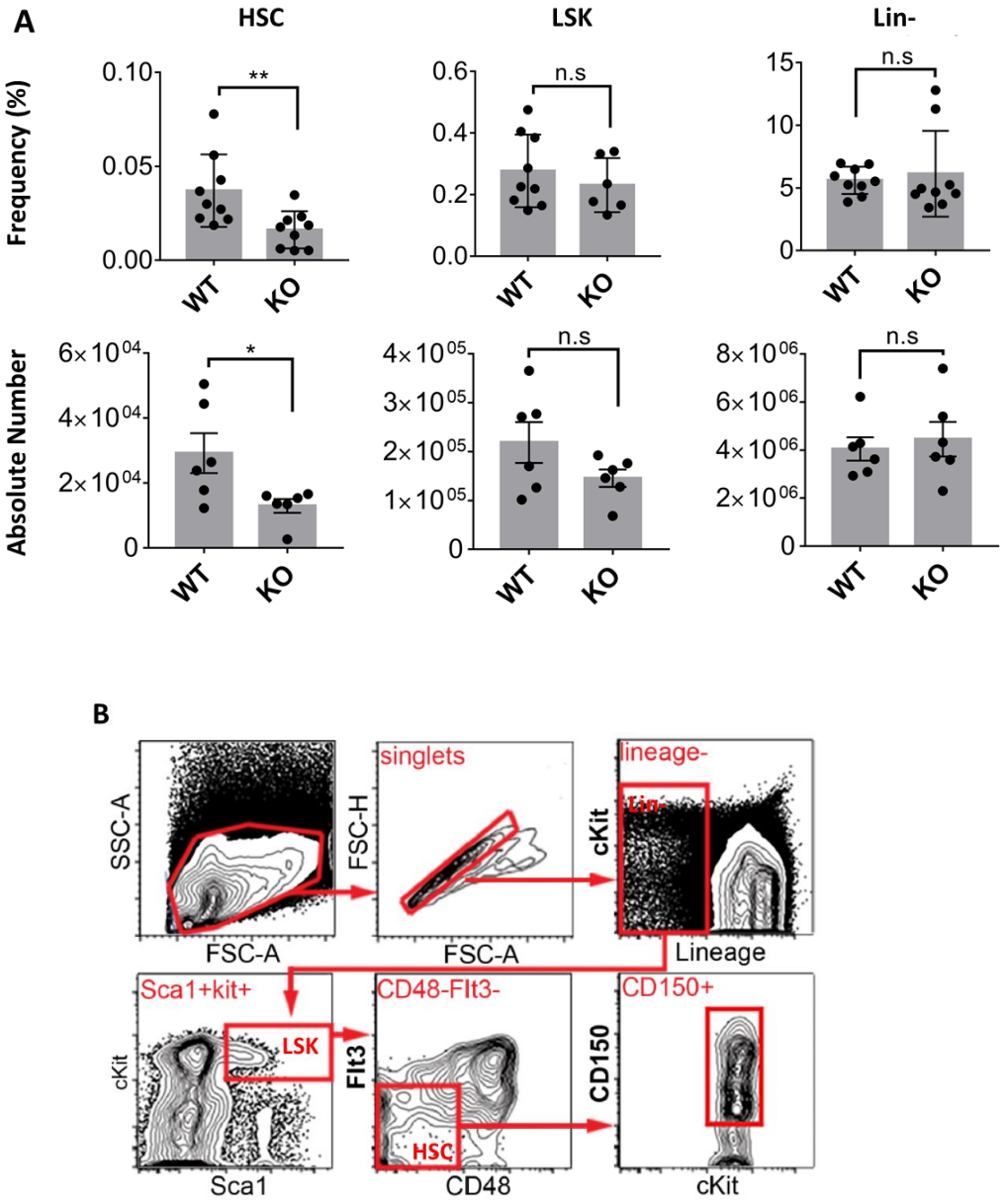

Figure 4-2: Lowered HSC frequency and absolute number in *Prdm16*$^{fl/fl}$*.Vav-Cre* mice. (**A**) Frequency (*n* = 9) and absolute number (*n* = 6) of HSCs (Lin^{-}cKit^{+}Sca^{+}Flt3^{-}CD48^{-}CD150^{+}), LSKs (Lin^{-}cKit^{+}Sca1^{+}) and Lineage negative cells in bone marrow of adult *Vav-Cre*$^{-/-}$ *Prdm16*$^{fl/fl}$ (WT) and *Vav-Cre*$^{+/-}$ *Prdm16*$^{fl/fl}$ (KO) mice. (**B**) Representative flow plot depicting HSC, LSK, and Lineage negative gating scheme. (n.s = $P > 0.05$; * = $P < 0.05$; ** = $P < 0.01$, Student's t-test for single comparisons).

We then analyzed the peripheral blood of *Prdm16*-deficient mice to determine if hematopoietic output was broadly impacted by *Prdm16* deletion. To examine this, we performed a complete blood count (CBC) of peripheral blood (PB) harvested from *Prdm16$^{fl/fl}$.Vav-Cre^{+}* mice or WT littermate controls. No differences were detected in any PB component between *Prdm16$^{fl/fl}$.Vav-Cre^{+}* or WT mice, including lymphocytes, neutrophils, monocytes, granulocytes, red blood cells, reticulocytes, or platelets (**Figure 4-3**), indicating that in adult mice, Prdm16 was not required to maintain steady-state hematopoietic levels.

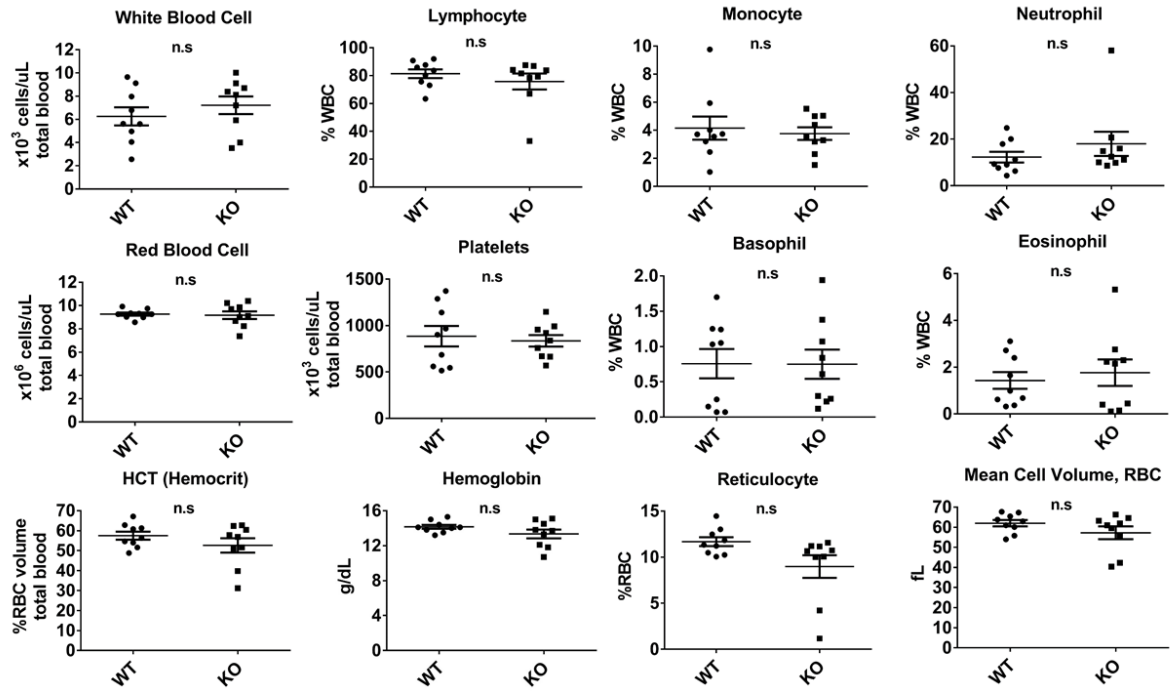

Figure 4-3: Similar peripheral blood composition of *Prdm16$^{fl/fl}$.Vav-Cre* and WT littermates. Complete blood counts from peripheral blood of 12-week adult *Prdm16$^{fl/fl}$.Vav-Cre* (KO) and WT littermates (n=9). All populations assayed, including white blood cells, lymphocytes, monocytes, neutrophils, red blood cells, platelets, basophils, eosinophils, and reticulocytes were unchanged ($P > 0.05$, Student's t-test). Counts of hemoglobin, hematocrit ratio and mean cell volume were also unchanged between WT and KO. Y-axis indicates the measurement taken, which varies for each blood population.

4.1.2 Functional competitive reconstitution defects of *Prdm16$^{fl/fl}$.Vav-Cre^{+}* HSCs

Many genes important for HSC maintenance are nonetheless able to maintain steady-state hematopoiesis in mice when deleted. MPPs and other short-term HSPCs are typically able to contribute the bulk of hematopoietic output if necessary. A more complete understanding of LT-HSC maintenance must therefore be measured in other ways, with competitive transplantations being the most effective. We therefore performed transplants of *Prdm16$^{fl/fl}$.Vav-Cre^{+}* and WT littermate HSCs and found that *Prdm16*-deficient HSCs had a significant defect in long-term repopulation capacity (**Figure 4-4A**). Analysis of peripheral blood of recipient mice revealed a low donor chimerism in mice transplanted with *Prdm16$^{fl/fl}$.Vav-Cre^{+}* HSCs, but no apparent lymphoid/myeloid bias of the repopulating cells compared to WT, suggesting that the reconstitution defect observed in *Prdm16*-deficient HSCs is not specifically biased toward either hematopoietic lineage (**Figure 4-4B**). We also performed secondary transplants to determine whether hematopoietic output of *Prdm16*-deficient HSCs would continue to diminish over time. Secondary transplants revealed this to be the case – WT HSCs generated similar chimerism levels in secondary transplants as they did in primary transplants, whereas secondary *Prdm16*-deficient transplants had a lower donor chimerism than what was observed after 16-week primary transplants (**Figure 4-4C**). A continuous decrease in hematopoietic output over time indicates a long-term self-renewal defect in *Prdm16$^{fl/fl}$.Vav-Cre^{+}* HSCs.

The most effective way to estimate functional HSC frequency is through limiting dilution analysis (LDA). We therefore performed an LDA analysis of *Prdm16$^{fl/fl}$.Vav-Cre^{+}* HSCs compared to WT. We found that HSC frequency in WT mice was approximately 1/8 cells, whereas HSC frequency in *Prdm16*-deficient bone marrow was significantly lower (approximately 1/47) ($P < 0.0001$, ELDA analysis) (**Figure 4-4D**).

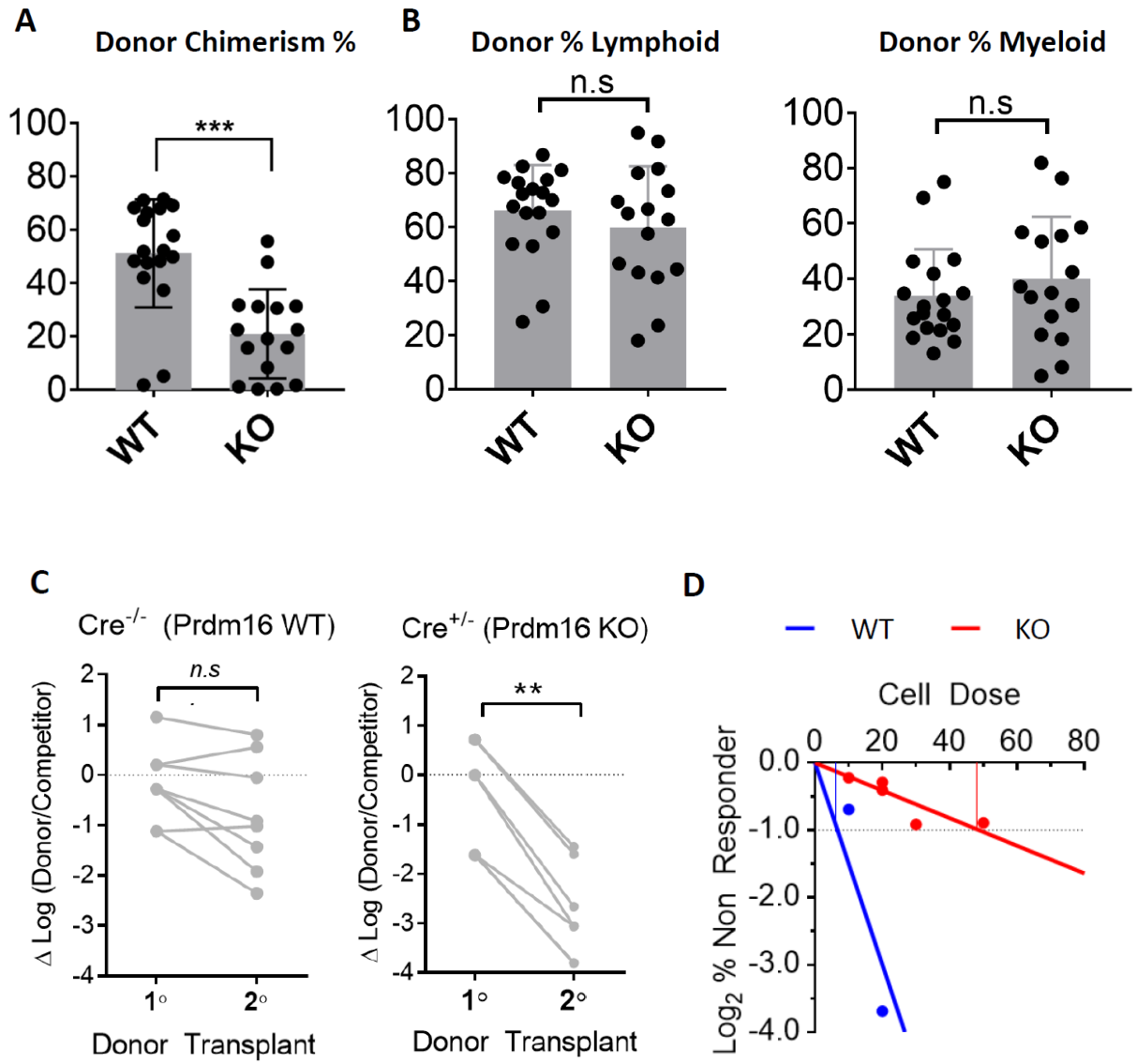

Figure 4-4: Defective HSC maintenance in *Prdm16$^{fl/fl}$.Vav-Cre^{+}* mice. (**A**) Peripheral blood (PB) donor chimerism of transplanted *Cre^{-}* (WT) or *Prdm16$^{fl/fl}$.Vav-Cre^{+}* (KO) BM HSCs in competitive transplants with CD45.1 BM, measured 16-weeks post-transplant. (*n* = 16-18 mice, 3 independent transplants). (**B**) Percentage of donor cells from (A) that were lymphoid (CD19^{+} or CD3^{+}) or myeloid (Gr-1^{+} or Mac1^{+}) (*n* = 16-18 mice). (**C**) Change in donor/competitor ratio (log_{10} scale) between primary competitive transplants and secondary transplants of primary recipient BM. (*n* = 8 mice, 2 independent transplants). (**D**) Limiting dilution assay of WT vs KO BM HSCs. (n.s = $P > 0.05$; * = $P < 0.05$; ** = $P < 0.01$; *** = $P < 0.001$, Student's t-test for single comparisons, ELDA calculation for LDA analysis).

A previous report from our lab characterized fetal liver HSCs in an embryonically-lethal global *Prdm16*$^{-/-}$ mouse. This study found extremely low levels of chimerism in competitive transplants. We observed a significant phenotype in adult *Prdm16*$^{fl/fl}$*.Vav-Cre*$^{+}$ but it was less severe than in fetal liver *Prdm16*$^{-/-}$ HSCs. We sought to determine whether this was a result of different severity of *Prdm16*-deletion in fetal liver compared to adult HSCs. We therefore performed competitive transplants with fetal liver HSCs from *Prdm16*$^{fl/fl}$*.Vav-Cre*$^{+}$ mice. These experiments did indeed show a more severe effect on competitive repopulation ability in *Prdm16*$^{fl/fl}$*.Vav-Cre*$^{+}$ HSCs, with a median peripheral blood donor chimerism of only 2% (**Figure 4-5A**). Further analysis of peripheral blood of recipient mice showed that, as with the adult HSCs, there was no particular lineage bias of the few reconstituting *Prdm16*$^{fl/fl}$*.Vav-Cre*$^{+}$ HSCs, as the donor percent lymphoid/myeloid were unchanged compared to WT controls (**Figure 4-5B**).

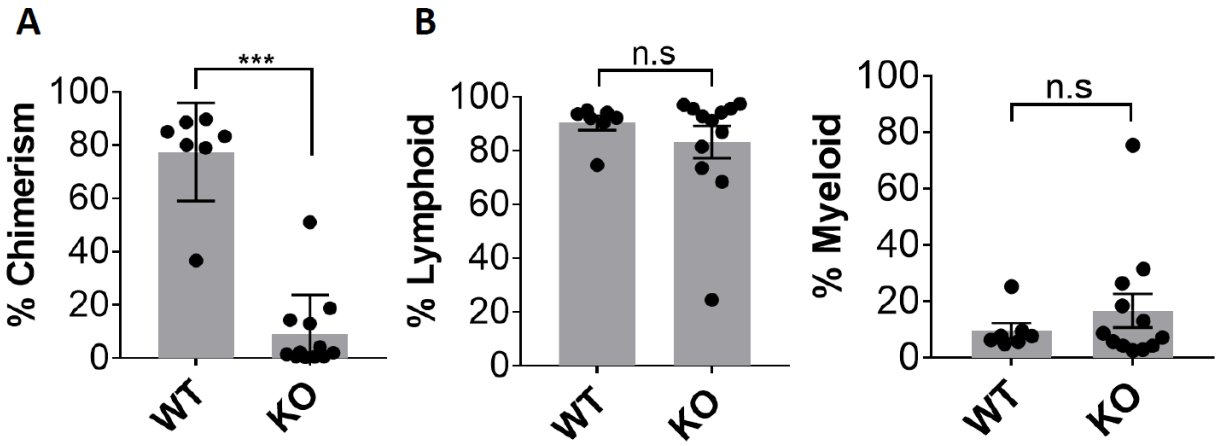

Figure 4-5: Severe defects in HSC function in *Prdm16*$^{fl/fl}$*.Vav-Cre*$^{+}$ fetal liver. (**A**) Peripheral blood donor chimerism of *Cre*$^{-}$ (WT) or *Prdm16*$^{fl/fl}$*.Vav-Cre*$^{+}$ (KO) fetal liver HSCs in competitive transplants with CD45.1 BM, 16-weeks post-transplant. (*n* = 8-10 mice, 2 independent transplants) (**B**) Percentage of lymphoid (CD19+ or CD3+) or myeloid (Mac1+ or Gr1+) donor cells from (A) (*n* = 8-10 mice). (n.s = $P > 0.05$; * = $P < 0.05$; ** = $P < 0.01$; *** = $P < 0.001$, Student's t-test for single comparisons).

4.1.3 *Prdm16*-deficient cells have normal cycling, apoptosis and engraftment potential

We next performed a phenotypic analysis of *Prdm16*-deficient HSCs to investigate changes in these cells that could potentially account for the defects observed in competitive transplant experiments. One possibility is that *Prdm16$^{fl/fl}$.Vav-Cre^{+}* HSCs could have a loss of quiescence and increased cycling. This typically results in exhaustion of the HSC compartment and loss of reconstitution potential. Another possibility is that HSCs could have higher levels of apoptosis, which would deplete the HSC compartment. Finally, apparent competitive repopulation defects can be caused by a loss of homing and engraftment ability. In this case, an inability of transplanted cells to migrate from the periphery (via tail vein injection) into the bone marrow would result in a loss of donor chimerism.

Our analysis of these fundamental HSC properties did not show any pronounced effects. Ki-67 staining labels cycling cells that are no longer in the highly quiescent G0 phase. Sorted *Prdm16*-deficient HSCs did not have a statistically significant increase in Ki-67 staining (**Figure 4-6A**). Similarly, we assessed levels of apoptosis by staining for cleaved Caspase-3 in sorted HSCs from WT and *Prdm16$^{fl/fl}$.Vav-Cre^{+}* mice. Again, we did not see a significant difference (**Figure 4-6B**). Notably, although we did not observe a statistically significant difference in cycling or apoptosis, we did find a potentially slight increase. This minor increase, however, would be unlikely to explain the drastic differences in HSC potential we observed in *Prdm16*-deficient mice.

These findings are consistent with previously published data in fetal liver *Prdm16$^{-/-}$* HSCs, where a very slight but significant increase in cycling and apoptosis was observed. We then measured engraftment potential by quantifying the frequency of engrafted cells (distinguished by donor CD45.2 staining as in competitive transplants) in recipient mice 24 hours after tail vein injection. Engraftment potential was unchanged between *Prdm16$^{fl/fl}$.Vav-Cre^{+}* progenitors (**Figure 4-6C**) and WT controls. One caveat of this

experiment is that LSK cells were used in place of HSCs in order to have enough transplantable cells to detect within 24 hours.

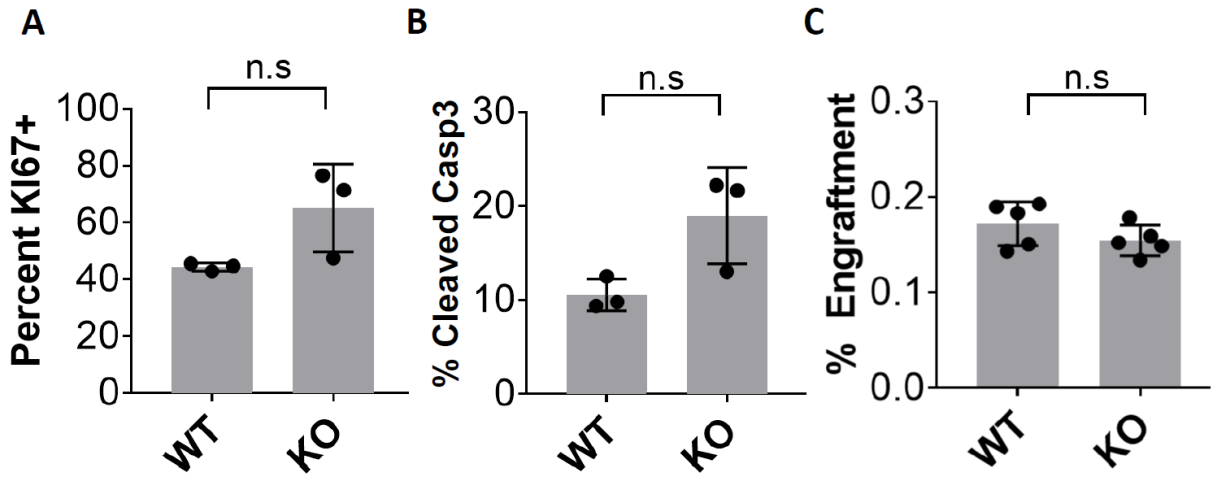

Figure 4-6: Cycling, apoptosis, and engraftment are similar between *Prdm16$^{fl/fl}$.Vav-Cre^{+}* and WT HSCs. (**A**) Percentage of KI-67^{+} and (**B**) Cleaved caspase-3^{+} bone marrow HSCs from *Cre*$^{-}$ (WT) and *Prdm16$^{fl/fl}$.Vav-Cre^{+}* (KO) mice (*n* = 3 mice). (**C**) Percent of WT or KO donor CD45.2 cells in BM of recipient mice 24-hours post-transplant. (*n* = 5 recipient mice). (n.s. = *P* > 0.05, Student's t-test for single comparisons).

Section 4.2. Gene expression and mechanistic studies of *Prdm16*-deficient HSCs

4.2.1 RNAseq expression analysis of adult *Prdm16$^{fl/fl}$.Vav-Cre^{+}* HSCs

In order to gain further insight into potential mechanisms by which Prdm16 may regulate and maintain HSCs, we performed RNAseq of HSCs from *Prdm16$^{fl/fl}$.Vav-Cre^{+}* mice and WT littermate controls. We first analyzed adult HSCs (a parallel analysis using fetal liver HSCs is described in section 4.2.3). We isolated RNA from bone marrow Lin^{-}cKit^{+}Sca1^{+}CD48^{-}Flt3^{-} HSCs from 4 *Prdm16$^{fl/fl}$.Vav-Cre^{+}* mice or WT littermates, amplified RNA and performed RNA sequencing. 561 genes were significantly downregulated, while 411 genes were upregulated. The top 50 genes upregulated and downregulated are presented in **Figure 4-7**. Principal component analysis (PCA) of the samples showed a clear distinction between WT and *Prdm16*-deficient HSCs, an indicator of both experimental quality and of a significant, detectable difference in gene expression patterns between the two populations (**Figure 4-8A**). As expected based on the design of the *Prdm16$^{fl/fl}$* mice, an exon analysis of *Prdm16$^{fl/fl}$.Vav-Cre^{+}* HSCs showed an overall reduction in *Prdm16* mRNA, with a complete absence of mRNA expression within exons 6 and 7 (**Figure 4-8B**). A loss of exons 6 and 7 leads to a frameshift, resulting in a change in amino acid sequence and early termination 25 amino acids downstream of the deletion (**Figure 4-8C**).

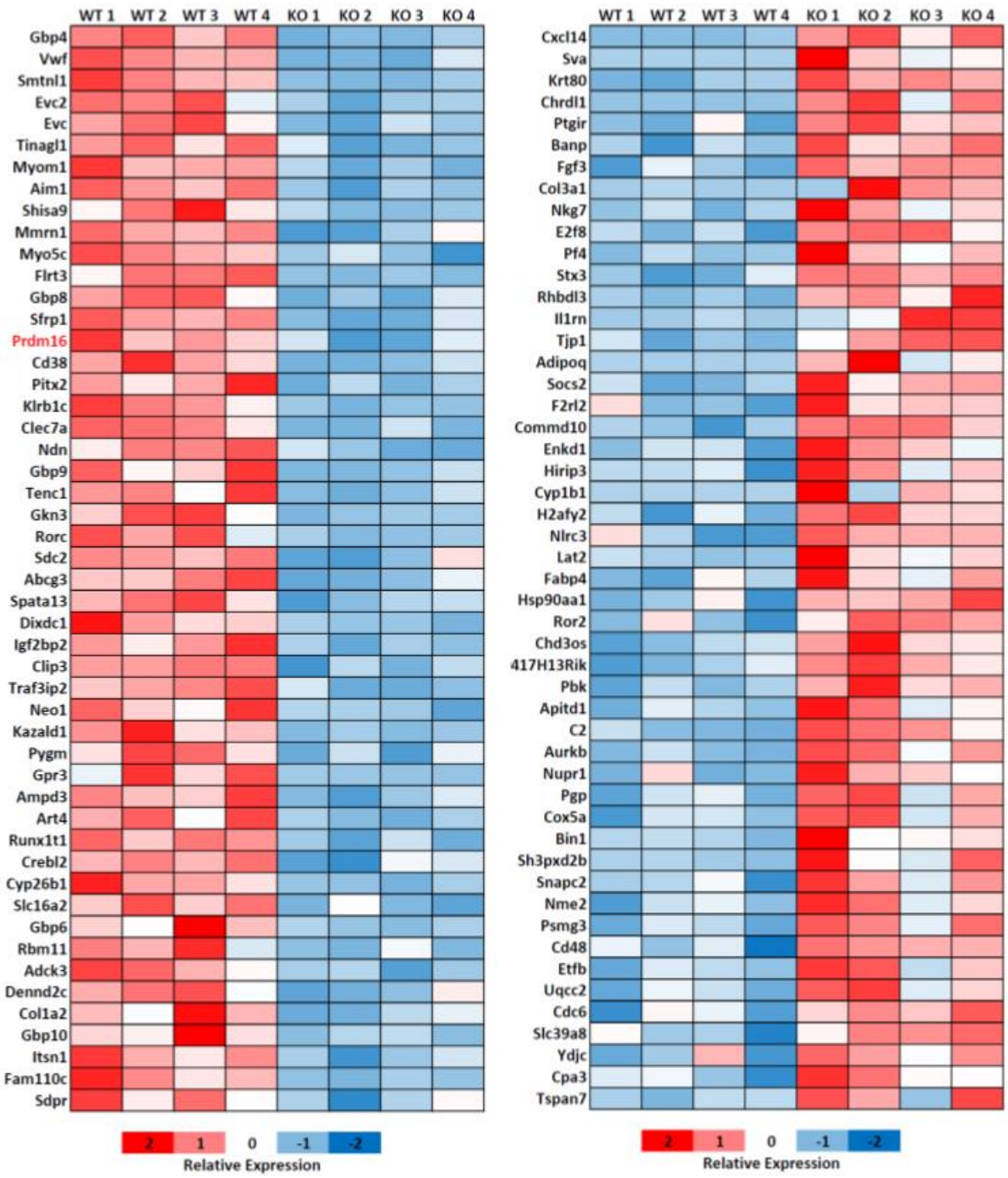

Figure 4-7: Genome-wide expression analysis of *Prdm16$^{fl/fl}$.Vav-Cre* bone marrow HSCs Heatmap of the top 50 genes (by *P*-value) upregulated in *Cre*$^{-}$ (WT, left panel) and *Vav-Cre*$^{+/-}$ *Prdm16*$^{fl/fl}$ (KO, right panel) bone marrow HSCs, for each sample, as determined by RNAseq. Of note, *Prdm16* (highlighted in red) appears in the list of genes most highly downregulated in the KO samples.

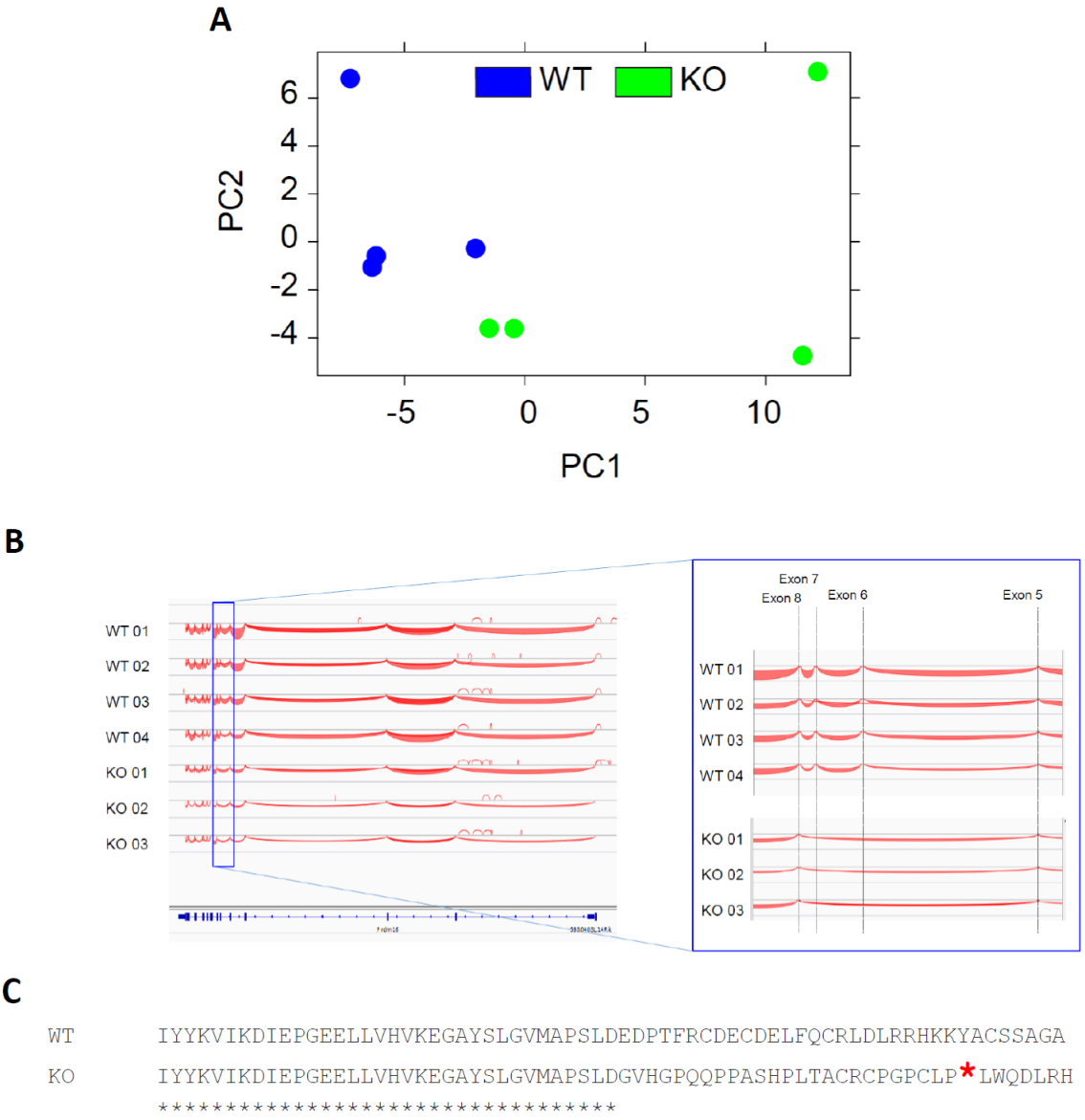

Figure 4-8: Principal component and exon analysis of *Prdm16$^{fl/fl}$.Vav-Cre* HSCs. (**A**) Principal component analysis (PCA) of individual RNAseq samples from *Cre*- (WT) and *Prdm16$^{fl/fl}$.Vav-Cre* (KO) bone marrow HSCs (**B**) Quantification of *Prdm16* exons in RNAseq analysis of WT and KO littermate HSCs using the Integrative Genomics Viewer (IGV), showing absence of reads at exons 6 and 7 in KO samples. (**C**) Analysis of *Prdm16$^{fl/fl}$.Vav-Cre* and WT littermate Prdm16 amino acid sequences showing a frameshift and early termination 25 amino acids downstream of the C-terminus of exon 5

We then performed pathway analysis to determine biological pathways differentially regulated in WT and *Prdm16*-deficient HSCs. We performed a statistical enrichment test using the PANTHER algorithm[352,353] with the set of genes selected using a 0.1 false discovery rate (FDR) cutoff. A broad set of pathways were

upregulated and downregulated by Prdm16 (**Figure 4-9A**). Pathways upregulated in WT HSCs and therefore likely induced by *Prdm16*, are largely related to Rho and Ras GTPase signaling and include blood vessel development and angiogenesis pathways, which contain a number of common genes. Other gene subsets upregulated by *Prdm16* include those with ubiquitin transferase activity and PDGF receptor binding activity, which can also serve as mediators of Ras GTPase signaling[354]. Pathways downregulated by Prdm16 were largely related to metabolism. These include respiratory pathways (oxidative phosphorylation, cellular respiration, electron transport chain, oxidoreductase activity, ATP metabolic process) and processes involving rRNA biosynthesis (ribosome biogenesis, rRNA binding, RNA processing) (**Figure 4-9A**). To obtain a clearer perspective on the specific respiratory genes downregulated by Prdm16, we analyzed which specific members of the five respiratory complexes were differentially expressed. A table of these genes is presented in **Table 1**. Our analysis demonstrated that of the 96 electron transport chain (ETC) genes, 31 were upregulated in *Prdm16*-deficient HSCs. Upregulation was observed in each of the five respiratory complexes (**Figure 4-9B**) and the observed value was significantly higher than expected by random chance (31/96 observed vs 4/96 expected, $P<0.0001$ determined by Chi-Square analysis).

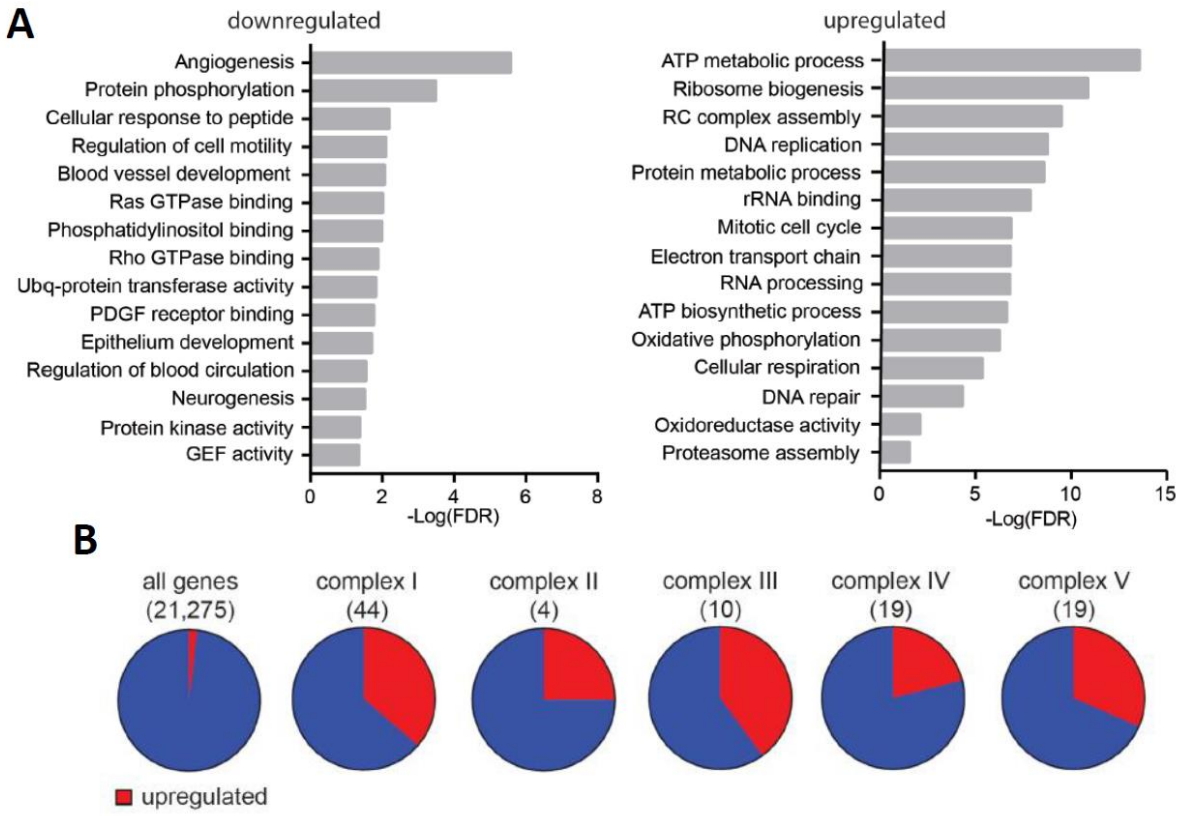

Figure 4-9: Pathway analysis of *Prdm16$^{fl/fl}$.Vav-Cre* HSCs shows that *Prdm16* induces GTPase signaling and represses oxidative phosphorylation. (**A**) GO pathways significantly up/downregulated in *Prdm16$^{fl/fl}$.Vav-Cre* HSCs compared to WT, determined by RNAseq, taking all differentially regulated genes using a 0.1 FDR cutoff. P-values presented as the $-\text{Log}_{10}$ of the P-value, determined by PANTHER algorithm. (**B**) Fraction of genes upregulated (red) in *Prdm16$^{fl/fl}$.Vav-Cre* HSCs among all genes and the five respiratory complexes illustrating overrepresentation of ETC genes ($P < 0.0001$ by Chi-Square test)

Table 1

Respiratory Complex Genes Elevated in Prdm16-deficient HSCs

Gene	Complex	Fold	P Value
NDUFS7	Complex I	1.32	4.8E-02
NDUFS8	Complex I	1.30	6.2E-02
NDUFV2	Complex I	1.33	4.5E-02
NDUFA1	Complex I	1.42	2.6E-02
NDUFA2	Complex I	1.45	5.0E-02
NDUFA3	Complex I	1.42	2.9E-02
NDUFA5	Complex I	1.40	3.7E-02
NDUFA8	Complex I	1.39	2.5E-02
NDUFA11	Complex I	1.51	2.8E-02
NDUFB2	Complex I	1.43	1.6E-02
NDUFB5	Complex I	1.34	4.9E-02
NDUFB7	Complex I	1.42	1.8E-02
NDUFB8	Complex I	1.46	9.5E-03
NDUFB10	Complex I	1.38	3.0E-02
NDUFB11	Complex I	1.36	3.5E-02
NDUFC1	Complex I	1.35	4.6E-02
SDHB	Complex II	1.33	4.7E-02
CYC1	Complex III	1.36	3.3E-02
UQCRQ	Complex III	1.51	1.4E-02
UQCR10	Complex III	1.44	1.5E-02
UQCR11	Complex III	1.43	3.7E-02
COX5A	Complex IV	1.52	3.9E-03
COX6A1	Complex IV	1.45	2.8E-02
COX6B2	Complex IV	1.56	1.6E-02
COX8A	Complex IV	1.42	4.3E-02
ATP5D	Complex V	1.45	3.7E-02
ATP5E	Complex V	1.47	2.1E-02
ATP5G1	Complex V	1.34	4.5E-02
ATP5H	Complex V	1.34	3.9E-02
ATP5J2	Complex V	1.47	2.3E-02
ATP5O	Complex V	1.40	2.0E-02

4.2.2 Adult *Prdm16*-deficient HSCs have higher respiratory metabolism

Based on our genome-wide expression analysis, we determined whether basal metabolic rates were altered in *Prdm16*-deficient HSCs compared to WT, using a Seahorse metabolic flux analyzer (**Figure 4-10A**). This machine requires a minimum of 50,000 cells for an effective measurement above background. For this reason, individual data points represent 5 pooled mice and HSCs were defined here as Lin^- $cKit^+Sca1^+Flt3^-$ cells, to obtain a larger cell number. The Seahorse Mitochondrial Stress Test, used to determine respiratory profiles of cell populations, detected elevated basal oxygen consumption (**Figure 4-10B**) and an increase in total respiratory ATP production (**Figure 4-10C**) in *Prdm16*-deficient HSCs compared to WT littermate controls. This increase in respiration was cell-type specific as we did not observe a difference in respiration in *Prdm16*-deficient mouse embryonic fibroblasts (MEFs) (**Figure 4-10D**). We then measured reactive oxygen species (ROS) levels in WT and *Prdm16*-deficient HSCs using CellROX-Deep Red staining. CellROX is a cell-permeable dye that is non-fluorescent in a reduced state but presents a Deep Red fluorescence upon oxidation. ROS levels were elevated in *Prdm16*-deficient HSCs compared to WT levels (**Figure 4-10E**). This finding is consistent with elevated levels of respiration, as ROS are a common byproduct of ETC activity.

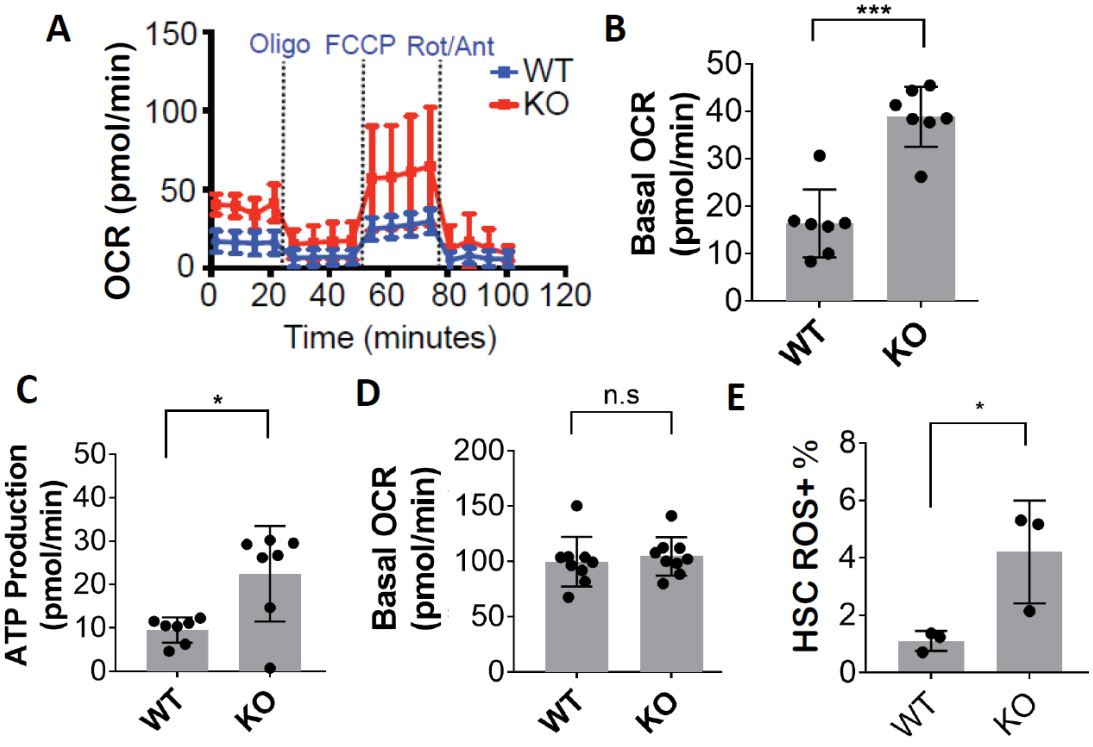

Figure 4-10: Elevated mitochondrial respiration and ROS in *Prdm16$^{fl/fl}$.Vav-Cre* adult HSCs. (**A**) Extracellular metabolic flux analysis of either *Cre*- (WT) or *Prdm16$^{fl/fl}$.Vav-Cre* (KO) HSCs. (*n* = 3 experiments in duplicate, 5 mice/experiment). First four data points represent basal respiration. Oligomycin treatment is used to calculate respiratory ATP production (positive readings here represent proton leak that does not generate ATP). FCCP is used to measure maximal respiratory capacity, and rotenone/antimycin treatment should reduce OCR to 0. (**B**) Basal oxygen consumption rate (OCR) and (**C**) Respiratory ATP production of either WT or KO HSCs. (**D**) Basal oxygen consumption rate (OCR) of WT and KO mouse embryonic fibroblasts (MEFs) (*n* = 3 experiments with technical triplicates) (**E**) Reactive oxygen species (ROS) measured by the percentage of CellROX-Deep Red positive WT or KO bone marrow HSCs (*n* = 3). (n.s = $P > 0.05$; * = $P < 0.05$; ** = $P < 0.01$; *** = $P < 0.001$, Student's t-test for single comparisons).

As we observed downregulation of Ras and Rho GTPase signaling pathways in *Prdm16*-deficient HSCs, and as these pathways play a major role in HSC homing and mobilization[355], we assessed the frequency of phenotypically defined HSCs in the peripheral blood of WT and *Prdm16*-deficient mice. We did not observe a difference, however, indicating that egress of HSCs from bone marrow into the periphery is likely not the cause of the hematopoietic defects observed in *Prdm16*-deficient mice (**Figure 4-11**).

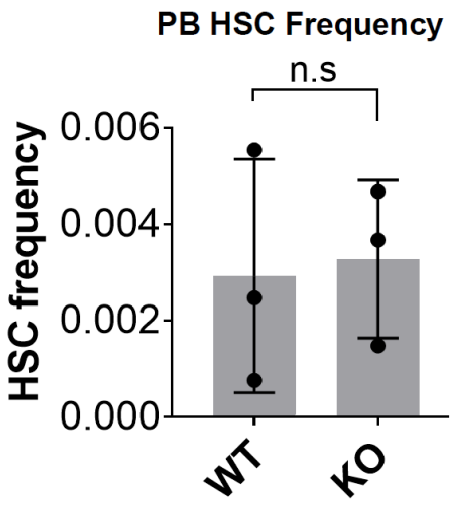

Figure 4-11: HSC peripheral blood frequency is unchanged in *Prdm16$^{fl/fl}$.Vav-Cre* mice. HSC frequency (percentage), defined as Lin$^-$Sca1$^+$cKit$^+$Flt3$^-$CD48$^+$, in the peripheral blood of 12-week old *Cre*- (WT) and *Vav-Cre$^{+/-}$ Prdm16$^{fl/fl}$* (KO) mice. (*n* = 3 mice) (P=0.79, Student's t-test for single comparisons)

4.2.3 Gene expression analysis of fetal liver *Prdm16$^{fl/fl}$.Vav-Cre$^+$* HSCs

Fetal and adult HSCs have functional and phenotypical differences. These include higher cycling levels, competitive repopulation efficiency, and a stronger lymphoid reconstitution bias in fetal liver HSCs compared to adult. They also express different transcription factors important for HSC maintenance, an example of which is Sox17 required for fetal liver, but not bone marrow, HSCs[356]. It remains unclear to what extent differences between fetal liver and bone marrow HSCs depend on intrinsic differences or external signaling from the microenvironment. *Prdm16$^{fl/fl}$.Vav-Cre$^+$* conditional deletion revealed significant defects in both adult and fetal liver HSCs, but effects were particularly severe in the fetal liver, with almost no donor chimerism detected in competitive transplants. We therefore performed RNAseq of fetal liver *Prdm16$^{fl/fl}$.Vav-Cre$^+$* HSCs to determine which pathways were similarly altered between *Prdm16*-deficient fetal liver and bone marrow HSCs. We isolated RNA from 3 biological replicates of (E)14.5 fetal liver Lin$^-$cKit$^+$Sca1$^+$CD48$^-$ HSCs, excluding Mac1 from the lineage cocktail, and performed RNA amplification and sequencing. 210 genes were significantly downregulated, while 242 genes were

upregulated. The top 50 upregulated and downregulated genes are presented in **Figure 4-12**. Principal component analysis (PCA) of the samples again showed a clear distinction between WT and *Prdm16*-deficient samples (**Figure 4-13A**). Pathway analysis revealed that, as with the adult HSCs, Rho and Ras GTPase signaling pathways, and related angiogenesis and cell migratory pathways, were downregulated in the *Prdm16*-deficient HSCs (**Figure 4-13B**). Importantly, we did not observe upregulation of respiratory pathways in the fetal liver *Prdm16*-deficient HSC cohort, as we observed in RNAseq and metabolic flux analysis of adult *Prdm16*$^{fl/fl}$*.Vav-Cre*$^{+}$ HSCs. Fetal liver HSCs are more oxidative and have higher basal levels of respiration compared to adult HSCs[28], which may explain why we did not detect respiratory differences between WT and *Prdm16*$^{fl/fl}$*.Vav-Cre*$^{+}$ HSCs in this compartment. It also suggests that it is unlikely that suppression of respiration by *Prdm16* in adult HSCs is the primary cause of HSC deficiency.

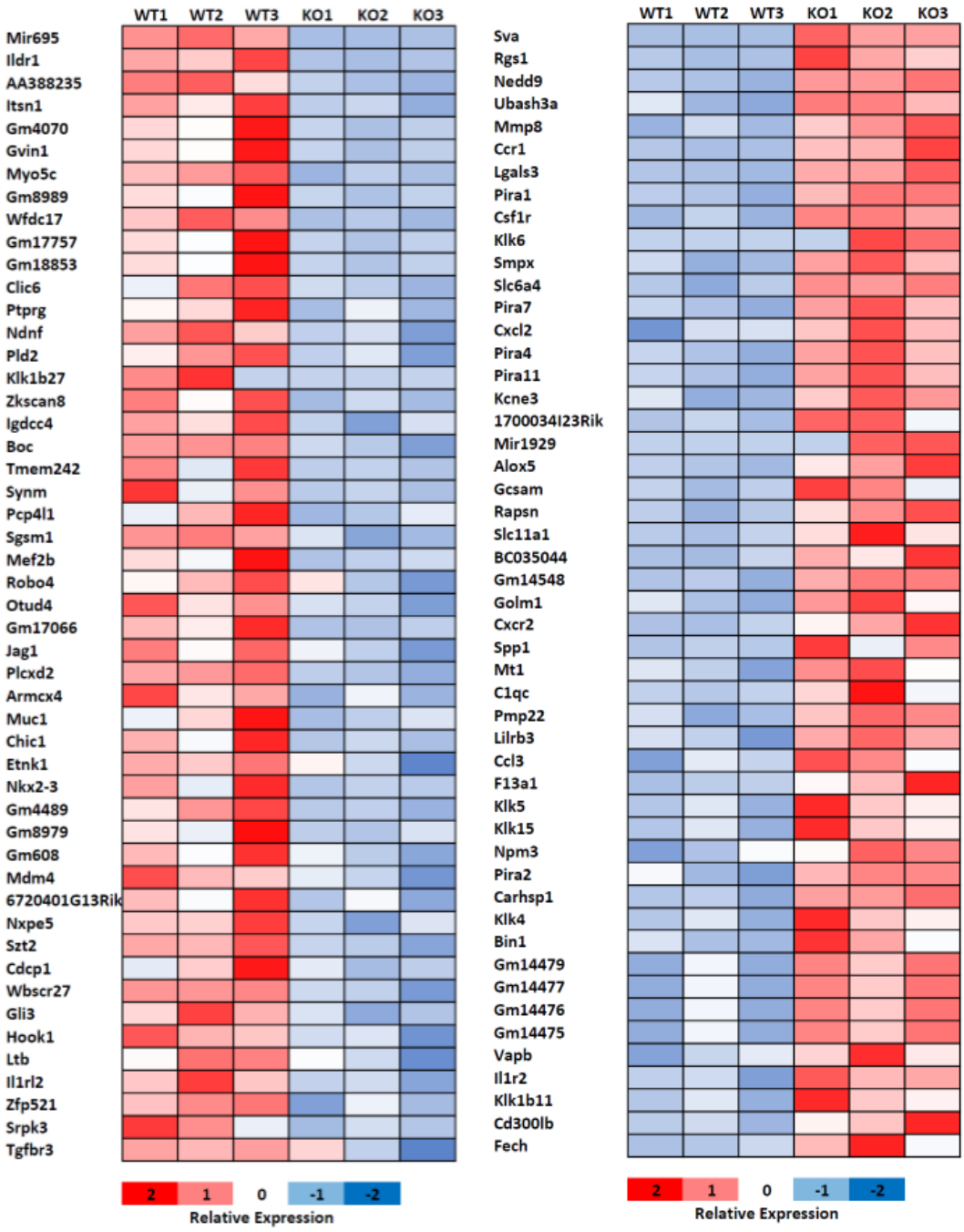

Figure 4-12: Genome-wide expression analysis of *Prdm16$^{fl/fl}$.Vav-Cre* fetal liver HSCs Heatmap of the top 50 genes (by *P*-value) upregulated in *Cre*$^{-}$ (WT, left panel) and *Vav-Cre*$^{+/-}$ *Prdm16$^{fl/fl}$* (KO, right panel) fetal liver HSCs, for each individual sample, as determined by RNAseq.

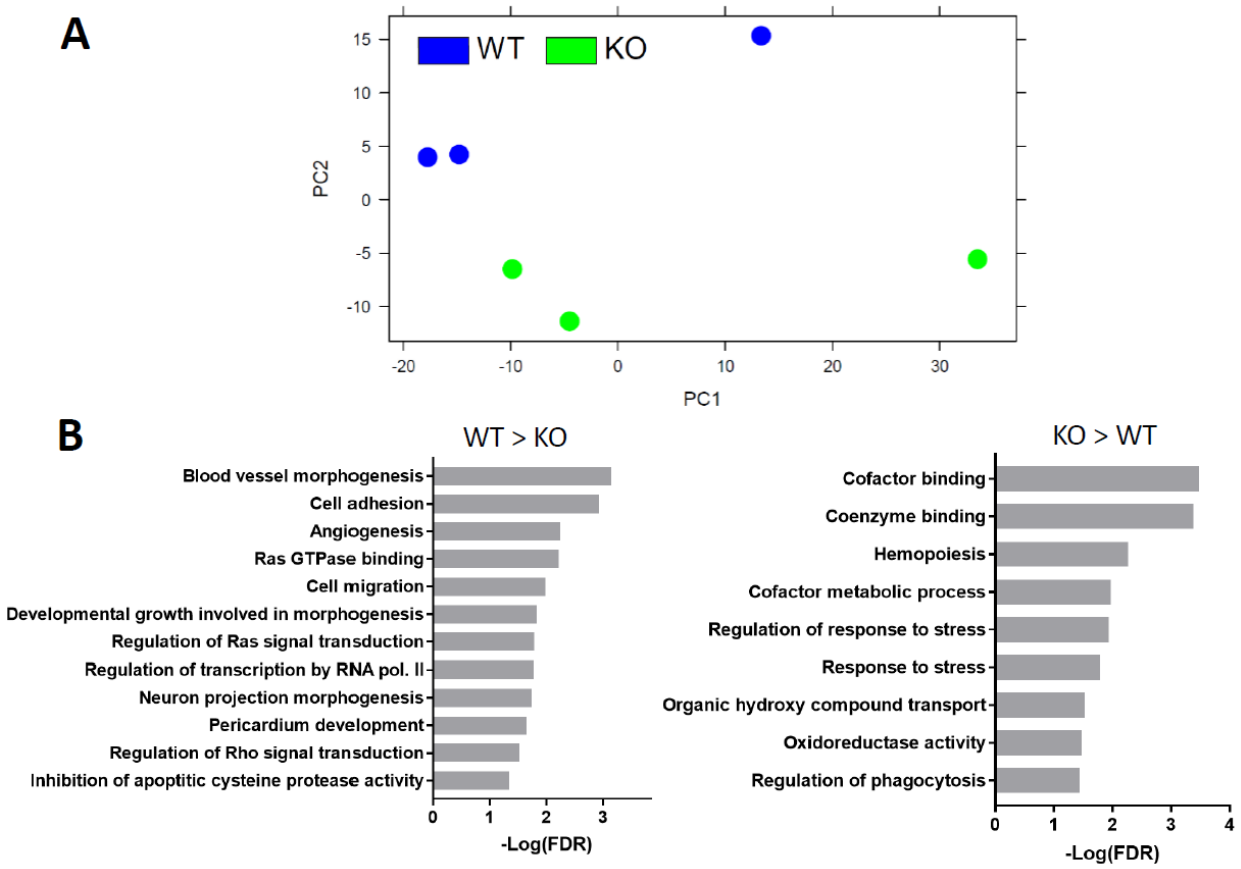

Figure 4-13: RNAseq Pathway analysis of *Prdm16$^{fl/fl}$.Vav-Cre* fetal liver HSCs (**A**) Principal component analysis (PCA) of individual WT and *Prdm16$^{fl/fl}$.Vav-Cre* (KO) fetal liver HSC RNAseq samples (**B**) GO pathways significantly downregulated in sorted Lin$^-$cKit$^+$Sca$^+$CD48$^-$CD150$^+$ KO fetal liver HSCs compared to WT littermates. (WT > KO – pathways downregulated in KO HSCs, KO > WT – pathways upregulated in KO HSCs). Values expressed as -Log$_{10}$ of the P-value, determined by PANTHER RNAseq analysis.

Section 4.3 – *f-Prdm16* is essential for HSC maintenance

4.3.1 Rationale/genetic overview of specific *f-Prdm16* and *s-Prdm16* deletion

In order to investigate the specific roles of each Prdm16 isoform in normal and malignant hematopoiesis, we attempted to generate mice with specific deletions of each isoform. As described in the introduction, the *f-Prdm16* gene contains 17 exons. The short isoform, *s-Prdm16*, begins translation within exon 4 of *f-Prdm16*. Therefore, exons 1-3 of *f-Prdm16* are specific to the full isoform, and perturbation of these exons should not affect *s-Prdm16*, making this a promising pathway to specific *f-Prdm16* deletion. We designed guide RNA (gRNA) sequences targeting exon 2 for CRISPR/Cas9-mediated disruption of the mouse genome (**Table 2**), to create indels for the purpose of inducing frameshifts and causing specific *f-Prdm16* deletion (**Figure 4-14**)

Table 2 - gRNA sequences used for CRISPR/Cas9 Prdm16 isoform deletion

CRISPR/Cas9 gRNA sequences	20bp gRNA sequence
Exon 2 Indel gRNA1	GACTCTCGTAGCTCGAAGTC
Exon 2 Indel gRNA2	CAAGGAGGGCTCGCCCTATG
Exon 2 Indel gRNA3	GGGGGACAGGATGCCGTCTT
SLTSS Intron 3 deletion 5' gRNA 1	AAGCTGCCAGCCCGTGGTCC
SLTSS Intron 3 deletion 5' gRNA 2	ACTGGCCTCGGGGGTCAGGC
SLTSS Intron 3 deletion 3' gRNA 1	CTTACAAGCAACCTCGGGGT
SLTSS Intron 3 deletion 3' gRNA 2	CTGTACTGGCCTCGGGGGTC

Specific deletion of *s-Prdm16* is conceptually more challenging. The entire *s-Prdm16* coding region is contained within the *f-Prdm16* coding region, and therefore any deletion would affect both isoforms. Furthermore, the translational start AUG is the only codon that produces a methionine residue, and therefore mutation of the *s-Prdm16* start ATG to prevent *s-Prdm16* translation would correspondingly mutate a methionine in *f-Prdm16* and make unclear whether any phenotype in these mice could be ascribed to either loss of *s-Prdm16* or mutation of *f-Prdm16*. If *f-Prdm16* and *s-Prdm16* are translated from separate mRNA molecules, blockade of *s-Prdm16* transcription would be an alternative method to

specifically delete *s-Prdm16*. The literature has proposed a number of potential transcriptional start sites (TSS) for *s-Prdm16*. These include sites in intron 1 (co-transcription with *f-Prdm16*), a distinct TSS within *Prdm16* exon 2 (which would disrupt *f-Prdm16* and is therefore not applicable), and a specific *s-Prdm16* TSS at the C-terminus of intron 3. The intron 3 TSS presented the only potential method for *s-Prdm16* deletion without affecting *f-Prdm16* (**Figure 4-14)**. We therefore designed CRISPR/Cas9 gRNA sequences flanking a 600bp region containing this putative *s-Prdm16* TSS (two gRNAs for the 5'end and two for the 3'end, listed in **Table 2**) in an attempt to specifically ablate *s-Prdm16*.

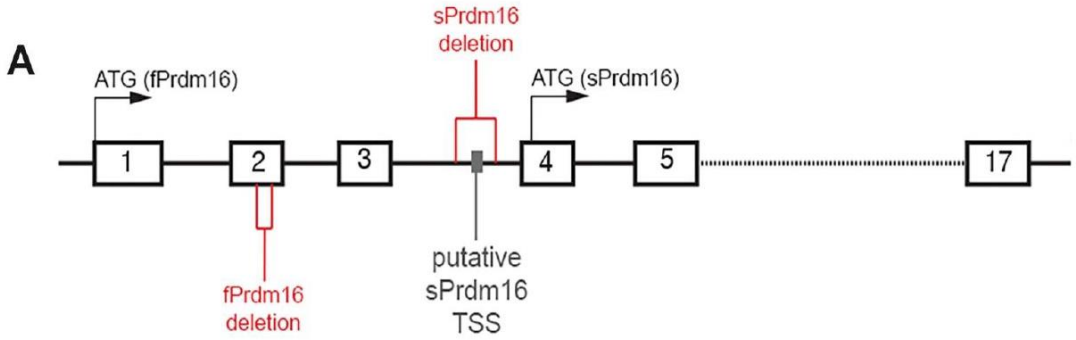

Figure 4-14: Schematic of CRISPR/Cas9 targeting strategies for *f-Prdm16* and *s-Prdm16* deletion. Schematic representation of regions targeted in CRISPR/Cas9 *Prdm16* isoform-deletion experiment, highlighting exon structure, *f-Prdm16* and *siPrdm16* start codons, and putative *sPrdm16* TSS in intron 3. Deletion of *f-Prdm16* was attempted by CRISPR/Cas9 targeting of Exon 2. Deletion of *s-Prdm16* was attempted by using CRISPR/Cas9 to delete a region containing a putative transcriptional start site (TSS) for *s-Prdm16* in intron 3.

4.3.2 Deletion of the putative intron 3 *s-Prdm16* TSS does not delete *s-Prdm16* in HSCs

Fertilized C57BL/6 embryos were injected with a cocktail of PX330 plasmid DNA containing gRNA sequences (**Table 2**) designed to specifically flank and delete the *s-Prdm16* TSS in intron 3. PX330 is an all-in-one vector containing CRISPR/Cas9 and the targeting gRNA. Blastocyst injection was performed by Victor Lin at the Columbia Mouse Transgenic Core. We obtained chimeric mice containing a fraction of somatic cells and gametes with the 600bp region deleted. These mice were crossed to WT C57BL/6 mice

to generate heterozygotes, which were then crossed together to produced homozygous WT, homozygously-deleted (*SL-TSS*$^{-/-}$), or heterozygous (*SL-TSS*$^{+/-}$) progeny. DNA sequencing confirmed a deletion of approximately 600bp, from positions -641 to -76 of intron 3, which included the putative TSS located at position -470 (**Figure 4-15**). Thus, we did in fact delete the desired region in these mice.

```
Intron3     AGATTAGAGCTTACCATAGGCACTGAGCAAAGCAGGCAAGAGCTGGAAAGGTCTATTGCACCTAAAGCTGCCAGCCCGTGGTCCAGGTCTTCTTACAAGC   -656
WT          AGATTAGAGCTTACCATAGGCACTGAGCAAAGCAGGCAAGAGCTGGAAAGGTCTATTGCACCTAAAGCTGCCAGCCCGTGGTCCAGGTCTTCTTACAAGC   -656
SLTSS KO    AGATTAGAGCTTACCATAGGCACTGAGCAAAGCAGGCAAGAGCTGGAAAGGTCTATTGCACCTAAAGCTGCCAGCCCGTGGTCCAGGTCTTCTTACAAGC   -656

Intron3     AACCTCGGGGTGGGGGTGGGGAGACAGAGATCAGCAAACCAGTCTCTGCAGCTAAGTTCAGAAGATAGCATCAACAACAAAGAGAATGAGCAGAACACGG   -556
WT          AACCTCGGGGTGGGGGTGGGGAGACAGAGATCAGCAAACCAGTCTCTGCAGCTAAGTTCAGAAGATAGCATCAACAACAAAGAGAATGAGCAGAACACGG   -556
SLTSS KO    AACCTCGGGGTGGGGG----------------------------------------------------------------------------------   -556

                                                                                          Putative S-PRDM16 TSS
Intron3     TGAGGAAGCTGAGCATCTGTGTGCTGGCCAGGGCCAAACTGAGACTTTCCAGTTGAAAGGAAACAATGTTTTCTGGCATTCAGGTGGTGTGATGTCCGAC   -456
WT          TGAGGAAGCTGAGCATCTGTGTGCTGGCCAGGGCCAAACTGAGACTTTCCAGTTGAAAGGAAACAATGTTTTCTGGCATTCAGGTGGTGTGATGTCCGAC   -456
SLTSS KO    ----------------------------------------------------------------------------------------------------   -456

Intron3     AGGAGCAGGTACACTCAGGCAAAAGTGTTGTGCACGCACAGGCTCACACACCAGGACTTGGGTGCAGCCACACACCCTCATAACACCTTTAGCTTCAGAC   -356
WT          AGGAGCAGGTACACTCAGGCAAAAGTGTTGTGCACGCACAGGCTCACACACCAGGACTTGGGTGCAGCCACACACCCTCATAACACCTTTAGCTTCAGAC   -356
SLTSS KO    ----------------------------------------------------------------------------------------------------   -356

Intron3     ATGCTCTTTCTAGGTCAACACCCCACTGTCTTTGGGGGGTCATGTCAGACACAAGAAGGCTCTGCTTTCTCACACCTGGACAGCCTACTGGAAGGTTTTA   -256
WT          ATGCTCTTTCTAGGTCAACACCCCACTGTCTTTGGGGGGTCATGTCAGACACAAGAAGGCTCTGCTTTCTCACACCTGGACAGCCTACTGGAAGGTTTTA   -256
SLTSS KO    ----------------------------------------------------------------------------------------------------   -256

Intron3     CTGTGCTAGAGACTCGTCATTGCCTAACCTGACTGAAAGCTATTCTCTACGAACTAGAAAGGCCACCTGCTTCTCTCCTCCAATCTCCTGGAGGTTCCTA   -156
WT          CTGTGCTAGAGACTCGTCATTGCCTAACCTGACTGAAAGCTATTCTCTACGAACTAGAAAGGCCACCTGCTTCTCTCCTCCAATCTCCTGGAGGTTCCTA   -156
SLTSS KO    ----------------------------------------------------------------------------------------------------   -156

Intron3     GGACCAGGTGGCCTGGGTGGACAGAGTCTCTCCTTGCCTAGAACTGGGTGAGGTCTTAGACAACCTGCCATCCTGCCTGACCCCCGAGGCCAGTACAGCG   -56
WT          GGACCAGGTGGCCTGGGTGGACAGAGTCTCTCCTTGCCTAGAACTGGGTGAGGTCTTAGACAACCTGCCATCCTGCCTGACCCCCGAGGCCAGTACAGCG   -56
SLTSS KO    ----------------------------------------------------------CCATCCTGCCTGACCCCCGAGGCCAGTACAGCG   -56

Intron3     TGATATAACACACACAGGACAGGCACCTCTGACCTCAGGTGTGTTTCTTCCCCAG   0
WT          TGATATAACACACACAGGACAGGCACCTCTGACCTCAGGTGTGTTTCTTCCCCAG   0
SLTSS KO    TGATATAACACACACAGGACAGGCACCTCTGACCTCAGGTGTGTTTCTTCCCCAG   0
```

Figure 4-15: *SL-TSS*$^{-/-}$ mice have a 600bp deletion which includes the putative *s-Prdm16* TSS. Alignment of sequencing results from intron 3 of a WT mouse and a putative *sPrdm16-TSS KO* (SLTSS KO). Sequencing results are aligned to the final 755 nucleotides of *Prdm16* intron 3 and illustrate loss of the putative *s-Prdm16* TSS from the SLTSS KO mice, which is highlighted in yellow.

SL-TSS$^{-/-}$ mice were viable and born in Mendelian ratios (**Figure 4-16A**), in contrast to the global *Prdm16* deletion which is not viable. To compare mRNA expression of individual *Prdm16* isoforms, we developed a method of subtractive qPCR. We designed primers specific for *f-Prdm16* across the exon 2/3 junction, and primers for total *Prdm16* across the exon 14/15 junction (**Figure 4-16B**). Using this method in

conjunction with a standard curve, copy number per cell estimates for each isoform were obtained. *S-Prdm16* is calculated by subtracting *f-Prdm16* from total *Prdm16.* We isolated HSCs from adult *SL-TSS*$^{-/-}$ mice and WT littermate controls and performed subtractive qPCR. Our results showed that there was no specific loss of *s-Prdm16* mRNA in the HSCs of these mice (**Figure 4-16C**).

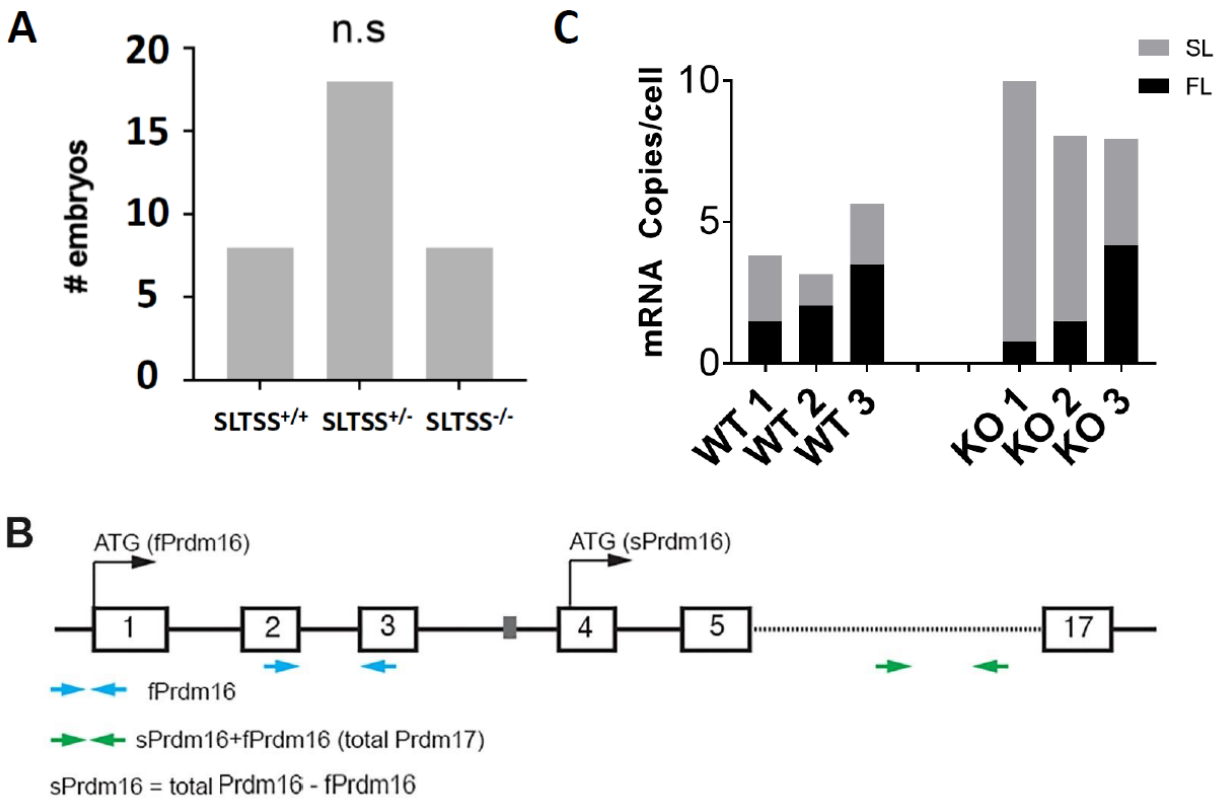

Figure 4-16: Characterization of *SL-TSS* mouse and description of *Prdm16* isoform-specific qPCR. (**A**) *SLTSS*$^{-/-}$ mice are viable and born in Mendelian ratios. Quantification of number of mice born with each indicated genotype (n = 34 mice from 4 litters). (**B**) Schematic of subtractive qPCR used to determine copy number of *s-Prdm16* mRNA. Probes in exon 2/3 are specific for *f-Prdm16* and probes in exon 14/15 are used to calculate total *Prdm16*. *S-Prdm16* is calculated by subtracting *f-Prdm16* from total *Prdm16*. (**C**) Quantification based on subtractive qPCR of *Prdm16* isoform copy number from mice deleted for the *sPrdm16* putative TSS (KO) compared to WT littermates shows no decrease in *s-Prdm16* mRNA copy number.

Although isoform-specific qPCR demonstrated that deletion of the intron 3 putative *s-Prdm16* TSS did not affect the expression of this isoform, we nonetheless examined hematopoietic phenotypes in these mice,

to confirm the absence of any hematopoietic defect. *SL-TSS*$^{-/-}$ mice did not have any differences in bone marrow HSC frequency or absolute number (**Figure 4-17A**). More importantly, competitive transplantations of *SL-TSS*$^{-/-}$ bone marrow did not show any defects compared to bone marrow from HSC littermates (**Figure 4-17B**). Taken together, the lack of a decrease in *s-Prdm16* mRNA message and the absence of any discernable hematopoietic phenotype indicates that deletion of the putative TSS in intron 3 does not affect *s-Prdm16* expression. It is likely, therefore, that at least in the hematopoietic system *s-Prdm16* is transcribed from an alternate TSS, a conclusion supported by the multiple potential TSS for *s-Prdm16* described in the literature.

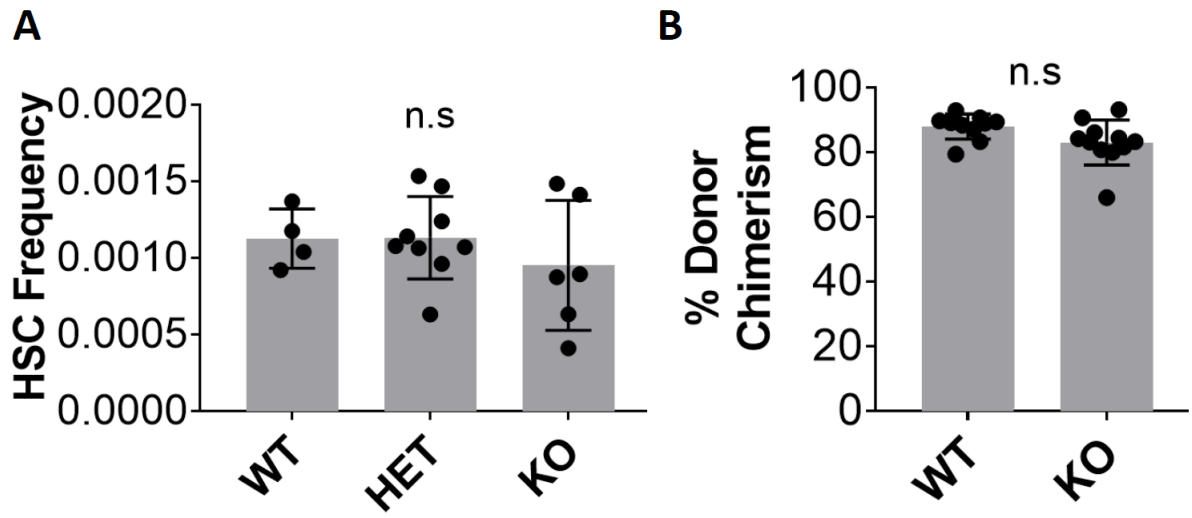

Figure 4-17: *SL-TSS*$^{-/-}$ mice have a normal hematopoietic phenotype. (**A**) Bone marrow HSC frequency ($Lin^-Sca1^+cKit^+Flt3^-CD48^-CD150^+$) in WT, KO, or SL-TSS-heterozygous (HET) mice. (**B**) Peripheral blood (PB) donor chimerism of transplanted WT or KO bone marrow HSCs in competitive transplants with CD45.1 BM, measured 16-weeks post-transplant (*n* = 10-11 recipients from 3 independent experiments). (n.s = *P* > 0.05; One-way ANOVA for multiple comparisons or Student's t-test for single comparisons).

4.3.3 Generation of a specific *f-Prdm16* deletion in mice which is lethal and causes a severe defect in HSC maintenance

To specifically delete *f-Prdm16*, we injected fertilized C57BL/6 embryos with PX330 plasmid containing gRNA sequences targeting exon 2 of *Prdm16*. Two chimeric mice were obtained from the litter, which

were bred to WT C57BL/6 mice to generate heterozygotes. Sequencing of DNA from the two mice revealed two distinct indels, one 47bp long and another 13bp long (*Δ47-fPrdm16*$^{+/-}$ and *Δ13-fPrdm16*$^{+/-}$) (**Figure 4-18A**). Both of these deletions are indivisible by three and therefore frameshifting, and both lead to premature stop codons shortly after deletion (**Figure 4-18B**).

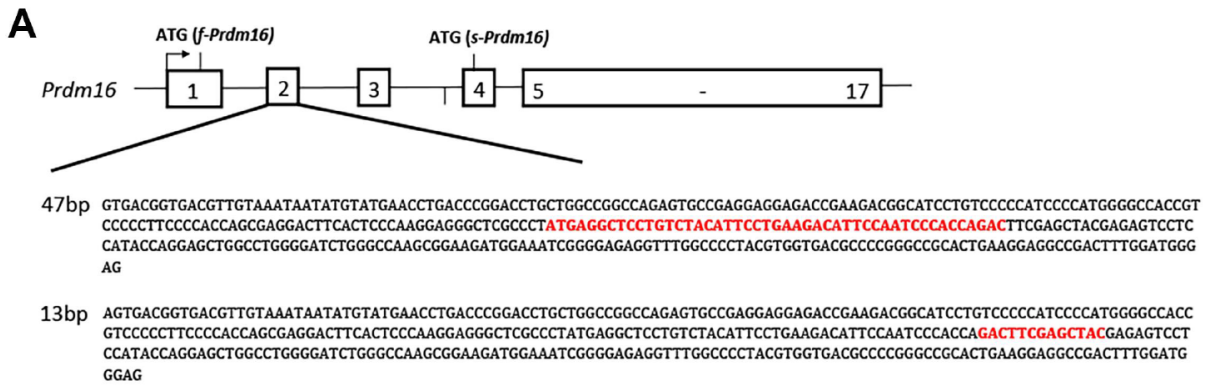

Figure 4-18: Generation of two mouse strains with frameshifting indels in *Prdm16* exon 2. (**A**) Map of the 47bp and 13bp deletions (in red) obtained from mice using CRISPR/Cas9 pronuclear injection of gRNA targeting *Prdm16* exon 2. (**B**) Comparison of the frameshifted amino acid sequences (red) from 47bp and 13bp deletions to WT. Both frameshifts lead to premature stop codons (*) shortly after deletion.

Paired breeding of either heterozygous *Δ47-fPrdm16*$^{+/-}$ or *Δ13-fPrdm16*$^{+/-}$ mice produced progeny with no homozygous deleted mice, signifying that a global deletion of *f-Prdm16* is a lethal mutation in mice. Therefore, as with the global *Prdm16*$^{-/-}$ deletion, fetal liver needed to be studied to discern hematopoietic properties. Day (E)13.5-16.5 embryos were distributed in Mendelian ratios (**Figure 4-19A**). To confirm a specific loss of *f-Prdm16* in these mice, we employed subtractive qPCR of fetal liver HSCs as described in Figure 4-16B. We detected a loss of *f-Prdm16,* but not *s-Prdm16* in these cells, when calculated as either

mRNA molecules per cell or by percentage (**Figure 4-19B**). We therefore concluded that the *Δ47-fPrdm16*$^{-/-}$ and *Δ13-fPrdm16*$^{-/-}$ frameshifting mutations result in a specific, global deletion of *f-Prdm16*, or, viewed from the opposite perspective, a "*s-Prdm16*-only" genotype.

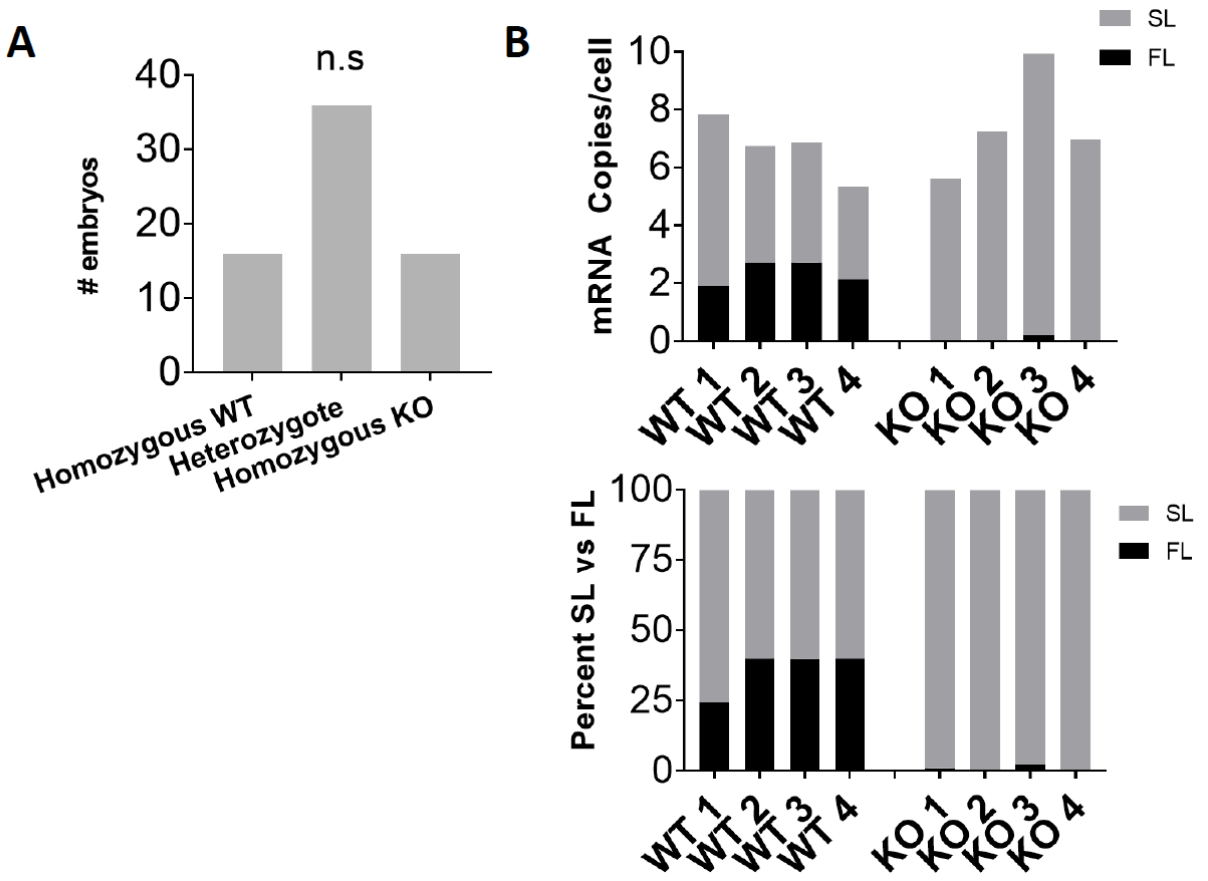

Figure 4-19: Global *f-Prdm16* deletion is embryonic lethal and retains expression of *s-Prdm16*. (**A**) Mendelian distribution of E13.5-15.5 embryos of *Δ47-fPrdm16* mice (*n* = 62). (**B**) Subtractive qPCR quantification of *Prdm16* isoform mRNA copy number (top panel) and percent isoform expression (bottom panel) from fetal liver HSCs of *Δ47-fPrdm16*$^{-/-}$ (KO) and WT littermates shows selective loss of *f-Prdm16* in the mutants. (n.s = *P* > 0.05, Chi-square test)

Having confirmed the specificity of *f-Prdm16* global deletion, we next assessed the hematopoietic phenotype of these mice, using fetal livers. In both the *Δ47-fPrdm16*$^{-/-}$ and *Δ13-fPrdm16*$^{-/-}$ mice, the frequency (**Figure 4-20A**) and absolute number (**Figure 4-20B**) of HSCs ($Lin^{-}cKit^{+}Sca1^{+}CD48^{-}CD150^{+}$) was significantly reduced compared to WT littermates. There was no difference in the frequency of LSK cells,

however, indicating a specific depletion in HSCs without a loss of downstream progenitors (**Figure 4-20C**). Notably, we saw an intermediate phenotype in heterozygous *Δ47-fPrdm16*$^{+/-}$ and *Δ13-fPrdm16*$^{+/-}$ fetal liver. This is similar to what our lab previously observed in total *Prdm16*$^{+/-}$ fetal liver, where heterozygotes had an intermediate phenotype between WT and homozygous KO. Because we observed an identical phenotype in both *Δ47-fPrdm16*$^{-/-}$ and *Δ13-fPrdm16*$^{-/-}$ fetal liver, further experiments were performed with *Δ47-fPrdm16*$^{-/-}$ mice. Furthermore, the strong similarity between the *Δ47-fPrdm16*$^{-/-}$ and *Δ13-fPrdm16*$^{-/-}$ fetal liver compartments substantially reduces the chances of artifacts due to a non-specific gRNA targeting event. Experimental WT littermate controls were also derived from CRISPR/Cas9 blastocyst injection. Therefore, any non-specific off-target deletions should be randomly distributed between WT and *Δ47-fPrdm16*$^{-/-}$ or *Δ13-fPrdm16*$^{-/-}$ mice. Finally, the fact that *SL-TSS*$^{-/-}$ mice had no hematopoietic phenotype argues against the possibility of off-target effects.

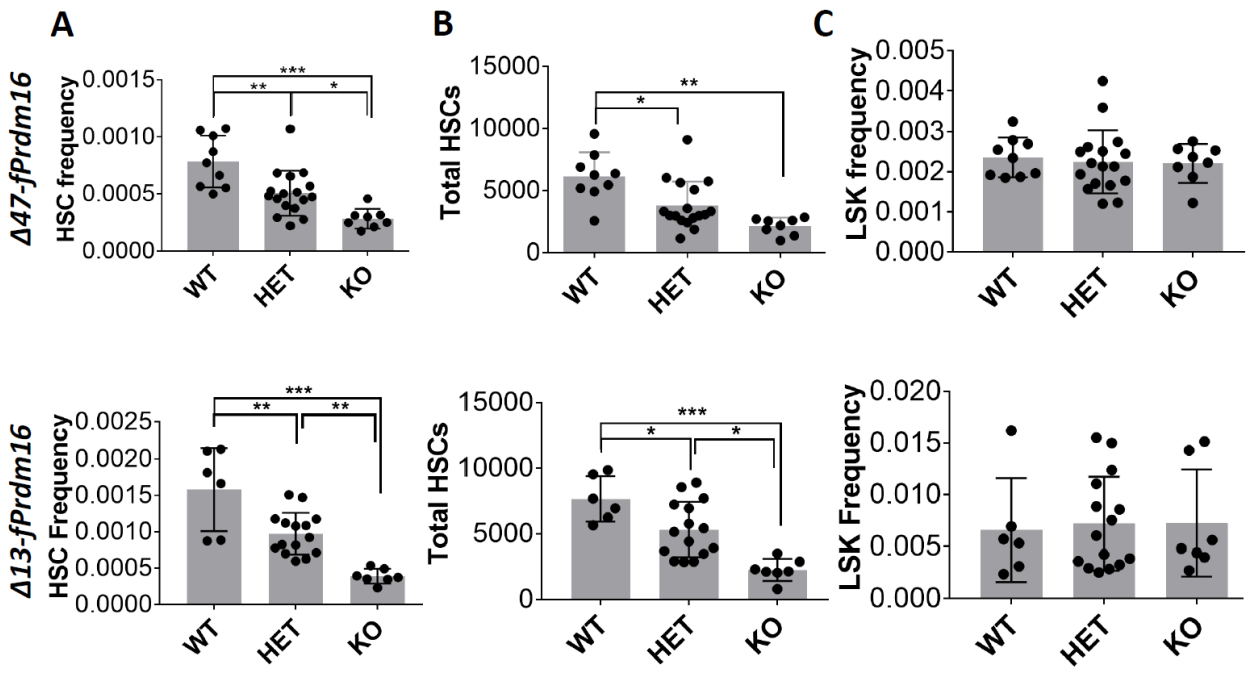

Figure 4-20: Specific loss of HSCs in *f-Prdm16*$^{-/-}$ fetal liver. (**A**) Frequency (%) and (**B**) absolute number of HSCs (Lin$^-$cKit$^+$Sca1$^+$CD48$^-$CD150$^+$) in fetal liver of *Δ47-fPrdm16*$^{-/-}$ (KO), *Δ47-fPrdm16*$^{+/-}$ (HET) and WT littermate mice (n = 34 mice), or *Δ13-fPrdm16*$^{-/-}$ (KO), *Δ13-fPrdm16*$^{+/-}$ (HET) and WT (n = 28 mice). (**C**) Frequency of LSK cells (Lin$^-$Sca1$^+$cKit$^+$) using the same fetal liver samples from (A). (P > 0.25 for all comparisons). (n.s = P > 0.05; * = P < 0.05; ** = P < 0.01; *** = P < 0.001, One-way ANOVA for multiple comparisons)

We then performed competitive transplants of *Δ47-fPrdm16*$^{-/-}$ and WT littermate fetal liver to compare the effect of *f-Prdm16* deletion on HSC maintenance. *Δ47-fPrdm16*$^{-/-}$ fetal liver cells showed a severe repopulation defect, on a similar order to that observed in *Prdm16*$^{-/-}$ fetal liver (**Figure 4-21A**). However, in stark contrast to *Prdm16*$^{-/-}$ competitive transplants, the few reconstituting donor *Δ47-fPrdm16*$^{-/-}$ cells were strongly lymphoid biased compared to repopulating WT cells, and within the lymphoid population, were further biased toward the B-cell lineage (**Figure 4-21B**). A comparison of proliferation and apoptosis between *Δ47-fPrdm16*$^{-/-}$ and WT HSCs showed no significant differences – both HSC populations had similar levels of cycling (**Figure 4-21C**), as measured by Ki-67 staining, and apoptosis, measured as the percentage of HSCs expressing cleaved Caspase3 (**Figure 4-21D**). Furthermore, and similar to global

Prdm16$^{-/-}$ fetal liver and *Prdm16*$^{fl/fl}$*.Vav-Cre* bone marrow, there was no defect in engraftment of donor cells to the bone marrow after 24 hours in *Δ47-fPrdm16*$^{-/-}$ fetal liver cells (**Figure 4-21E**).

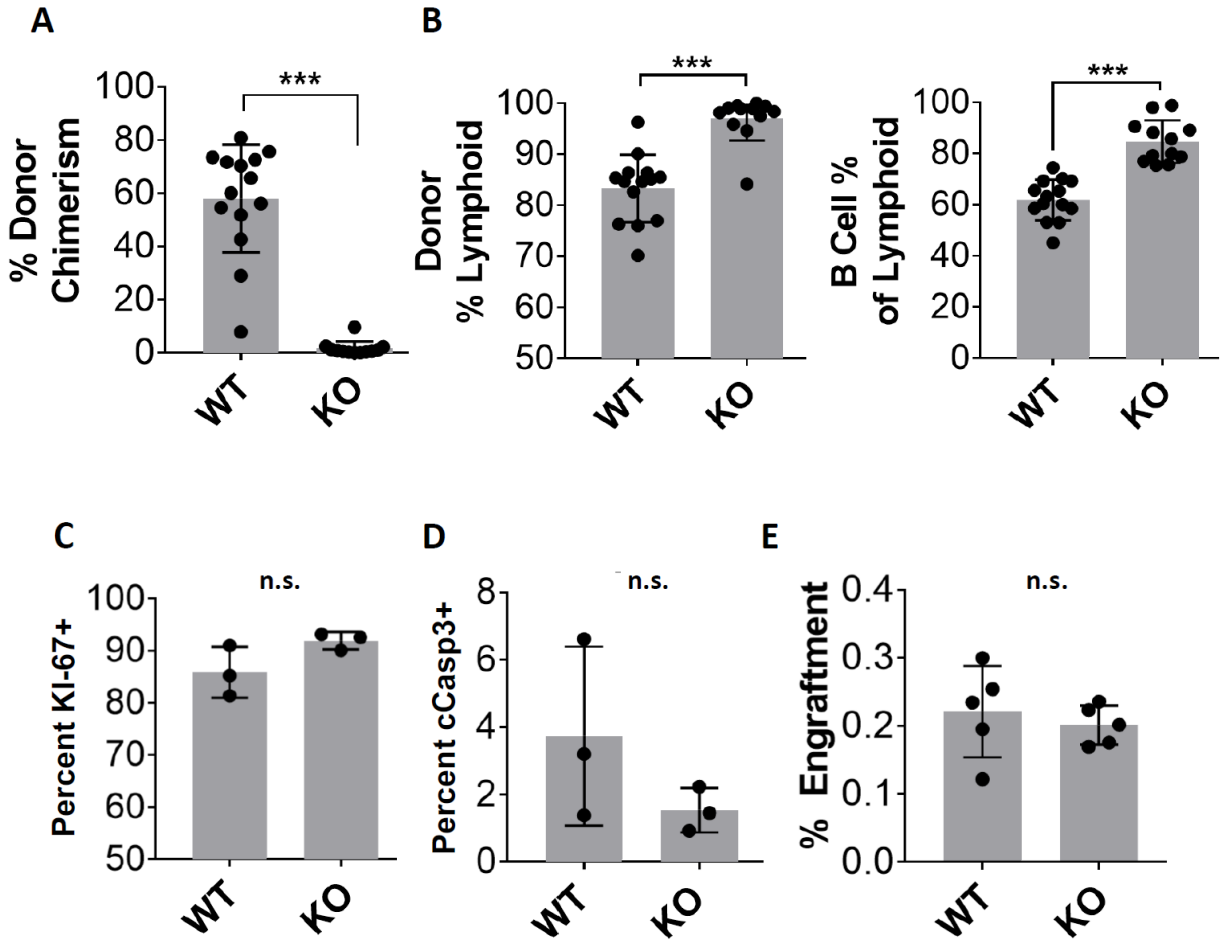

Figure 4-21: Severe HSC reconstitution defect and B-cell bias in *Δ47-fPrdm16*$^{-/-}$ HSCs. (**A**) Peripheral blood donor chimerism of transplanted *Δ47-fPrdm16*$^{-/-}$ (KO) and WT littermate fetal liver HSCs in competitive transplants with CD45.1 bone marrow, measured 16-weeks post-transplant (*n* = 12-14 mice, 3 independent transplants). (**B**) Percent of donor cells from (A) that were lymphoid (CD19^{+} or CD3^{+}) and the percentage of those that were B-cells (CD19^{+}) (*n* = 12-14). (**C**) Percent KI-67^{+} and (**D**) cleaved Caspase3^{+} FL HSCs in *Δ47-fPrdm16*$^{-/-}$ and WT littermate embryos (*n* = 3). (**E**) Percent donor CD45.2 cells in bone marrow of recipient mice 24 hours after transplantation of fetal liver cells from either *Δ47-fPrdm16* (KO) or WT littermates. (*n* = 5 recipient mice). (n.s = $P > 0.05$; * = $P < 0.05$; ** = $P < 0.01$; *** = $P < 0.001$, One-way ANOVA for multiple comparisons or Student's t-test for single comparisons).

Repopulating fetal liver HSCs are lymphoid-biased compared to adult HSCs, but even taking this into account, *Δ47-fPrdm16*$^{-/-}$ repopulation was exceptionally lymphoid-biased – almost entirely comprised of lymphoid cells, particularly CD19^{+} B-cells. Our results demonstrate that the *f-Prdm16* isoform is essential to HSC maintenance as deletion results in a defect in competitive transplantation similar to the *Prdm16*$^{-/-}$ and *Prdm16*$^{fl/fl}$*.Vav-Cre*$^{+}$ deletions. The *Δ47-fPrdm16*$^{-/-}$ mouse, however, can conversely be thought of as a "*s-Prdm16* only" mouse, and the fact that there is a strong lymphoid bias among the few reconstituting cells suggest that *s-Prdm16* supports limited lymphoid reconstitution, but is not sufficient for the effective maintenance of HSCs.

Section 4.4 – *s-Prdm16* supports the development of a Lin-Sca1+cKit- B-cell precursor

4.4.1 Bone marrow analysis of *Δ47-fPrdm16*$^{-/-}$ competitive transplantations reveals selective maintenance of LSK- precursors

To further investigate the apparent lymphoid and B-cell bias of *Δ47-fPrdm16*$^{-/-}$ mice, we performed a tissue analysis of recipient mice from *Δ47-fPrdm16*$^{-/-}$ or WT littermate fetal liver competitive transplantations. Analysis was performed on sacrificed recipients after 16-week peripheral blood collection. Analysis of donor chimerism in different tissues revealed that *Δ47-fPrdm16*$^{-/-}$ HSCs have a similarly severe repopulation defect in recipient bone marrow, spleen, and thymus (**Figure 4-22A**). Within the bone marrow, donor-derived LSK cells, common lymphoid progenitors (CLPs), common myeloid progenitors (CMPs), granulocyte-monocyte progenitors (GMPs) and megakaryocyte-erythroid progenitors (MEPs) were all similarly reduced in recipients of *Δ47-fPrdm16*$^{-/-}$ cells compared to WT littermates, determined by comparing relative donor frequency between *Δ47-fPrdm16*$^{-/-}$ and WT transplants (**Figure 4-22B**). However, a population of Lin^{-}Sca1^{+}cKit^{-} (termed LSK-) cells was strikingly overrepresented relative to all other donor populations in the bone marrow of recipients of *Δ47-fPrdm16*$^{-/-}$ cells (**Figure 4-22C**). In the *Δ47-fPrdm16*$^{-/-}$ recipients, the donor frequency of LSK- cells was approximately 20-fold higher than the relative frequency of other cell populations, strongly suggesting that *Δ47-fPrdm16*$^{-/-}$ mice, though severely impaired in HSC maintenance, are nonetheless able to selectively generate this LSK- progenitor compartment, pointing to a role for *s-Prdm16* (which remains expressed in *Δ47-fPrdm16*$^{-/-}$ mice) in the differentiation or maintenance of these cells. A representative flow plot illustrating the surface phenotype of LSK- cells is provided in **Figure 4-23**.

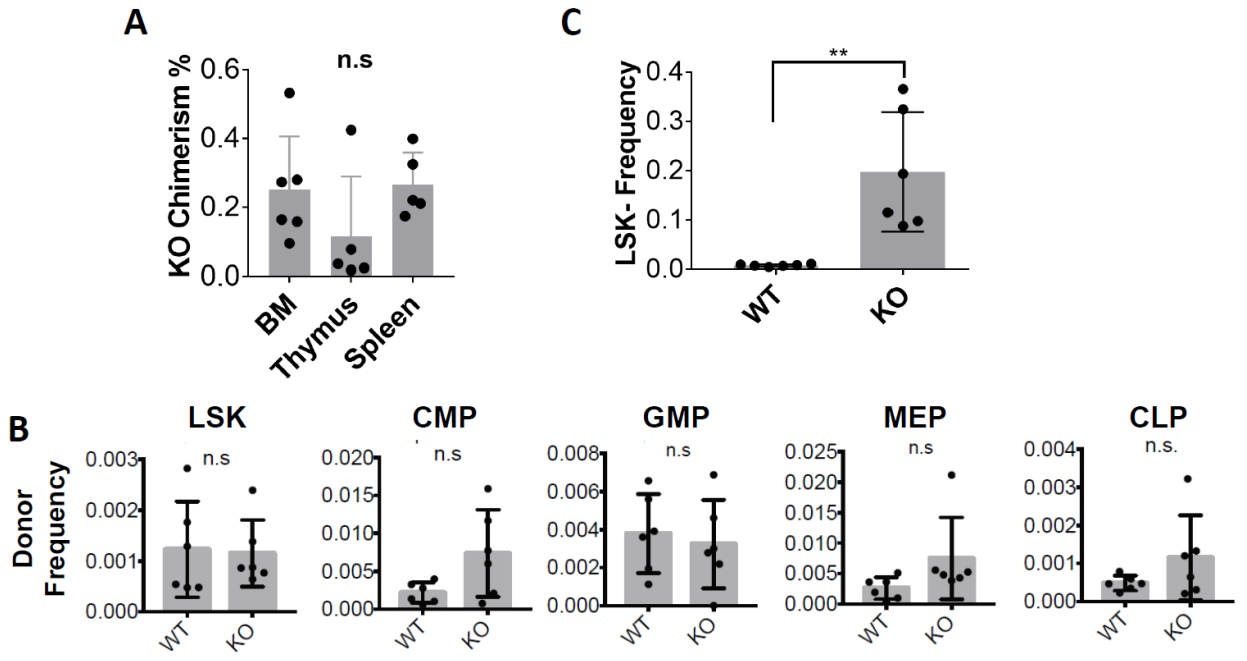

Figure 4-22: Selective maintenance of LSK- cells in *Δ47-fPrdm16*$^{-/-}$ competitive transplants. (**A**) Donor chimerism of transplanted *Δ47-fPrdm16*$^{-/-}$ fetal liver (KO) cells in bone marrow (BM), thymus, and spleen, 16-weeks after competitive transplant with CD45.1 BM (n = 6). (**B**) Donor frequency of progenitor populations 16 weeks after competitive transplantation of *Δ47-fPrdm16*$^{-/-}$ (KO) or WT littermate fetal liver cells, expressed as percent of CD45.2 donor cells in each progenitor population: LSK ($Lin^-Sca1^+cKit^+$), CMP ($Lin^-Sca1^-cKit^+CD34^+CD16/32^{lo}$), GMP ($Lin^-Sca1^-cKit^+CD34^+CD16/32^{mid}$), MEP ($Lin^-Sca1^-cKit^+CD34^-CD16/32^{lo}$), and CLP ($Lin^-Sca1^{lo}cKit^{lo}IL7ra^+Flt3^+$) ($n$ = 6 recipients from 2 independent transplants). (**C**) Donor LSK^- frequency in recipients of WT and *Δ47-fPrdm16*$^{-/-}$ (KO) fetal liver cells (n = 6). (n.s = $P > 0.05$; * = $P < 0.05$; ** = $P < 0.01$; *** = $P < 0.001$, One-way ANOVA for multiple comparisons or Student's t-test for single comparisons).

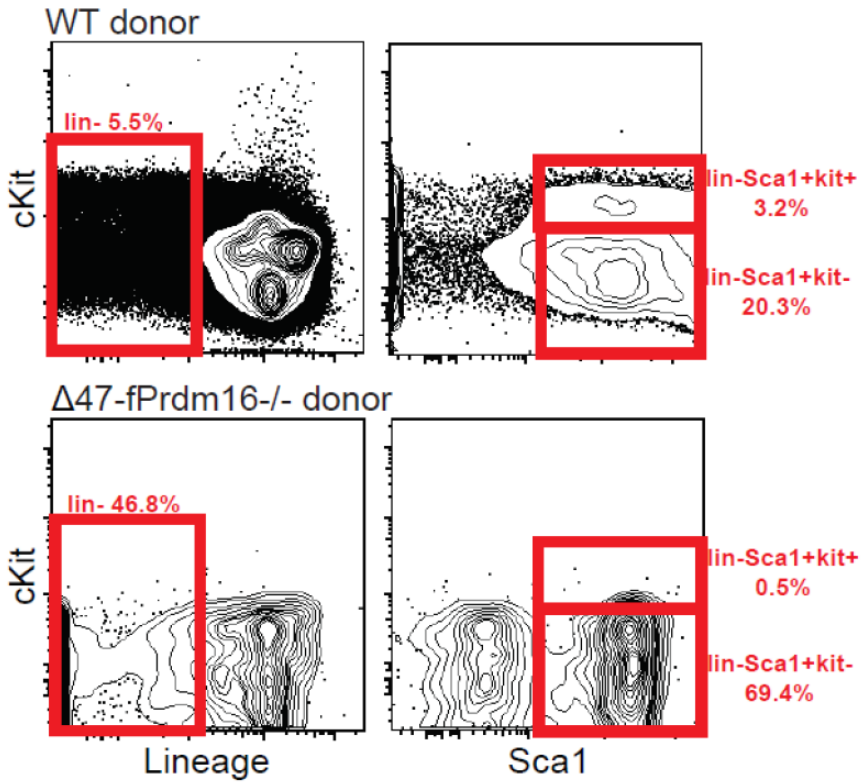

Figure 4-23: Representative flow plots of LSK- cells in *Δ47-fPrdm16*$^{-/-}$ and WT transplants. Representative flow plots illustrating the gating of Lin^{-}Sca1^{+}cKit^{-} (LSK^{-} cells) and showing the difference in LSK^{-} frequency between *Δ47-fPrdm16*$^{-/-}$ (KO) and WT littermate transplants.

A previous publication from our lab showed that the LSK- population, which does not express cKit but expresses more Sca1 than LSK cells, is enriched for a specific lymphoid progenitor distinct from CLPs[67]. Further work showed that LSK- cells possessed mainly B-cell potential and displayed a higher propensity to generate splenic marginal zone (MZ) B-cells in comparison to CLPs. This can be quantified by calculating the proportion of MZ B-cells (expressing the B-cell marker CD19 with a CD21^{hi}CD23^{lo} phenotype) to follicular (FO) B-cells (expressing CD19 and CD21^{lo}CD23^{hi})[68]. In addition, our lab showed that B-cells generated from LSK- cells had higher expression of Sca1 than those derived from CLPs.

We analyzed spleens of recipient mice from *Δ47-fPrdm16*$^{-/-}$ and WT competitive transplants and found that within the population of splenic donor B-cells (CD19^{+} cells), there was a significantly higher

percentage of donor CD21^{hi} MZ cells and a lower percentage of CD23^{hi} FO cells, presented as the MZ/FO ratio (**Figure 4-24A** with representative flow plot in **Figure 4-24B**). Furthermore, flow cytometric analysis revealed increased Sca1 mean fluorescence intensity (MFI) on donor MZ B-cells from *Δ47-fPrdm16*$^{-/-}$ compared to WT transplants (**Figure 4-24C** and **24D**). Taken together, these results show that *Δ47-fPrdm16*$^{-/-}$ HSPCs can generate LSK- cells, suggesting a role for *s-Prdm16* in this process.

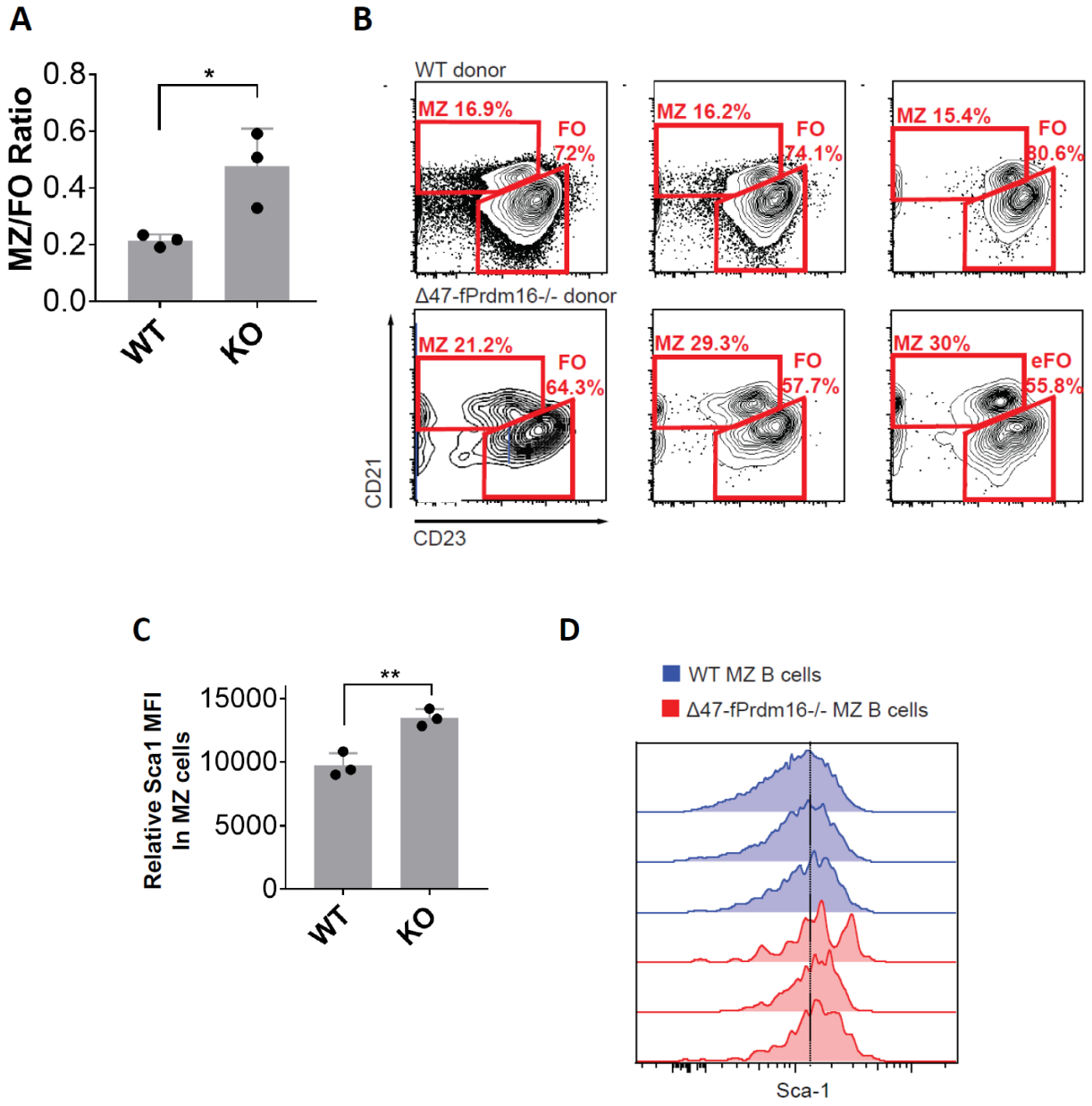

Figure 4-24: Donor *Δ47-fPrdm16*$^{-/-}$ cells are biased for MZ B-cells with elevated Sca1. (**A**) Ratio of marginal zone (CD21^{hi}CD23^{lo}) to follicular B-cells (CD23^{hi}CD21^{lo}) (MZ/FO) among donor splenic B-cells (CD19^{+}) in recipients of *Δ47-fPrdm16*$^{-/-}$ (KO) and WT fetal liver cells (*n* = 3 recipients). (**B**) Flow cytometry plots of donor-derived splenic B-cells 16 weeks after competitive transplantation from (A) (MZ: marginal zone B-cells; FO: follicular B-cells). (**C**) Sca1 mean fluorescence intensity (MFI) of donor MZ cells from recipients in (A) (*n* = 3). (**D**) Histograms of Sca1 MFI in donor MZ B-cells illustrating higher Sca1 in the MZ B-cells from *Δ47-fPrdm16*$^{-/-}$ than from WT littermate fetal liver cells (histograms to accompany (C)). (n.s = $P > 0.05$; * = $P < 0.05$; ** = $P < 0.01$; *** = $P < 0.001$, Student's t-test for single comparisons).

4.4.2 *s-Prdm16* supports differentiation of HSCs into LSK- cells but does not selectively maintain them

These experiments did not clearly elucidate whether *s-Prdm16* promotes the development of HSCs into LSK- cells or is instead involved in the maintenance of LSK- cells once established. Competitive transplants in Section 4.3 were performed using unsorted fetal liver cells. This has certain advantages over sorted HSCs – for example, if a given perturbation alters HSC surface phenotype, the typical sorting scheme ($Lin^-cKit^+Sca1^+CD48^-CD150^+$) could miss functional HSCs and cause a misinterpretation of results. Transplantation of total fetal liver or bone marrow ensures that all functional HSCs will be transplanted irrespective of changes in surface phenotype.

However, our transplantation of *Δ47-fPrdm16*$^{-/-}$ fetal liver into recipient mice meant that both HSCs and LSK- cells were transplanted into recipients, making it impossible to determine whether repopulating donor LSK- cells and MZ B-cell progeny originated from HSCs or were instead derived from pre-existing fetal liver LSK- cells. We therefore repeated competitive transplants with sorted HSCs instead of total fetal liver. Results were very similar to those performed with fetal liver, with extremely low chimerism in the *Δ47-fPrdm16*$^{-/-}$ cohort and a nearly absolute lymphoid and B-cell bias among the few donor cells (**Figure 4-25A**). Furthermore, qPCR analysis of sorted fetal liver LSK- cells revealed a very low, nearly undetectable level of *Prdm16* expression in these cells compared to HSCs (**Figure 4-25B**). Taken together, these results indicate that *s-Prdm16* promotes the differentiation of HSCs into LSK- cells but does not selectively maintain LSK- cells once established.

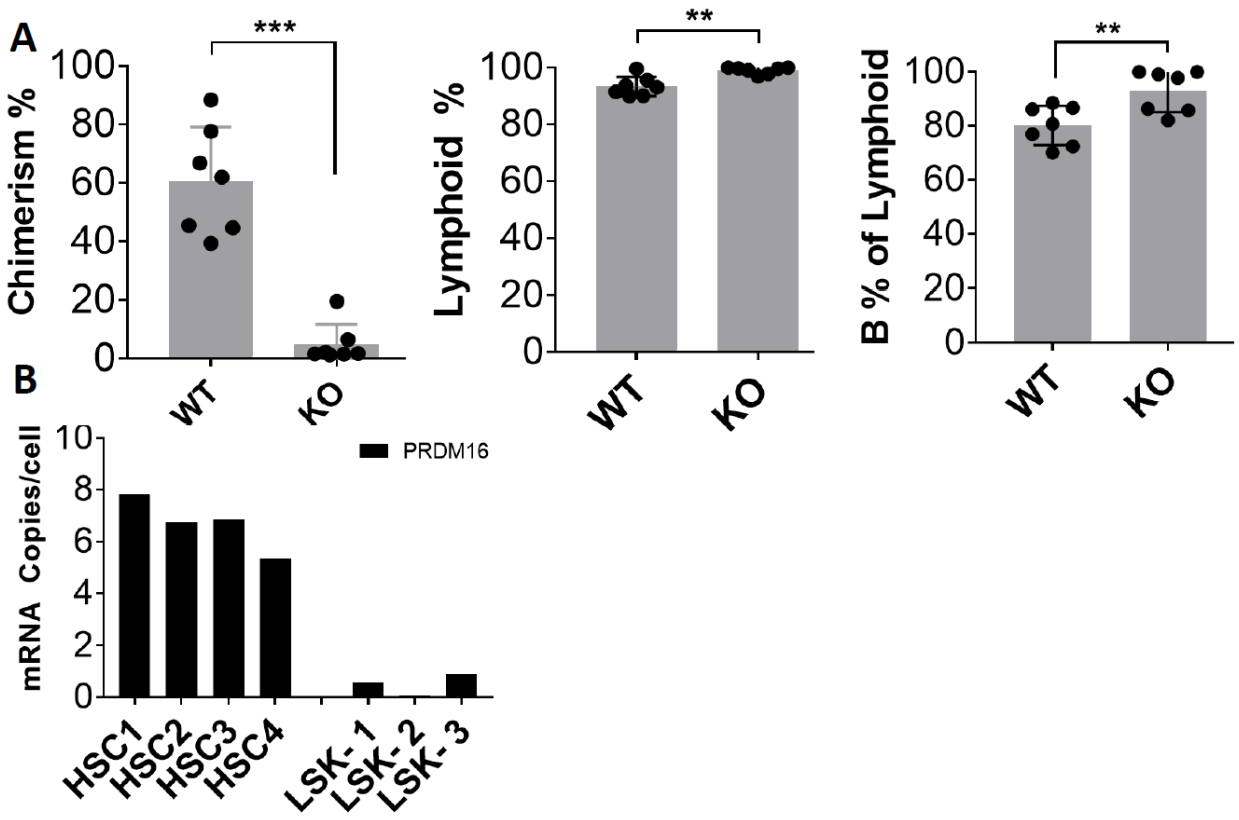

Figure 4-25: *s-Prdm16* promotes differentiation of LSK- cells but not their maintenance. (**A**) Competitive transplantation of sorted HSCs ($Lin^-cKit^+Sca^+CD48^-CD150^+$) from either WT or *Δ47-fPrdm16*$^{-/-}$ (KO) fetal liver, with peripheral blood donor chimerism, lymphoid percent of donor ($CD19^+$ or $CD3^+$), and B-cell percent of lymphoid ($CD19^+$) displayed. Recipient mice were analyzed 16-weeks post-transplant. (*n* = 7-8 recipients from 2 independent transplants). (**B**) Quantitative PCR for total *Prdm16* in sorted HSCs ($Lin^-cKit^+Sca^+CD48^-CD150^+$) or LSK- cells ($Lin^-Sca1^+cKit^-$) from WT mouse fetal liver, expressed as mRNA copies per cell. (*n* = 3-4 embryos). (n.s = $P > 0.05$; * = $P < 0.05$; ** = $P < 0.01$; *** = $P < 0.001$, Student's t-test for single comparisons).

These results prompted us to examine the *Δ47-fPrdm16*$^{-/-}$ and WT fetal liver compartments in more detail. Given the significant bias in *Δ47-fPrdm16*$^{-/-}$ donor cells toward LSK- progenitors and their B-cell progeny, we determined the frequency of LSK- cells in fetal livers of *Δ47-fPrdm16*$^{-/-}$ and WT littermates. Fetal liver LSK- cells are rare, with a frequency comparable to that of HSCs, becoming more frequent in bone marrow and increasing in frequency with age. Although the frequency was low, we did indeed observe that LSK- frequency was approximately 30% higher in *Δ47-fPrdm16*$^{-/-}$ than in WT fetal liver, with heterozygotes displaying an intermediate phenotype (**Figure 4-26A**). This is in agreement with results from competitive

transplants. Furthermore, among phenotypic HSCs, relative CD150 MFI was lower in *Δ47-fPrdm16*$^{-/-}$ compared to WT (**Figure 4-26B**). This finding is consistent with the lymphoid bias of *Δ47-fPrdm16*$^{-/-}$ HSCs, as low CD150 expression has been associated with higher lymphoid potential and a decrease in long-term repopulation capacity[357]. Finally, as we observed an elevation in ROS levels in *Prdm16*$^{fl/fl}$*.Vav-Cre*$^{+}$ HSCs, we measured ROS in *Δ47-fPrdm16*$^{-/-}$ compared to WT HSCs. We did not detect a difference, however (**Figure 4-26C**). Our conclusion from *Prdm16*$^{fl/fl}$*.Vav-Cre*$^{+}$ mice was that elevated ROS in bone marrow HSCs could result from increased oxidative phosphorylation and ETC activity in these cells. This pathway was not upregulated in *Prdm16*-deficient fetal liver. It is therefore consistent that ROS would not be elevated in *Δ47-fPrdm16*$^{-/-}$ fetal liver HSCs, as this may be specific to the bone marrow compartment. In conclusion, our analysis of *Δ47-fPrdm16*$^{-/-}$ fetal liver yielded results that were in accord with the LSK- and lymphoid bias observed in competitive transplants.

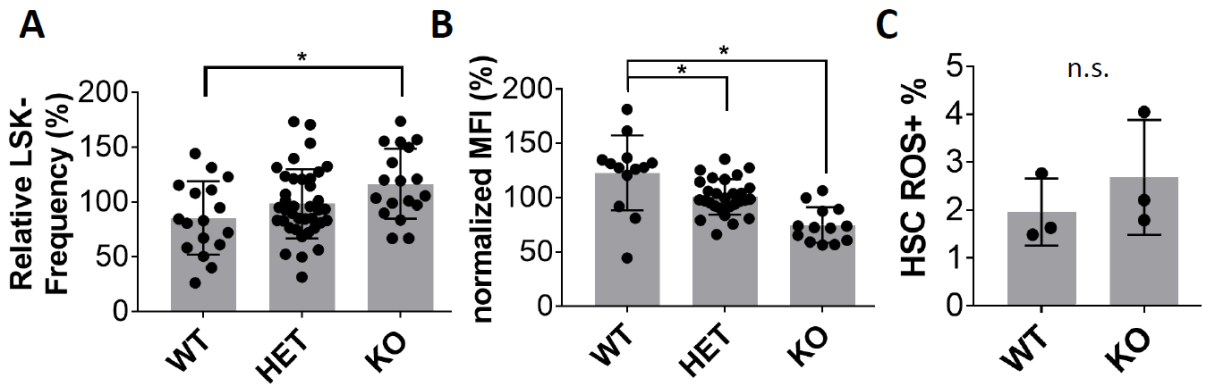

Figure 4-26: Altered LSK- frequency and HSC CD150 expression in *f-Prdm16*$^{-/-}$ fetal liver. (**A**) LSK^{-} (Lin^{-}Sca1^{+}cKit^{-}) frequency (*n* = 73 mice) in fetal livers from WT, *Δ47-fPrdm16*$^{+/-}$ (HET), and *Δ47-fPrdm16*$^{-/-}$ (KO) embryos, expressed as a percentage relative to the litter average. (**B**) Relative CD150 MFI of fetal liver HSCs from WT, HET, or KO embryos, expressed as percentage relative to litter average (*n* = 54 mice). (**C**) Percentage of fetal liver HSCs from WT or KO embryos with positive expression of the ROS indicator CellROX (*n* = 3 embryos). (n.s = $P > 0.05$; * = $P < 0.05$; ** = $P < 0.01$; *** = $P < 0.001$, One-way ANOVA for multiple comparisons or Student's t-test for single comparisons).

Section 4.5 – Prdm16 isoforms oppositely regulate inflammatory HSC signaling

We performed a gene expression analysis using RNAseq to elucidate additional gene expression patterns that may account for the phenotypes observed in *Δ47-fPrdm16*$^{-/-}$ fetal liver HSCs. We sorted HSCs ($Lin^-cKit^+Sca1^+CD48^-CD150^+$, excluding Mac1), amplified RNA and performed RNAseq analysis. 578 genes were upregulated and 694 downregulated genes were found in *Δ47-fPrdm16*$^{-/-}$ HSCs. The top 50 upregulated and downregulated genes by P-value are presented in **Figure 4-27**. PCA of individual samples again showed a clear distinction in gene expression patterns between WT and *Δ47-fPrdm16*$^{-/-}$ fetal liver HSCs (**Figure 4-28A**). We used this data to quantify mRNA expression of full and short-length *Prdm16* isoforms. We mapped sequencing reads to specific exons using the Tophat program to obtain individual RPKM values for each exon. This allowed for calculation of *Prdm16* exon 1-3 RPKM (*f-Prdm16* only) and exon 4-17 RPKM corresponding to total *Prdm16* expression (*f-Prdm16* plus *s-Prdm16*). By subtracting *f-Prdm16* RPKM from total RPKM, we calculated *s-Prdm16* RPKM. In WT HSCs, *f-Prdm16* represented the majority (about 60%) of *Prdm16* expression. In *Δ47-fPrdm16*$^{-/-}$ HSCs, however, very little *f-Prdm16* was detected. On the other hand, *s-Prdm16* RPKM was similar between the WT and *Δ47-fPrdm16*$^{-/-}$ samples (**Figure 4-28B**). This analysis was in agreement with qPCR analysis (Figure 4-19B), providing further confidence that the *Δ47* deletion specifically deletes *f-Prdm16* as intended.

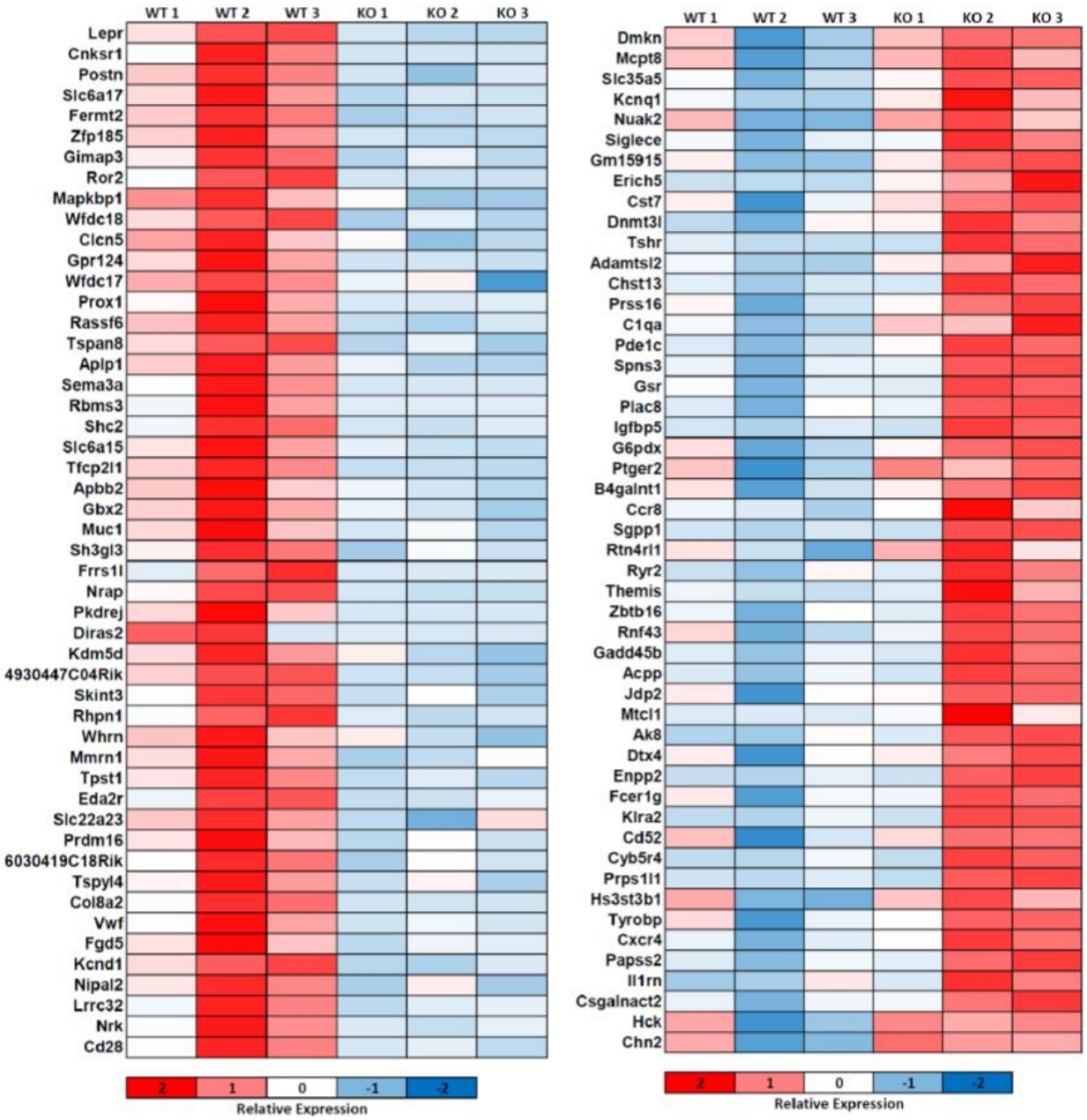

Figure 4-27: Genome-wide expression analysis of *Δ47-fPrdm16*$^{-/-}$ fetal liver HSCs. Heatmap of the top 50 genes (by *P*-value) upregulated in WT (left panel) and *Δ47-fPrdm16*$^{-/-}$ (KO, right panel) fetal liver HSCs, for each individual sample, as determined by RNAseq. Of note, *Prdm16* appears in the list of genes downregulated in KO.

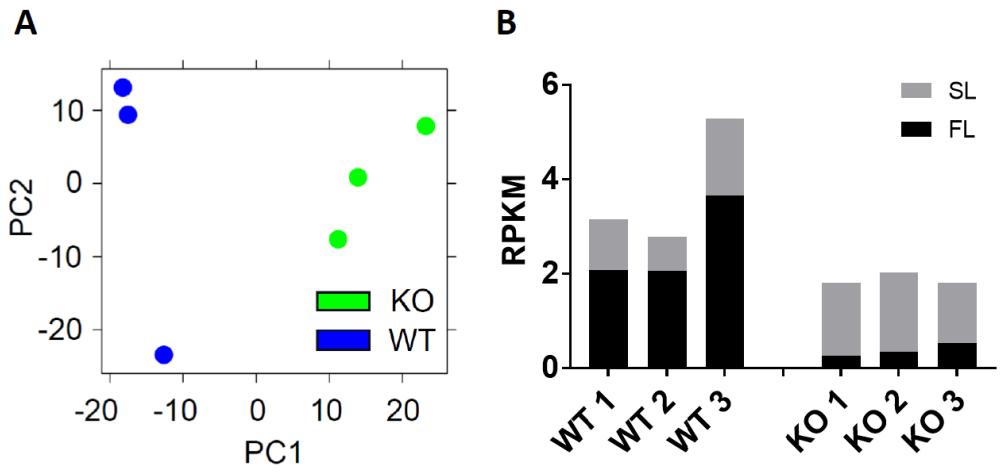

Figure 4-28: PCA and isoform RPKM analysis of *Δ47-fPrdm16*$^{-/-}$ HSCs. (**A**) Principal component analysis of individual RNAseq samples comparing WT and *Δ47-fPrdm16*$^{-/-}$ (KO) fetal liver HSCs (Lin^{-}cKit^{+}Sca^{+}CD48^{-} CD150^{+}). (**B**) RPKM values from individual RNAseq samples for *f-Prdm16* (FL), represented as Exon 1-3 RPKM, and *s-Prdm16* (SL), calculated by subtracting *f-Prdm16* RPKM from total *Prdm16* RPKM (Exons 1-17).

Pathway analysis using the PANTHER algorithm (**Figure 4-29**) of WT and *Δ47-fPrdm16*$^{-/-}$ HSC samples illustrated two significant findings. Firstly, we observed that, as with both fetal and adult *Prdm16*$^{fl/fl}$*.Vav-Cre*$^{+}$ HSCs, GTPase signaling pathways and pathways associated with them (Ras and Rho GTPase binding, angiogenesis, blood vessel development, cell motility, and Rho/Ras GEF activity pathways) were downregulated in *Δ47-fPrdm16*$^{-/-}$ HSCs compared to WT, indicating that the *f-Prdm16* isoform positively regulates these pathways. The lack of a *s-Prdm16*$^{-/-}$ mouse makes unclear whether the short isoform also regulates GTPase signaling. Nonetheless, the downregulation of Rho and Ras GTPase pathways in all HSC cohorts examined by RNAseq, and the fact that all cohorts have deficient HSC maintenance and competitive reconstitution, raises the strong possibility that these pathways are important for HSC maintenance. A list of genes downregulated in the various *Prdm16*-deficient RNAseq cohorts is presented in **Table 3**. This will be discussed further in the Discussion section (Chapter 8).

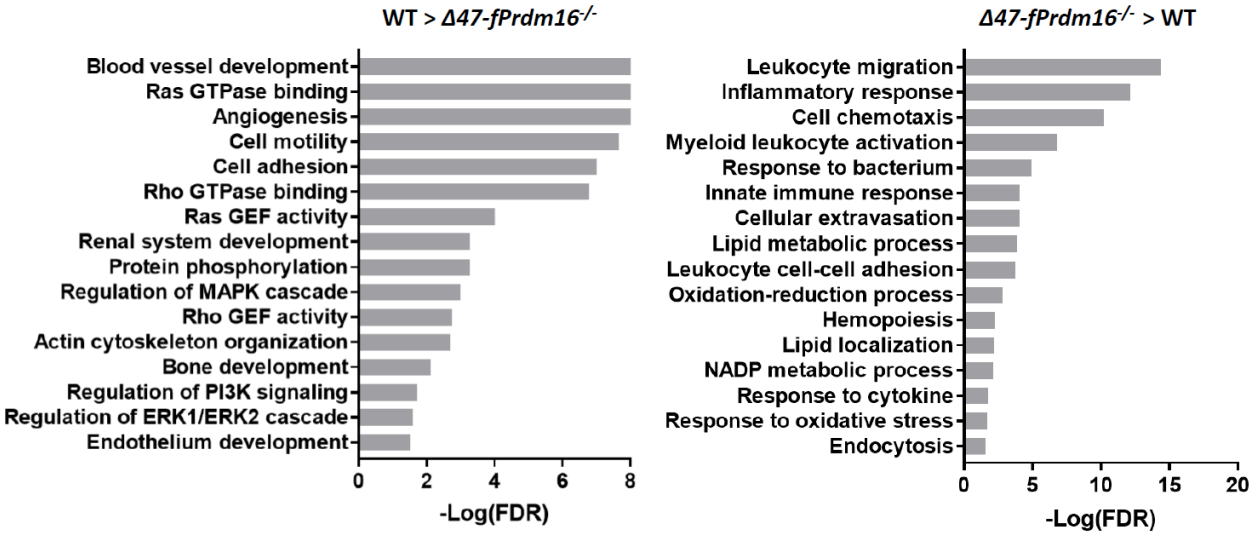

Figure 4-29: Pathways differentially regulated in *Δ47-fPrdm16*$^{-/-}$ HSCs. (**A**) GO pathways significantly downregulated (left panel) or upregulated (right panel) in sorted ($Lin^{-}cKit^{+}Sca^{+}CD48^{-}CD150^{+}$) *Δ47-fPrdm16*$^{-/-}$ fetal liver HSCs compared to WT littermates. Values expressed as -Log_{10} of the P-value, determined by PANTHER pathway analysis algorithm.

Table 3: GTPase-related genes upregulated by *Prdm16*

	Fold change (WT vs Vav-Cre.Prdm16$^{-/-}$ BM HSCs)	FDR	Fold change (WT vs f-Prdm16$^{-/-}$ FL HSCs)	FDR
Als2cl	1.9	0.02	2.74	0.026
Arhgef10	1.38	0.1	2.86	0.001
Dennd2c	2.83	0	1.71	0.071
Fgd5	1.4	0.035	2.24	0.005
Itsn1	1.73	0	2.91	0.1
Mtss1l	1.86	0.005	2.25	0.05
Nckap1	1.44	0.097	1.53	0.055
Obscn	2.17	0.002	2.73	0.004
Rab11fip3	1.43	0.029	1.6	0.045
Rgl1	1.56	0.041	1.69	0.07
Sbf2	2.52	0.001	1.85	0.02

The pathways upregulated in *Δ47-fPrdm16*$^{-/-}$ HSCs (which express only *s-Prdm16)* (Figure 4-29) were equally intriguing. Our analysis showed that nearly all upregulated pathways in these samples were inflammatory or somehow related to immune activation. It is unclear if inflammatory gene expression is related to the selective maintenance of LSK- cells and their differentiated progeny, but notably, upregulation of Sca1 is associated with elevated inflammatory signaling in HSCs, raising the possibility that these two findings may be related. The strong upregulation of inflammatory gene expression in *Δ47-fPrdm16*$^{-/-}$ HSCs, with only a mild change in *Prdm16*$^{fl/fl}$*.Vav-Cre*$^{+}$ HSCs (FDR of 0.13, indicating a potentially slight difference shy of statistical significance), suggests that *s-Prdm16* induces inflammatory gene expression and *f-Prdm16* conversely represses inflammatory genes. Importantly, this finding will have significant implications regarding the role of *s-Prdm16* in leukemia, discussed in Chapter 5.

Chapter 5 – The Role of PRDM16 Isoforms in Leukemia

Section 5.0 – Introduction

Chapter 4 describes a role for PRDM16 isoforms in HSC maintenance, and RNAseq analysis revealed pathways differentially regulated by these isoforms in hematopoietic progenitors. Evidence, described in Section 3.1, has also implicated PRDM16 in leukemia. It has been proposed that the full-length isoforms of several *PRDM* family members may function as tumor suppressors in human malignancies[311,358]. This is based on the fact that many tumors show deletion or inactivation of a long *PRDM* isoform, while overexpression induces apoptosis or cell cycle arrest. This has been demonstrated for *PRDM1*[359], *PRDM2*[360] and *PRDM5*[361], among others. A recent study using a murine MLL-AF9 model also showed that *f-Prdm16* inhibits leukemogenesis through induction of *Gfi1b*, which in turn represses *HOXA* genes[314]. In this study, no biological role could be discerned for an H3K4 methyltransferase-dead mutant, suggesting that the short isoform of *Prdm16* may have no biological function. These findings, taken together, suggest that *f-Prdm16* is a suppressor of leukemia.

Several lines of evidence, however, support an oncogenic role for *s-Prdm16*. In leukemic translocations involving *PRDM16*, the PR domain is often deleted[344]. These leukemias show dysplastic features and are associated with poor survival[340,362,363]. The N-terminal region of *Prdm16* is also a frequent target of retroviral insertional mutagenesis leading to immortalization[346] and leukemia[347] in mice. Furthermore, overexpression of *s-Prdm16*, but not *f-Prdm16*, in progenitor cells from *p53*$^{-/-}$ mice induces leukemic transformation[344], and forced expression of *s-Prdm16* promotes leukemic transformation during HOXB4-mediated immortalization of HSCs[50]. Collectively, these findings suggest an oncogenic role for *s-Prdm16*.

We therefore examined the role of both *Prdm16* isoforms in a mouse model of human MLL-AF9 leukemia, presenting this work in Chapter 5. We first compared the effect of complete *Prdm16* deletion in a mouse

model of AML. These findings are presented in Section 5.1. We next determined the effect of forced expression of each Prdm16 isoform on AML progression. These experiments were performed in a *Prdm16*$^{-/-}$ background to avoid the effects of endogenous expression of the other isoform. These results are described in Section 5.2. We analyzed gene expression patterns of these leukemic populations to elucidate potential mechanisms underlying differences in leukemic latency between WT and *Prdm16*$^{-/-}$ leukemias (Section 5.1), and those overexpressing either *s-Prdm16* or *f-Prdm16*, presented in Section 5.3. We employed the Cancer Genome Atlas (CGA), a publicly available database containing gene expression data from 179 human AML samples, to determine the effect of *PRDM16* isoform expression on patient survival and on the regulation of different biological pathways. Data from human AML revealed meaningful similarities with our experiments in mice, as described in Section 5.4. Finally, we compared our gene expression results to known gene expression signatures found in human MDS, uncovering interesting similarities between *s-Prdm16*-expressing AML and MDS. This is presented in Section 5.5.

Section 5.1 – Prdm16-deficient MLL-AF9 cells have a longer leukemic latency and distinct gene expression patterns

5.1.1 Prdm16 shortens latency of MLL-AF9 leukemia without affecting *in vitro* growth

General overview of MLL-AF9 experiments

We employed a mouse model of MLL-AF9 leukemia to investigate the role of Prdm16 isoforms in leukemia. As described in Section 2.2.2, this was the first mouse model of MLL-rearranged leukemia to be developed and is often used because of its relative genetic simplicity and reliable recapitulation of AML[364]. We generated MLL-AF9 cells by transduction of a retroviral vector expressing MLL-AF9 fusion protein and a human NGFR reporter (**Figure 5-1A**). Immortalized hNGFR$^+$ MLL-AF9 cells were expanded *in vitro* supplemented with SCF, IL-6 and IL-3. After 3-4 days of expansion, 2x10^4 hNGFR$^+$ cells (**Figure 5-1B**) were transplanted into irradiated recipient mice together with 2x10^5 supporting WT bone marrow cells (schematic in **Figure 5-1C**). Development of myeloid leukemia was confirmed by staining bone marrow for hNGFR$^+$Mac1$^+$Gr1$^+$ cells (example in **Figure 5-1D**) and by hematoxylin/eosin staining of peripheral blood (**Figure 5-1E**). *In vitro* colony assays were performed with 1000 MLL-AF9 cells in methylcellulose media and assayed after 7 days. All biological replicates were derived from independent MLL-AF9 cell lines originating from different retroviral transductions.

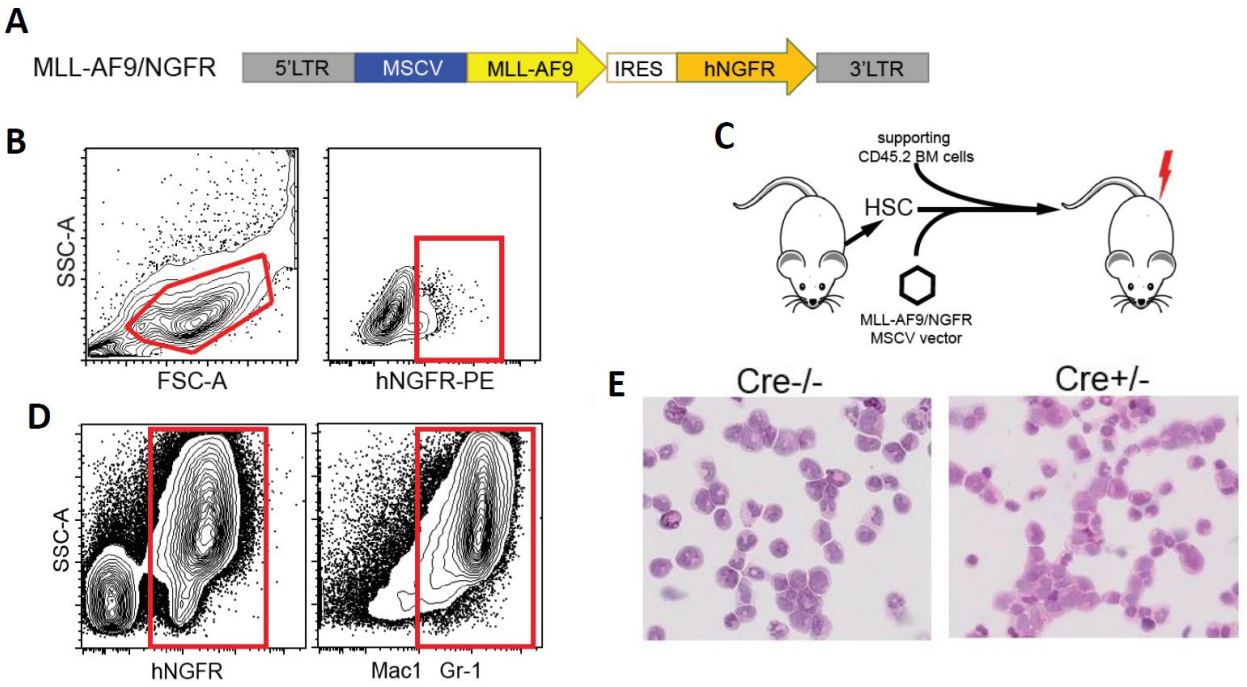

Figure 5-1: Overview of MLL-AF9 retroviral transduction and mouse transplants. (**A**) Map of retroviral MLL-AF9 vector under an MSCV promoter and co-expressing human NGFR. (**B**) Representative flow cytometry plot showing hNGFR expression after transformation of HSCs with MSCV-MLL-AF9-hNGFR retroviral vector. (**C**) Experimental design of MLL-AF9 leukemia studies. (**D**) Representative flow cytometry plot showing hNGFR and myeloid (Mac1, Gr-1) marker expression in peripheral blood of moribund mice at the endpoint of survival experiments. (**E**) Representative hematoxylin and eosin (H&E) staining of purified hNGFR$^+$ cells from moribund mice transplanted with either *Prdm16$^{fl/fl}$.Vav-Cre* (Cre+/-) or WT littermate (Cre-/-) MLL-AF9 cells.

To determine the effect of *Prdm16* deletion on leukemogenesis, we retrovirally transduced bone marrow HSCs (Lin$^-$cKit$^+$Sca1$^+$Flt3$^-$) from *Prdm16$^{fl/fl}$.Vav-Cre$^+$* mice and WT littermates with MLL-AF9. Leukemic latency was significantly extended in mice transplanted with *Prdm16$^{fl/fl}$.Vav-Cre$^+$* compared to WT MLL-AF9 cells (**Figure 5-2A**). Despite accelerating development of leukemia *in vivo*, colony forming assays showed that Prdm16 did not affect proliferation *in vitro*, with no difference between *Prdm16$^{fl/fl}$.Vav-Cre$^+$* or WT MLL-AF9 cells (**Figure 5-2B**). Leukemic cell-of-origin can have a significant impact on resulting leukemia. To investigate the effect of *Prdm16* deletion on MLL-AF9 cells generated from other cells-of-origin, we transduced Lin$^-$Sca1$^-$Kit$^+$ progenitors (a population containing GMPs, CMPs, and MEPs)

with MLL-AF9. Mice transplanted with these *Prdm16*$^{fl/fl}$.*Vav-Cre*$^{+}$ cells also had a longer leukemic latency compared to WT, although both cohorts had increased latency compared to mice receiving HSC-derived MLL-AF9 cells, a finding that is consistent with published data (**Figure 5-2C**).

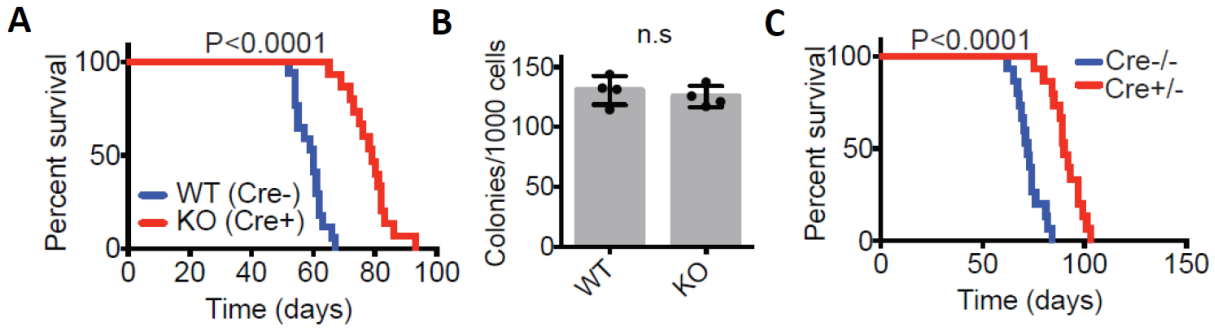

Figure 5-2: Extended leukemic latency in *Prdm16*-deficient MLL-AF9 cells. (**A**) Survival of lethally irradiated mice transplanted with bone marrow HSC-derived MLL-AF9 cells from *Vav-Cre*$^{-/-}$ *Prdm16*$^{fl/fl}$ (WT) and *Vav-Cre*$^{+/-}$ *Prdm16*$^{fl/fl}$ (KO) mice. (**B**) *In vitro* colony-forming assays of MLL-AF9 cells corresponding to (A). (n = 4 independent assays in duplicate). (**C**) Survival of lethally irradiated mice transplanted with MLL-AF9 cells generated from bone marrow Lin^{-}Sca1^{-}kit^{+} cells from *Vav-Cre*$^{-/-}$ *Prdm16*$^{fl/fl}$ (WT) and *Vav-Cre*$^{+/-}$ *Prdm16*$^{fl/fl}$ (KO) mice. (n.s = $P > 0.05$; * = $P < 0.05$; ** = $P < 0.01$; *** = $P < 0.001$, Student's t-test for single comparisons and Gehan-Breslow-Wilcoxon test for comparison of survival curves).

We obtained similar results using MLL-AF9 transduction of HSCs from germline-deleted *Prdm16*$^{-/-}$ mice. As these mice die perinatally, fetal liver cells were used. We also assayed *Prdm16*$^{+/-}$ MLL-AF9 cells, as our previous report showed an intermediate phenotype of heterozygote HSCs indicating *Prdm16* haploinsufficiency. Mice transplanted with *Prdm16*$^{-/-}$ MLL-AF9 cells had a significantly increased leukemic latency compared to WT, with heterozygotes showing an intermediate phenotype (**Figure 5-3A**). As with bone marrow-derived *Prdm16*$^{fl/fl}$.*Vav-Cre*$^{+}$ deletion, germline-deleted *Prdm16*$^{-/-}$ MLL-AF9 cells did not, however, exhibit *in vitro* growth defects in colony-forming assays (**Figure 5-3B**). To determine if physiological levels of *f-Prdm16* suppress leukemogenesis, we transduced fetal liver HSCs from *f-Prdm16*-deleted *Δ47-fPrdm16*$^{-/-}$ mice with MLL-AF9. In contrast to the *Prdm16*$^{-/-}$ deletion, leukemic latency was unchanged between mice transplanted with either *Δ47-fPrdm16*$^{-/-}$ or WT cells (**Figure 5-3C**).

As *Δ47-fPrdm16*$^{-/-}$ cells express normal levels of *s-Prdm16*, our results taken together support the conclusion that *s-Prdm16* is required for normal latency of murine MLL-AF9 leukemia, whereas *f-Prdm16* is not required. Furthermore, because *Δ47-fPrdm16*$^{-/-}$ MLL-AF9 cells did not have a shorter latency than WT, our data argue that physiological levels of *f-Prdm16* do not have a tumor suppressor effect.

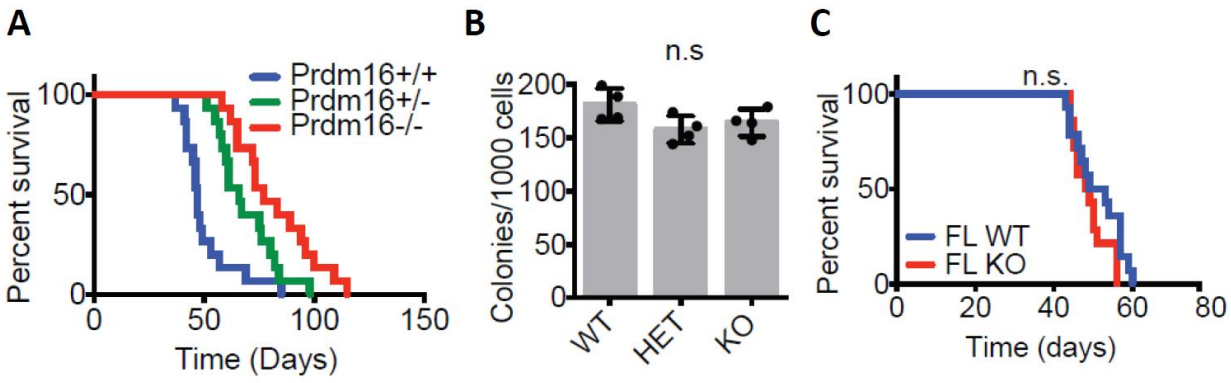

Figure 5-3: *s-Prdm16* is required for efficient MLL-AF9 leukemogenesis. (**A**) Survival of lethally irradiated mice transplanted with *Prdm16*$^{+/+}$ (WT), *Prdm16*$^{+/-}$ (HET), or *Prdm16*$^{-/-}$ (KO) fetal liver HSC-derived MLL-AF9 cells. (*n* = 14-15 recipients, 3 independently-derived MLL-AF9 lines). (**B**) *In vitro* colony-forming assays of MLL-AF9 cells from (A) (*n* = 4 independent assays in duplicate). (**C**) Survival of mice transplanted with fetal liver HSC-derived MLL-AF9 cells from *Δ47-fPrdm16*$^{-/-}$ (KO) or WT littermate mice. (n.s = $P > 0.05$; * = $P < 0.05$; ** = $P < 0.01$; *** = $P < 0.001$, One-way ANOVA for multiple comparisons, Gehan-Breslow-Wilcoxon test for comparison of survival curves)

As MLL-AF9 leukemia from *Prdm16*-deficient mice exhibits a delayed latency, *Prdm16* must be required in either the cell-of-origin and/or the resulting leukemic cells. We know from our previous publications that both *Prdm16* isoforms are highly expressed in HSCs, the cell-of-origin in our model. We therefore performed qPCR on *ex vivo* MLL-AF9 cells from the bone marrow of moribund recipient mice and found that in these cells *Prdm16* levels were undetectable (**Figure 5-4A**). Similar results were obtained with MLL-AF9 cells cultured *in vitro* (**Figure 5-4B**). Therefore, expression of *s-Prdm16* in HSCs at the time of leukemic transformation is likely the determinant of MLL-AF9 latency *in vivo*. Previous findings in mouse models of MLL-AF9 are in accord with this conclusion, demonstrating that differences in the cell-of-origin can significantly influence latency and gene expression patterns of the resulting leukemia[224]. The authors

found significant epigenetic differences in the resulting leukemic cells, leading us to speculate that *s-Prdm16* may possibly function through a similar mechanism, inducing an inheritable epigenetic signature that promotes leukemogenesis at the time of MLL-AF9 transformation.

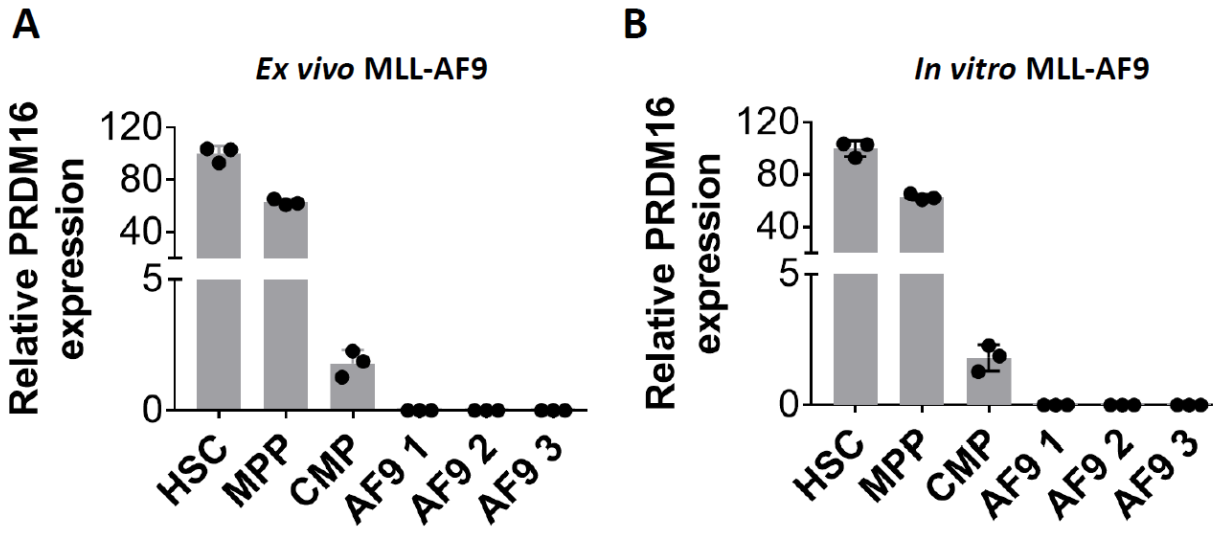

Figure 5-4: Undetectable expression of *Prdm16* in MLL-AF9 cells. (**A**) Quantitative PCR showing percent expression of *Prdm16* relative to WT HSC controls in other stem and progenitor cells (MPPs and CMPs) and in *ex vivo* WT MLL-AF9 leukemic cells (sorted hNGFR+ cells from bone marrow of moribund mice). (*n* = 3, in triplicate). (**B**) Relative percent mRNA expression of *Prdm16* in *in vitro* cultured MLL-AF9 cells compared to HSC controls. (*n* = 3, in triplicate).

5.1.2 Prdm16 in MLL-AF9 cell-of-origin induces an inflammatory and GTPase gene signature

Physiological expression of *s-Prdm16* in the cell-of-origin promotes development of MLL-AF9 leukemia. To better understand the mechanism underlying this effect, we performed RNAseq on sorted hNGFR$^+$ cells isolated *ex vivo* from bone marrow of moribund recipient mice of either *Prdm16$^{fl/fl}$.Vav-Cre$^+$* or WT MLL-AF9 cells. 817 genes were significantly upregulated and 708 genes were downregulated in *Prdm16$^{fl/fl}$.Vav-Cre$^+$* MLL-AF9 cells using a 0.1 false discovery rate (FDR) cutoff. The top 50 upregulated and downregulated genes by P-value are presented in **Figure 5-5**. PCA analysis showed clear separation

between the two populations (**Figure 5-6A**). Consistent with qPCR data, we observed very few *Prdm16* counts in the WT sample, indicating near-undetectable expression (data not shown).

Pathway analysis using the PANTHER algorithm showed a broad group of differentially regulated pathways. A representative list of these is provided in **Figure 5-6B**. Most strikingly, GTPase and inflammatory pathways were downregulated in *Prdm16*$^{fl/fl}$*.Vav-Cre*$^{+}$ leukemic cells. Both results are consistent with RNAseq analysis from HSCs. In both *Prdm16*-deficient and *f-Prdm16*-deficient HSCs, GTPase pathways were downregulated. Inflammatory pathways were upregulated in *Δ47-fPrdm16*$^{-/-}$ HSCs, which suggested that s-Prdm16 may positively regulate inflammatory signaling in opposition to f-Prdm16.

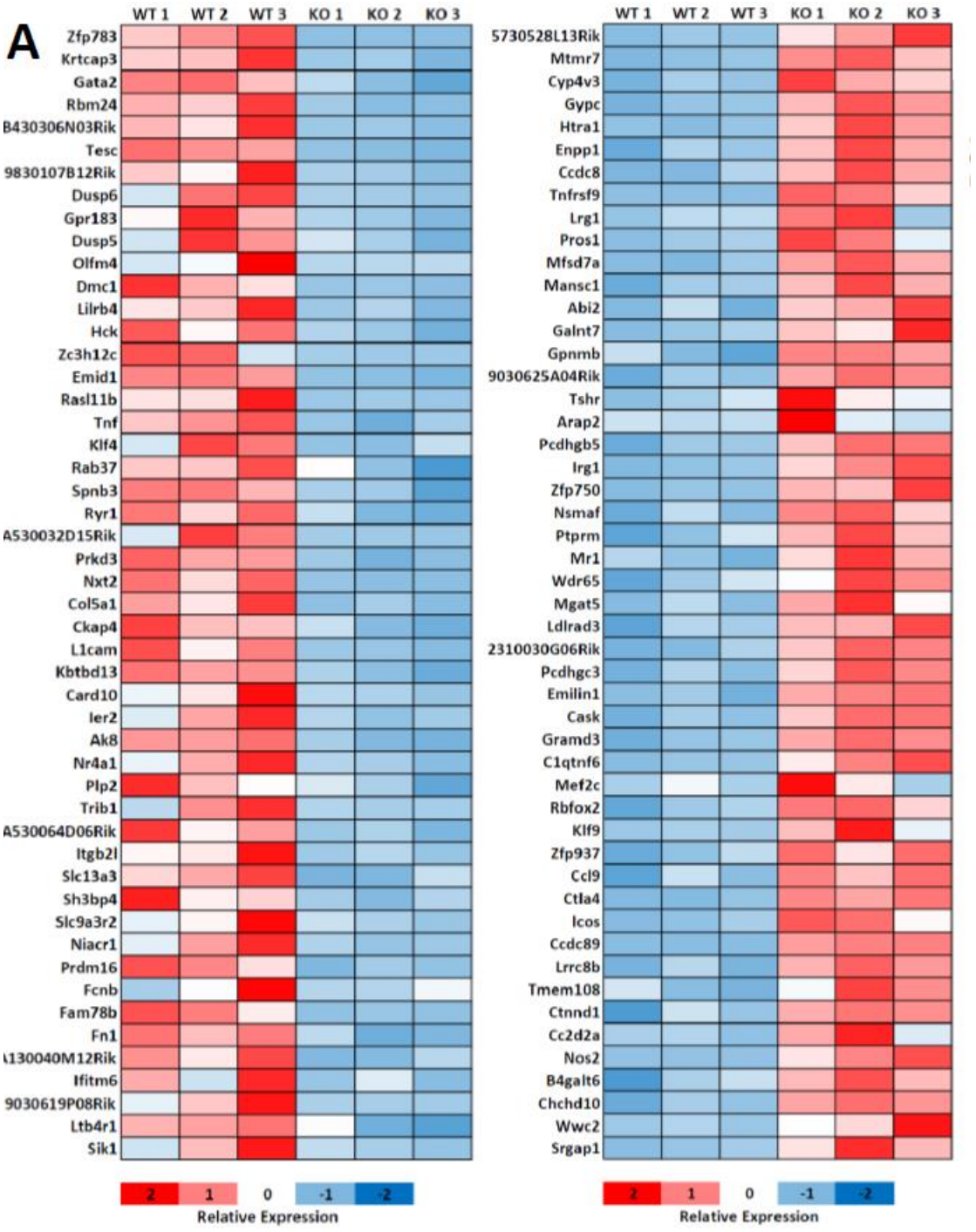

Figure 5-5: Genome-wide expression analysis of *Prdm16$^{fl/fl}$.Vav-Cre^{+}* MLL-AF9 leukemia. Heatmap of the top 50 genes (by *P*-value) upregulated in each individual sample of WT (left panel) and *Prdm16$^{fl/fl}$.Vav-Cre^{+}* (KO) (right panel) sorted MLL-AF9 cells (hNGFR^{+}) from moribund transplanted mice, as determined by RNAseq.

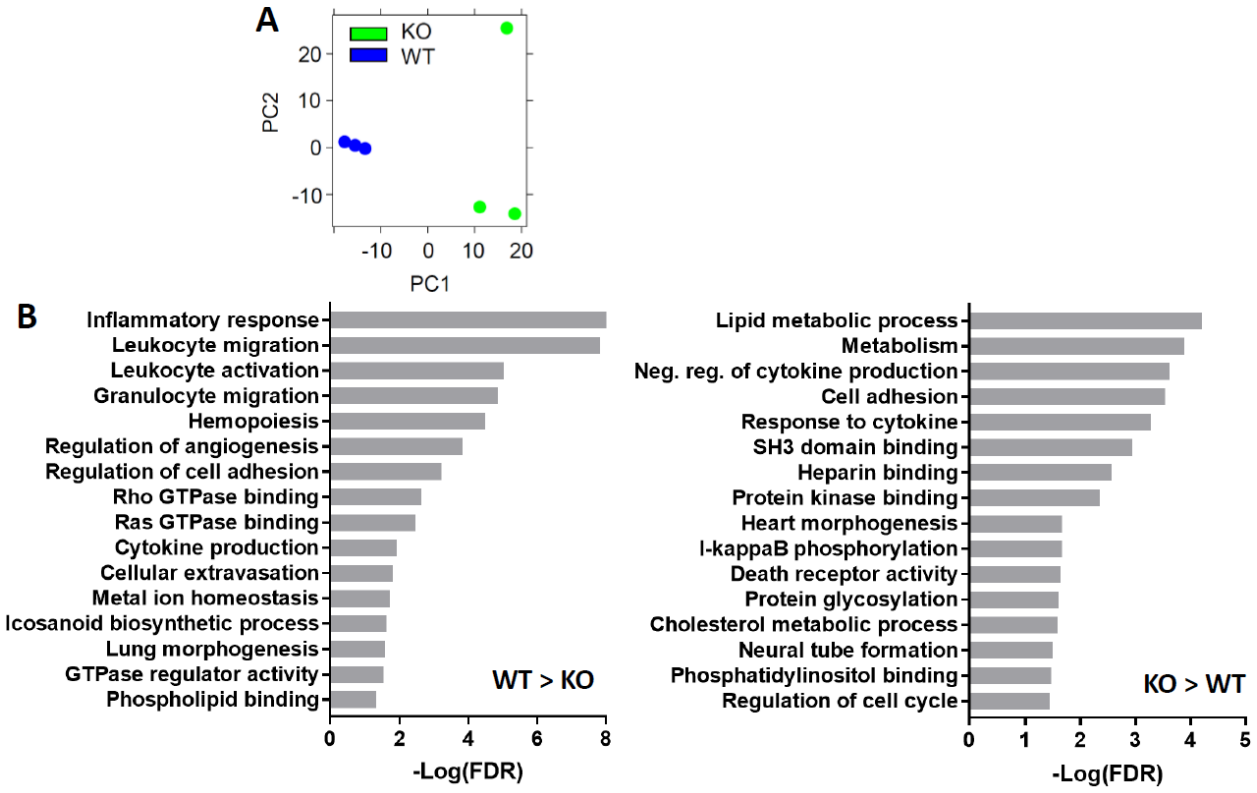

Figure 5-6: Pathways differentially expressed in *Prdm16$^{fl/fl}$.Vav-Cre^{+}* MLL-AF9 leukemia. (**A**) Principal component analysis of individual RNAseq samples from sorted WT and *Prdm16$^{fl/fl}$.Vav-Cre^{+}* (KO) MLL-AF9 cells (hNGFR^{+}) from moribund transplanted mice. (**B**) GO pathways significantly upregulated (right panel) or downregulated (left panel) in *ex vivo* KO MLL-AF9 relative to WT cells from (A). Values expressed as $-Log_{10}$ of the P-value, determined by PANTHER algorithm.

Section 5.2 – Opposing effects of forced expression of *Prdm16* isoforms on MLL-AF9 latency

In Section 5.1 we showed that physiological expression of *s-Prdm16* in HSCs shortens the latency of resulting MLL-AF9 leukemia. *Prdm16* expression, however, was downregulated in the MLL-AF9-transformed cells. Nonetheless, *PRDM16* is often expressed in leukemic cells. Our previous data did not investigate the effect of forced *Prdm16* expression. We therefore retrovirally overexpressed individual *Prdm16* isoforms in MLL-AF9 cells using an MSCV-IRES-GFP construct (vector maps in **Figure 5-7A**). We used the *Prdm16*$^{fl/fl}$*.Vav-Cre*$^{+}$ background which allowed for the forced expression of one *Prdm16* isoform without a risk of endogenous expression of the other, to distinguish the individual biological effects of each isoform. Furthermore, to mitigate potential artifacts from retroviral insertion at different sites, we expressed *Prdm16* isoforms after MLL-AF9 immortalization, thereby using the same pool of leukemic cells for transduction of either empty vector, *f-Prdm16*, or *s-Prdm16*. This is illustrated schematically in **Figure 5-7B**. Cells transduced with either of these three constructs had similar levels of GFP expression (**Figure 5-7C**) and there were also comparable levels of mRNA expression in the *Prdm16*-overexpressing samples as measured by subtractive qPCR (**Figure 5-7D**), indicating that the two *Prdm16* isoforms were overexpressed at similar levels.

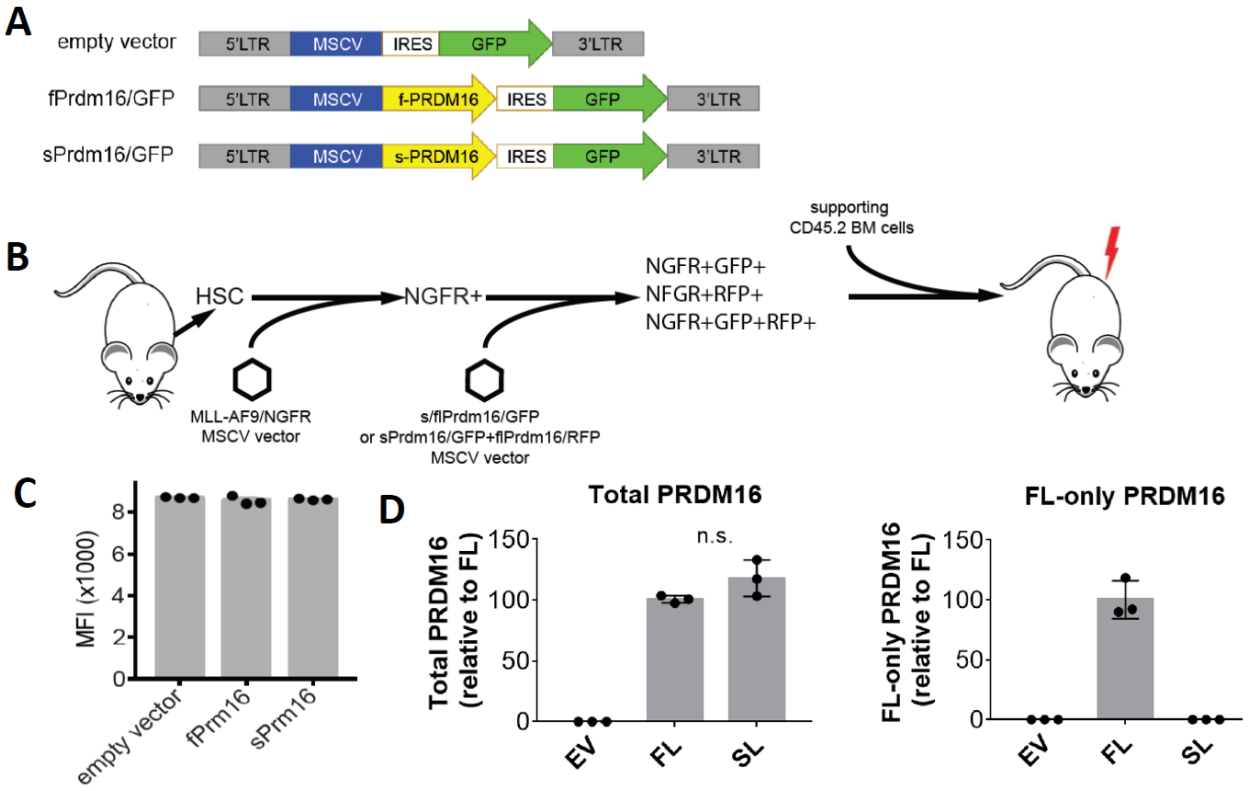

Figure 5-7: Forced expression of *Prdm16* isoforms in *Prdm16*$^{fl/fl}$*.Vav-Cre*$^{+}$ MLL-AF9 cells. (**A**) Maps of retroviral *Prdm16* expression vectors used in MLL-AF9 leukemia studies. (**B**) Schematic of MLL-AF9 transformation of HSCs followed by forced expression of either empty vector, *f-Prdm16*-GFP, *s-Prdm16*-GFP, or *s-Prdm16*-GFP/*f-Prdm16*-RFP. (**C**) Quantification of GFP mean fluorescence intensity (MFI) of *Prdm16*$^{fl/fl}$*.Vav-Cre* MLL-AF9 cells expressing either empty vector, *f-Prdm16*-GFP or *s-Prdm16*-GFP (*n* = 3). (**D**) Quantitative PCR of MLL-AF9 leukemia expressing either empty vector, *f-Prdm16*, or *s-Prdm16*, using probes for total *Prdm16* (exon 14/15 junction, left panel) or *f-Prdm16*-only (exons 2/3, right panel) demonstrating selective expression of the correct isoform and similar total expression levels. (n.s – *P* > 0.05, One-way ANOVA for multiple comparisons).

Forced expression of either *f-Prdm16* or *s-Prdm16* did not have an effect on *in vitro* growth of MLL-AF9 cells in colony forming assays (**Figure 5-8A**). This finding was consistent with the lack of an *in vitro* growth phenotype in MLL-AF9 cells with *Prdm16* deletion. However, transplantation of recipient mice with these cells revealed that forced expression of *s-Prdm16* shortened latency, to near the latency of WT leukemia, whereas overexpression of *f-Prdm16* further increased leukemic latency beyond that observed with the empty vector *Prdm16*$^{fl/fl}$*.Vav-Cre*$^{+}$ MLL-AF9 cells (**Figure 5-8B**). Co-expression of both *s-Prdm16* and *f-Prdm16* yielded a leukemic latency between those two extremes. To rule out the possibility that

differences in leukemic latency could be ascribed to defects in engraftment into recipient bone marrow, we measured engraftment of MLL-AF9 cells 24 hours after transplantation. We found that *f-Prdm16*-overexpressing MLL-AF9 cells did not have an engraftment defect and in fact homed more effectively to bone marrow than leukemic cells expressing *s-Prdm16* (**Figure 5-8C**). Additionally, *s-Prdm16*-overexpressing MLL-AF9 populations had fewer cycling cells than those expressing either *f-Prdm16* or empty vector, eliminating defects in proliferation as a cause of extended latency in *f-Prdm16*-expressing leukemia (**Figure 5-8D**). These findings suggest an oncogenic role for s-Prdm16 and a tumor suppressor role for f-Prdm16 after forced expression in MLL-AF9 that is unrelated to differences in engraftment potential or cycling.

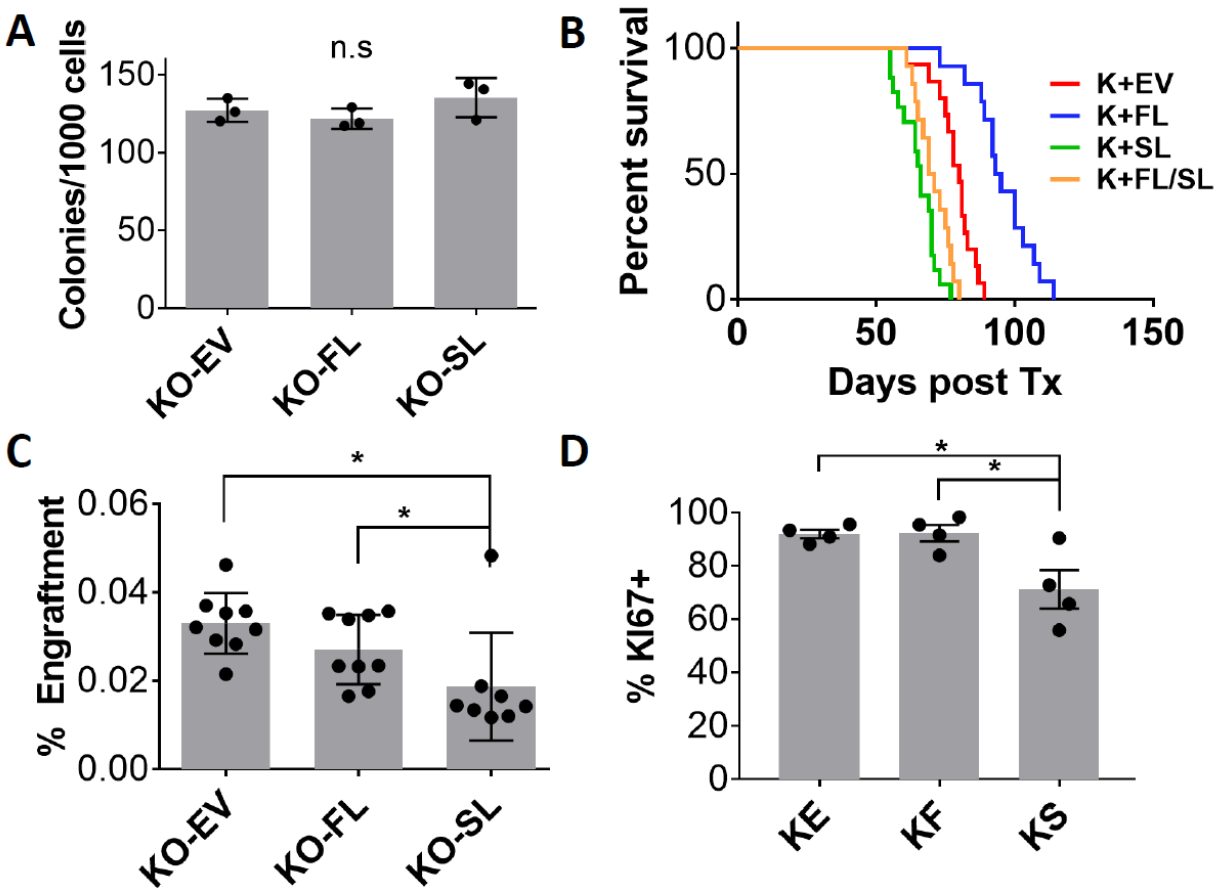

Figure 5-8: Forced expression of *s-Prdm16* and *f-Prdm16* have opposite effects on MLL-AF9 latency. (**A**) Colony-forming assays of *Prdm16*-deficient *Vav-Cre*$^{+/-}$ *Prdm16*$^{fl/fl}$ (KO) MLL-AF9 cells expressing empty vector, *f-Prdm16*, or *s-Prdm16*. (*n* = 3 independent assays in duplicate). (**B**) Survival of lethally irradiated mice transplanted with the MLL-AF9 cells described in (A), as well as a KO MLL-AF9 line co-expressing both *Prdm16* isoforms. (*n* = 14-15 recipients from 3 independent experiments). (**C**) Percent of MLL-AF9 cells in bone marrow of recipient mice 24-hours post-transplant. (*n* = 9 recipients, 3 independent transplants). (**D**) Percentage of KI-67+ *ex vivo* MLL-AF9 cells isolated *ex vivo* from moribund mice transplanted MLL-AF9 cells described in (A) (*n* = 4 recipients). (n.s = $P > 0.05$; * = $P < 0.05$; ** = $P < 0.01$; *** = $P < 0.001$, One-way ANOVA for multiple comparisons, Gehan-Breslow-Wilcoxon test for comparison of survival curves)

We performed bone marrow smears from moribund mice to check for visible differences between leukemic cells expressing either *f-Prdm16* or *s-Prdm16* compared to empty vector. Hematoxylin/eosin staining showed that in MLL-AF9 leukemias overexpressing *s-Prdm16* in comparison to empty vector or *f-Prdm16*, there was a significant increase in the fraction of cells with abnormal or fragmented nuclei (**Figure 5-9A** with representative pictures in **Figure 5-9B**). This finding is consistent with previous work

showing dysplastic changes in AML with *PRDM16* translocations in which the PR domain is absent[362,363,365,366].

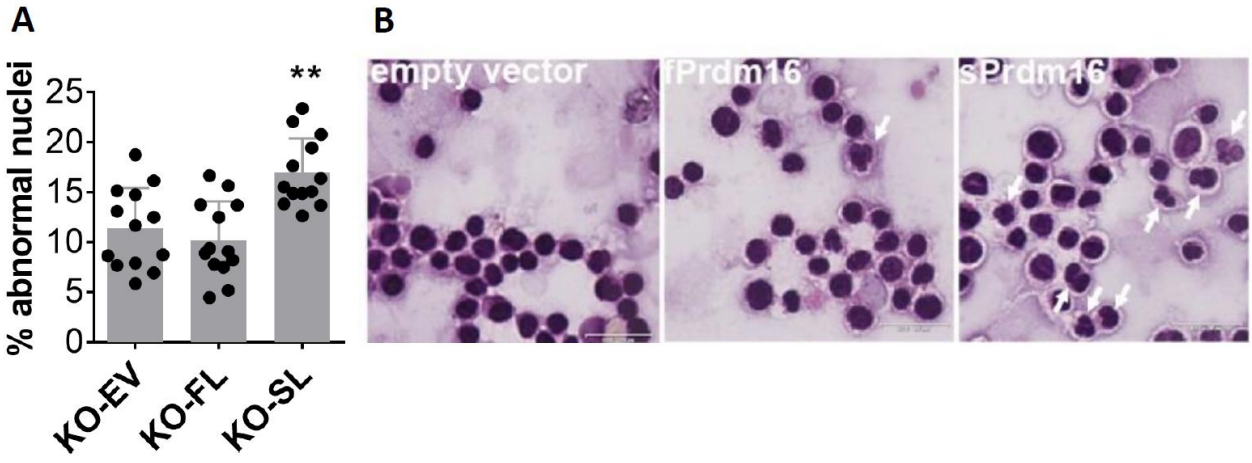

Figure 5-9: Dysplastic phenotype of MLL-AF9 cells expressing *s-Prdm16.* (**A**) Percent of cells with abnormal (elongated or multi-lobed) nuclei in bone marrow of leukemic mice transplanted with *Prdm16*$^{fl/fl}$*.Vav-Cre* MLL-AF9 cells expressing either empty vector, *f-Prdm16*-GFP or *s-Prdm16*-GFP (*n* = 4 fields from 3 independent mice, each field containing at least 50 bone marrow cells, (** = *P* < 0.01, One-way ANOVA for multiple comparisons). (**B**) Representative images of the data presented in (A). White arrows indicate abnormal nuclei.

Section 5.3 – Gene expression profiling reveals differential pathways induced by s-Prdm16 and f-Prdm16 in leukemic cells

5.3.1 Leukemic cells expressing *f-Prdm16* have increased oxidative phosphorylation and ROS

To explore mechanisms underlying the opposing effects of s-Prdm16 and f-Prdm16 in MLL-AF9, we performed gene expression analysis using RNAseq on GFP^+ cells isolated from moribund mice transplanted with either empty vector, *f-Prdm16*-expressing, or *s-Prdm16*-expressing MLL-AF9 cells. 398 genes were significantly upregulated and 760 genes were downregulated in *f-Prdm16*-expressing MLL-AF9 cells. A larger set of genes was differentially regulated by *s-Prdm16* – 1608 were significantly upregulated and 1924 genes were downregulated. Tables of the top 50 differentially regulated genes are presented in **Figure 5-10** (*f-Prdm16* vs empty vector) and **Figure 5-11** (*s-Prdm16* vs empty vector). Principal component analysis of individual samples showed very distinct clustering of the three leukemic populations (empty vector, *f-Prdm16*-expressing, *s-Prdm16*-expressing), indicating substantial differences in gene expression patterns (**Figure 5-12A**). Differentially regulated pathways are presented in **Figure 5-12B** (*f-Prdm16* vs empty vector) and **Figure 5-12C** (*s-Prdm16* vs empty vector).

Figure 5-10: Genome-wide expression analysis of *f-Prdm16*-expressing MLL-AF9 leukemia. Heatmap of the top 50 genes (by *P*-value) upregulated in either empty vector (left panel) of *f-Prdm16*-expressing (right panel) *Prdm16*$^{fl/fl}$*.Vav-Cre*$^{+}$ MLL-AF9 cells isolated from transplanted moribund mice. Mice were sacrificed and GFP^{+} cells were isolated from bone marrow. Columns represent individual independent samples. (*n* = 3).

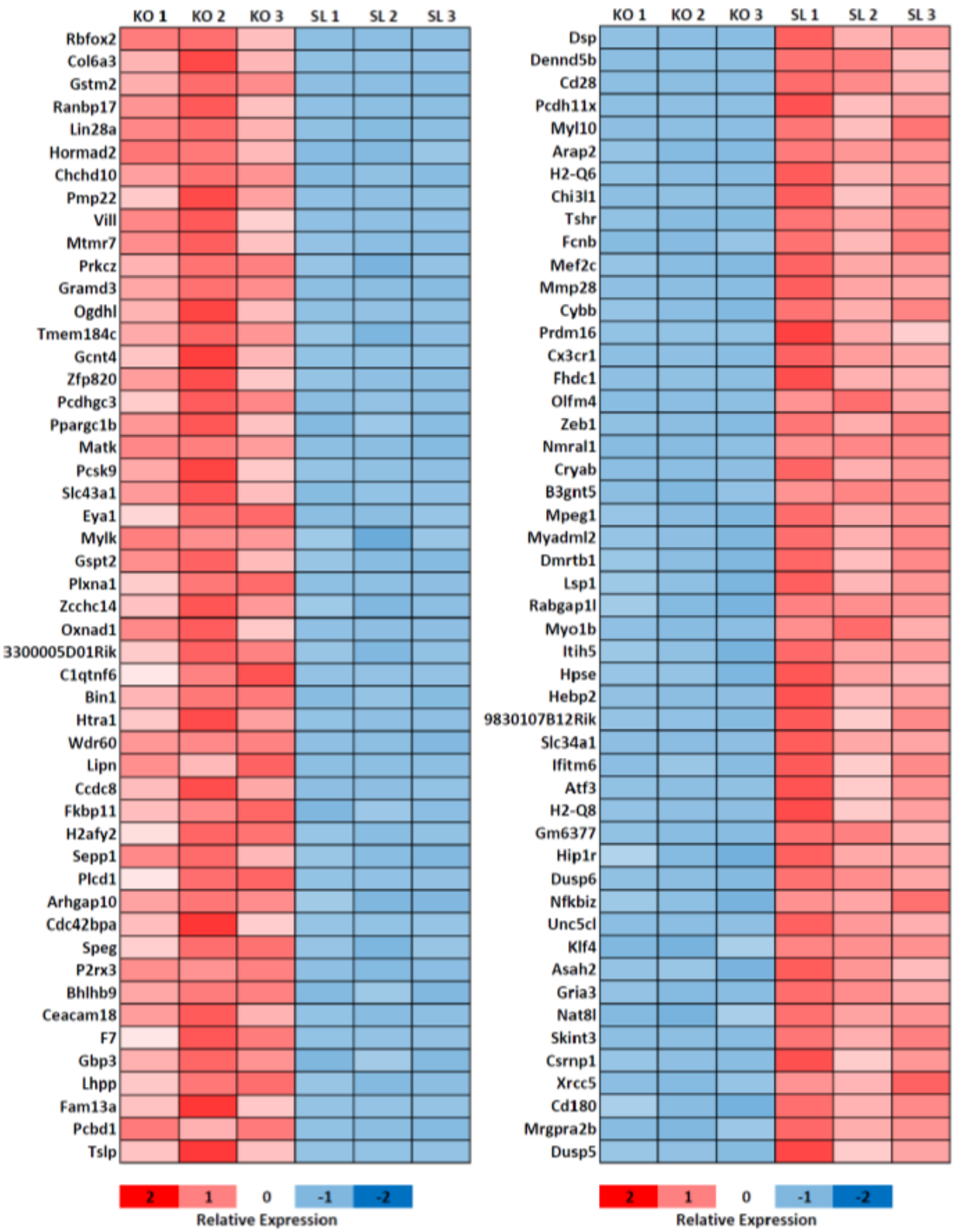

Figure 5-11: Genome-wide expression analysis of *s-Prdm16*-expressing MLL-AF9 leukemia. Heatmap of the top 50 genes (by *P*-value) upregulated in either empty vector (left panel) of *s-Prdm16*-expressing (right panel) *Prdm16*$^{fl/fl}$*.Vav-Cre*$^{+}$ MLL-AF9 cells isolated from transplanted moribund mice. Mice were sacrificed and GFP^{+} cells were isolated from bone marrow. Columns represent individual independent samples. (*n* = 3).

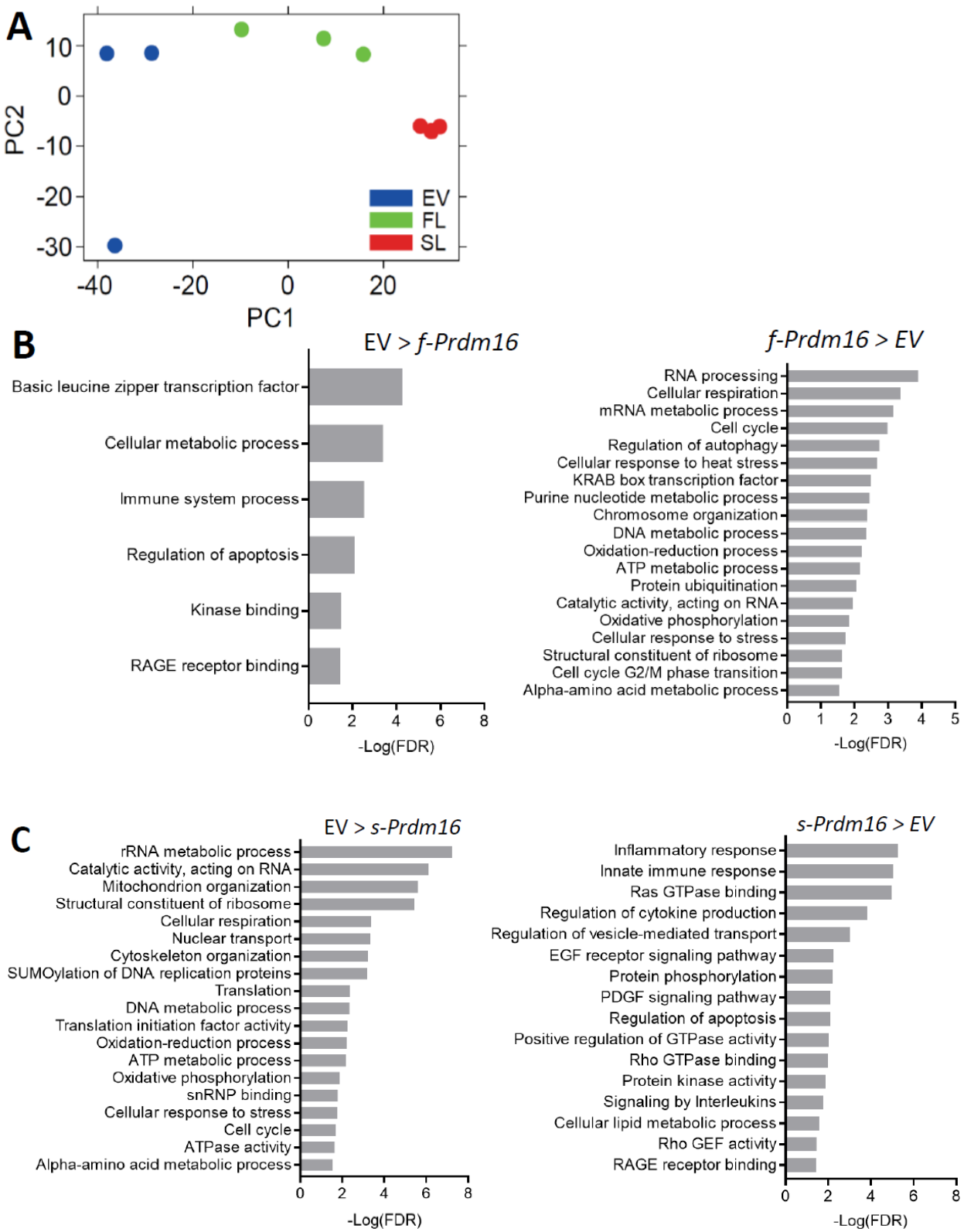
A
PC2
PC1
EV
FL
SL
B
EV > f-Prdm16
Basic leucine zipper transcription factor
Cellular metabolic process
Immune system process
Regulation of apoptosis
Kinase binding
RAGE receptor binding
-Log(FDR)
f-Prdm16 > EV
RNA processing
Cellular respiration
mRNA metabolic process
Cell cycle
Regulation of autophagy
Cellular response to heat stress
KRAB box transcription factor
Purine nucleotide metabolic process
Chromosome organization
DNA metabolic process
Oxidation-reduction process
ATP metabolic process
Protein ubiquitination
Catalytic activity, acting on RNA
Oxidative phosphorylation
Cellular response to stress
Structural constituent of ribosome
Cell cycle G2/M phase transition
Alpha-amino acid metabolic process
-Log(FDR)
C
EV > s-Prdm16
rRNA metabolic process
Catalytic activity, acting on RNA
Mitochondrion organization
Structural constituent of ribosome
Cellular respiration
Nuclear transport
Cytoskeleton organization
SUMOylation of DNA replication proteins
Translation
DNA metabolic process
Translation initiation factor activity
Oxidation-reduction process
ATP metabolic process
Oxidative phosphorylation
snRNP binding
Cellular response to stress
Cell cycle
ATPase activity
Alpha-amino acid metabolic process
-Log(FDR)
s-Prdm16 > EV
Inflammatory response
Innate immune response
Ras GTPase binding
Regulation of cytokine production
Regulation of vesicle-mediated transport
EGF receptor signaling pathway
Protein phosphorylation
PDGF signaling pathway
Regulation of apoptosis
Positive regulation of GTPase activity
Rho GTPase binding
Protein kinase activity
Signaling by Interleukins
Cellular lipid metabolic process
Rho GEF activity
RAGE receptor binding
-Log(FDR)

Figure 5-12: Pathway analysis of *f-Prdm16*-expressing and *s-Prdm16*-expressing MLL-AF9. (**A**) Principal component analysis of RNAseq samples of *Prdm16$^{fl/fl}$.Vav-Cre^{+}* MLL-AF9 cells expressing either empty vector (EV), *f-Prdm16* (FL), or *s-Prdm16* (SL), isolated from moribund recipient mice. (**B**) GO Pathways significantly downregulated (left panel) or upregulated (right panel) in *f-Prdm16*-expressing MLL-AF9 leukemia compared to empty vector, determined using the PANTHER algorithm. (**C**) GO Pathways significantly downregulated (left panel) or upregulates (right panel) in *s-Prdm16*-expressing MLL-AF9 leukemia compared to empty vector, determined using the PANTHER algorithm.

Leukemic cells expressing *f-Prdm16*, but not *s-Prdm16*, upregulated respiratory and oxidative phosphorylation gene expression pathways. We therefore used the Seahorse metabolic flux analyzer to determine levels of respiration and glycolysis in *Prdm16$^{fl/fl}$.Vav-Cre^{+}* MLL-AF9 cells expressing either empty vector, *f-Prdm16* or *s-Prdm16*. Leukemic cells expressing *f-Prdm16* had higher basal oxygen consumption (**Figure 5-13A**) and spare respiratory capacity (**Figure 5-13B**) than those expressing either empty vector or *s-Prdm16*. However, these cells also displayed a significantly higher rate of proton leak (**Figure 5-13C**) and, as a result, there was no difference in total respiratory ATP production from any population (**Figure 5-13D**). These results raise the possibility that f-Prdm16 may inhibit leukemogenesis in part through induction of metabolic inefficiency by increased uncoupling of respiration. Alternately, *f-Prdm16*-expressing MLL-AF9 cells may be under increased oxidative stress as a result of enhanced electron transport chain activity, as measurements of ROS using the fluorescent CellROX dye demonstrate elevated ROS levels in *f-Prdm16*-expressing leukemic cells than in those expressing empty vector or *s-Prdm16* (**Figure 5-13E**).

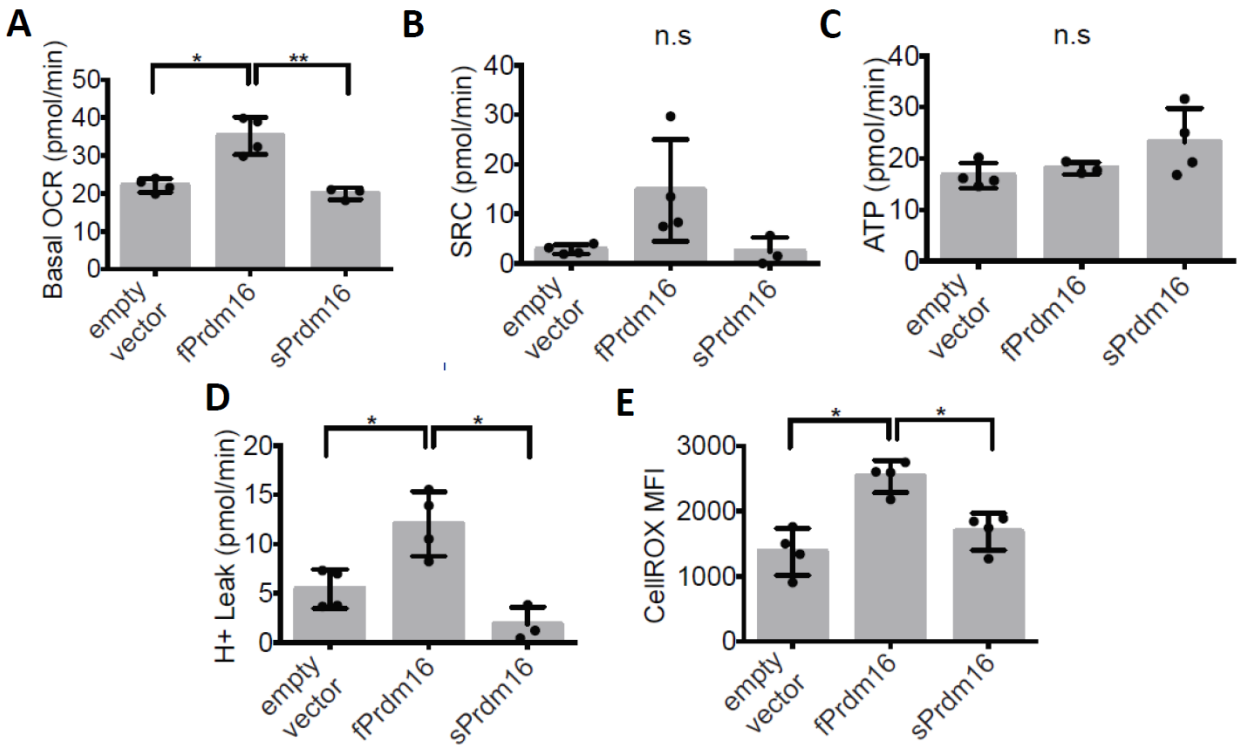

Figure 5-13: Increased basal respiration and ETC uncoupling in *f-Prdm16*-expressing MLL-AF9. (**A**) Basal oxygen consumption rate (OCR), (**B**) Spare respiratory capacity (SRC) (*P*(EV/*fPrdm16)*=0.07; *P(fPrdm16/sPrdm16*)=0.08), (**C**) Respiratory ATP production, and (**D**) proton leak from *ex vivo* *Prdm16*$^{fl/fl}$*.Vav-Cre*$^{+}$ MLL-AF9 cells expressing either empty vector, *f-Prdm16*, or *s-Prdm16,* isolated from moribund mice. (*n* = 4). (**E**) Reactive oxygen species (ROS) as measured by mean fluorescence intensity of CellROX-Deep Red from *in vitro* MLL-AF9 cells (*n* = 4*)*. (n.s = *P* > 0.05; * = *P* < 0.05; ** = *P* < 0.01; *** = *P* < 0.001, One-way ANOVA for multiple comparisons)

5.3.2 *s-Prdm16* expression induces inflammatory gene expression in MLL-AF9 leukemia

Pathway analysis of *s-Prdm16*-expressing MLL-AF9 leukemia (above in **Figure 5-12C**) indicated that the short Prdm16 isoform regulates a substantially different gene expression network than that of *f-Prdm16*. MLL-AF9 cells expressing *s-Prdm16* had a striking induction of immune and inflammatory pathways. This finding is consistent with increased inflammatory gene expression in WT leukemia (which expresses *s-Prdm16* in the cell-of-origin) compared to *Prdm16*$^{fl/fl}$*.Vav-Cre*$^{+}$ leukemic cells, and in *Δ47-fPrdm16*$^{-/-}$ HSCs (expressing only *s-Prdm16*) compared to WT. These results suggest that s-Prdm16, in both normal and leukemic cells, induces an inflammatory gene signature.

We performed an in-depth analysis of these three RNAseq datasets (*s-Prdm16*-expressing vs empty vector MLL-AF9, WT vs *Prdm16$^{fl/fl}$.Vav-Cre^{+}* MLL-AF9, and *Δ47-fPrdm16$^{-/-}$* vs WT HSCs). These data are presented in **Table 4**. We compared genes from the GO term "inflammatory process," which was significantly upregulated in all three datasets. Of the 418 genes with this classification, 151 were upregulated in at least one dataset. Of those, 56 (37%) were upregulated in at least two, and 13 (9%) were upregulated in all three datasets. This suggests a common mechanism of s-Prdm16 activation of inflammatory gene expression. Inflammatory genes upregulated in multiple datasets include *Tnfa, Il1b, S100A8/9, Tlr9, Tlr13, Hck, Mac1*, and NFkB family members. S-Prdm16-mediated induction of inflammatory signaling is a plausible mechanism by which this isoform may shorten leukemic latency, which will be discussed further in the discussion (Chapter 8).

A previous report suggested that f-Prdm16, but not a mutant without methyltransferase activity, represses HoxA genes through induction of Gfi1b to prevent leukemogenesis[314]. We analyzed *HoxA* and *Gfi1b* RNAseq data to determine if these genes were affected by f-Prdm16. *Gfi1b* expression was very low in all populations (empty vector, *f-Prdm16*-expressing and *s-Prdm16*-expressing) and was not elevated in leukemia expressing *f-Prdm16*. Furthermore, *f-Prdm16*-expressing MLL-AF9 did not exhibit downregulation any *HoxA* gene compared to empty vector (**Table 5**). We conclude that, in our experiments, f-Prdm16 did not induce Gfi1b or thereby indirectly suppress HoxA genes. This discrepancy may be a result of methodological differences, described in more detail in the Discussion (Chapter 8).

Table 4: Genes in GO term 'inflammatory process' upregulated in s-Prdm16-expressing MLL-AF9 cells and HSCs (part 1)

	WT vs. Prdm16$^{-/-}$ MLL-AF9	s-Prdm16 vs EV MLL-AF9	f-Prdm16$^{-/-}$ vs.WT HSC	WT vs. Prdm16$^{-/-}$ MLL-AF9		s-Prdm16 vs EV MLL-AF9		f-Prdm16$^{-/-}$ vs. wt HSC	
	Changed	Changed	Changed	Fold Change	P-Value	Fold Change	P-Value	Fold Change	P-Value
Anxa1	x	x	x	3.73	1.7E-05	3.76	1.5E-07	2.89	7.9E-04
Chil1	x	x	x	2.04	2.3E-03	41.41	6.1E-74	3.76	1.7E-05
Clec7a	x	x	x	1.46	4.6E-02	2.14	4.0E-06	2.17	6.6E-02
Ffar2	x	x	x	1.90	1.1E-02	4.84	7.5E-10	1.87	5.7E-02
Fpr2	x	x	x	5.46	1.4E-02	24.35	1.1E-06	5.61	1.5E-03
Hck	x	x	x	4.28	7.1E-09	11.13	1.6E-23	3.33	5.9E-04
Itgam	x	x	x	1.50	1.7E-02	2.26	1.2E-07	2.43	2.3E-02
Itgb2l	x	x	x	6.31	8.7E-07	10.71	1.3E-14	3.61	9.3E-03
Ly86	x	x	x	5.67	3.6E-04	6.48	1.6E-08	3.22	3.3E-02
Ncf1	x	x	x	1.97	5.5E-04	4.60	5.5E-22	2.57	2.6E-02
Pik3cb	x	x	x	1.71	2.1E-03	1.37	4.4E-02	2.32	5.9E-02
S100a8	x	x	x	4.84	4.7E-02	19.84	1.5E-04	3.54	1.6E-03
S100a9	x	x	x	6.60	2.6E-03	28.12	5.5E-08	3.34	3.3E-03
Adora3	x	x		2.26	2.5E-02	1.50	3.4E-01	3.52	2.0E-02
Alox5	x	x		2.62	1.2E-02	1.05	8.5E-01	3.33	2.5E-03
Alox5ap	x	x		1.44	4.1E-02	1.23	1.7E-01	1.56	5.7E-03
C5ar1	x	x		3.18	1.5E-04	1.35	5.1E-01	3.53	2.0E-05
Calca	x	x		6.20	9.0E-04	0.86	9.2E-01	16.36	2.9E-03
Ccl3	x	x		3.33	7.2E-04	2.47	2.0E-04	1.27	7.9E-01
Ccl4	x	x		2.69	9.0E-03	2.58	6.1E-03	0.59	2.0E-03
Ccl6	x	x		2.15	1.4E-02	2.93	3.9E-08	2.01	3.7E-01
Ccrl2	x	x		2.10	4.7E-04	4.41	1.9E-13	1.18	5.3E-01
Cd14	x	x		1.83	7.2E-02	3.72	1.8E-05	2.65	3.8E-01
Cnr2	x	x		1.35	1.0E-01	1.03	7.8E-01	2.02	2.5E-03
Crlf2	x	x		1.49	3.0E-02	1.72	5.5E-04	0.84	3.6E-01
Csf1r	x	x		2.00	1.9E-02	3.58	8.4E-05	2.01	3.1E-01
Cxcl12	x	x		1.62	6.6E-02	1.78	3.9E-02	n/a	n.a
Cxcl2	x	x		10.43	3.9E-03	12.17	1.0E-02	1.31	8.3E-01
Fcer1g	x	x		1.72	3.4E-03	1.10	5.4E-01	2.84	1.0E-03
Fn1	x	x		4.51	2.1E-06	2.71	2.6E-02	0.74	4.9E-01
Ggt5	x	x		3.45	2.3E-02	4.14	3.0E-03	0.91	9.1E-01
Hmox1	x	x		1.74	6.2E-03	2.48	2.3E-06	1.29	2.4E-01
Il15	x	x		2.29	7.9E-05	4.47	4.2E-16	0.95	9.1E-01
Il1b	x	x		3.33	1.1E-02	8.88	1.8E-11	2.79	1.1E-01
Itgb2	x	x		1.59	7.8E-03	0.70	2.2E-02	2.67	4.8E-02
Jak2	x	x		1.38	7.7E-02	2.70	5.3E-10	1.04	9.9E-01
Kdm6b	x	x		2.13	9.7E-04	3.25	4.2E-05	0.90	8.7E-01
Mmp25	x	x		4.66	2.9E-02	1.85	5.5E-01	6.06	3.9E-02
Nfkb2	x	x		1.39	9.5E-02	2.55	2.1E-05	0.74	6.8E-02
Nfkbid	x	x		1.48	5.4E-02	2.26	6.4E-07	0.98	1.0E+00

Table 4: Genes in GO term 'inflammatory process' upregulated in s-Prdm16-expressing MLL-AF9 cells and HSCs (part 2)

	WT vs. Prdm16$^{-/-}$ MLL-AF9	s-Prdm16 vs EV MLL-AF9	f-Prdm16$^{-/-}$ vs.WT HSC	WT vs. Prdm16$^{-/-}$ MLL-AF9		s-Prdm16 vs EV MLL-AF9		f-Prdm16$^{-/-}$ vs. wt HSC	
	Changed	Changed	Changed	Fold Change	P-Value	Fold Change	P-Value	Fold Change	P-Value
Nfkbiz	x	x		2.37	2.2E-02	9.09	1.5E-34	0.68	5.6E-01
Nlrp3	x	x		13.08	2.2E-05	19.82	1.1E-06	3.98	2.8E-01
Polb	x	x		1.60	8.3E-03	1.45	2.5E-02	0.94	8.1E-01
Ptafr	x	x		1.86	1.4E-03	2.76	9.8E-05	1.27	4.7E-01
Ptgs2	x	x		6.37	2.6E-04	7.16	2.4E-05	0.81	8.5E-01
Rel	x	x		1.43	6.2E-02	2.41	5.6E-07	0.95	9.1E-01
Relb	x	x		1.61	9.3E-02	3.88	1.0E-06	0.62	1.1E-02
Sgms1	x	x		1.93	4.7E-03	6.73	6.7E-19	0.70	5.0E-02
Slc11a1	x	x		2.46	3.9E-03	1.51	2.2E-01	3.60	1.9E-02
Thbs1	x	x		11.30	1.0E-01	6.16	2.1E-04	3.75	3.9E-01
Tlr13	x	x		3.10	8.2E-03	2.14	9.9E-02	2.53	7.0E-04
Tlr9	x	x		2.71	9.2E-03	1.96	3.4E-02	n/a	n.a
Tnf	x	x		3.12	5.1E-08	3.27	1.4E-05	1.01	9.3E-01
Tnfaip3	x	x		2.21	1.1E-04	3.91	3.5E-16	0.96	9.8E-01
Tnfrsf18	x	x		2.17	3.0E-03	2.52	4.3E-04	0.58	3.8E-02
Tnfrsf23	x	x		1.42	5.0E-02	0.86	5.2E-01	3.95	1.2E-04
Unc13d	x	x		1.33	9.6E-02	1.84	7.7E-05	0.98	9.3E-01
Adora3	x		x	2.26	2.5E-02	1.50	3.4E-01	3.52	2.0E-02
Alox5	x		x	2.62	1.2E-02	1.05	8.5E-01	3.33	2.5E-03
Alox5ap	x		x	1.44	4.1E-02	1.23	1.7E-01	1.56	5.7E-03
C5ar1	x		x	3.18	1.5E-04	1.35	5.1E-01	3.53	2.0E-05
Calca	x		x	6.20	9.0E-04	0.86	9.2E-01	16.36	2.9E-03
Cnr2	x		x	1.35	1.0E-01	1.03	7.8E-01	2.02	2.5E-03
Fcer1g	x		x	1.72	3.4E-03	1.10	5.4E-01	2.84	1.0E-03
Itgb2	x		x	1.59	7.8E-03	0.70	2.2E-02	2.67	4.8E-02
Mmp25	x		x	4.66	2.9E-02	1.85	5.5E-01	6.06	3.9E-02
Slc11a1	x		x	2.46	3.9E-03	1.51	2.2E-01	3.60	1.9E-02
Tlr13	x		x	3.10	8.2E-03	2.14	9.9E-02	2.53	7.0E-04
Tnfrsf23	x		x	1.42	5.0E-02	0.86	5.2E-01	3.95	1.2E-04
Bcl6		x	x	1.05	8.3E-01	4.13	1.7E-13	3.42	8.5E-04
C3		x	x	1.06	6.3E-01	2.32	2.3E-07	3.67	6.5E-03
Cd24a		x	x	0.86	5.8E-01	3.39	7.9E-07	1.34	4.8E-02
Cd300a		x	x	1.26	1.9E-01	1.51	7.2E-03	1.67	6.0E-03
Cxcr2		x	x	1.55	2.4E-01	2.56	1.4E-02	3.77	3.7E-05
Cybb		x	x	1.16	3.5E-01	19.01	8.5E-64	3.52	8.2E-03
Fpr1		x	x	3.57	1.5E-01	12.84	3.1E-03	2.53	1.7E-02
Hp		x	x	0.99	9.6E-01	1.70	1.1E-02	3.34	5.2E-03
Nlrc4		x	x	1.19	3.1E-01	1.88	6.6E-05	2.12	1.0E-01
Pstpip1		x	x	1.31	1.1E-01	1.75	2.2E-04	1.50	8.0E-02
Ptgs1		x	x	0.86	4.3E-01	1.56	3.0E-03	1.41	2.8E-02

Table 5: Expression of Gfib and HOX genes in MLL-AF9 leukemia

	Average RPKM		
Overexpressed Gene	EV	f-Prdm16	s-Prdm16
Gfi1b	0.01	0.23	0.13
Hoxa1	0.61	0.49	0.56
Hoxa10	89.36	63.81	60.40
Hoxa11	11.54	5.74	1.29
Hoxa11os	2.18	1.11	0.39
Hoxa2	1.76	4.22	4.25
Hoxa3	10.94	16.88	16.35
Hoxa4	2.09	2.06	1.58
Hoxa5	32.87	39.18	38.68
Hoxa6	8.25	10.27	8.99
Hoxa7	10.98	16.58	14.32
Hoxa9	76.94	79.23	66.37

Section 5.4 – Association between *PRDM16* and inflammation in subsets of human AML

5.4.1 PRDM16 is associated with worse prognosis in human AML and correlated with *HOX* gene expression

Our results using a murine model of MLL-AF9 suggested that *s-Prdm16* overexpression plays an oncogenic role in leukemia and that induction of inflammation may be involved. To connect our findings to human AML, we used gene expression data publically available in the Cancer Genome Atlas[272], a database containing 179 cases of human AML with both clinical information and gene expression data at the individual exon level. We compared *PRDM16* expression (calculated as Reads Per Kilobase of transcript per Million mapped reads or RPKM) and overall patient survival in these samples and found a negative correlation between the two (**Figure 5-14A**). This data was in agreement with other reports describing PRDM16 as a negative prognostic factor in AML[340,366,367]. We then determined the specific effect of *s-Prdm16* and *f-Prdm16* on prognosis, calculating individual isoform RPKM by determining exon 1-3 RPKM (*f-Prdm16* only) and exon 4-17 RPKM (total *PRDM16*), and using the difference between those two values to calculate *s-Prdm16* RPKM. Expression of *f-Prdm16* and *s-Prdm16* were significantly correlated with each other, and most AML cases with *PRDM16* expression showed some expression of each isoform (**Figure 5-14B**). *s-Prdm16* expression, however, had a stronger negative correlation with overall survival, with a more negative correlation coefficient and lower P-value than for *f-Prdm16* (**Figure 5-14C**). These data are consistent with our findings in an MLL-AF9 mouse model which demonstrated a shorter latency in leukemias expressing *s-Prdm16* and are consistent with a primary negative prognostic role of *s-Prdm16* in AML.

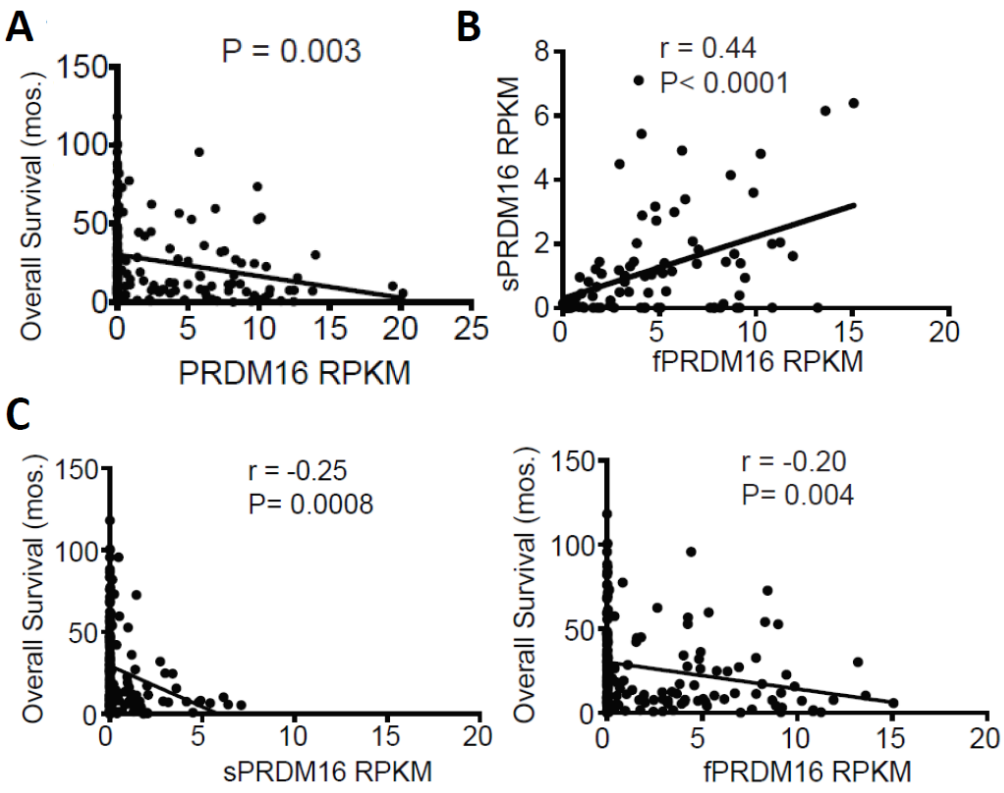

Figure 5-14: Negative correlation of *PRDM16* with survival in human AML. (**A**) Correlation between PRDM16 RPKM vs Overall Survival in all 179 human AML cases with gene expression data available in the Cancer Genome Atlas (CGA) (*n* =179). (**B**) Correlation between *f-PRDM16* and *s-PRDM16* mRNA expression (RPKM) among the set of *PRDM16*-expressing human AML cases in the Cancer Genome Atlas (CGA) cohort (corresponding to Q3 and Q4, with RPKM > 0.1, as described in the manuscript and in Figure 5-15A) (*n* = 90). (**C**) Negative correlation between both *s-PRDM16* and *f-PRDM16* mRNA expression (RPKM) and overall survival among 179 AML cases in the CGA.

We next compared cases of human AML with high *PRDM16* expression to those with little or no expression of *PRDM16.* We divided the CGA cohort of 179 AML cases into four quartiles based on *PRDM16* expression (shown graphically in **Figure 5-15A**). Quartiles 1 and 2 had very little or no *PRDM16* expression and were grouped together as *PRDM16*^{lo} AML (RPKM < 0.1). Quartile 4 had substantial *PRDM16* expression (RPKM > 5.0) and was classified as *PRDM16*^{hi}*.* Because quartile 3 contained a very broad range of *PRDM16* expression values (RPKM between 0.1 and 5), it was not considered in our analysis. We performed RNAseq, using gene counts provided in the CGA, comparing *PRDM16*^{lo} and *PRDM16*^{hi} cohorts. Principal

component analysis of all 179 samples showed no discernable clustering between *PRDM16*^{lo} and *PRDM16*^{hi} samples (**Figure 5-15B**). This suggests that *PRDM16* expression does not enough have statistical power to overcome the considerable heterogeneity found among all 179 cases of AML to reveal a detectable gene expression pattern – other factors, for example the driver mutations that form the basis of AML classification, account for too large a difference between samples.

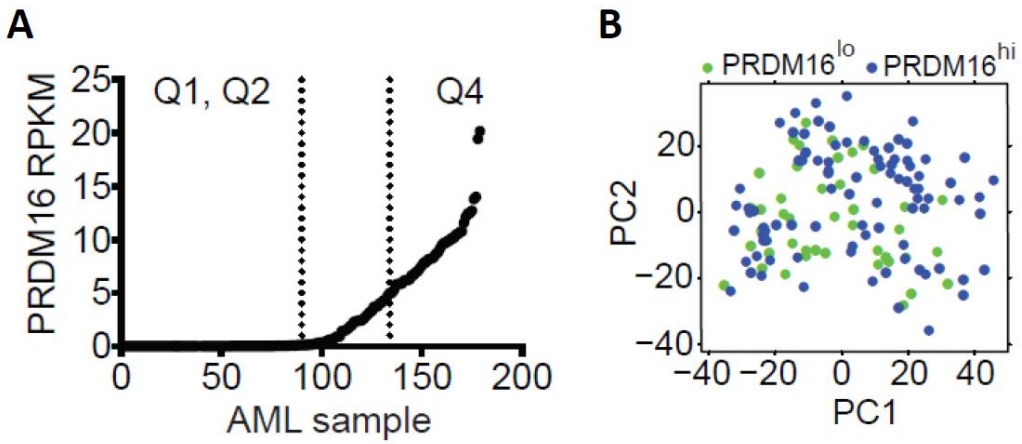

Figure 5-15: No difference in gene expression of *PRDM16*^{lo} and *PRDM16*^{hi} AML in the complete CGA. (**A**) Graph of PRDM16 RPKM for all AML samples in the Cancer Genome Atlas (CGA), ranked by RPKM, illustrating Q1/Q2 (*PRDM16*^{lo} cohort) and Q4 (*PRDM16*^{hi} cohort). (**B**) Principal component analysis (PCA) of RNAseq comparing *PRDM16*^{lo} and *PRDM16*^{hi} AML cases among all 179 in the CGA database shows no discernable clustering.

An examination of differentially expressed genes from this analysis, however, illustrated that *HOX* genes appeared to be significantly upregulated in the *PRDM16*^{hi} cohort. As presented in **Table 6**, 13 of the 40 HOX genes were upregulated in AML samples with high *PRDM16*. Only 2.4% of total genes were significantly upregulated, implying that only 0.53 HOX genes should be upregulated by chance. Therefore, significantly more HOX genes were upregulated than expected ($P < 0.001$, Chi-square test). Among the 179 AML cases, we stratified expression of the *HOXA* and *HOXB* clusters, using HOXA9 and HOXB3 as representative genes. Cases were classified into one of four clusters – those without *HOX* expression, expressing one *HOX* cluster (either *HOXA* or *HOXB*), expressing both *HOX* clusters, and a separate

classification for *NPM1*-mutated leukemias (all of which are both *HOXA*$^{+}$ and *HOXB*$^{+}$). Quite strikingly, in the *HOX*-negative and single *HOX* cluster AML cohorts, *PRDM16* expression was low or undetectable. Of the 66 *HOX*-negative samples, none had a *PRDM16* RPKM >5, and only 4 of 66 (6%) of cases had a *PRDM16* RPKM >1. In contrast, in both *HOXA/B* double-positive AML and *NPM1*-mutated AML, the mean *PRDM16* RPKM was >5 **(Figure 5-16)**. We did not detect differences in *Hox* gene expression in our mouse model after overexpression of either *f-Prdm16* or *s-Prdm16*. The association between *PRDM16* and *HOX* cluster expression in human AML therefore suggests that *PRDM16* may not, as has been suggested[314], repress *HOX* genes, but that in fact, *HOX* genes may upregulate *PRDM16*.

Table 6: HOX genes upregulated in PRDM16hi AML

Gene	fold change	P Value
HOXB3	4.89	4.2E-16
HOXB4	4.34	8.5E-13
HOXB2	3.39	6.2E-08
HOXB6	5.04	1.2E-07
HOXA6	3.26	3.2E-07
HOXA7	2.74	9.0E-06
HOXA3	2.79	1.2E-05
HOXB5	5.44	3.6E-05
HOXA5	2.92	4.4E-05
HOXA4	3.11	1.4E-04
HOXA9	2.46	1.1E-03
HOXA10	1.97	2.0E-02
HOXA1	1.83	2.5E-02

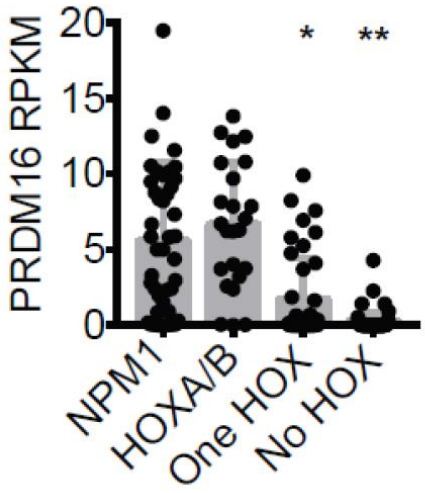

Figure 5-16: Elevated *PRDM16* expression in HOXA or HOXB-expressing AML. PRDM16 RPKM compared within 4 mutually exclusive groups from the CGA AML cohort. These include – NPM1-mutated, NPM1wt HOXA9/B4 double-positive (HOXA/B), HOXA9 or HOXB4 single-positive (one HOX), and HOXA9/HOXB4 double-negative (No HOX) (*n* = 179). (n.s = $P > 0.05$; * = $P < 0.05$; ** = $P < 0.01$; *** = $P < 0.001$, One-way ANOVA for multiple comparisons)

5.4.2 PRDM16 expression is associated with inflammatory gene expression in NPM1-mutated and MLL-rearranged AML

We did not observe statistically significant clustering between *PRDM16*^{lo} and *PRDM16*^{hi} AML cohorts when analyzing the entire CGA dataset of all 179 AML cases. This dataset is representative of all AML and therefore contains all AML classifications, rendering it highly heterogeneous. We therefore isolated two subsets from the CGA samples – those with NPM1-mutations and those with MLL-rearrangements. We selected these two AML subsets because of the previously demonstrated expression of PRDM16 in many NPM1-mutated leukemias[344] and because we found a role for *Prdm16* in an MLL-AF9 mouse model. There were 47 NPM1-mutated AML samples and 21 samples with MLL-rearrangements in the CGA dataset. As with the total AML cohort, *PRDM16* expression negatively correlated with overall survival in the NPM1-mutated subset of AML (**Figure 5-17A**). A similar trend was observed in the MLL-rearranged AML

subset, but the results were not significant, likely owing to the relatively small sample size available (**Figure 5-17B**).

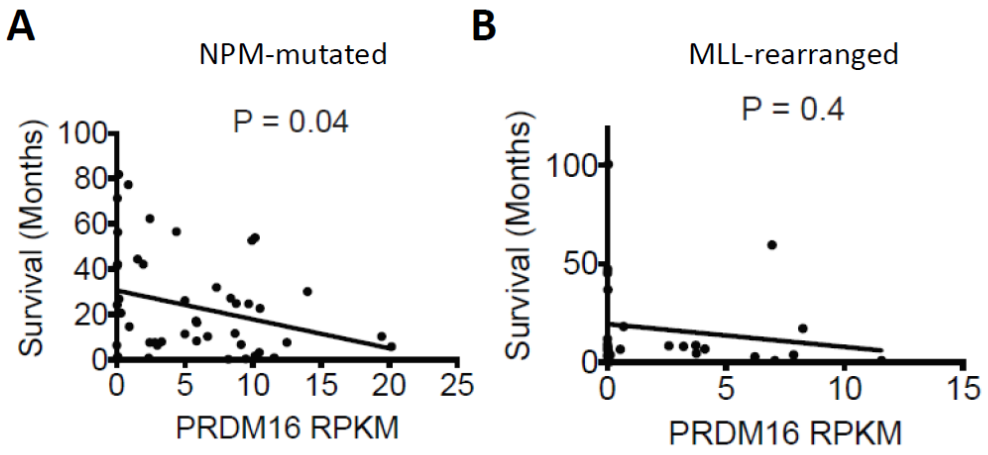

Figure 5-17: *PRDM16* expression negatively correlates with outcome in *NPM1*-rearranged AML. (**A**) Correlation between *PRDM16* RPKM and Overall Survival among *NPM1*-mutated AML cases (*n* = 47) and (**B**) MLL-rearranged AML cases in the CGA (*n* = 21), with *P*-values listed within the graph.

We then divided both leukemic subsets (NPM1-mutated and MLL-rearranged) into $PRDM16^{lo}$ and $PRDM16^{hi}$ groups and performed gene analysis similar to that for the entire population using quartiles Q1/Q2 vs Q4, determined from the entire dataset. In sharp contrast to the complete CGA dataset, principal component analysis clearly separated the $PRDM16^{lo}$ and $PRDM16^{hi}$ cohorts in both the NPM1-mutant (**Figure 5-18A**) and MLL-rearranged leukemias (**Figure 5-18B**). This indicates that, within these two leukemic subsets, the effect of *PRDM16* expression is significant enough to overcome statistical noise and cause differential gene expression patterns, likely because these specific leukemic subsets are considerably more homogenous than the entire AML cohort. Pathway analysis using the PANTHER algorithm revealed that, in both subsets, $PRDM16^{hi}$ samples exhibited an upregulated inflammatory gene expression signature compared to $PRDM16^{lo}$ leukemias (**Figure 5-18C and D**). Collectively, these findings demonstrate that, in human AML and among particular AML subsets, *PRDM16* expression is associated

with a worse prognosis overall. Furthermore, at least within the NPM1-mutant and MLL-rearranged AML subsets, *PRDM16* expression associates with an inflammatory gene expression signature, consistent with our findings in murine AML showing induction of inflammatory gene expression by s-Prdm16.

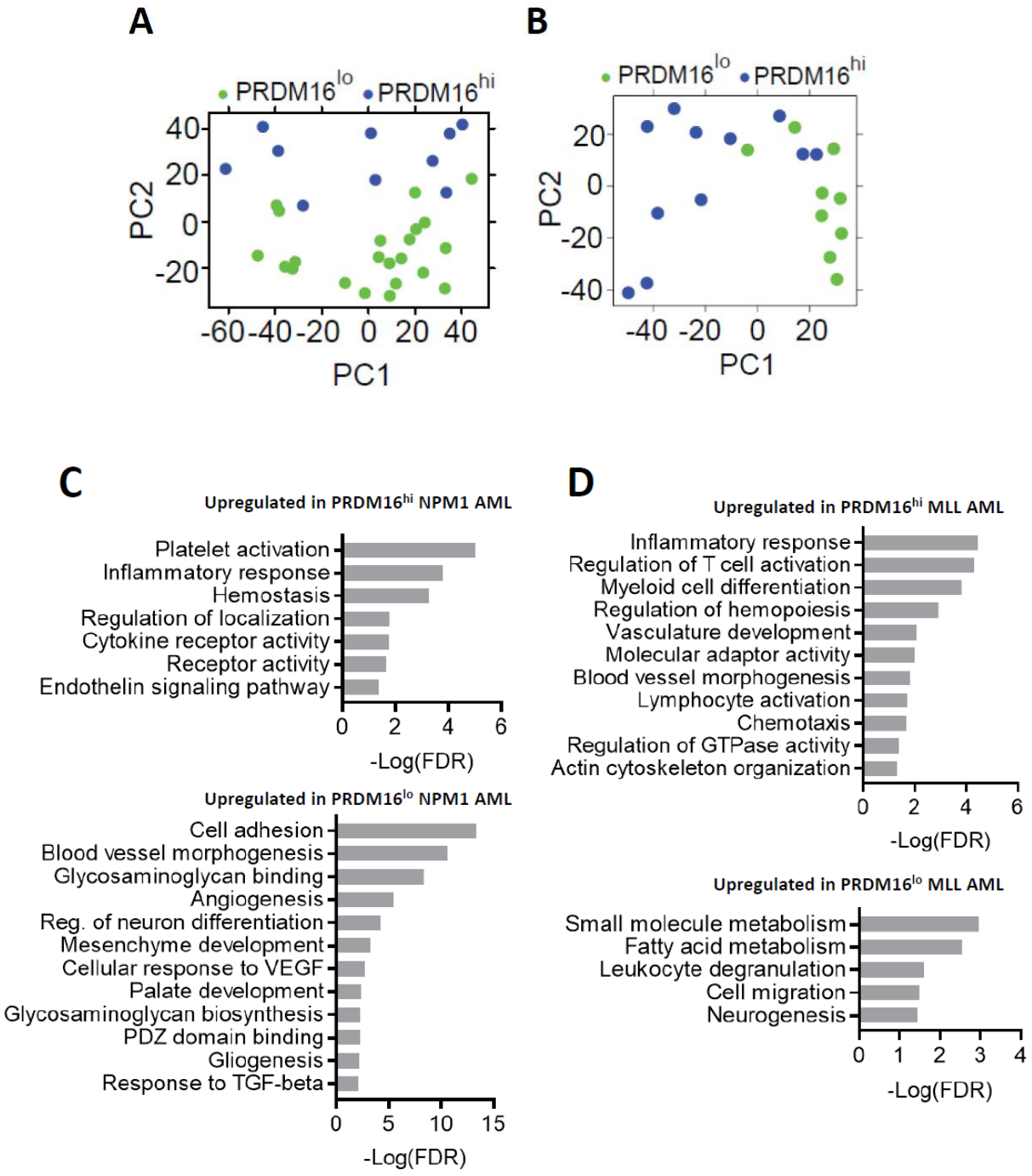

Figure 5-18: Inflammatory pathways are upregulated in *PRDM16^{hi}* human AML subsets. (**A**) PCA of RNAseq performed on NPM1-mutated and (**B**) MLL-rearranged AML cases from the CGA, comparing *Prdm16^{hi}* and *Prdm16^{lo}* cohorts. (**C**) Representative list of GO pathways upregulated in *Prdm16^{hi}* or *Prdm16^{lo}* cohorts of NPM1-mutated or (**D**) MLL-rearranged AML cases in the CGA. Values expressed as $-\text{Log}_{10}$ of the P-value, determined by PANTHER algorithm.

Section 5.5 – Inflammatory gene signature induced by *s-Prdm16* shows commonalities with myelodysplastic syndromes

The fact that *s-Prdm16* induced an inflammatory gene signature in an MLL-AF9 mouse model, and also that in certain human AML subsets, *PRDM16* correlated with inflammatory gene expression and worse prognosis, lead us to speculate that inflammation plays an important role in the decreased leukemic latency resulting from forced *s-Prdm16* expression. MDS, as described in Section 2.1.3., is a malignancy related to AML characterized by clonal expansion of malignant progenitors and ineffective hematopoiesis. Interestingly, inflammation is increasingly seen as a key feature of MDS[368]. Furthermore, PR-deleting leukemic rearrangements of *PRDM16* show dysplastic features and importantly, we found that bone marrow smears of *s-Prdm16*-expressing MLL-AF9 leukemia showed an increase in abnormal and fragmented nuclei (Figure 5-9).

We therefore selected from our RNAseq data all genes from the GO term "inflammatory process" that were upregulated in MLL-AF9 cells by *s-Prdm16* compared to empty vector in forced expression experiments, or upregulated in WT MLL-AF9 cells compared to *Prdm16*$^{fl/fl}$*.Vav-Cre*$^{+}$ cells lacking *s-Prdm16*. We cross-referenced this list to a consensus list of inflammatory genes frequently dysregulated in MDS[368]. A table documenting this comparison is provided in **Table 7**. Significantly more genes than would be expected by chance matched this consensus list in the WT vs *Prdm16*$^{-/-}$ and the *s-Prdm16*-expressed vs empty vector analyses, but not for the *f-Prdm16*-expressed vs empty vector analysis (**Figure 5-19**). We conclude that s-Prdm16, but not f-Prdm16, induces an inflammatory gene signature that overlaps with inflammatory signatures known to be observed in MDS.

Table 7: Genes differentially expressed by sPrdm16-expressing leukemia and MDS

	change in MDS	WT MLL-AF9 vs Prdm16$^{fl/fl}$.Vav-Cre		s-Prdm16 MLL-AF9 vs. empty vector	
		fold change	P-value	fold change	P-value
Ccl5	Lower	0.34	9.4E-03	0.32	3.5E-03
Csf1r	Higher	2.00	1.9E-02	3.58	8.4E-05
Tnf	Higher	3.12	5.1E-08	3.27	1.4E-05
Il1r2	Higher	2.60	4.1E-02	11.28	3.9E-06
Il15	Higher	2.29	7.9E-05	4.47	4.2E-16
Vegfa	Higher	*1.06*	*6.9E-01*	1.49	1.0E-02
Ccl3	Higher	3.33	7.2E-04	2.47	2.0E-04
Ccl4	Higher	2.69	9.0E-03	2.58	6.1E-03
Hgf	Higher	*1.18*	*4.8E-01*	3.28	3.6E-07
Tlr2	Higher	0.92	6.2E-01	2.43	1.4E-05
Tlr9	Higher	2.71	9.2E-03	1.96	3.4E-02

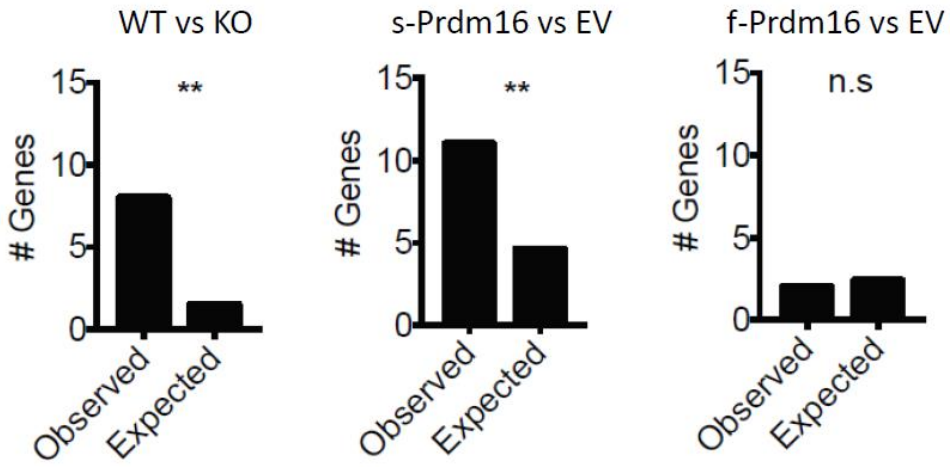

Figure 5-19: MLL-AF9 expressing *s-Prdm16* has common inflammatory gene expression with human MDS. Chi-square analysis of observed vs expected number of dysregulated inflammatory MDS-related genes in common with genes from our various MLL-AF9 RNAseq analyses (WT vs *Prdm16$^{fl/fl}$.Vav-Cre^{+}*, *s-Prdm16*-expressing vs empty vector, *f-Prdm16*-expressing vs empty vector). (n.s = $P > 0.05$; * = $P < 0.05$; ** = $P < 0.01$; *** = $P < 0.001$, Chi-square analysis)

Chapter 6 – MLL-AF9 LSCs have different mitochondrial properties than blasts, independent of PRDM16

Section 6.0 – Introduction

Our work, presented in Chapter 5, confirmed that the short isoform of PRDM16 functions as an oncogene, and concluded that inflammatory gene expression induced by s-Prdm16 may contribute to leukemogenesis. Previous work from our lab has demonstrated that Prdm16, specifically s-Prdm16, regulates expression of the mitofusin Mfn2. Furthermore, HSCs deficient for *Prdm16* have fragmented mitochondrial morphology compared to WT. We therefore speculated that mitochondrial dynamics may play a role in promoting leukemogenesis and that Prdm16 may be involved through regulation of Mfn2. We address this hypothesis in Chapter 6. We used fluorescently-labeled mitochondria in MLL-AF9 cells to determine that leukemic stem cells have different mitochondrial properties than blasts, specifically in regard to mitochondrial length, mass, and polarization. Further investigation, however, using *Prdm16*-deficient MLL-AF9 cells indicated that Prdm16 was not involved. We then ended this investigation, deciding that Prdm16-independent functions of mitochondrial dynamics in LSC maintenance was beyond the scope of our project. Nonetheless, this work revealed interesting findings regarding the role of mitochondrial dynamics in LSCs which could serve as the basis for future studies.

Section 6.1 – LSCs have distinct mitochondrial properties compared to blast cells, independently of Prdm16

Based on previous findings regarding Prdm16, and our work presented in Chapter 5, we hypothesized that mitochondrial dynamics may play a Prdm16-dependent role in MLL-AF9 oncogenesis. We therefore devised methods to visualize mitochondria in MLL-AF9 cells to correlate mitochondrial properties with leukemogenicity in these cells.

Different AML subsets have distinct surface markers which can be used to enrich for leukemic stem cell (LSC) activity. In murine models of MLL-AF9, LSCs are not known to exhibit a unique surface phenotype allowing for isolation with high purity. It has been shown, however, that essentially all cells with LSC activity are $cKit^+$, with LSC activity further concentrated in cells with lower "Lineage" staining (Gr1/Mac1 for myeloid leukemias)[369]. The $cKit^-$ population consists almost entirely of blast cells with no capacity to regenerate leukemia. We therefore sorted MLL-AF9 cells into $Lin^{lo}cKit^+$ and $cKit^-$ subsets to determine if these two populations had different mitochondrial properties. We stained cells with Mitotracker Red (MTR), a red-fluorescent dye that stains mitochondria with intact membrane potential, selectively staining functional mitochondria. Visualization of individual mitochondria (and therefore measurement of mitochondrial length) was difficult with MTR, owing to mild background staining. We did note, however, that mitochondria in the $Lin^{lo}cKit^+$ population appeared to be more polarized than in the $cKit^-$ cells. To calculate this, we developed a method of quantification, described in the Methods section (7.9), to assign individual cells a polarization score between 0 (homogenous mitochondrial staining in all 8 octants of the cell) and 100 (all mitochondrial intensity localized within one specific octant). Illustrative schematic (**Figure 6-1A**) and MTR-stained cell (**Figure 6-1B**) examples are provided below for reference. Quantification of polarization score from 45 $Lin^{lo}cKit^+$ and $cKit^-$ cells confirmed that $Lin^{lo}cKit^+$ cells were indeed more polarized than $cKit^-$ blast cells (**Figure 6-2A**). Furthermore, we verified, in our murine MLL-AF9 model, that

the $Lin^{lo}cKit^{+}$ population was enriched for colony-forming cells (approximately 16%) compared to $cKit^{-}$ cells (1% forming colonies), consistent with other published work (**Figure 6-2B**).

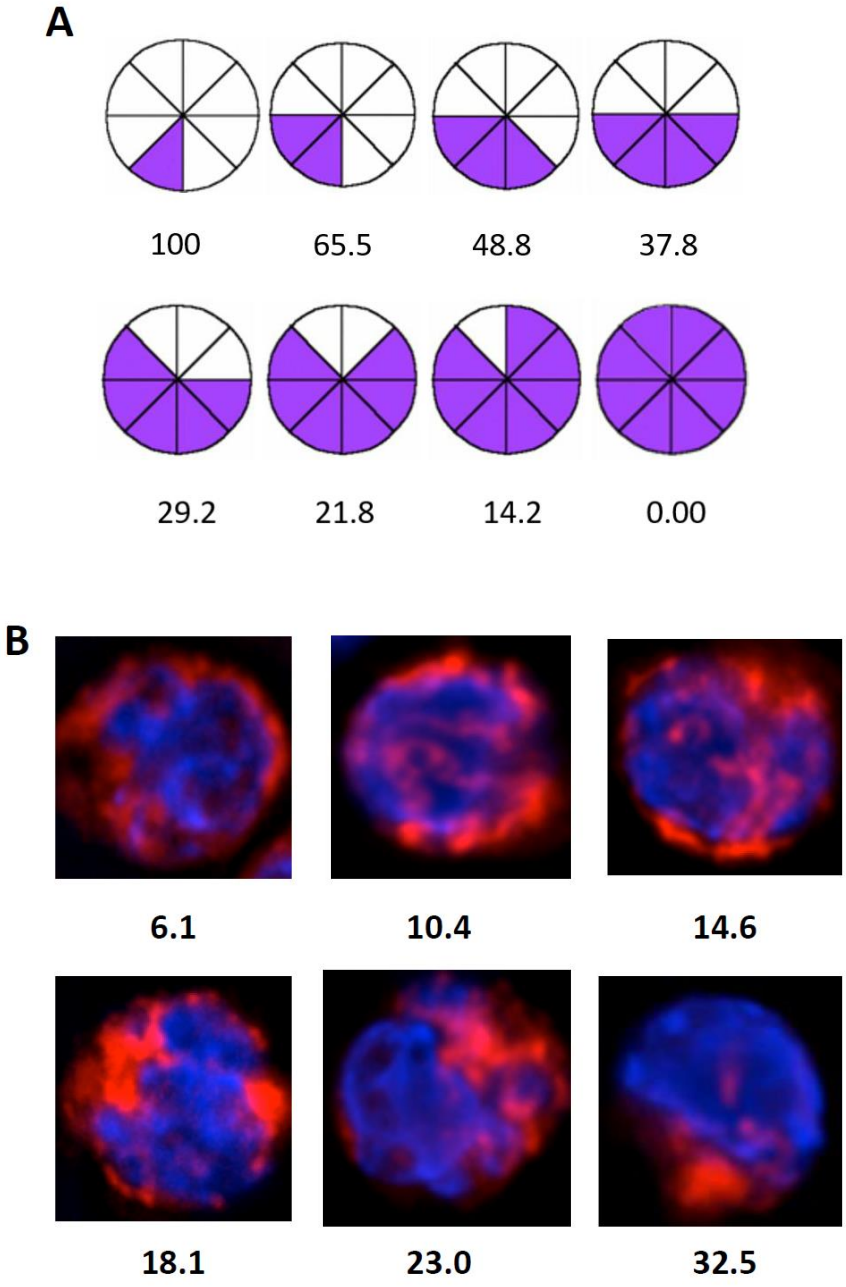

Figure 6-1: Illustrative examples of mitochondrial polarization scoring: (**A**) Schematic representation of mitochondrial polarization scores (mitochondria represented as violet staining) ranging from 100 (all mitochondria localized in one octant) to 0 (homogenous mitochondrial intensity in all octants). (**B**) Six cellular examples of polarization scores (mitochondria stained with Mitotracker Red), ranging from unpolarized (score = 6.1) to polarized (score = 32.5)

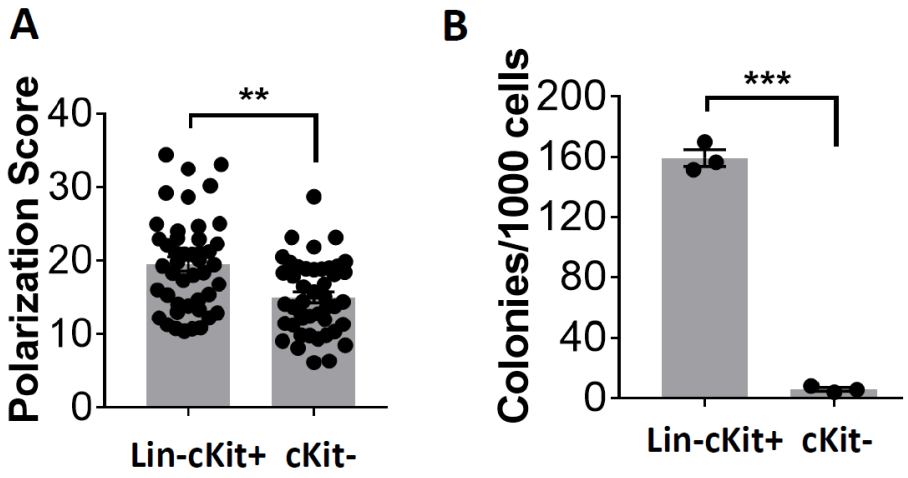

Figure 6-2: Cells with enriched LSC potential have increased mitochondrial polarization. (**A**) Polarization scores of MTR-stained $Lin^{-}cKit^{+}$ or $cKit^{-}$ MLL-AF9 cells (*n* = 45). (**B**) Colony assays of $Lin^{-}cKit^{+}$ or $cKit^{-}$ MLL-AF9 cells (*n* = 45). (n.s = *P* > 0.05; * = *P* < 0.05; ** = *P* < 0.01; *** = *P* < 0.001, Student's t-test for single comparisons)

Quantification of mitochondrial polarization using MTR suggested that LSCs may be more polarized than blast cells. As mentioned previously, however, the $Lin^{lo}cKit^{+}$ population is only enriched for colony-forming cells, with at least 80% of cells failing to form colonies. Therefore, a more direct single-cell comparison between mitochondrial phenotype and colony-forming ability was warranted. MTR specifically stains mitochondria but is toxic to MLL-AF9 cells. We therefore used other methods to clearly visualize mitochondria without inducing toxicity, allowing us to measure mitochondrial properties of individual MLL-AF9 cells and then track their LSC potential in colony-forming assays. We transduced MLL-AF9 cell lines with a retroviral vector expressing a mitochondrially-targeted red fluorescent protein (RFP) to generate a leukemic line (AF9-RFP) with clearly distinguishable mitochondria (examples in **Figure 6-3**).

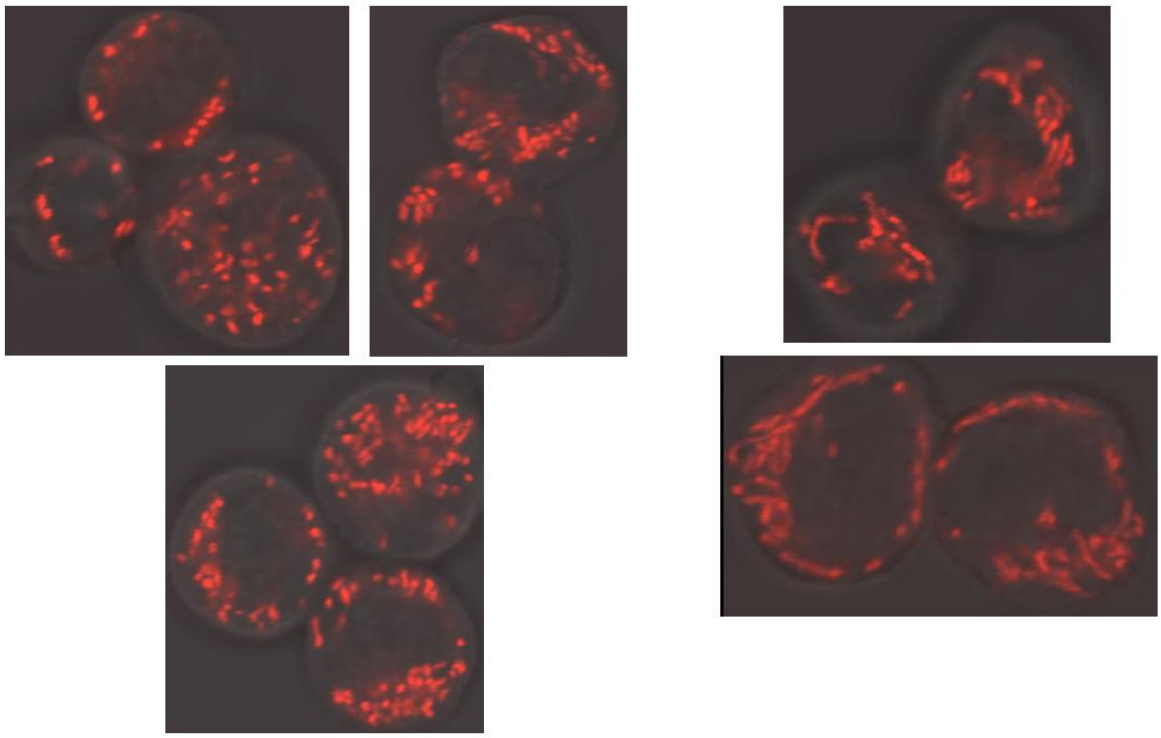

Figure 6-3: Representative AF9-RFP images with specifically stained mitochondria. Representative images of cells retrovirally transduced with a vector encoding a mitochondrially-targeted red fluorescent protein (RFP). Cells imaged at 63x magnification. Cells with fragmented mitochondria are displayed on the left, with elongated mitochondria illustrated on the right.

We devised a single-cell assay in which cells were sorted into 96-well plates containing semisolid methylcellulose media to immobilize them. Clear mitochondrial staining allowed us to score mitochondrial length, which was not possible using MTR. We therefore scored the cells as either polarized or unpolarized, and as having either fragmented or elongated mitochondria. We then determined which cells formed colonies after 7 days, an indicator of LSC potential. We scored a total of 624 cells. The overall score distribution is displayed in **Figure 6-4A**. Analysis of colony-forming cells indicated that MLL-AF9 cells with polarized mitochondria were more likely to form colonies than unpolarized cells, consistent what we found using MTR (**Figure 6-4B**). This difference was slight, though statistically significant (P=0.015). More strikingly, we determined that MLL-AF9 cells with elongated mitochondria were significantly

(approximately 2.5 times) more likely to form colonies than cells with fragmented mitochondria (P<0.0001) (**Figure 6-4C**).

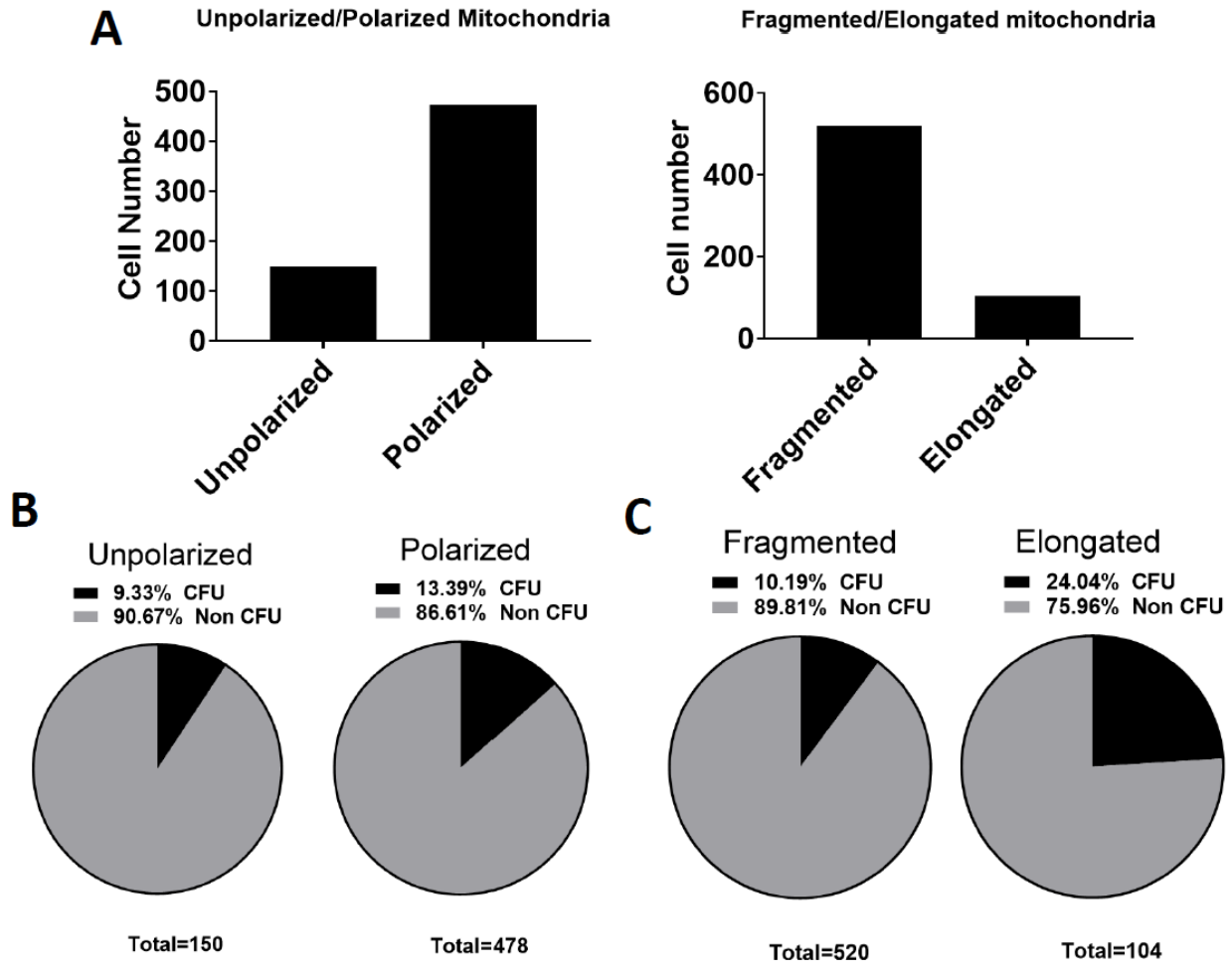

Figure 6-4: MLL-AF9 cells with polarized or elongated mitochondria have higher colony-forming ability. (**A**) Distribution of cellular scores from single-cell assays of RFP-expressing MLL-AF9 cells. Mitochondria scored as either unpolarized or polarized (left panel) and either fragmented or elongated (right panel) (*n* = 5 experiments and 624 individual cells). (**B**) Percentage of mito-RFP-expressing MLL-AF9 cells with either unpolarized or polarized mitochondria that form colonies (*P* = 0.015, Chi-Square test). (**C**) Percentage of mito-RFP-expressing MLL-AF9 cells with either fragmented or elongated mitochondria that form colonies (*P* < 0.0001, Chi-Square test).

We also stained MLL-AF9 cells with mitotracker green (MTG), a commonly used flow cytometric determinant of mitochondrial mass which does not induce toxicity. We sorted leukemic cells into three populations based on MTG fluorescence – MTG^{lo}, MTG^{med} and MTG^{hi}. Colony assays with these

populations revealed that MTG^{hi} cells were significantly more likely to form colonies than MTG^{lo} cells. MTG^{med} cells showed an intermediate phenotype (**Figure 6-5**). Thus, we concluded that multiple mitochondrial phenotypes, including mitochondrial length, mass, and polarization, correlate with LSC potential in MLL-AF9 cells.

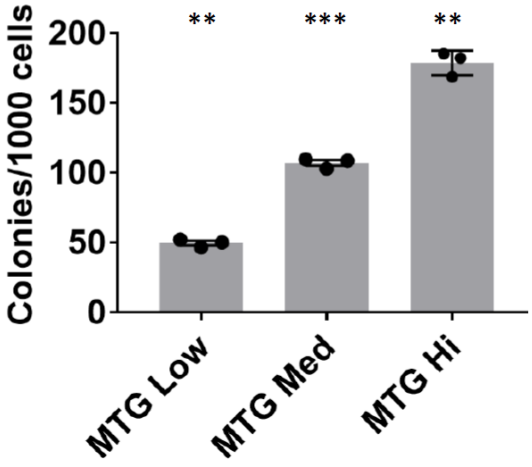

Figure 6-5: MLL-AF9 cells with high MTG staining are more likely to form colonies. Colony-forming assay of mitotracker green (MTG)-stained cells sorted into either low, medium, or high populations based on MTG fluorescence. Displayed as colonies formed per 1000 cells (n = 3 independent experiments, $P < 0.01$ for all comparisons, One-way ANOVA for multiple comparisons)

These experiments did not distinguish whether mitochondrial dynamics were a cause of differences in LSC potential, which would suggest a potential mechanism of LSC maintenance, or rather served only as indicators of LSC potential. We used the phenotype of mitochondrial elongation, which exhibited the strongest correlation with colony-forming potential, to investigate this question further. Although there was a quantitative difference between colony-forming capacity of fragmented vs elongated MLL-AF9 cells, both populations were nonetheless able to generate colonies (10% of fragmented cells compared to 25% of elongated cells). If colonies formed from clones of different mitochondrial length continued to exhibit differences in serial experiments, this would be more indicative of a mechanistic relationship between mitochondrial length and LSC potential. We therefore collected individual colonies originating from either

fragmented or elongated clones and analyzed these cells. Fragmented-derived or elongated-derived colonies were similar in secondary colony-forming ability (**Figure 6-6A**) and, more importantly, in leukemic latency after transplantation into irradiated mice (**Figure 6-6B**). Therefore, colonies derived from either fragmented or elongated clones were functionally similar. This result suggested that the altered mitochondrial structure (increased length, mass, and polarization) enriched in LSCs may only indicate LSC potential rather than function as a mechanistic determinant of LSC maintenance.

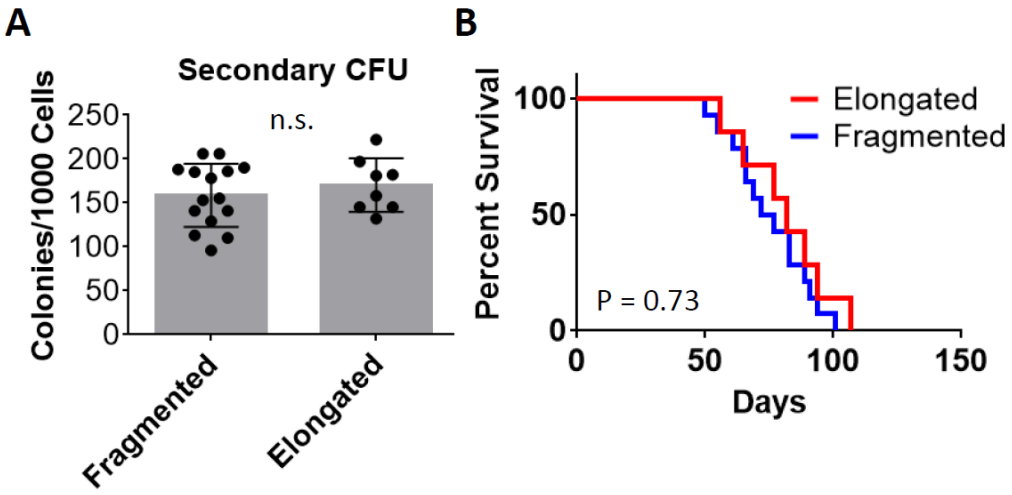

Figure 6-6: Colonies formed by fragmented or elongated MLL-AF9 clones are functionally similar. (**A**) Secondary colony-forming assay of cells taken from primary colonies generated from single MLL-AF9 cells with either fragmented or elongated mitochondria. Expressed as number of colonies per 1000 plated cells. (**B**) Survival curve of recipient mice transplanted with the same cells from (A). (*n* = 8-15 primary colonies, each plated in duplicate for colony assays, or transplanted into one recipient mouse in transplants). (Student's t-test for single comparisons and Gehan-Breslow-Wilcoxon test for comparison of survival curves)

To determine if this mitochondrial phenotype was *Prdm16*-dependent, we compared mitochondrial lengths of MLL-AF9 cells derived from *Prdm16*$^{-/-}$, *Prdm16*$^{+/-}$ or WT *Prdm16*$^{+/+}$ mice that we transduced with mito-RFP retrovirus. These three MLL-AF9 populations exhibit clear differences in leukemic latency (Figure 5-3A). We found that mitochondrial lengths were not different within the three populations (**Figure 6-7**),

indicating that regulation of mitochondrial dynamics is not a mechanism by which Prdm16 affects leukemogenesis.

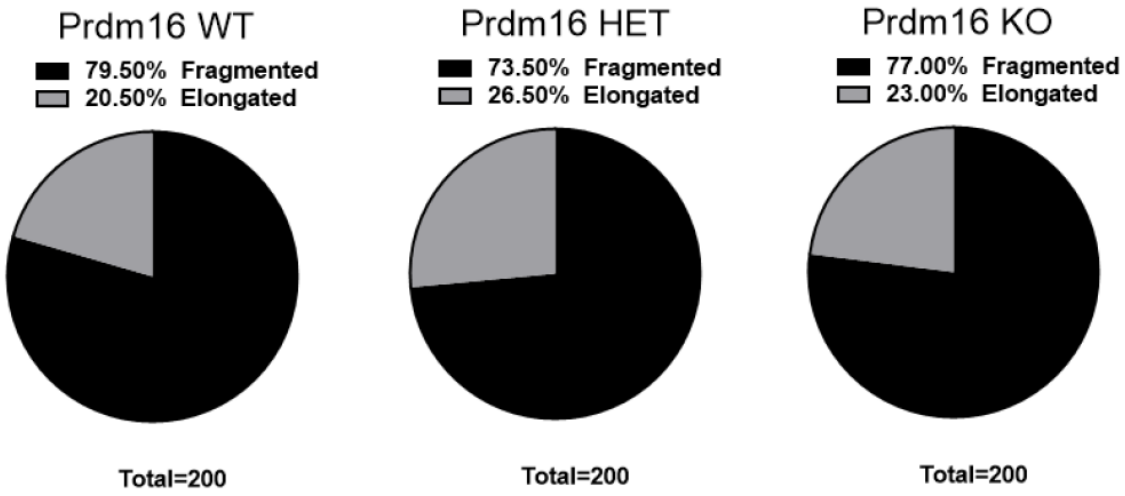

Figure 6-7: Prdm16 does not affect mitochondrial length of MLL-AF9 cells. MLL-AF9 cells derived from *Prdm16*$^{-/-}$, *Prdm16*$^{+/-}$ or WT *Prdm16*$^{+/+}$ mice were transduced with mito-RFP retrovirus, RFP+ cells were sorted and mitochondrial lengths scored as either fragmented or elongated. Scores presented above show no significant difference in length distribution in any population (*n* = 200 cells, P > 0.5 for all comparisons by Chi-square test)

Lastly, because Prdm16 regulates expression of *Mfn2* in HSCs, and as *Mfn2* deletion has a deleterious effect on HSC maintenance, particularly of those with lymphoid potential, we determined if deletion of *Mfn2* affects MLL-AF9 leukemogenesis. We transduced HSCs from adult *Mfn2*$^{fl/fl}$*.Vav-Cre*$^{+}$ mice and WT littermate controls with MLL-AF9. These mice have conditional deletion of *Mfn2* in the hematopoietic system similar to the *Prdm16* conditional deletion. We observed that *in vitro* growth (**Figure 6-8A**) and leukemic latency (**Figure 6-8B**) of *Mfn2*$^{fl/fl}$*.Vav-Cre*$^{+}$ cells were not different from WT leukemia. Furthermore, we analyzed RNAseq data comparing *Prdm16*$^{fl/fl}$*.Vav-Cre*$^{+}$ and WT MLL-AF9 cells and found that expression of *Mfn2* in these cohorts was unchanged (**Figure 6-8C**). Taken in totality, the data presented in Chapter 6 led us to conclude that, although there appears to be some correlation between mitochondrial dynamics and LSC potential, it is unclear if mitochondrial dynamics function as a causative

factor in LSC maintenance. Furthermore, our data indicated that neither Prdm16, nor its downstream target in HSCs, Mfn2, were related to the changes in mitochondrial dynamics observed. Considering this, we decided that a study of mitochondrial dynamics in LSC maintenance was beyond the scope of this thesis, though it could serve as a promising basis for future investigations.

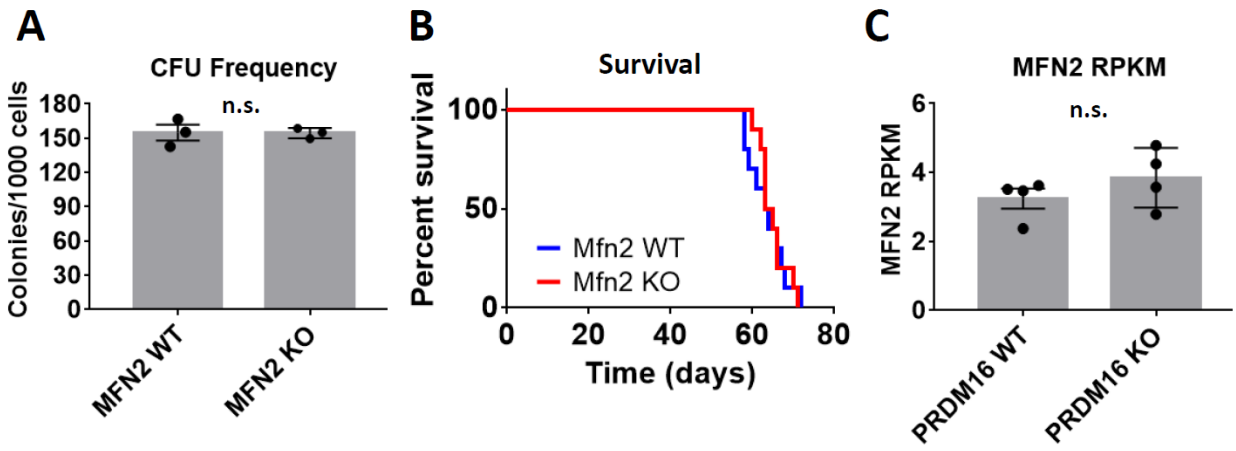

Figure 6-8: *Mfn2* deletion does not affect MLL-AF9 leukemogenesis. (**A**) Colony forming assays of MLL-AF9 cells derived from either *Mfn2*$^{fl/fl}$*.Vav-Cre*$^{+}$ (Mfn2 KO) mice or WT littermates. (*n* = 3 experiments) (**B**) Survival curves of recipient mice transplanted with either Mfn2 WT or Mfn2 KO MLL-AF9 cells. (*n* = 10 mice from 2 independent transplants) (**C**) Calculated RPKM from RNAseq samples of MLL-AF9 cells from *Prdm16*$^{fl/fl}$*.Vav-Cre*$^{+}$ (Prdm16 KO) or WT littermate mice. (*n* = 4 samples)

Chapter 7 – Materials and Methods

7.1. Experimental mice

C57BL/6J mice (CD45.2) and competitor B6.SJL-Ptprca$^{Pep3b/BoyJ}$ (CD45.1) mice were purchased from the Jackson Laboratory (Bar Harbor, ME).

Prdm16$^{fl/fl}$ mice were generated by Ingenious Targeted Laboratory, Inc. (Stony Brook, NY). A neomycin resistance cassette flanked by *FRT* and a 3' *LoxP* site were inserted upstream of exon 6 and another *LoxP* site was inserted downstream of exon 7 in a 10.2 Kb fragment from a C57NL/6 bacterial artificial chromosome (BAC) clone, extending from intron 5 through exon 9. The modified BAC clone was electroporated into mouse embryonic stem cells, and Neo resistant clones were expanded, screened for retention of the Neo cassette and for the second *LoxP* site, and injected into B6 blastocysts to generate chimeric mice. Removal of the Neo cassette was accomplished by crossing to *FLP* heterozygous mice, resulting in mutant, *Prdm16$^{fl/fl}$* mice with *LoxP* sites flanking exon 6 and 7.

Isoform-specific *Prdm16* knockout mice were generated using CRISPR/Cas9. PX330-based plasmids (200ng/µL), containing CRISPR/Cas9 expression cassettes and specific gRNAs (see **Table 8,** primers and gRNA), were injected into fertilized B6 blastocysts. Mice chimeric for CRISPR-initiated mutations were bred to WT C57BL/6J. Heterozygous siblings were mated to generate a homozygous mutant.

Prdm16$^{+/-}$ mice were derived from sperm saved from *Prdm16$^{Gt(OST67423)Lex}$* mice (Lexicon Genetics, Basking Ridge, NJ) obtained from a gene-trap library[370]. Mice were reconstituted by in vitro fertilization and bred as heterozygotes.

7.2. MLL-AF9 transduction and cell culture

pMSCV-FPRDM16-IRES-GFP/RFP and pMSCV-SPRDM16-IRES-GFP/RFP plasmids were cloned by XhoI/EcoRI-insertion of *f-Prdm16* or *s-Prdm16* cDNA into a backbone pMSCV-IRES-GFP or pMSCV-IRES-

RFP plasmid (Addgene). pMSCV-MLL-AF9-IRES-hNGFR was cloned by deletion of GFP from a pMSCV-MLL-AF9-IRES-GFP plasmid and insertion of hNGFR cDNA[371]. Retroviral particles were produced by seeding PlatE cells (Cell Biolabs, San Diego, CA) at $7x10^5/cm^2$ overnight followed by transfection of each packaging and expression construct (1:1:1) using Lipofectamine 3000 (Invitrogen, Carlsbad, CA) according to manufacturer's instructions. Media were pooled after 48 hours, clarified and concentrated by ultracentrifugation (100,000xg), resuspended in RPMI media (Corning/Cellgro, Corning, NY) and stored at -80^{o}C. MLL-AF9 cells were generated by transduction of sorted HSCs ($Lin^-cKit^+Sca1^+Flt3^-$) or $Lin^-cKit^+Sca1^-CD16/32^+$ cells (a population containing committed myeloid and erythroid progenitors) with an MSCV-MLL-AF9-hNGFR retroviral construct by spinfection at 750 RCF, 22°C for 90 minutes. $hNGFR^+$ cells were sorted and expanded in RPMI media (Corning/Cellgro) containing 15% FBS (Atlanta Biologicals, Flowery Branch, GA), 1x Glutamax (Gibco, Gaithersburg, MD), penicillin/streptomycin (Gibco), 1x MEM Non-Essential Amino Acids (Gibco), SCF (50ng/mL), IL-6 (20ng/mL), and IL-3 (10ng/mL) (all peptides from Peprotech, Rocky Hill, NJ). For *in vitro* growth assays, 1000 cells were plated in 1ml media of the same composition additionally containing 1.5% methylcellulose (Sigma-Aldritch, St. Louis MO) and colony number was counted after 7 days.

7.3. MLL-AF9 leukemia and hematopoietic stem cell transplantation

200 purified HSCs, $2x10^5$ unsorted bone marrow (BM) or fetal liver (FL) cells, or $2x10^4$ purified MLL-AF9 immortalized cells as indicated, were injected together with $2x10^5$ competitor BM cells ($CD45.1^+$ for competitive transplants to distinguish from CD45.2 donor cells, $CD45.2^+$ for leukemic transplants) into lethally irradiated mice (two doses of 475 cGy using a Rad Source RS-200 X-ray irradiator [Rad Source, Brentwood, TN]) by tail vein injection. Survival in leukemia experiments was determined as the number of days post-transplant before the mouse became moribund, at which time mice were euthanized.

7.4. Quantitative RT-PCR

After cell lysis (Trizol, Invitrogen, Carlsbad, CA), RNA was isolated according to manufacturer's instructions, using a chloroform/isopropanol extraction, and washing with 70% ethanol. cDNA was prepared using Superscript III Reverse Transcriptase (Invitrogen). PCR was performed using the Viia7 Real Time PCR System (Applied Biosystems), using either inventoried or custom Taqman probes, or using custom primers and SYBRGreen enzyme (primers are listed in **Table 8,** primers and gRNA). Relative mRNA content was determined by the ΔΔCT method with normalization based on GAPDH-VIC, or 18S-VIC housekeeping genes. To determine copy number of *Prdm16* isoforms, a Taqman probe was designed that was specific to *f-Prdm16* (exon2/3 junction), and another probe (exon 14/15 junction) was used to quantify total *Prdm16* (*t-Prdm16*). Copy number was calculated from a linear regression of serial dilutions of a *Prdm16*-containing plasmid, and *s-Prdm16* copy number was calculated via subtraction. (*s-Prdm16* = *t-Prdm16 – f-Prdm16*). A parallel method was used to quantify *s-Prdm16* RPKM from RNAseq experiments.

7.5. Flow cytometry and cell staining

Cells were analyzed on a BD LSRII flow cytometer, BD Fortessa flow cytometer, or BD Canto flow cytometer (Becton Dickinson, Mountain View, CA). Cells were sorted using a BD Influx cell sorter. For BM analysis, bones were crushed, lysed with ACK lysis buffer, and filtered through a 0.22um filter prior to staining. For FL analysis, livers were isolated from (E)13-15 embryos, passed through a 0.22uM filter to separate from tissue, and lysed with ACK lysis buffer prior to staining. For peripheral blood (PB) analysis, blood obtained by submandibular bleeding was lysed twice with ACK lysis buffer prior to staining. Staining was performed by incubating cells with an antibody cocktail in FACS buffer for 30 minutes at 4°C and then washing in FACS buffer before analysis. Antibodies are listed in **Table 9**. All data were analyzed using FlowJo 9.6 (TreeStar Inc., Ashland, OR). BM and PB from select moribund mice was stained for hematoxylin/eosin (Vector Laboratories, Burlingame, CA). Undiluted PB or BM diluted in 50uL/femur was smeared on slides, fixed with methanol, and stained with hematoxylin/eosin according to manufacturer's protocol.

7.6. Seahorse metabolic flux analysis

Respiratory oxygen consumption rate (OCR) and glycolytic acidification (mpH/sec) were determined using a Seahorse XFe96, or XFp metabolic flux analyzer (Seahorse Bioscience, North Billerica, MA). MLL-AF9 cells ($1x10^6$ cells/well) or enriched HSCs ($Lin^-cKit^+Sca1^+Flt3^-$, $7.5x10^4$ cells/well), were suspended in unbuffered medium, equilibrated at 37°C in a CO_2-free incubator, transferred to the Seahorse Bioanalyzer and assayed. The Mitochondrial Stress Test (Seahorse) was used to measure the respiratory properties of the cells, and the Glycolysis Test (Seahorse) was used to measure glycolytic properties.

7.7. Measurement of reactive oxygen species (ROS)

Cells were suspended in 500µL of PBS ($1x10^5$ cells/mL) at room temperature with 1µL CellROX Deep Red (Thermo Fisher, Waltham, MA) for 45 minutes, washed, resuspended in FACS buffer, and analyzed by flow cytometry in the APC channel. Cells treated with both CellROX and tert-butyl hydroperoxide (TBHP) were used as positive controls.

7.8. RNAseq analysis, principal component analysis, pathway analysis

mRNA from total RNA samples (400ng per sample) was enriched by poly-A pull down. Libraries were prepared using TruSeq RNA prep kit (Illumina, San Diego, CA)) and sequenced using Illumina HiSeq2000 at the Columbia Genome Center. Samples were multiplexed in each lane. Base calling was performed using RTA (Illumina). BCL and bcl2fastq programs were used to convert BCL to FASTQ format, coupled with adaptor trimming. Reads were mapped to a reference genome (UCSC/mm9) using Tophat with 4 mismatches and 10 maximum multiple hits. Binary alignment (BAM) files were generated by Tophat to map reads to annotated genes, and converted to an annotated count matrix, using the Rsamtools and GenomicAlignments packages in R. Data was then analyzed using DESeq to obtain differential expression analysis and principal component analysis. Pathway analysis was performed using PATHER, with pathway data from the GO gene ontology database.

7.9. Mitochondrial Staining and Quantification of Mitochondrial Polarization

Mitochondria were stained with 200nM of Mitotracker Red (Invitrogen) and 300nM DAPI for 30 minutes at 37^{o}C, washed with PBS and visualized using a Leica DMI 6000B microscope (Leica, Wetzlar, Germany). Pictures of each cell were saved and analyzed using ImageJ (public domain). We placed ovals manually over each cell image, which was then divided into octants using ImageJ. Mitotracker Red MFI was then calculated for each octant. Octant MFI was then normalized such that the total MFI per cell was adjusted to 100. The standard deviation of the normalized eight octants was then calculated and divided by 0.3535534, the maximum standard deviation for eight positive numbers totaling 1 (with octants 1, 0, 0, 0, 0, 0, 0, 0 or all intensity contained in one octant). In this way, a cell with all intensity in one octant would have a polarization score of 100, and a cell with equivalent MFI in all octants would have a score of 0.

7.10. Single-cell MLL-AF9 assays

Single MLL-AF9 cells were retrovirally transduced with a mitochondrially-targeted RFP protein. Sorted RFP^{+} cells were placed single wells of 96-well plates containing activation media with 1.5% methylcellulose. Cells were then visualized in a Leica DMI 6000B microscope and manually score as having either “polarized or unpolarized” mitochondria and having either “fragmented or elongated” mitochondria. These cells were then incubated for 7 days, at which point their colony-forming ability was determined and matched back to the original scoring of the cell.

7.11. Statistics

Statistical analysis was performed using PRISM software. Primary statistical tests include Student’s t-test for single comparisons of normally-distributed data, one-way ANOVA for multiple comparisons, Pearson’s correlation test for comparisons of Prdm16 RPKM vs Survival, Gehan-Breslow-Wilcoxon log-rank tests to compare the survival of recipient mice after leukemic transplants. For RNAseq analysis, the statistical P-value for individual genes was calculated from the DeSeq package in the statistical software R using a

binomial test that accounts for size factors and intragene sample variance, and principal component analysis was also performed with this software. Pathway analysis from RNAseq was performed using the statistical overrepresentation test from PANTHER, with a Bonferroni correction for multiple testing. Chi-square tests were also used to test whether the observed frequency of selected "hits" from RNAseq analysis were larger than the expected frequency.

7.12. Study Approval

Experiments and animal care were performed in accordance with the Columbia University Institutional Animal Care and Use Committee, under the approved mouse protocol AC-AAAM4750, of which all contributing authors are approved.

Table 8 -- List of primers and gRNA sequences

TAQMAN Primers (commercial)	**Taqman ID Number**	
Total PRDM16 (Exon 14/15)	Mm01266512_m1	
GAPDH	Mm99999915_g1	
Custom TAQMAN Primers	**Forward Primer**	**Reverse Primer**
Full-length PRDM16 (Exon 2/3)	5′-TGAAGGAGGCCGACTTTG-3′	5′-CCTGGGATGACACCTCTGTA-3′
	5'-Internal Probe	
	5′-TCCGTCAGCATCTGCTCCCATC-3′	
Primers	**Forward Primer**	**Reverse Primer**
CRISPR/Cas9 Exon 2 Indel Sequencing	5'-CCCGGTTCACCAACCTCCGAGGCTAC-3'	5'-GGCGTCACCACGTAGGGGCCAAACCTC-3'
CRISPR/Cas9 Intron 3 TSS-deletion Sequencing	5'-GCATGCCTGGTTAGCCACCCCAGTTG-3'	5'-GTCATCACAGGAACACGCTACACGG-3'
Vav-Cre Genotyping	5'-AGATGCCAGGACATCAGGAACCTG-3'	5-ATCAGCCACACCAGACACAGAGATC-3'
Prdm16 Floxed LOX1/SDL1 Genotyping	5'-AACACTATCCTGGGTGGTCTTTGG-3'	5-CGACAGTGGCAAGCGCTTCGAATG-3'
5'LAN1 and 3'LOX1 excision	5'-CCAGAGGCCACTTGTGTAGC-3'	5'-AACACTATCCTGGGTGGTCTTTGG-3'
CRISPR/Cas9 gRNA sequences	**20bp gRNA sequence**	
Exon 2 Indel gRNA1	GACTCTCGTAGCTCGAAGTC	
Exon 2 Indel gRNA2	CAAGGAGGGCTCGCCCTATG	
Exon 2 Indel gRNA3	GGGGGACAGGATGCCGTCTT	
Intron 3 deletion 5' gRNA 1	AAGCTGCCAGCCCGTGGTCC	
Intron 3 deletion 5' gRNA 2	ACTGGCCTCGGGGGTCAGGC	
Intron 3 deletion 3' gRNA 1	CTTACAAGCAACCTCGGGGT	
Intron 3 deletion 3' gRNA 2	CTGTACTGGCCTCGGGGGTC	

Table 9 - List of antibodies

Antibody	Company	Catalog #
Bone Marrow/Fetal Liver		
Lineage-FITC (CD2, CD3e, CD4, CD8, Ter119, GR-1, B220, CD19, Mac1)	eBioscience	11-0021-85, 11-0031-85, 11-0041-85, 11-0081-85, 11-5921-85, 3010-02, 11-5931-85, 11-0193-85, 11-0112-85
Sca1-Pac Blue	BD	560563
cKit-APC-Cy7	eBioscience	47-1171-82
CD48-A700	BioLegend	103426
CD150-PE-Cy7	BioLegend	115914
Flt3-PE	eBioscience	12-1351-82
Tissue Analysis - Competitive CD45.1/2 transplants		
Donor/Competitor		
CD45.1-Pac Blue	Tonbo	75-0453
CD45.2-PerCP5.5	BioLegend	109828
CD45.1-PE-Cy7	Tonbo	60-0453
CD45.2-FITC	Tonbo	35-0454
CD45.1-BV650	BioLegend	110735
Spleen/Peripheral Blood		
CD3-Pac Blue	BioLegend	100214
B220-BUV395	BD	563793
Mac1-PE	Tonbo	50-0112
GR-1-APC	Tonbo	20-5931
CD19-APC-Cy7	BD	557655
CD21-FITC	BioLegend	123407
CD23-PE-Cy7	BioLegend	101613
cKit-PE-Cy7	BD	558163
Bone Marrow		
Sca1-PE	BioLegend	108107
Flt3-APC	eBioscience	12-1351-83
Sca1-APC	BioLegend	122511
CD34-PE	BD	551387
IL7Rα-PE	BD	552543
CD16/32-Pac Blue	BD	560539
Thymus		
cKit-BUV395	BD	745740
CD25-PE	BioLegend	102007
CD44-APC	BioLegend	103011
CD8-APC-Cy7	BD	561967
MLL-AF9-hNGFR Isolation		
human hNGFR-PE	BD	557196
Cell Cycle/Apoptosis analysis		
7AAD	Tonbo	13-6993
KI-67-PE	eBioscience	12-5698
cCaspase-3-Rabbit	Cell Signaling	9664S
Donkey anti-Rabbit-Alexa Fluor 647	Invitrogen	A-31573

Chapter 8 – Discussion and Future Directions

8.0. Graphical Summary

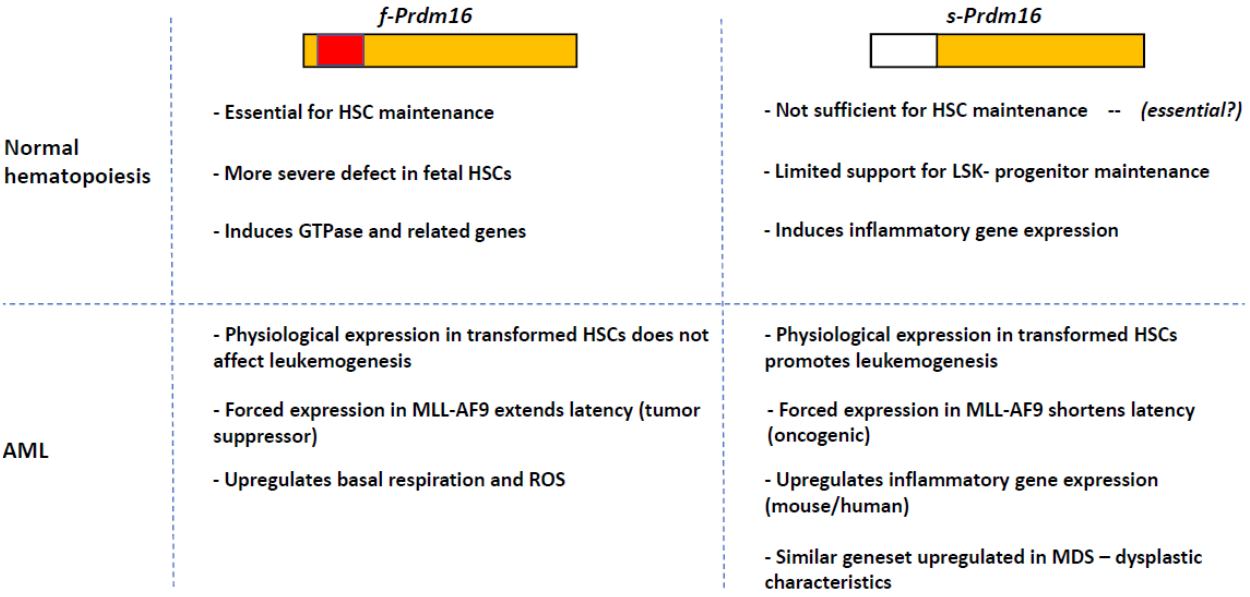

Figure 8-1: Graphical summary of key findings in normal hematopoiesis and AML. Graphical summary highlighting the essential findings of this thesis project, divided based on the two models studied (normal hematopoiesis and acute myeloid leukemia) and listing the key differences between the full-length isoform of *Prdm16* (*f-Prdm16*) and the short isoform (*s-Prdm16*).

8.1. Prdm16 is essential for adult HSC maintenance and regulates GTPase signaling

We first demonstrated the importance of Prdm16 in the maintenance of adult HSCs, showing that Prdm16 is essential for their long-term maintenance, as deletion of *Prdm16* in hematopoietic cells resulted in HSCs with lower competitive reconstitution with even more pronounced defects upon serial transplantation. Importantly, the *Vav-Cre* conditional deletion model, in contrast to the global deletion previously reported, revealed that the HSC defect in *Prdm16*-deficient HSCs was cell autonomous and not a result of Prdm16-dependent changes in external signaling from niche cells. The HSC phenotype of adult *Prdm16*$^{fl/fl}$*.Vav-Cre*$^{+}$ HSCs, while significant, was less severe than that observed in the global deletion.

Transplants using *Prdm16*$^{fl/fl}$*.Vav-Cre*$^{+}$ fetal liver HSCs, however, showed a more pronounced defect and demonstrated that fetal liver HSCs exhibit a more severe Prdm16 phenotype than adult HSCs.

Gene expression analysis demonstrated that Prdm16 positively regulated Rho and Ras GTPase signaling in HSCs. Further gene expression profiling of HSCs specifically deleted for *f-Prdm16* ascribed this effect specifically to the full-length isoform. Pathways involving angiogenesis and cell motility, in which small GTPases play important roles[372-374], were also upregulated by *f-Prdm16*. Functions of GTPases in vasculogenesis include modulation of endothelial permeability, extracellular matrix remodeling, and control of endothelial migration[375]. These pathways play important roles in HSC function, including in cytoskeletal regulation, which modulates niche interactions and affects HSC proliferation and self-renewal[355], migration and mobilization[376], and HSC aging[377]. Furthermore, a number of the genes downregulated in both *Prdm16*$^{fl/fl}$*.Vav-Cre* and *Δ47-fPrdm16*$^{-/-}$ HSCs are involved in vesicle trafficking, including *Als2cl*[378], *Arhgef10*[379], and *Rap11fip3*[380]. Currently, little is known regarding the role of vesicular or endosomal trafficking in HSC function. A large-scale shRNA screen for HSPC competitive repopulation activity, however, did uncover several vesicular trafficking genes whose depletion reduced HSPC repopulation in recipient mice. The authors offered the regulation of stable HSC-niche interactions, or transduction of key survival signals during hematopoietic stress, as potential mechanisms[381]. It is therefore plausible that *f-Prdm16* may regulate vesicular trafficking in HSCs, and that this could play important roles currently underappreciated in HSC function.

We observed an increase in mitochondrial respiration in *Prdm16*-deficient adult HSCs. This may account for some of observed HSC defects, as increased respiration is associated with an increase in cycling, HSC exhaustion, and oxidative stress. These changes are thought to begin with a metabolic switch to oxidative phosphorylation, leading to an accumulation of ROS triggering entry into cell cycle[382]. The activity of metabolic regulators such as pyruvate dehydrogenase kinases (Pdks) which promote glycolysis, enhance HSC maintenance, quiescence and competitive reconstitution capacity[383]. Deletion of *Prdm16* in adult

HSCs caused an increase in mitochondrial ROS in addition to elevated oxidative phosphorylation, as well as a slight increase in cycling just shy of statistical significance, lending plausibility to the conclusion that Prdm16 may maintain HSCs partially by promoting glycolytic metabolism or suppressing respiration and oxidative stress.

However, we did not observe changes in respiratory gene expression in fetal liver HSCs deleted for either *Prdm16* or *f-Prdm16*. Unfortunately, as the *f-Prdm16* deletion was global and embryonic lethal, we were unable to obtain adult *f-Prdm16*-deficient HSCs and were therefore unable to ascribe changes in mitochondrial respiration to either f-Prdm16 or s-Prdm16 specifically.

The absence of a respiratory or oxidative phosphorylation gene expression signature in either *Prdm16*$^{-/-}$ or *f-Prdm16*$^{-/-}$ fetal liver HSCs indicates that Prdm16 likely promotes HSC maintenance through additional important mechanisms and that the respiratory phenotype may not be linked. This is particularly true because *Prdm16*$^{-/-}$ and *f-Prdm16*$^{-/-}$ fetal liver HSCs, despite the absence of a respiratory phenotype, have a severe defect in HSC frequency and competitive reconstitution. Fetal liver HSCs have higher levels of both proliferation and respiratory ATP production, however[28], which may account for why no differences in respiration were observed in these cells. Differences in Rho and Ras GTPase gene expression, however, were consistently observed in all gene expression studies comparing *Prdm16* or *f-Prdm16*-deficient HSCs to WT controls, and we therefore conclude that differences in GTPase signaling, or processes dependent on this activity, my account for the defect observed in *Prdm16*-deficient HSCs, irrespective of HSC developmental stage.

8.2. f-Prdm16 is essential for HSC maintenance whereas s-Prdm16 supports limited lymphopoiesis through a Lin-Sca1+cKit- progenitor

Our generation and analysis of a specific *f-Prdm16*-deleted mouse model demonstrated that the full-length Prdm16 isoform is essential for HSC maintenance, with a similarly severe defect in HSC frequency and competitive transplantation as the complete *Prdm16* deletion. This is the first work to develop and characterize a mouse with specific deletion of the *f-Prdm16* isoform.

Although we were not able to generate a specific *s-Prdm16*$^{-/-}$ mouse, we could infer some of the hematopoietic functions of *s-Prdm16* by comparing *f-Prdm16*$^{-/-}$ fetal liver HSCs (which express *s-Prdm16*) to the complete deletion lacking both Prdm16 isoforms. We found that *s-Prdm16* is required for the generation of a Lin^{-}Sca1^{+}cKit^{-} (LSK-) lymphoid progenitor distinct from CLPs. In bone marrow from competitive transplant recipients, *f-Prdm16*$^{-/-}$ donor cell chimerism was severely reduced (approximately 1% the level of WT) in all cell populations except for LSK- cells, whose reconstitution was comparable to WT levels. Consistent with previous findings in our lab[67,68], LSK- progenitors have the capacity for lymphoid (predominantly B-cell) development and their progeny have elevated surface expression of Sca1. Gene expression studies indicated that *f-Prdm16*$^{-/-}$ HSCs had an inflammatory gene expression signature, suggesting that *s-Prdm16* may promote and *f-Prdm16* may suppress inflammation, a finding consistent with what we observed in *s-Prdm16*-expressing leukemia (Section 8.3). Inflammatory mediators, including TNF which was upregulated in *f-Prdm16*$^{-/-}$ HSCs, have been shown to induce Sca1 expression[384]. Sca1, despite being well known as a murine HSC marker, does not currently have a characterized hematopoietic function. However, as Sca1 is expressed in LSK- progenitors, and differentiated progeny retain elevated Sca1 expression, it is plausible that Sca1 may be involved in LSK- regulation, and that inflammatory signaling may contribute to this. Acute inflammation activates HSCs but becomes detrimental to HSC function and preservation when chronic[385]. It is therefore possible that specific deletion of *s-Prdm16*

would also demonstrate a critical role for this isoform and that normal HSC function requires a balance between both isoforms, making targeted deletion of *s-Prdm16* a worthy pursuit for future investigation.

8.3. s-Prdm16 is an oncogene that may contribute to leukemogenesis by inducing inflammation

Experiments using a murine model of MLL-AF9 indicated that forced expression of *s-Prdm16* shortened leukemic latency, demonstrating an oncogenic role for this Prdm16 isoform. Furthermore, physiological levels of *s-Prdm16* in leukemic cell-of-origin support MLL-AF9 leukemogenesis, as the expression of *s-Prdm16,* as in *Δ47-fPrdm16*$^{-/-}$ HSCs, was sufficient to reverse the increased latency observed in *Prdm16*$^{fl/fl}$*.Vav-Cre* leukemia back to that of WT. Because in these experiments *Prdm16* was not detectably expressed in MLL-AF9 cells, but only the originating HSCs from which the leukemia was derived, the effect of *s-Prdm16* may therefore be epigenetic. This finding would be consistent with published work using the murine MLL-AF9 model, which demonstrated that differences in cell-of-origin can lead to significant differences in the resulting leukemia in terms of epigenetics, gene expression, and leukemic latency[224].

We observed an increase in inflammatory gene expression in *s-Prdm16*-overexpressing MLL-AF9 cells, similar to that found in *f-Prdm16*$^{-/-}$ HSCs which express only the short isoform. We also observed increased inflammatory signaling in WT MLL-AF9 (expressing *s-Prdm16* in the leukemia-initiating HSCs) compared to *Prdm16*$^{fl/fl}$*.Vav-Cre* leukemia. Our detection of inflammatory gene expression in each of these experiments suggests that this may be an important mechanism underlying the role of *s-Prdm16* in leukemia. As described in Section 2.3.4, recent work has identified an association between inflammation and outcome in both AML and MDS, as well as other hematopoietic malignancies. Novel therapeutic strategies to treat MDS through anti-inflammatory strategies are currently being explored[386]. In some studies, pre-existing inflammation plays a role in predisposition to malignancy[387]. Our results suggest that, in the case of *s-Prdm16*, direct induction of inflammation from the leukemic cells may also play a role in leukemic progression. We corroborated this hypothesis by analyzing samples from the Cancer Genome

Atlas. Expression levels of *PRDM16,* predominantly *s-PRDM16,* were associated with inflammatory gene expression and a decrease in overall patient survival in NPM1-mutated and MLL-rearranged AML.

A comparison of the inflammatory genes upregulated by *s-Prdm16* with those known to be associated with prognosis in MDS revealed a statistically-significant overlap between the two lists. Common upregulated genes included hepatocyte growth factor (*Hgf*), vascular endothelial growth factor A (*Vegfa*), and tumor necrosis factor (*Tnf*). Interestingly, we also observed that expression of *Ccl5*, one of the few consensus genes in MDS in which lower levels correlate with worse prognosis[388], was similarly downregulated by *s-Prdm16* in the MLL-AF9 mouse model. We observed an increased frequency of abnormal or fragmented nuclei in bone marrow smears of leukemic mice transplanted with *s-Prdm16*-expressing MLL-AF9 cells. Taken together, we conclude that *s-Prdm16* may regulate leukemogenesis in a manner similar to that seen in MDS, though further experiments are required to state this definitively. These data are also consistent with the fact that cases of AML with *PRDM16* translocations show dysplastic changes. The inflammatory signaling induced by *s-Prdm16* may provide a competitive advantage to leukemic cells by influencing the surrounding bone marrow environment to suppress normal hematopoiesis. *Ccl3,* for example, one of the inflammatory chemokines induced by *s-Prdm16*, suppresses the activity of MEP progenitors when released by leukemic cells[389]. The expression of inflammatory mediators by AML cells has also recently been shown to promote leukemogenesis by remodeling the bone marrow endosteal zone resulting in suppression of normal hematopoiesis[293]. Our findings, taken in the context of the existing literature, therefore support a model in which *s-Prdm16* induces the expression of inflammatory mediators which suppress normal hematopoiesis and cause a more rapid progression of leukemia in transplanted mice. Importantly, this model would also explain why we do not observe an *in vitro* growth advantage of MLL-AF9 cells expressing *s-Prdm16*.

8.4. Tumor suppressor function after forced expression of f-Prdm16

The full-length isoform of Prdm16 is purported to function as a tumor suppressor, largely because most leukemic translocations involving *PRDM16* delete the N-terminal PR domain, and because overexpression of *s-Prdm16* (but not *f-Prdm16*) induces leukemia in certain contexts. Our work suggests that this is partially true – forced overexpression of *f-Prdm16* caused an increase in leukemic latency compared to empty vector, indicating that f-Prdm16 can function as a tumor suppressor. However, *f-Prdm16*-deficient MLL-AF9 cells had a similar leukemic latency as WT MLL-AF9 cells. If physiological levels of *f-Prdm16* in the cell-of-origin have tumor suppressor function, we would expect that *f-Prdm16*$^{-/-}$ leukemic cells (which express the oncogenic *s-Prdm16* isoform but no *f-Prdm16*) would in fact have a shorter leukemic latency than WT cells expressing both isoforms. We conclude that *f-Prdm16* appears to have a tumor suppressor effect in MLL-AF9 cells but not when physiologically expressed in the cell-of-origin.

RNAseq studies indicated an elevation in respiratory and oxidative phosphorylation pathways in leukemic cells with forced expression of *f-Prdm16*, a finding that we corroborated using Seahorse metabolic flux analysis. Leukemic and other cancer cells typically shift their primary metabolism from oxidative phosphorylation to glycolysis during tumor development, a phenomenon known as the Warburg effect[390]. Many cells undergo oxidative phosphorylation because this process is substantially more efficient in terms of ATP production. However, glycolysis promotes tumor growth, as it generates ATP more quickly and, importantly, provides most of the building blocks required for cell proliferation. Therefore, glycolysis is believed to allow leukemic cells to expand and proliferate more quickly. We observed that MLL-AF9 cells overexpressing *f-Prdm16* not only had higher rates of respiration, but also higher rates of proton leak and a similar energy derivation from respiration overall. This could result in *f-Prdm16*-overexpressing cells becoming metabolically inefficient, with a slower progression of leukemia in recipient mice. It could also lead to the generation of more ROS and higher stress levels within these cells. Experiments using the

CellROX ROS indicator revealed that indeed MLL-AF9 cells expressing *f-Prdm16* had higher ROS levels than those expressing empty vector or *s-Prdm16*.

A previous report concluded that *f-Prdm16* was a tumor suppressor but suggested that the short isoform did not promote leukemia. They also demonstrated H3K4 methyltransferase activity in the PR domain[314]. The authors used the same murine model, concluding that forced *f-Prdm16* expression completely blocked leukemogenesis and *in vitro* survival of MLL-AF9 cells. They showed that a mutant lacking H3K4 methyltransferase activity had no effect, and furthermore, that knockdown of *Prdm16* shortened leukemic latency. They concluded that inhibition of leukemogenesis by *f-Prdm16* occurs through induction of *Gfi1b*, which in turn reduced *HoxA* gene expression, preventing leukemogenesis. We did observe an inhibitory effect of *f-Prdm16* on leukemogenesis *in vivo* but no differences in growth *in vitro*. Furthermore, we observed an oncogenic effect of *s-Prdm16*, which should resemble the methyltransferase-dead mutant from Zhou et al. That publication did not specifically analyze expression of *s-Prdm16*. Furthermore, we did not observe any downregulation of *HoxA* genes upon *f-Prdm16* expression, and in fact, in human AML data from the CGA, we observed a positive correlation between *PRDM16* and *HOXA* gene expression, suggestive of *HOXA* regulation of *PRDM16*, in concurrence with other published work suggesting that *HoxA9* and *HoxA10* induce *Prdm16*[50].

Two important methodological differences may account for the discrepancies between our findings and those in Zhou et al. Firstly, their forced expression experiments were performed in a WT background. It is therefore unclear whether or to what extent the knockdown or forced expression of one *Prdm16* isoform may have induced homeostatic mechanisms altering the expression of the other isoform. We performed forced expression experiments in a *Prdm16*-deleted background to avoid this confounding possibility. Secondly, in Zhou et al, the authors did not begin their forced expression experiments from the same existing pool of MLL-AF9 cells, instead co-transducing bone marrow cells with both MLL-AF9 and

Prdm16-GFP retroviral vectors simultaneously. We preferred the generation of one homogenous pool of MLL-AF9 cells before expressing *Prdm16* isoforms as there can be clonal differences in MLL-AF9 populations based on the initiating retroviral insertion site, leading to artifactual differences based on this, and not based on the specific overexpression of either *Prdm16* isoform.

8.5. Cells with leukemic stem cell potential may have an altered mitochondrial phenotype

We observed that MLL-AF9 cells with increased mitochondrial polarization, mitochondrial length, or mitochondrial mass were more likely to have colony-forming ability, indicative of LSC potential. We were unable to clearly distinguish whether this change in mitochondrial phenotype between LSCs and blast cells was important mechanistically to the function of LSCs. However, we found that MLL-AF9 colonies formed from clones with either elongated or fragmented mitochondria exhibited no differences in leukemogenicity or secondary colony-forming ability. This, coupled with our finding the mitochondrial differences between LSCs and blast cells were independent of Prdm16, caused us to end this investigation, considering it to be beyond the scope of this thesis project. Nonetheless, these are interesting findings worthy of future investigation. As a key player in cellular energy production, mitochondrial properties are intimately involved in metabolism, and highly regulated by metabolic signaling within the cell[391]. LSCs are thought to have elevated rates of oxidative phosphorylation and to be more quiescent than blast cells[392]. This altered metabolic phenotype could therefore be reflected in a distinct mitochondrial patterning in LSCs compared to blast cells.

Our experiments in regard to mitochondrial mass were conducted using flow cytometric staining with mitotracker green (MTG). As mentioned in Section 1.3.3, our lab has recently demonstrated possible artifacts with the use of MTG in HSCs, as a result of enhanced efflux of this dye from HSCs leading to an underestimation of mitochondrial mass[117]. However, we in fact observed a higher mitochondrial mass in LSCs than in blast cells, reducing the chances of underestimation due to efflux and making us more

confident in this finding than we would be in measuring mitochondrial mass in HSCs. Nonetheless, any future investigation should verify increased mitochondrial mass in LSCs using an alternative method.

8.6. Future Directions

A number of questions could be pursued in future work building on the findings presented in this thesis. One key observation derived from gene expression studies was that Rho and Ras GTPase gene expression was downregulated in both *Prdm16*$^{fl/fl}$*.Vav-Cre* (total *Prdm16*-deletion) and in *Δ47-fPrdm16*$^{-/-}$ (*f-Prdm16*-deleted) HSCs. Both deletions led to severe HSC deficiency, leading us to hypothesize that GTPase signaling, or a biological process dependent on GTPase signaling, may play an important role in HSC maintenance. Future work could investigate this in more detail. GTPases are involved in the regulation of many processes, including cell motility, endosomal and vesicle trafficking, intracellular signaling, and membrane protein translocation. A future project could investigate whether perturbation of any of these pathways leads to HSC defects mirroring those observed in the *Prdm16* deletion.

Our investigation made a significant contribution to the field through the generation of both an adult *Vav-Cre Prdm16* conditional hematopoietic mouse deletion, and a global *f-Prdm16*-specific mouse deletion. Additional genetic manipulations could yield further important results. Firstly, global deletion of *f-Prdm16* was embryonically lethal, as we similarly observed in the *Prdm16*$^{-/-}$ global deletion. Generation of a specific *f-Prdm16* conditional deletion in the hematopoetic system could be pursued by insertion of *LoxP* sites within the first three exons of *Prdm16*, corresponding to the full-length isoform. One risk of this approach, however, is that a large-scale deletion could disrupt expression of *s-Prdm16*, even if its coding sequence is not deleted. In our *Δ47-fPrdm16*$^{-/-}$ model, only 47 base pairs were deleted. Nonetheless, an attempt to develop a *f-Prdm16* conditionally-deleted mouse could yield further insights into the roles of individual *Prdm16* isoforms in adult hematopoiesis.

Similarly, an attempt could be made to generate a *s-Prdm16* deletion. As described in Section 4.3.1, we deleted a putative *s-Prdm16* transcriptional start site (TSS), but this did not cause a loss of transcription of *s-Prdm16*. Other putative TSS sites occur within the *f-Prdm16* coding region, making them unacceptable targets. The only potential approach would be to mutate the *s-Prdm16* start codon. This would block translation of *s-Prdm16*, while mutating *f-Prdm16* but not disrupting its translation. This is not ideal, as any phenotype observed in these mice would then have to be ascribed to either *s-Prdm16*-deletion or *f-Prdm16* mutation, possibly by forced expression experiments to determine which isoform reversed any observed phenotype. Though technically challenging, this would be a worthy subject of further investigation.

Our leukemia experiments using forced expression of *s-Prdm16* revealed an oncogenic role for this isoform and an induction of inflammatory gene expression. As described in Sections 8.3 and 2.3.4, a significant volume of published work exists that is consistent with the hypothesis that inflammation induced by *s-Prdm16* could serve an oncogenic role. Several experiments could be performed to investigate this further. Analysis of peripheral blood or bone marrow of recipient mice could reveal which extracellular inflammatory mediators are released by *s-Prdm16*-expressing leukemias. Forced expression experiments of genes induced by *s-Prdm16* in MLL-AF9 leukemia could be performed in leukemic cells from *Prdm16*$^{fl/fl}$*.Vav-Cre* mice to determine whether any individual inflammatory mediator could reverse the increased leukemic latency observed in these cells. As inflammation is a complex process, however, it is possible that no individual gene could replace the inflammatory signaling program induced by *s-Prdm16.* A more in-depth study of human AML samples could provide further insight and reveal a more limited number of individual inflammatory gene candidates. Our RNAseq analysis was performed on only 3 AML samples, whereas human data are available for thousands of patients, which could be sorted and grouped according to specific clinical and genetic subsets, allowing for a more refined bioinformatic analysis. Lastly, a potentially promising future study could explore the potential for specific anti-inflammatory or immune

suppressive treatments to improve prognosis of AMLs with the inflammatory and dysplastic characteristics observed in *s-Prdm16*-expressing leukemias. We anticipate, based on other published work, that *s-Prdm16* may be one of a number of genes which may promote leukemogenesis through inflammatory signaling, highlighting the importance of searching for ways to suppress this process to improve outcome for patients with these subsets of AML.

References

1 Till, J. E. & Mc, C. E. A direct measurement of the radiation sensitivity of normal mouse bone marrow cells. *Radiat Res* **14**, 213-222 (1961).

2 Challen, G. A., Boles, N., Lin, K. K. & Goodell, M. A. Mouse hematopoietic stem cell identification and analysis. *Cytometry A* **75**, 14-24, doi:10.1002/cyto.a.20674 (2009).

3 Fantoni, A., Bank, A. & Marks, P. A. Globin composition and synthesis of hemoglobins in developing fetal mice erythroid cells. *Science* **157**, 1327-1329 (1967).

4 Choi, K., Kennedy, M., Kazarov, A., Papadimitriou, J. C. & Keller, G. A common precursor for hematopoietic and endothelial cells. *Development* **125**, 725-732 (1998).

5 Dieterlen-Lievre, F. On the origin of haemopoietic stem cells in the avian embryo: an experimental approach. *J Embryol Exp Morphol* **33**, 607-619 (1975).

6 Nakano, H. *et al.* Haemogenic endocardium contributes to transient definitive haematopoiesis. *Nat Commun* **4**, 1564, doi:10.1038/ncomms2569 (2013).

7 Li, Z. *et al.* Mouse embryonic head as a site for hematopoietic stem cell development. *Cell Stem Cell* **11**, 663-675, doi:10.1016/j.stem.2012.07.004 (2012).

8 Dzierzak, E. & Speck, N. A. Of lineage and legacy: the development of mammalian hematopoietic stem cells. *Nat Immunol* **9**, 129-136, doi:10.1038/ni1560 (2008).

9 Medvinsky, A. & Dzierzak, E. Definitive hematopoiesis is autonomously initiated by the AGM region. *Cell* **86**, 897-906 (1996).

10 Ivanovs, A., Rybtsov, S., Anderson, R. A., Turner, M. L. & Medvinsky, A. Identification of the niche and phenotype of the first human hematopoietic stem cells. *Stem Cell Reports* **2**, 449-456, doi:10.1016/j.stemcr.2014.02.004 (2014).

11 Ivanovs, A. *et al.* Highly potent human hematopoietic stem cells first emerge in the intraembryonic aorta-gonad-mesonephros region. *J Exp Med* **208**, 2417-2427, doi:10.1084/jem.20111688 (2011).

12 de Bruijn, M. F., Speck, N. A., Peeters, M. C. & Dzierzak, E. Definitive hematopoietic stem cells first develop within the major arterial regions of the mouse embryo. *EMBO J* **19**, 2465-2474, doi:10.1093/emboj/19.11.2465 (2000).

13 Arora, N. *et al.* Effect of developmental stage of HSC and recipient on transplant outcomes. *Dev Cell* **29**, 621-628, doi:10.1016/j.devcel.2014.04.013 (2014).

14 Benz, C. *et al.* Hematopoietic stem cell subtypes expand differentially during development and display distinct lymphopoietic programs. *Cell Stem Cell* **10**, 273-283, doi:10.1016/j.stem.2012.02.007 (2012).

15 Zovein, A. C. *et al.* Fate tracing reveals the endothelial origin of hematopoietic stem cells. *Cell Stem Cell* **3**, 625-636, doi:10.1016/j.stem.2008.09.018 (2008).

16 Jordan, H. E. Aortic Cell Clusters in Vertebrate Embryos. *Proc Natl Acad Sci U S A* **3**, 149-156 (1917).

17 Lancrin, C. *et al.* The haemangioblast generates haematopoietic cells through a haemogenic endothelium stage. *Nature* **457**, 892-895, doi:10.1038/nature07679 (2009).

18 Mack, M., Riethmuller, G. & Kufer, P. A small bispecific antibody construct expressed as a functional single-chain molecule with high tumor cell cytotoxicity. *Proc Natl Acad Sci U S A* **92**, 7021-7025 (1995).

19 Shivdasani, R. A., Mayer, E. L. & Orkin, S. H. Absence of blood formation in mice lacking the T-cell leukaemia oncoprotein tal-1/SCL. *Nature* **373**, 432-434, doi:10.1038/373432a0 (1995).

20 Okuda, T., van Deursen, J., Hiebert, S. W., Grosveld, G. & Downing, J. R. AML1, the target of multiple chromosomal translocations in human leukemia, is essential for normal fetal liver hematopoiesis. *Cell* **84**, 321-330 (1996).

21 Lancrin, C. *et al.* GFI1 and GFI1B control the loss of endothelial identity of hemogenic endothelium during hematopoietic commitment. *Blood* **120**, 314-322, doi:10.1182/blood-2011-10-386094 (2012).

22 Chen, M. J., Yokomizo, T., Zeigler, B. M., Dzierzak, E. & Speck, N. A. Runx1 is required for the endothelial to haematopoietic cell transition but not thereafter. *Nature* **457**, 887-891, doi:10.1038/nature07619 (2009).

23 Kissa, K. & Herbomel, P. Blood stem cells emerge from aortic endothelium by a novel type of cell transition. *Nature* **464**, 112-115, doi:10.1038/nature08761 (2010).

24 Minegishi, N. *et al.* Expression and domain-specific function of GATA-2 during differentiation of the hematopoietic precursor cells in midgestation mouse embryos. *Blood* **102**, 896-905, doi:10.1182/blood-2002-12-3809 (2003).

25 Morrison, S. J., Hemmati, H. D., Wandycz, A. M. & Weissman, I. L. The purification and characterization of fetal liver hematopoietic stem cells. *Proc Natl Acad Sci U S A* **92**, 10302-10306 (1995).

26 Kim, I., He, S., Yilmaz, O. H., Kiel, M. J. & Morrison, S. J. Enhanced purification of fetal liver hematopoietic stem cells using SLAM family receptors. *Blood* **108**, 737-744, doi:10.1182/blood-2005-10-4135 (2006).

27 Copley, M. R. *et al.* The Lin28b-let-7-Hmga2 axis determines the higher self-renewal potential of fetal haematopoietic stem cells. *Nat Cell Biol* **15**, 916-925, doi:10.1038/ncb2783 (2013).

28 Manesia, J. K. *et al.* Highly proliferative primitive fetal liver hematopoietic stem cells are fueled by oxidative metabolic pathways. *Stem Cell Res* **15**, 715-721, doi:10.1016/j.scr.2015.11.001 (2015).

29 Martin, M. A. & Bhatia, M. Analysis of the human fetal liver hematopoietic microenvironment. *Stem Cells Dev* **14**, 493-504, doi:10.1089/scd.2005.14.493 (2005).

30 Chou, S. & Lodish, H. F. Fetal liver hepatic progenitors are supportive stromal cells for hematopoietic stem cells. *Proc Natl Acad Sci U S A* **107**, 7799-7804, doi:10.1073/pnas.1003586107 (2010).

31 Ye, M. *et al.* C/EBPa controls acquisition and maintenance of adult haematopoietic stem cell quiescence. *Nat Cell Biol* **15**, 385-394, doi:10.1038/ncb2698 (2013).

32 Kim, I., Yilmaz, O. H. & Morrison, S. J. CD144 (VE-cadherin) is transiently expressed by fetal liver hematopoietic stem cells. *Blood* **106**, 903-905, doi:10.1182/blood-2004-12-4960 (2005).

33 Ciriza, J. *et al.* Single-cell analysis of murine long-term hematopoietic stem cells reveals distinct patterns of gene expression during fetal migration. *PLoS One* **7**, e30542, doi:10.1371/journal.pone.0030542 (2012).

34 Emery, J. L. & Follett, G. F. Regression of Bone-Marrow Haemopoiesis from the Terminal Digits in the Foetus and Infant. *Br J Haematol* **10**, 485-489 (1964).

35 Ricci, C. *et al.* Normal age-related patterns of cellular and fatty bone marrow distribution in the axial skeleton: MR imaging study. *Radiology* **177**, 83-88, doi:10.1148/radiology.177.1.2399343 (1990).

36 Morrison, S. J., Wandycz, A. M., Akashi, K., Globerson, A. & Weissman, I. L. The aging of hematopoietic stem cells. *Nat Med* **2**, 1011-1016 (1996).

37 Rossi, D. J. *et al.* Cell intrinsic alterations underlie hematopoietic stem cell aging. *Proc Natl Acad Sci U S A* **102**, 9194-9199, doi:10.1073/pnas.0503280102 (2005).

38 Beerman, I. *et al.* Functionally distinct hematopoietic stem cells modulate hematopoietic lineage potential during aging by a mechanism of clonal expansion. *Proc Natl Acad Sci U S A* **107**, 5465-5470, doi:10.1073/pnas.1000834107 (2010).

39 Busque, L. *et al.* Recurrent somatic TET2 mutations in normal elderly individuals with clonal hematopoiesis. *Nat Genet* **44**, 1179-1181, doi:10.1038/ng.2413 (2012).

40 Thomas, E. D., Lochte, H. L., Jr., Lu, W. C. & Ferrebee, J. W. Intravenous infusion of bone marrow in patients receiving radiation and chemotherapy. *N Engl J Med* **257**, 491-496, doi:10.1056/NEJM195709122571102 (1957).

41 Gale, R. P. *et al.* Prevention of graft rejection following bone marrow transplantation. *Blood* **57**, 9-12 (1981).

42 Graw, R. G., Jr. *et al.* Graft-versus-host reaction complicating HL-A matched bone-marrow transplantation. *Lancet* **2**, 1053-1055 (1970).

43 Prentice, H. G. *et al.* Depletion of T lymphocytes in donor marrow prevents significant graft-versus-host disease in matched allogeneic leukaemic marrow transplant recipients. *Lancet* **1**, 472-476 (1984).

44 Ljungman, P. *et al.* Allogeneic and autologous transplantation for haematological diseases, solid tumours and immune disorders: definitions and current practice in Europe. *Bone Marrow Transplant* **37**, 439-449, doi:10.1038/sj.bmt.1705265 (2006).

45 Gratwohl, A. *et al.* Hematopoietic stem cell transplantation: a global perspective. *JAMA* **303**, 1617-1624, doi:10.1001/jama.2010.491 (2010).

46 Andrade-Zaldivar, H., Santos, L. & De Leon Rodriguez, A. Expansion of human hematopoietic stem cells for transplantation: trends and perspectives. *Cytotechnology* **56**, 151-160, doi:10.1007/s10616-008-9144-1 (2008).

47 Schuster, J. A. *et al.* Expansion of hematopoietic stem cells for transplantation: current perspectives. *Exp Hematol Oncol* **1**, 12, doi:10.1186/2162-3619-1-12 (2012).

48 Sauvageau, G., Iscove, N. N. & Humphries, R. K. In vitro and in vivo expansion of hematopoietic stem cells. *Oncogene* **23**, 7223-7232, doi:10.1038/sj.onc.1207942 (2004).

49 Antonchuk, J., Sauvageau, G. & Humphries, R. K. HOXB4-induced expansion of adult hematopoietic stem cells ex vivo. *Cell* **109**, 39-45 (2002).

50 Yu, H. *et al.* Downregulation of Prdm16 mRNA is a specific antileukemic mechanism during HOXB4-mediated HSC expansion in vivo. *Blood* **124**, 1737-1747, doi:10.1182/blood-2013-10-534735 (2014).

51 Boitano, A. E. *et al.* Aryl hydrocarbon receptor antagonists promote the expansion of human hematopoietic stem cells. *Science* **329**, 1345-1348, doi:10.1126/science.1191536 (2010).

52 Fares, I. *et al.* Cord blood expansion. Pyrimidoindole derivatives are agonists of human hematopoietic stem cell self-renewal. *Science* **345**, 1509-1512, doi:10.1126/science.1256337 (2014).

53 Takahashi, K., Okita, K., Nakagawa, M. & Yamanaka, S. Induction of pluripotent stem cells from fibroblast cultures. *Nat Protoc* **2**, 3081-3089, doi:10.1038/nprot.2007.418 (2007).

54 Kennedy, M. *et al.* T lymphocyte potential marks the emergence of definitive hematopoietic progenitors in human pluripotent stem cell differentiation cultures. *Cell Rep* **2**, 1722-1735, doi:10.1016/j.celrep.2012.11.003 (2012).

55 Sturgeon, C. M., Ditadi, A., Awong, G., Kennedy, M. & Keller, G. Wnt signaling controls the specification of definitive and primitive hematopoiesis from human pluripotent stem cells. *Nat Biotechnol* **32**, 554-561, doi:10.1038/nbt.2915 (2014).

56 Pereira, C. F. *et al.* Induction of a hemogenic program in mouse fibroblasts. *Cell Stem Cell* **13**, 205-218, doi:10.1016/j.stem.2013.05.024 (2013).

57 Riddell, J. *et al.* Reprogramming committed murine blood cells to induced hematopoietic stem cells with defined factors. *Cell* **157**, 549-564, doi:10.1016/j.cell.2014.04.006 (2014).

58 Elcheva, I. *et al.* Direct induction of haematoendothelial programs in human pluripotent stem cells by transcriptional regulators. *Nat Commun* **5**, 4372, doi:10.1038/ncomms5372 (2014).

59 Morrison, S. J. & Weissman, I. L. The long-term repopulating subset of hematopoietic stem cells is deterministic and isolatable by phenotype. *Immunity* **1**, 661-673 (1994).

60 Pietras, E. M. *et al.* Functionally Distinct Subsets of Lineage-Biased Multipotent Progenitors Control Blood Production in Normal and Regenerative Conditions. *Cell Stem Cell* **17**, 35-46, doi:10.1016/j.stem.2015.05.003 (2015).

61 Park, I. K. *et al.* Differential gene expression profiling of adult murine hematopoietic stem cells. *Blood* **99**, 488-498 (2002).

62 Okada, S. *et al.* In vivo and in vitro stem cell function of c-kit- and Sca-1-positive murine hematopoietic cells. *Blood* **80**, 3044-3050 (1992).

63 Seita, J. & Weissman, I. L. Hematopoietic stem cell: self-renewal versus differentiation. *Wiley Interdiscip Rev Syst Biol Med* **2**, 640-653, doi:10.1002/wsbm.86 (2010).

64 Kondo, M., Weissman, I. L. & Akashi, K. Identification of clonogenic common lymphoid progenitors in mouse bone marrow. *Cell* **91**, 661-672 (1997).

65 Akashi, K., Traver, D., Miyamoto, T. & Weissman, I. L. A clonogenic common myeloid progenitor that gives rise to all myeloid lineages. *Nature* **404**, 193-197, doi:10.1038/35004599 (2000).

66 Cavazzana-Calvo, M. *et al.* Is normal hematopoiesis maintained solely by long-term multipotent stem cells? *Blood* **117**, 4420-4424, doi:10.1182/blood-2010-09-255679 (2011).

67 Kumar, R., Fossati, V., Israel, M. & Snoeck, H. W. Lin-Sca1+kit- bone marrow cells contain early lymphoid-committed precursors that are distinct from common lymphoid progenitors. *J Immunol* **181**, 7507-7513 (2008).

68 Fossati, V., Kumar, R. & Snoeck, H. W. Progenitor cell origin plays a role in fate choices of mature B cells. *J Immunol* **184**, 1251-1260, doi:10.4049/jimmunol.0901922 (2010).

69 Labastie, M. C., Thiery, J. P. & Le Douarin, N. M. Mouse yolk sac and intraembryonic tissues produce factors able to elicit differentiation of erythroid burst-forming units and colony-forming units, respectively. *Proc Natl Acad Sci U S A* **81**, 1453-1456 (1984).

70 van Os, R. P., Dethmers-Ausema, B. & de Haan, G. In vitro assays for cobblestone area-forming cells, LTC-IC, and CFU-C. *Methods Mol Biol* **430**, 143-157, doi:10.1007/978-1-59745-182-6_10 (2008).

71 Ploemacher, R. E., van der Sluijs, J. P., Voerman, J. S. & Brons, N. H. An in vitro limiting-dilution assay of long-term repopulating hematopoietic stem cells in the mouse. *Blood* **74**, 2755-2763 (1989).

72 Sutherland, H. J., Eaves, C. J., Eaves, A. C., Dragowska, W. & Lansdorp, P. M. Characterization and partial purification of human marrow cells capable of initiating long-term hematopoiesis in vitro. *Blood* **74**, 1563-1570 (1989).

73 Harrison, D. E. Competitive repopulation: a new assay for long-term stem cell functional capacity. *Blood* **55**, 77-81 (1980).

74 Peters, S. O., Kittler, E. L., Ramshaw, H. S. & Quesenberry, P. J. Ex vivo expansion of murine marrow cells with interleukin-3 (IL-3), IL-6, IL-11, and stem cell factor leads to impaired engraftment in irradiated hosts. *Blood* **87**, 30-37 (1996).

75 Szilvassy, S. J., Humphries, R. K., Lansdorp, P. M., Eaves, A. C. & Eaves, C. J. Quantitative assay for totipotent reconstituting hematopoietic stem cells by a competitive repopulation strategy. *Proc Natl Acad Sci U S A* **87**, 8736-8740 (1990).

76 Taswell, C. Limiting dilution assays for the determination of immunocompetent cell frequencies. III. Validity tests for the single-hit Poisson model. *J Immunol Methods* **72**, 29-40 (1984).

77 Busch, K. *et al.* Fundamental properties of unperturbed haematopoiesis from stem cells in vivo. *Nature* **518**, 542-546, doi:10.1038/nature14242 (2015).

78 Sun, J. *et al.* Clonal dynamics of native haematopoiesis. *Nature* **514**, 322-327, doi:10.1038/nature13824 (2014).

79 Crisan, M. & Dzierzak, E. The many faces of hematopoietic stem cell heterogeneity. *Development* **143**, 4571-4581, doi:10.1242/dev.114231 (2016).

80 Osawa, M., Hanada, K., Hamada, H. & Nakauchi, H. Long-term lymphohematopoietic reconstitution by a single CD34-low/negative hematopoietic stem cell. *Science* **273**, 242-245 (1996).

81 Sieburg, H. B. *et al.* The hematopoietic stem compartment consists of a limited number of discrete stem cell subsets. *Blood* **107**, 2311-2316, doi:10.1182/blood-2005-07-2970 (2006).

82 Smith, L. G., Weissman, I. L. & Heimfeld, S. Clonal analysis of hematopoietic stem-cell differentiation in vivo. *Proc Natl Acad Sci U S A* **88**, 2788-2792 (1991).

83 van der Wath, R. C., Wilson, A., Laurenti, E., Trumpp, A. & Lio, P. Estimating dormant and active hematopoietic stem cell kinetics through extensive modeling of bromodeoxyuridine label-retaining cell dynamics. *PLoS One* **4**, e6972, doi:10.1371/journal.pone.0006972 (2009).

84 Wilson, A. *et al.* Hematopoietic stem cells reversibly switch from dormancy to self-renewal during homeostasis and repair. *Cell* **135**, 1118-1129, doi:10.1016/j.cell.2008.10.048 (2008).

85 Sanjuan-Pla, A. *et al.* Platelet-biased stem cells reside at the apex of the haematopoietic stem-cell hierarchy. *Nature* **502**, 232-236, doi:10.1038/nature12495 (2013).

86 Ema, H., Morita, Y. & Suda, T. Heterogeneity and hierarchy of hematopoietic stem cells. *Exp Hematol* **42**, 74-82 e72, doi:10.1016/j.exphem.2013.11.004 (2014).

87 Pang, W. W. *et al.* Human bone marrow hematopoietic stem cells are increased in frequency and myeloid-biased with age. *Proc Natl Acad Sci U S A* **108**, 20012-20017, doi:10.1073/pnas.1116110108 (2011).

88 Morita, Y., Ema, H. & Nakauchi, H. Heterogeneity and hierarchy within the most primitive hematopoietic stem cell compartment. *J Exp Med* **207**, 1173-1182, doi:10.1084/jem.20091318 (2010).

89 Denis, C. *et al.* A mouse model of severe von Willebrand disease: defects in hemostasis and thrombosis. *Proc Natl Acad Sci U S A* **95**, 9524-9529 (1998).

90 Challen, G. A., Boles, N. C., Chambers, S. M. & Goodell, M. A. Distinct hematopoietic stem cell subtypes are differentially regulated by TGF-beta1. *Cell Stem Cell* **6**, 265-278, doi:10.1016/j.stem.2010.02.002 (2010).

91 Crisan, M. *et al.* BMP signalling differentially regulates distinct haematopoietic stem cell types. *Nat Commun* **6**, 8040, doi:10.1038/ncomms9040 (2015).

92 Luchsinger, L. L., de Almeida, M. J., Corrigan, D. J., Mumau, M. & Snoeck, H. W. Mitofusin 2 maintains haematopoietic stem cells with extensive lymphoid potential. *Nature* **529**, 528-531, doi:10.1038/nature16500 (2016).

93 Spangrude, G. J., Heimfeld, S. & Weissman, I. L. Purification and characterization of mouse hematopoietic stem cells. *Science* **241**, 58-62 (1988).

94 Kiel, M. J. *et al.* SLAM family receptors distinguish hematopoietic stem and progenitor cells and reveal endothelial niches for stem cells. *Cell* **121**, 1109-1121, doi:10.1016/j.cell.2005.05.026 (2005).

95 Notta, F. *et al.* Isolation of single human hematopoietic stem cells capable of long-term multilineage engraftment. *Science* **333**, 218-221, doi:10.1126/science.1201219 (2011).

96 Majeti, R., Park, C. Y. & Weissman, I. L. Identification of a hierarchy of multipotent hematopoietic progenitors in human cord blood. *Cell Stem Cell* **1**, 635-645, doi:10.1016/j.stem.2007.10.001 (2007).

97 Hackney, J. A. *et al.* A molecular profile of a hematopoietic stem cell niche. *Proc Natl Acad Sci U S A* **99**, 13061-13066, doi:10.1073/pnas.192124499 (2002).

98 Calvi, L. M. *et al.* Osteoblastic cells regulate the haematopoietic stem cell niche. *Nature* **425**, 841-846, doi:10.1038/nature02040 (2003).

99 Visnjic, D. *et al.* Hematopoiesis is severely altered in mice with an induced osteoblast deficiency. *Blood* **103**, 3258-3264, doi:10.1182/blood-2003-11-4011 (2004).

100 Zhu, J. *et al.* Osteoblasts support B-lymphocyte commitment and differentiation from hematopoietic stem cells. *Blood* **109**, 3706-3712, doi:10.1182/blood-2006-08-041384 (2007).

101 Acar, M. *et al.* Deep imaging of bone marrow shows non-dividing stem cells are mainly perisinusoidal. *Nature* **526**, 126-130, doi:10.1038/nature15250 (2015).

102 Chen, J. Y. *et al.* Hoxb5 marks long-term haematopoietic stem cells and reveals a homogenous perivascular niche. *Nature* **530**, 223-227, doi:10.1038/nature16943 (2016).

103 Zou, Y. R., Kottmann, A. H., Kuroda, M., Taniuchi, I. & Littman, D. R. Function of the chemokine receptor CXCR4 in haematopoiesis and in cerebellar development. *Nature* **393**, 595-599, doi:10.1038/31269 (1998).

104 Sugiyama, T., Kohara, H., Noda, M. & Nagasawa, T. Maintenance of the hematopoietic stem cell pool by CXCL12-CXCR4 chemokine signaling in bone marrow stromal cell niches. *Immunity* **25**, 977-988, doi:10.1016/j.immuni.2006.10.016 (2006).

105 Tzeng, Y. S. *et al.* Loss of Cxcl12/Sdf-1 in adult mice decreases the quiescent state of hematopoietic stem/progenitor cells and alters the pattern of hematopoietic regeneration after myelosuppression. *Blood* **117**, 429-439, doi:10.1182/blood-2010-01-266833 (2011).

106 Ikuta, K. & Weissman, I. L. Evidence that hematopoietic stem cells express mouse c-kit but do not depend on steel factor for their generation. *Proc Natl Acad Sci U S A* **89**, 1502-1506 (1992).

107 Barker, J. E. Sl/Sld hematopoietic progenitors are deficient in situ. *Exp Hematol* **22**, 174-177 (1994).

108 Ding, L. & Morrison, S. J. Haematopoietic stem cells and early lymphoid progenitors occupy distinct bone marrow niches. *Nature* **495**, 231-235, doi:10.1038/nature11885 (2013).

109 Sorrentino, B. P., McDonagh, K. T., Woods, D. & Orlic, D. Expression of retroviral vectors containing the human multidrug resistance 1 cDNA in hematopoietic cells of transplanted mice. *Blood* **86**, 491-501 (1995).

110 Zhou, S. *et al.* The ABC transporter Bcrp1/ABCG2 is expressed in a wide variety of stem cells and is a molecular determinant of the side-population phenotype. *Nat Med* **7**, 1028-1034, doi:10.1038/nm0901-1028 (2001).

111 Zhou, S., Zong, Y., Lu, T. & Sorrentino, B. P. Hematopoietic cells from mice that are deficient in both Bcrp1/Abcg2 and Mdr1a/1b develop normally but are sensitized to mitoxantrone. *Biotechniques* **35**, 1248-1252 (2003).

112 Goodell, M. A., Brose, K., Paradis, G., Conner, A. S. & Mulligan, R. C. Isolation and functional properties of murine hematopoietic stem cells that are replicating in vivo. *J Exp Med* **183**, 1797-1806 (1996).

113 Migliaccio, G., Baiocchi, M., Adamson, J. W. & Migliaccio, A. R. Isolation and biological characterization of two classes of blast-cell colony-forming cells from normal murine marrow. *Blood* **87**, 4091-4099 (1996).

114 Simsek, T. *et al.* The distinct metabolic profile of hematopoietic stem cells reflects their location in a hypoxic niche. *Cell Stem Cell* **7**, 380-390, doi:10.1016/j.stem.2010.07.011 (2010).

115 Romero-Moya, D. *et al.* Cord blood-derived CD34+ hematopoietic cells with low mitochondrial mass are enriched in hematopoietic repopulating stem cell function. *Haematologica* **98**, 1022-1029, doi:10.3324/haematol.2012.079244 (2013).

116 Vannini, N. *et al.* Specification of haematopoietic stem cell fate via modulation of mitochondrial activity. *Nat Commun* **7**, 13125, doi:10.1038/ncomms13125 (2016).

117 de Almeida, M. J., Luchsinger, L. L., Corrigan, D. J., Williams, L. J. & Snoeck, H. W. Dye-Independent Methods Reveal Elevated Mitochondrial Mass in Hematopoietic Stem Cells. *Cell Stem Cell* **21**, 725-729 e724, doi:10.1016/j.stem.2017.11.002 (2017).

118 Aguilo, F. *et al.* Prdm16 is a physiologic regulator of hematopoietic stem cells. *Blood* **117**, 5057-5066, doi:10.1182/blood-2010-08-300145 (2011).

119 Santel, A. & Fuller, M. T. Control of mitochondrial morphology by a human mitofusin. *J Cell Sci* **114**, 867-874 (2001).

120 Rapaport, D., Brunner, M., Neupert, W. & Westermann, B. Fzo1p is a mitochondrial outer membrane protein essential for the biogenesis of functional mitochondria in Saccharomyces cerevisiae. *J Biol Chem* **273**, 20150-20155 (1998).

121 Hales, K. G. & Fuller, M. T. Developmentally regulated mitochondrial fusion mediated by a conserved, novel, predicted GTPase. *Cell* **90**, 121-129 (1997).

122 Misaka, T., Miyashita, T. & Kubo, Y. Primary structure of a dynamin-related mouse mitochondrial GTPase and its distribution in brain, subcellular localization, and effect on mitochondrial morphology. *J Biol Chem* **277**, 15834-15842, doi:10.1074/jbc.M109260200 (2002).

123 Bleazard, W. *et al.* The dynamin-related GTPase Dnm1 regulates mitochondrial fission in yeast. *Nat Cell Biol* **1**, 298-304, doi:10.1038/13014 (1999).

124 James, D. I., Parone, P. A., Mattenberger, Y. & Martinou, J. C. hFis1, a novel component of the mammalian mitochondrial fission machinery. *J Biol Chem* **278**, 36373-36379, doi:10.1074/jbc.M303758200 (2003).

125 Ito, K. & Suda, T. Metabolic requirements for the maintenance of self-renewing stem cells. *Nat Rev Mol Cell Biol* **15**, 243-256, doi:10.1038/nrm3772 (2014).

126 Parmar, K., Mauch, P., Vergilio, J. A., Sackstein, R. & Down, J. D. Distribution of hematopoietic stem cells in the bone marrow according to regional hypoxia. *Proc Natl Acad Sci U S A* **104**, 5431-5436, doi:10.1073/pnas.0701152104 (2007).

127 Winkler, I. G. *et al.* Positioning of bone marrow hematopoietic and stromal cells relative to blood flow in vivo: serially reconstituting hematopoietic stem cells reside in distinct nonperfused niches. *Blood* **116**, 375-385, doi:10.1182/blood-2009-07-233437 (2010).

128 Spencer, J. A. *et al.* Direct measurement of local oxygen concentration in the bone marrow of live animals. *Nature* **508**, 269-273, doi:10.1038/nature13034 (2014).

129 Takubo, K. *et al.* Regulation of the HIF-1alpha level is essential for hematopoietic stem cells. *Cell Stem Cell* **7**, 391-402, doi:10.1016/j.stem.2010.06.020 (2010).

130 Ogawa, M. *et al.* Expression and function of c-kit in hemopoietic progenitor cells. *J Exp Med* **174**, 63-71 (1991).

131 Kimura, S., Roberts, A. W., Metcalf, D. & Alexander, W. S. Hematopoietic stem cell deficiencies in mice lacking c-Mpl, the receptor for thrombopoietin. *Proc Natl Acad Sci U S A* **95**, 1195-1200 (1998).

132 Qian, H. *et al.* Critical role of thrombopoietin in maintaining adult quiescent hematopoietic stem cells. *Cell Stem Cell* **1**, 671-684, doi:10.1016/j.stem.2007.10.008 (2007).

133 Crane, G. M., Jeffery, E. & Morrison, S. J. Adult haematopoietic stem cell niches. *Nat Rev Immunol* **17**, 573-590, doi:10.1038/nri.2017.53 (2017).

134 Himburg, H. A. *et al.* Pleiotrophin regulates the expansion and regeneration of hematopoietic stem cells. *Nat Med* **16**, 475-482, doi:10.1038/nm.2119 (2010).

135 Himburg, H. A. *et al.* Pleiotrophin regulates the retention and self-renewal of hematopoietic stem cells in the bone marrow vascular niche. *Cell Rep* **2**, 964-975, doi:10.1016/j.celrep.2012.09.002 (2012).

136 Gerber, H. P. *et al.* VEGF regulates haematopoietic stem cell survival by an internal autocrine loop mechanism. *Nature* **417**, 954-958, doi:10.1038/nature00821 (2002).

137 Rehn, M. *et al.* Hypoxic induction of vascular endothelial growth factor regulates murine hematopoietic stem cell function in the low-oxygenic niche. *Blood* **118**, 1534-1543, doi:10.1182/blood-2011-01-332890 (2011).

138 Puri, M. C. & Bernstein, A. Requirement for the TIE family of receptor tyrosine kinases in adult but not fetal hematopoiesis. *Proc Natl Acad Sci U S A* **100**, 12753-12758, doi:10.1073/pnas.2133552100 (2003).

139 Takakura, N. *et al.* Critical role of the TIE2 endothelial cell receptor in the development of definitive hematopoiesis. *Immunity* **9**, 677-686 (1998).

140 Arai, F. *et al.* Tie2/angiopoietin-1 signaling regulates hematopoietic stem cell quiescence in the bone marrow niche. *Cell* **118**, 149-161, doi:10.1016/j.cell.2004.07.004 (2004).

141 Sitnicka, E., Ruscetti, F. W., Priestley, G. V., Wolf, N. S. & Bartelmez, S. H. Transforming growth factor beta 1 directly and reversibly inhibits the initial cell divisions of long-term repopulating hematopoietic stem cells. *Blood* **88**, 82-88 (1996).

142 Capron, C. *et al.* A major role of TGF-beta1 in the homing capacities of murine hematopoietic stem cell/progenitors. *Blood* **116**, 1244-1253, doi:10.1182/blood-2009-05-221093 (2010).

143 Yamazaki, S. *et al.* Nonmyelinating Schwann cells maintain hematopoietic stem cell hibernation in the bone marrow niche. *Cell* **147**, 1146-1158, doi:10.1016/j.cell.2011.09.053 (2011).

144 Avagyan, S., Aguilo, F., Kamezaki, K. & Snoeck, H. W. Quantitative trait mapping reveals a regulatory axis involving peroxisome proliferator-activated receptors, PRDM16, transforming growth factor-beta2 and FLT3 in hematopoiesis. *Blood* **118**, 6078-6086, doi:10.1182/blood-2011-07-365080 (2011).

145 Karlsson, G. *et al.* Smad4 is critical for self-renewal of hematopoietic stem cells. *J Exp Med* **204**, 467-474, doi:10.1084/jem.20060465 (2007).

146 Harrison, D. E. & Lerner, C. P. Most primitive hematopoietic stem cells are stimulated to cycle rapidly after treatment with 5-fluorouracil. *Blood* **78**, 1237-1240 (1991).

147 Mancini, S. J. *et al.* Jagged1-dependent Notch signaling is dispensable for hematopoietic stem cell self-renewal and differentiation. *Blood* **105**, 2340-2342, doi:10.1182/blood-2004-08-3207 (2005).

148 Varnum-Finney, B., Brashem-Stein, C. & Bernstein, I. D. Combined effects of Notch signaling and cytokines induce a multiple log increase in precursors with lymphoid and myeloid reconstituting ability. *Blood* **101**, 1784-1789, doi:10.1182/blood-2002-06-1862 (2003).

149 Reya, T. *et al.* A role for Wnt signalling in self-renewal of haematopoietic stem cells. *Nature* **423**, 409-414, doi:10.1038/nature01593 (2003).

150 Murdoch, B. *et al.* Wnt-5A augments repopulating capacity and primitive hematopoietic development of human blood stem cells in vivo. *Proc Natl Acad Sci U S A* **100**, 3422-3427, doi:10.1073/pnas.0130233100 (2003).

151 Nemeth, M. J., Topol, L., Anderson, S. M., Yang, Y. & Bodine, D. M. Wnt5a inhibits canonical Wnt signaling in hematopoietic stem cells and enhances repopulation. *Proc Natl Acad Sci U S A* **104**, 15436-15441, doi:10.1073/pnas.0704747104 (2007).

152 Scumpia, P. O. *et al.* Cutting edge: bacterial infection induces hematopoietic stem and progenitor cell expansion in the absence of TLR signaling. *J Immunol* **184**, 2247-2251, doi:10.4049/jimmunol.0903652 (2010).

153 Baldridge, M. T., King, K. Y., Boles, N. C., Weksberg, D. C. & Goodell, M. A. Quiescent haematopoietic stem cells are activated by IFN-gamma in response to chronic infection. *Nature* **465**, 793-797, doi:10.1038/nature09135 (2010).

154 Essers, M. A. *et al.* IFNalpha activates dormant haematopoietic stem cells in vivo. *Nature* **458**, 904-908, doi:10.1038/nature07815 (2009).

155 Sato, T. *et al.* Interferon regulatory factor-2 protects quiescent hematopoietic stem cells from type I interferon-dependent exhaustion. *Nat Med* **15**, 696-700, doi:10.1038/nm.1973 (2009).

156 Verma, A. *et al.* Activation of the p38 mitogen-activated protein kinase mediates the suppressive effects of type I interferons and transforming growth factor-beta on normal hematopoiesis. *J Biol Chem* **277**, 7726-7735, doi:10.1074/jbc.M106640200 (2002).

157 Brown, J., Wang, H., Hajishengallis, G. N. & Martin, M. TLR-signaling networks: an integration of adaptor molecules, kinases, and cross-talk. *J Dent Res* **90**, 417-427, doi:10.1177/0022034510381264 (2011).

158 Nagai, Y. *et al.* Toll-like receptors on hematopoietic progenitor cells stimulate innate immune system replenishment. *Immunity* **24**, 801-812, doi:10.1016/j.immuni.2006.04.008 (2006).

159 Zhao, J. L. *et al.* Conversion of danger signals into cytokine signals by hematopoietic stem and progenitor cells for regulation of stress-induced hematopoiesis. *Cell Stem Cell* **14**, 445-459, doi:10.1016/j.stem.2014.01.007 (2014).

160 Wiedmann, M. W., Mossner, J., Baerwald, C. & Pierer, M. TNF alpha inhibition as treatment modality for certain rheumatologic and gastrointestinal diseases. *Endocr Metab Immune Disord Drug Targets* **9**, 295-314 (2009).

161 Dufour, C. *et al.* TNF-alpha and IFN-gamma are overexpressed in the bone marrow of Fanconi anemia patients and TNF-alpha suppresses erythropoiesis in vitro. *Blood* **102**, 2053-2059, doi:10.1182/blood-2003-01-0114 (2003).

162 Pronk, C. J., Veiby, O. P., Bryder, D. & Jacobsen, S. E. Tumor necrosis factor restricts hematopoietic stem cell activity in mice: involvement of two distinct receptors. *J Exp Med* **208**, 1563-1570, doi:10.1084/jem.20110752 (2011).

163 Morishita, K. *et al.* Retroviral activation of a novel gene encoding a zinc finger protein in IL-3-dependent myeloid leukemia cell lines. *Cell* **54**, 831-840 (1988).

164 Mochizuki, N. *et al.* A novel gene, MEL1, mapped to 1p36.3 is highly homologous to the MDS1/EVI1 gene and is transcriptionally activated in t(1;3)(p36;q21)-positive leukemia cells. *Blood* **96**, 3209-3214 (2000).

165 Kataoka, K. *et al.* Evi1 is essential for hematopoietic stem cell self-renewal, and its expression marks hematopoietic cells with long-term multilineage repopulating activity. *J Exp Med* **208**, 2403-2416, doi:10.1084/jem.20110447 (2011).

166 Goyama, S. *et al.* Evi-1 is a critical regulator for hematopoietic stem cells and transformed leukemic cells. *Cell Stem Cell* **3**, 207-220, doi:10.1016/j.stem.2008.06.002 (2008).

167 Lacombe, J. *et al.* Scl regulates the quiescence and the long-term competence of hematopoietic stem cells. *Blood* **115**, 792-803, doi:10.1182/blood-2009-01-201384 (2010).

168 Wadman, I. A. *et al.* The LIM-only protein Lmo2 is a bridging molecule assembling an erythroid, DNA-binding complex which includes the TAL1, E47, GATA-1 and Ldb1/NLI proteins. *EMBO J* **16**, 3145-3157, doi:10.1093/emboj/16.11.3145 (1997).

169 Nottingham, W. T. *et al.* Runx1-mediated hematopoietic stem-cell emergence is controlled by a Gata/Ets/SCL-regulated enhancer. *Blood* **110**, 4188-4197, doi:10.1182/blood-2007-07-100883 (2007).

170 Semerad, C. L., Mercer, E. M., Inlay, M. A., Weissman, I. L. & Murre, C. E2A proteins maintain the hematopoietic stem cell pool and promote the maturation of myelolymphoid and myeloerythroid progenitors. *Proc Natl Acad Sci U S A* **106**, 1930-1935, doi:10.1073/pnas.0808866106 (2009).

171 Li, L. *et al.* Nuclear adaptor Ldb1 regulates a transcriptional program essential for the maintenance of hematopoietic stem cells. *Nat Immunol* **12**, 129-136, doi:10.1038/ni.1978 (2011).

172 Yamada, Y. *et al.* The T cell leukemia LIM protein Lmo2 is necessary for adult mouse hematopoiesis. *Proc Natl Acad Sci U S A* **95**, 3890-3895 (1998).

173 Pearson, J. C., Lemons, D. & McGinnis, W. Modulating Hox gene functions during animal body patterning. *Nat Rev Genet* **6**, 893-904, doi:10.1038/nrg1726 (2005).

174 Alharbi, R. A., Pettengell, R., Pandha, H. S. & Morgan, R. The role of HOX genes in normal hematopoiesis and acute leukemia. *Leukemia* **27**, 1000-1008, doi:10.1038/leu.2012.356 (2013).

175 Shen, W. F. *et al.* Hox homeodomain proteins exhibit selective complex stabilities with Pbx and DNA. *Nucleic Acids Res* **24**, 898-906 (1996).

176 Shen, W. F. *et al.* AbdB-like Hox proteins stabilize DNA binding by the Meis1 homeodomain proteins. *Mol Cell Biol* **17**, 6448-6458 (1997).

177 Schuettengruber, B., Chourrout, D., Vervoort, M., Leblanc, B. & Cavalli, G. Genome regulation by polycomb and trithorax proteins. *Cell* **128**, 735-745, doi:10.1016/j.cell.2007.02.009 (2007).

178 Daser, A. & Rabbitts, T. H. Extending the repertoire of the mixed-lineage leukemia gene MLL in leukemogenesis. *Genes Dev* **18**, 965-974, doi:10.1101/gad.1195504 (2004).

179 Yu, B. D., Hess, J. L., Horning, S. E., Brown, G. A. & Korsmeyer, S. J. Altered Hox expression and segmental identity in Mll-mutant mice. *Nature* **378**, 505-508, doi:10.1038/378505a0 (1995).

180 Jude, C. D. *et al.* Unique and independent roles for MLL in adult hematopoietic stem cells and progenitors. *Cell Stem Cell* **1**, 324-337, doi:10.1016/j.stem.2007.05.019 (2007).

181 Artinger, E. L. *et al.* An MLL-dependent network sustains hematopoiesis. *Proc Natl Acad Sci U S A* **110**, 12000-12005, doi:10.1073/pnas.1301278110 (2013).

182 Radulovic, V., de Haan, G. & Klauke, K. Polycomb-group proteins in hematopoietic stem cell regulation and hematopoietic neoplasms. *Leukemia* **27**, 523-533, doi:10.1038/leu.2012.368 (2013).

183 Kamminga, L. M. *et al.* The Polycomb group gene Ezh2 prevents hematopoietic stem cell exhaustion. *Blood* **107**, 2170-2179, doi:10.1182/blood-2005-09-3585 (2006).

184 Abdel-Wahab, O. *et al.* Deletion of Asxl1 results in myelodysplasia and severe developmental defects in vivo. *J Exp Med* **210**, 2641-2659, doi:10.1084/jem.20131141 (2013).

185 Okano, M., Xie, S. & Li, E. Cloning and characterization of a family of novel mammalian DNA (cytosine-5) methyltransferases. *Nat Genet* **19**, 219-220, doi:10.1038/890 (1998).

186 Challen, G. A. *et al.* Dnmt3a is essential for hematopoietic stem cell differentiation. *Nat Genet* **44**, 23-31, doi:10.1038/ng.1009 (2011).

187 Challen, G. A. *et al.* Dnmt3a and Dnmt3b have overlapping and distinct functions in hematopoietic stem cells. *Cell Stem Cell* **15**, 350-364, doi:10.1016/j.stem.2014.06.018 (2014).

188 Tahiliani, M. *et al.* Conversion of 5-methylcytosine to 5-hydroxymethylcytosine in mammalian DNA by MLL partner TET1. *Science* **324**, 930-935, doi:10.1126/science.1170116 (2009).

189 Moran-Crusio, K. *et al.* Tet2 loss leads to increased hematopoietic stem cell self-renewal and myeloid transformation. *Cancer Cell* **20**, 11-24, doi:10.1016/j.ccr.2011.06.001 (2011).

190 Harris, N. L. *et al.* World Health Organization classification of neoplastic diseases of the hematopoietic and lymphoid tissues: report of the Clinical Advisory Committee meeting-Airlie House, Virginia, November 1997. *J Clin Oncol* **17**, 3835-3849, doi:10.1200/JCO.1999.17.12.3835 (1999).

191 Vardiman, J. W. *et al.* The 2008 revision of the World Health Organization (WHO) classification of myeloid neoplasms and acute leukemia: rationale and important changes. *Blood* **114**, 937-951, doi:10.1182/blood-2009-03-209262 (2009).

192 Arber, D. A. *et al.* The 2016 revision to the World Health Organization classification of myeloid neoplasms and acute leukemia. *Blood* **127**, 2391-2405, doi:10.1182/blood-2016-03-643544 (2016).

193 Rowley, J. D. Letter: A new consistent chromosomal abnormality in chronic myelogenous leukaemia identified by quinacrine fluorescence and Giemsa staining. *Nature* **243**, 290-293 (1973).

194 Nowell, P. C. & Hungerford, D. A. Chromosome studies in human leukemia. II. Chronic granulocytic leukemia. *J Natl Cancer Inst* **27**, 1013-1035 (1961).

195 Nicholson, E. & Holyoake, T. The chronic myeloid leukemia stem cell. *Clin Lymphoma Myeloma* **9 Suppl 4**, S376-381, doi:10.3816/CLM.2009.s.037 (2009).

196 Score, J. *et al.* Analysis of genomic breakpoints in p190 and p210 BCR-ABL indicate distinct mechanisms of formation. *Leukemia* **24**, 1742-1750, doi:10.1038/leu.2010.174 (2010).

197 Haskovec, C. *et al.* P230 BCR/ABL protein may be associated with an acute leukaemia phenotype. *Br J Haematol* **103**, 1104-1108 (1998).

198 Chereda, B. & Melo, J. V. Natural course and biology of CML. *Ann Hematol* **94 Suppl 2**, S107-121, doi:10.1007/s00277-015-2325-z (2015).

199 Druker, B. J. *et al.* Five-year follow-up of patients receiving imatinib for chronic myeloid leukemia. *N Engl J Med* **355**, 2408-2417, doi:10.1056/NEJMoa062867 (2006).

200 Kantarjian, H. *et al.* Improved survival in chronic myeloid leukemia since the introduction of imatinib therapy: a single-institution historical experience. *Blood* **119**, 1981-1987, doi:10.1182/blood-2011-08-358135 (2012).

201 Gambacorti-Passerini, C. *et al.* Multicenter independent assessment of outcomes in chronic myeloid leukemia patients treated with imatinib. *J Natl Cancer Inst* **103**, 553-561, doi:10.1093/jnci/djr060 (2011).

202 Spivak, J. L. Polycythemia Vera. *Curr Treat Options Oncol* **19**, 12, doi:10.1007/s11864-018-0529-x (2018).

203 Meier, B. & Burton, J. H. Myeloproliferative Disorders. *Hematol Oncol Clin North Am* **31**, 1029-1044, doi:10.1016/j.hoc.2017.08.007 (2017).

204 Chai, S. K., Nichols, G. L. & Rothman, P. Constitutive activation of JAKs and STATs in BCR-Abl-expressing cell lines and peripheral blood cells derived from leukemic patients. *J Immunol* **159**, 4720-4728 (1997).

205 Warsch, W., Walz, C. & Sexl, V. JAK of all trades: JAK2-STAT5 as novel therapeutic targets in BCR-ABL1+ chronic myeloid leukemia. *Blood* **122**, 2167-2175, doi:10.1182/blood-2013-02-485573 (2013).

206 Klampfl, T. *et al.* Somatic mutations of calreticulin in myeloproliferative neoplasms. *N Engl J Med* **369**, 2379-2390, doi:10.1056/NEJMoa1311347 (2013).

207 Malcovati, L. *et al.* Time-dependent prognostic scoring system for predicting survival and leukemic evolution in myelodysplastic syndromes. *J Clin Oncol* **25**, 3503-3510, doi:10.1200/JCO.2006.08.5696 (2007).

208 Cazzola, M., Della Porta, M. G. & Malcovati, L. The genetic basis of myelodysplasia and its clinical relevance. *Blood* **122**, 4021-4034, doi:10.1182/blood-2013-09-381665 (2013).

209 Zoi, K. & Cross, N. C. Molecular pathogenesis of atypical CML, CMML and MDS/MPN-unclassifiable. *Int J Hematol* **101**, 229-242, doi:10.1007/s12185-014-1670-3 (2015).

210 Dores, G. M., Devesa, S. S., Curtis, R. E., Linet, M. S. & Morton, L. M. Acute leukemia incidence and patient survival among children and adults in the United States, 2001-2007. *Blood* **119**, 34-43, doi:10.1182/blood-2011-04-347872 (2012).

211 Bennett, J. M. *et al.* Proposals for the classification of the acute leukaemias. French-American-British (FAB) co-operative group. *Br J Haematol* **33**, 451-458 (1976).

212 Jiang, M., Bennani, N. N. & Feldman, A. L. Lymphoma classification update: T-cell lymphomas, Hodgkin lymphomas, and histiocytic/dendritic cell neoplasms. *Expert Rev Hematol* **10**, 239-249, doi:10.1080/17474086.2017.1281122 (2017).

213 Prochazkova, J. & Loizou, J. I. Programmed DNA breaks in lymphoid cells: repair mechanisms and consequences in human disease. *Immunology* **147**, 11-20, doi:10.1111/imm.12547 (2016).

214 Loghavi, S., Kutok, J. L. & Jorgensen, J. L. B-acute lymphoblastic leukemia/lymphoblastic lymphoma. *Am J Clin Pathol* **144**, 393-410, doi:10.1309/AJCPAN7BH5DNYWZB (2015).

215 Terwilliger, T. & Abdul-Hay, M. Acute lymphoblastic leukemia: a comprehensive review and 2017 update. *Blood Cancer J* **7**, e577, doi:10.1038/bcj.2017.53 (2017).

216 Roboz, G. J. Current treatment of acute myeloid leukemia. *Curr Opin Oncol* **24**, 711-719, doi:10.1097/CCO.0b013e328358f62d (2012).

217 Grosso, D. A., Hess, R. C. & Weiss, M. A. Immunotherapy in acute myeloid leukemia. *Cancer* **121**, 2689-2704, doi:10.1002/cncr.29378 (2015).

218 Fortier, J. M. & Graubert, T. A. Murine models of human acute myeloid leukemia. *Cancer Treat Res* **145**, 183-196, doi:10.1007/978-0-387-69259-3_11 (2010).

219 Deguchi, K. *et al.* MOZ-TIF2-induced acute myeloid leukemia requires the MOZ nucleosome binding motif and TIF2-mediated recruitment of CBP. *Cancer Cell* **3**, 259-271 (2003).

220 Kelly, L. M. *et al.* PML/RARalpha and FLT3-ITD induce an APL-like disease in a mouse model. *Proc Natl Acad Sci U S A* **99**, 8283-8288, doi:10.1073/pnas.122233699 (2002).

221 Kroon, E., Thorsteinsdottir, U., Mayotte, N., Nakamura, T. & Sauvageau, G. NUP98-HOXA9 expression in hemopoietic stem cells induces chronic and acute myeloid leukemias in mice. *EMBO J* **20**, 350-361, doi:10.1093/emboj/20.3.350 (2001).

222 Okuda, T. *et al.* Expression of a knocked-in AML1-ETO leukemia gene inhibits the establishment of normal definitive hematopoiesis and directly generates dysplastic hematopoietic progenitors. *Blood* **91**, 3134-3143 (1998).

223 Martin, M. E. *et al.* Dimerization of MLL fusion proteins immortalizes hematopoietic cells. *Cancer Cell* **4**, 197-207 (2003).

224 Krivtsov, A. V. *et al.* Cell of origin determines clinically relevant subtypes of MLL-rearranged AML. *Leukemia* **27**, 852-860, doi:10.1038/leu.2012.363 (2013).

225 Huntly, B. J. *et al.* MOZ-TIF2, but not BCR-ABL, confers properties of leukemic stem cells to committed murine hematopoietic progenitors. *Cancer Cell* **6**, 587-596, doi:10.1016/j.ccr.2004.10.015 (2004).

226 Sportoletti, P. *et al.* Mouse models of NPM1-mutated acute myeloid leukemia: biological and clinical implications. *Leukemia* **29**, 269-278, doi:10.1038/leu.2014.257 (2015).

227 Kelly, L. M. *et al.* FLT3 internal tandem duplication mutations associated with human acute myeloid leukemias induce myeloproliferative disease in a murine bone marrow transplant model. *Blood* **99**, 310-318 (2002).

228 Lapidot, T. *et al.* A cell initiating human acute myeloid leukaemia after transplantation into SCID mice. *Nature* **367**, 645-648, doi:10.1038/367645a0 (1994).

229 Bonnet, D. & Dick, J. E. Human acute myeloid leukemia is organized as a hierarchy that originates from a primitive hematopoietic cell. *Nat Med* **3**, 730-737 (1997).

230 O'Brien, J. A. & Rizzieri, D. A. Leukemic stem cells: a review. *Cancer Invest* **31**, 215-220, doi:10.3109/07357907.2012.700986 (2013).

231 Taussig, D. C. *et al.* Leukemia-initiating cells from some acute myeloid leukemia patients with mutated nucleophosmin reside in the CD34(-) fraction. *Blood* **115**, 1976-1984, doi:10.1182/blood-2009-02-206565 (2010).

232 Goardon, N. *et al.* Coexistence of LMPP-like and GMP-like leukemia stem cells in acute myeloid leukemia. *Cancer Cell* **19**, 138-152, doi:10.1016/j.ccr.2010.12.012 (2011).

233 van Rhenen, A. *et al.* High stem cell frequency in acute myeloid leukemia at diagnosis predicts high minimal residual disease and poor survival. *Clin Cancer Res* **11**, 6520-6527, doi:10.1158/1078-0432.CCR-05-0468 (2005).

234 Gentles, A. J., Plevritis, S. K., Majeti, R. & Alizadeh, A. A. Association of a leukemic stem cell gene expression signature with clinical outcomes in acute myeloid leukemia. *JAMA* **304**, 2706-2715, doi:10.1001/jama.2010.1862 (2010).

235 Jin, L. *et al.* Monoclonal antibody-mediated targeting of CD123, IL-3 receptor alpha chain, eliminates human acute myeloid leukemic stem cells. *Cell Stem Cell* **5**, 31-42, doi:10.1016/j.stem.2009.04.018 (2009).

236 Jaiswal, S. *et al.* CD47 is upregulated on circulating hematopoietic stem cells and leukemia cells to avoid phagocytosis. *Cell* **138**, 271-285, doi:10.1016/j.cell.2009.05.046 (2009).

237 Majeti, R. *et al.* CD47 is an adverse prognostic factor and therapeutic antibody target on human acute myeloid leukemia stem cells. *Cell* **138**, 286-299, doi:10.1016/j.cell.2009.05.045 (2009).

238 Kikushige, Y. *et al.* TIM-3 is a promising target to selectively kill acute myeloid leukemia stem cells. *Cell Stem Cell* **7**, 708-717, doi:10.1016/j.stem.2010.11.014 (2010).

239 Askmyr, M. *et al.* Selective killing of candidate AML stem cells by antibody targeting of IL1RAP. *Blood* **121**, 3709-3713, doi:10.1182/blood-2012-09-458935 (2013).

240 Guzman, M. L. *et al.* Nuclear factor-kappaB is constitutively activated in primitive human acute myelogenous leukemia cells. *Blood* **98**, 2301-2307 (2001).

241 Corces-Zimmerman, M. R. & Majeti, R. Pre-leukemic evolution of hematopoietic stem cells: the importance of early mutations in leukemogenesis. *Leukemia* **28**, 2276-2282, doi:10.1038/leu.2014.211 (2014).

242 Zuber, J. *et al.* RNAi screen identifies Brd4 as a therapeutic target in acute myeloid leukaemia. *Nature* **478**, 524-528, doi:10.1038/nature10334 (2011).

243 Keith, F. J., Bradbury, D. A., Zhu, Y. M. & Russell, N. H. Inhibition of bcl-2 with antisense oligonucleotides induces apoptosis and increases the sensitivity of AML blasts to Ara-C. *Leukemia* **9**, 131-138 (1995).

244 Lagadinou, E. D. *et al.* BCL-2 inhibition targets oxidative phosphorylation and selectively eradicates quiescent human leukemia stem cells. *Cell Stem Cell* **12**, 329-341, doi:10.1016/j.stem.2012.12.013 (2013).

245 Khwaja, A. *et al.* Acute myeloid leukaemia. *Nat Rev Dis Primers* **2**, 16010, doi:10.1038/nrdp.2016.10 (2016).

246 Balgobind, B. V., Zwaan, C. M., Pieters, R. & Van den Heuvel-Eibrink, M. M. The heterogeneity of pediatric MLL-rearranged acute myeloid leukemia. *Leukemia* **25**, 1239-1248, doi:10.1038/leu.2011.90 (2011).

247 He, N. *et al.* Human Polymerase-Associated Factor complex (PAFc) connects the Super Elongation Complex (SEC) to RNA polymerase II on chromatin. *Proc Natl Acad Sci U S A* **108**, E636-645, doi:10.1073/pnas.1107107108 (2011).

248 Dorrance, A. M. *et al.* Mll partial tandem duplication induces aberrant Hox expression in vivo via specific epigenetic alterations. *J Clin Invest* **116**, 2707-2716, doi:10.1172/JCI25546 (2006).

249 Tokita, K., Maki, K. & Mitani, K. RUNX1/EVI1, which blocks myeloid differentiation, inhibits CCAAT-enhancer binding protein alpha function. *Cancer Sci* **98**, 1752-1757, doi:10.1111/j.1349-7006.2007.00597.x (2007).

250 Gelmetti, V. *et al.* Aberrant recruitment of the nuclear receptor corepressor-histone deacetylase complex by the acute myeloid leukemia fusion partner ETO. *Mol Cell Biol* **18**, 7185-7191 (1998).

251 Kundu, M. *et al.* Role of Cbfb in hematopoiesis and perturbations resulting from expression of the leukemogenic fusion gene Cbfb-MYH11. *Blood* **100**, 2449-2456, doi:10.1182/blood-2002-04-1064 (2002).

252 De Braekeleer, E., Douet-Guilbert, N. & De Braekeleer, M. RARA fusion genes in acute promyelocytic leukemia: a review. *Expert Rev Hematol* **7**, 347-357, doi:10.1586/17474086.2014.903794 (2014).

253 Kraemer, D., Wozniak, R. W., Blobel, G. & Radu, A. The human CAN protein, a putative oncogene product associated with myeloid leukemogenesis, is a nuclear pore complex protein that faces the cytoplasm. *Proc Natl Acad Sci U S A* **91**, 1519-1523 (1994).

254 Martinelli, G. *et al.* Association of 3q21q26 syndrome with different RPN1/EVI1 fusion transcripts. *Haematologica* **88**, 1221-1228 (2003).

255 Testoni, N. *et al.* 3q21 and 3q26 cytogenetic abnormalities in acute myeloblastic leukemia: biological and clinical features. *Haematologica* **84**, 690-694 (1999).

256 Ley, T. J. *et al.* DNA sequencing of a cytogenetically normal acute myeloid leukaemia genome. *Nature* **456**, 66-72, doi:10.1038/nature07485 (2008).

257 Roti, G. *et al.* Denaturing high-performance liquid chromatography: a valid approach for identifying NPM1 mutations in acute myeloid leukemia. *J Mol Diagn* **8**, 254-259, doi:10.2353/jmoldx.2006.050098 (2006).

258 Haferlach, C. *et al.* AML with mutated NPM1 carrying a normal or aberrant karyotype show overlapping biologic, pathologic, immunophenotypic, and prognostic features. *Blood* **114**, 3024-3032, doi:10.1182/blood-2009-01-197871 (2009).

259 Vassiliou, G. S. *et al.* Mutant nucleophosmin and cooperating pathways drive leukemia initiation and progression in mice. *Nat Genet* **43**, 470-475, doi:10.1038/ng.796 (2011).

260 Rau, R. *et al.* NPMc+ cooperates with Flt3/ITD mutations to cause acute leukemia recapitulating human disease. *Exp Hematol* **42**, 101-113 e105, doi:10.1016/j.exphem.2013.10.005 (2014).

261 Zorko, N. A. *et al.* Mll partial tandem duplication and Flt3 internal tandem duplication in a double knock-in mouse recapitulates features of counterpart human acute myeloid leukemias. *Blood* **120**, 1130-1136, doi:10.1182/blood-2012-03-415067 (2012).

262 Greenblatt, S. *et al.* Knock-in of a FLT3/ITD mutation cooperates with a NUP98-HOXD13 fusion to generate acute myeloid leukemia in a mouse model. *Blood* **119**, 2883-2894, doi:10.1182/blood-2011-10-382283 (2012).

263 Kim, H. G. *et al.* FLT3-ITD cooperates with inv(16) to promote progression to acute myeloid leukemia. *Blood* **111**, 1567-1574, doi:10.1182/blood-2006-06-030312 (2008).

264 Stubbs, M. C. *et al.* MLL-AF9 and FLT3 cooperation in acute myelogenous leukemia: development of a model for rapid therapeutic assessment. *Leukemia* **22**, 66-77, doi:10.1038/sj.leu.2404951 (2008).

265 Lee, B. H. *et al.* FLT3 internal tandem duplication mutations induce myeloproliferative or lymphoid disease in a transgenic mouse model. *Oncogene* **24**, 7882-7892, doi:10.1038/sj.onc.1208933 (2005).

266 Choudhary, C. *et al.* Activation mechanisms of STAT5 by oncogenic Flt3-ITD. *Blood* **110**, 370-374, doi:10.1182/blood-2006-05-024018 (2007).

267 Grundler, R., Miething, C., Thiede, C., Peschel, C. & Duyster, J. FLT3-ITD and tyrosine kinase domain mutants induce 2 distinct phenotypes in a murine bone marrow transplantation model. *Blood* **105**, 4792-4799, doi:10.1182/blood-2004-11-4430 (2005).

268 Feinberg, A. P. & Vogelstein, B. Hypomethylation distinguishes genes of some human cancers from their normal counterparts. *Nature* **301**, 89-92 (1983).

269 Shlush, L. I. *et al.* Identification of pre-leukaemic haematopoietic stem cells in acute leukaemia. *Nature* **506**, 328-333, doi:10.1038/nature13038 (2014).

270 Guryanova, O. A. *et al.* Dnmt3a regulates myeloproliferation and liver-specific expansion of hematopoietic stem and progenitor cells. *Leukemia* **30**, 1133-1142, doi:10.1038/leu.2015.358 (2016).

271 Abdel-Wahab, O. *et al.* ASXL1 mutations promote myeloid transformation through loss of PRC2-mediated gene repression. *Cancer Cell* **22**, 180-193, doi:10.1016/j.ccr.2012.06.032 (2012).

272 Cancer Genome Atlas Research, N. *et al.* Genomic and epigenomic landscapes of adult de novo acute myeloid leukemia. *N Engl J Med* **368**, 2059-2074, doi:10.1056/NEJMoa1301689 (2013).

273 Chou, W. C. *et al.* The prognostic impact and stability of Isocitrate dehydrogenase 2 mutation in adult patients with acute myeloid leukemia. *Leukemia* **25**, 246-253, doi:10.1038/leu.2010.267 (2011).

274 Dang, L. *et al.* Cancer-associated IDH1 mutations produce 2-hydroxyglutarate. *Nature* **462**, 739-744, doi:10.1038/nature08617 (2009).

275 Ward, P. S. *et al.* The common feature of leukemia-associated IDH1 and IDH2 mutations is a neomorphic enzyme activity converting alpha-ketoglutarate to 2-hydroxyglutarate. *Cancer Cell* **17**, 225-234, doi:10.1016/j.ccr.2010.01.020 (2010).

276 Rakheja, D., Konoplev, S., Medeiros, L. J. & Chen, W. IDH mutations in acute myeloid leukemia. *Hum Pathol* **43**, 1541-1551, doi:10.1016/j.humpath.2012.05.003 (2012).

277 Figueroa, M. E. *et al.* Leukemic IDH1 and IDH2 mutations result in a hypermethylation phenotype, disrupt TET2 function, and impair hematopoietic differentiation. *Cancer Cell* **18**, 553-567, doi:10.1016/j.ccr.2010.11.015 (2010).

278 Wang, F. *et al.* Targeted inhibition of mutant IDH2 in leukemia cells induces cellular differentiation. *Science* **340**, 622-626, doi:10.1126/science.1234769 (2013).

279 Okoye-Okafor, U. C. *et al.* New IDH1 mutant inhibitors for treatment of acute myeloid leukemia. *Nat Chem Biol* **11**, 878-886, doi:10.1038/nchembio.1930 (2015).

280 Rohle, D. *et al.* An inhibitor of mutant IDH1 delays growth and promotes differentiation of glioma cells. *Science* **340**, 626-630, doi:10.1126/science.1236062 (2013).

281 Chaturvedi, A. *et al.* Pan-mutant-IDH1 inhibitor BAY1436032 is highly effective against human IDH1 mutant acute myeloid leukemia in vivo. *Leukemia* **31**, 2020-2028, doi:10.1038/leu.2017.46 (2017).

282 Hemmati, S., Haque, T. & Gritsman, K. Inflammatory Signaling Pathways in Preleukemic and Leukemic Stem Cells. *Front Oncol* **7**, 265, doi:10.3389/fonc.2017.00265 (2017).

283 Kerbauy, D. B. & Deeg, H. J. Apoptosis and antiapoptotic mechanisms in the progression of myelodysplastic syndrome. *Exp Hematol* **35**, 1739-1746, doi:10.1016/j.exphem.2007.09.007 (2007).

284 Kuo, H. P. *et al.* Epigenetic roles of MLL oncoproteins are dependent on NF-kappaB. *Cancer Cell* **24**, 423-437, doi:10.1016/j.ccr.2013.08.019 (2013).

285 Vaidya, R. *et al.* Plasma cytokines in polycythemia vera: phenotypic correlates, prognostic relevance, and comparison with myelofibrosis. *Am J Hematol* **87**, 1003-1005, doi:10.1002/ajh.23295 (2012).

286 Zhao, K. *et al.* IL1RAP as a surface marker for leukemia stem cells is related to clinical phase of chronic myeloid leukemia patients. *Int J Clin Exp Med* **7**, 4787-4798 (2014).

287 Katsumura, K. R., Ong, I. M., DeVilbiss, A. W., Sanalkumar, R. & Bresnick, E. H. GATA Factor-Dependent Positive-Feedback Circuit in Acute Myeloid Leukemia Cells. *Cell Rep* **16**, 2428-2441, doi:10.1016/j.celrep.2016.07.058 (2016).

288 Barreyro, L. *et al.* Overexpression of IL-1 receptor accessory protein in stem and progenitor cells and outcome correlation in AML and MDS. *Blood* **120**, 1290-1298, doi:10.1182/blood-2012-01-404699 (2012).

289 Rambaldi, A. *et al.* Modulation of cell proliferation and cytokine production in acute myeloblastic leukemia by interleukin-1 receptor antagonist and lack of its expression by leukemic cells. *Blood* **78**, 3248-3253 (1991).

290 Aguayo, A. *et al.* Plasma vascular endothelial growth factor levels have prognostic significance in patients with acute myeloid leukemia but not in patients with myelodysplastic syndromes. *Cancer* **95**, 1923-1930, doi:10.1002/cncr.10900 (2002).

291 Kim, J. G. *et al.* Clinical implications of angiogenic factors in patients with acute or chronic leukemia: hepatocyte growth factor levels have prognostic impact, especially in patients with acute myeloid leukemia. *Leuk Lymphoma* **46**, 885-891, doi:10.1080/10428190500054491 (2005).

292 Basiorka, A. A. *et al.* The NLRP3 inflammasome functions as a driver of the myelodysplastic syndrome phenotype. *Blood* **128**, 2960-2975, doi:10.1182/blood-2016-07-730556 (2016).

293 Duarte, D. *et al.* Inhibition of Endosteal Vascular Niche Remodeling Rescues Hematopoietic Stem Cell Loss in AML. *Cell Stem Cell* **22**, 64-77 e66, doi:10.1016/j.stem.2017.11.006 (2018).

294 Franceschi, C. & Campisi, J. Chronic inflammation (inflammaging) and its potential contribution to age-associated diseases. *J Gerontol A Biol Sci Med Sci* **69 Suppl 1**, S4-9, doi:10.1093/gerona/glu057 (2014).

295 Papaemmanuil, E. *et al.* Genomic Classification and Prognosis in Acute Myeloid Leukemia. *N Engl J Med* **374**, 2209-2221, doi:10.1056/NEJMoa1516192 (2016).

296 Fuster, J. J. *et al.* Clonal hematopoiesis associated with TET2 deficiency accelerates atherosclerosis development in mice. *Science* **355**, 842-847, doi:10.1126/science.aag1381 (2017).

297 Cull, A. H., Snetsinger, B., Buckstein, R., Wells, R. A. & Rauh, M. J. Tet2 restrains inflammatory gene expression in macrophages. *Exp Hematol* **55**, 56-70 e13, doi:10.1016/j.exphem.2017.08.001 (2017).

298 Leoni, C. *et al.* Dnmt3a restrains mast cell inflammatory responses. *Proc Natl Acad Sci U S A* **114**, E1490-E1499, doi:10.1073/pnas.1616420114 (2017).

299 Chi, J. & Cohen, P. The Multifaceted Roles of PRDM16: Adipose Biology and Beyond. *Trends Endocrinol Metab* **27**, 11-23, doi:10.1016/j.tem.2015.11.005 (2016).

300 Di Zazzo, E., De Rosa, C., Abbondanza, C. & Moncharmont, B. PRDM Proteins: Molecular Mechanisms in Signal Transduction and Transcriptional Regulation. *Biology (Basel)* **2**, 107-141, doi:10.3390/biology2010107 (2013).

301 Derunes, C. *et al.* Characterization of the PR domain of RIZ1 histone methyltransferase. *Biochem Biophys Res Commun* **333**, 925-934, doi:10.1016/j.bbrc.2005.05.190 (2005).

302 Eom, G. H. *et al.* Histone methyltransferase PRDM8 regulates mouse testis steroidogenesis. *Biochem Biophys Res Commun* **388**, 131-136, doi:10.1016/j.bbrc.2009.07.134 (2009).

303 Hayashi, K., Yoshida, K. & Matsui, Y. A histone H3 methyltransferase controls epigenetic events required for meiotic prophase. *Nature* **438**, 374-378, doi:10.1038/nature04112 (2005).

304 Hohenauer, T. & Moore, A. W. The Prdm family: expanding roles in stem cells and development. *Development* **139**, 2267-2282, doi:10.1242/dev.070110 (2012).

305 Katoh, K. *et al.* Blimp1 suppresses Chx10 expression in differentiating retinal photoreceptor precursors to ensure proper photoreceptor development. *J Neurosci* **30**, 6515-6526, doi:10.1523/JNEUROSCI.0771-10.2010 (2010).

306 Cretney, E. *et al.* The transcription factors Blimp-1 and IRF4 jointly control the differentiation and function of effector regulatory T cells. *Nat Immunol* **12**, 304-311, doi:10.1038/ni.2006 (2011).

307 Turner, C. A., Jr., Mack, D. H. & Davis, M. M. Blimp-1, a novel zinc finger-containing protein that can drive the maturation of B lymphocytes into immunoglobulin-secreting cells. *Cell* **77**, 297-306 (1994).

308 Yamaji, M. *et al.* Critical function of Prdm14 for the establishment of the germ cell lineage in mice. *Nat Genet* **40**, 1016-1022, doi:10.1038/ng.186 (2008).

309 Parvanov, E. D., Petkov, P. M. & Paigen, K. Prdm9 controls activation of mammalian recombination hotspots. *Science* **327**, 835, doi:10.1126/science.1181495 (2010).

310 Davis, C. A. *et al.* PRISM/PRDM6, a transcriptional repressor that promotes the proliferative gene program in smooth muscle cells. *Mol Cell Biol* **26**, 2626-2636, doi:10.1128/MCB.26.7.2626-2636.2006 (2006).

311 Mzoughi, S., Tan, Y. X., Low, D. & Guccione, E. The role of PRDMs in cancer: one family, two sides. *Curr Opin Genet Dev* **36**, 83-91, doi:10.1016/j.gde.2016.03.009 (2016).

312 Rea, S. *et al.* Regulation of chromatin structure by site-specific histone H3 methyltransferases. *Nature* **406**, 593-599, doi:10.1038/35020506 (2000).

313 Pinheiro, I. *et al.* Prdm3 and Prdm16 are H3K9me1 methyltransferases required for mammalian heterochromatin integrity. *Cell* **150**, 948-960, doi:10.1016/j.cell.2012.06.048 (2012).

314 Zhou, B. *et al.* PRDM16 Suppresses MLL1r Leukemia via Intrinsic Histone Methyltransferase Activity. *Mol Cell*, doi:10.1016/j.molcel.2016.03.010 (2016).

315 Kajimura, S. *et al.* Regulation of the brown and white fat gene programs through a PRDM16/CtBP transcriptional complex. *Genes Dev* **22**, 1397-1409, doi:10.1101/gad.1666108 (2008).

316 Kajimura, S. *et al.* Initiation of myoblast to brown fat switch by a PRDM16-C/EBP-beta transcriptional complex. *Nature* **460**, 1154-1158, doi:10.1038/nature08262 (2009).

317 Ohno, H., Shinoda, K., Ohyama, K., Sharp, L. Z. & Kajimura, S. EHMT1 controls brown adipose cell fate and thermogenesis through the PRDM16 complex. *Nature* **504**, 163-167, doi:10.1038/nature12652 (2013).

318 Seale, P. *et al.* Transcriptional control of brown fat determination by PRDM16. *Cell Metab* **6**, 38-54, doi:10.1016/j.cmet.2007.06.001 (2007).

319 Horn, K. H., Warner, D. R., Pisano, M. & Greene, R. M. PRDM16 expression in the developing mouse embryo. *Acta Histochem* **113**, 150-155, doi:10.1016/j.acthis.2009.09.006 (2011).

320 Trajkovski, M., Ahmed, K., Esau, C. C. & Stoffel, M. MyomiR-133 regulates brown fat differentiation through Prdm16. *Nat Cell Biol* **14**, 1330-1335, doi:10.1038/ncb2612 (2012).

321 Chou, C. F. *et al.* KSRP ablation enhances brown fat gene program in white adipose tissue through reduced miR-150 expression. *Diabetes* **63**, 2949-2961, doi:10.2337/db13-1901 (2014).

322 Sun, L. & Trajkovski, M. MiR-27 orchestrates the transcriptional regulation of brown adipogenesis. *Metabolism* **63**, 272-282, doi:10.1016/j.metabol.2013.10.004 (2014).

323 Liu, W. *et al.* miR-133a regulates adipocyte browning in vivo. *PLoS Genet* **9**, e1003626, doi:10.1371/journal.pgen.1003626 (2013).

324 Rosen, E. D. & Spiegelman, B. M. What we talk about when we talk about fat. *Cell* **156**, 20-44, doi:10.1016/j.cell.2013.12.012 (2014).

325 Tontonoz, P., Hu, E. & Spiegelman, B. M. Stimulation of adipogenesis in fibroblasts by PPAR gamma 2, a lipid-activated transcription factor. *Cell* **79**, 1147-1156 (1994).

326 Seale, P. *et al.* Prdm16 determines the thermogenic program of subcutaneous white adipose tissue in mice. *J Clin Invest* **121**, 96-105, doi:10.1172/JCI44271 (2011).

327 Harms, M. J. *et al.* Prdm16 is required for the maintenance of brown adipocyte identity and function in adult mice. *Cell Metab* **19**, 593-604, doi:10.1016/j.cmet.2014.03.007 (2014).

328 Chuikov, S., Levi, B. P., Smith, M. L. & Morrison, S. J. Prdm16 promotes stem cell maintenance in multiple tissues, partly by regulating oxidative stress. *Nat Cell Biol* **12**, 999-1006, doi:10.1038/ncb2101 (2010).

329 Chasman, D. I. *et al.* Genome-wide association study reveals three susceptibility loci for common migraine in the general population. *Nat Genet* **43**, 695-698, doi:10.1038/ng.856 (2011).

330 Sugiyama, T. *et al.* Reconstituting pancreas development from purified progenitor cells reveals genes essential for islet differentiation. *Proc Natl Acad Sci U S A* **110**, 12691-12696, doi:10.1073/pnas.1304507110 (2013).

331 Benitez, C. M. *et al.* An integrated cell purification and genomics strategy reveals multiple regulators of pancreas development. *PLoS Genet* **10**, e1004645, doi:10.1371/journal.pgen.1004645 (2014).

332 Bjork, B. C., Turbe-Doan, A., Prysak, M., Herron, B. J. & Beier, D. R. Prdm16 is required for normal palatogenesis in mice. *Hum Mol Genet* **19**, 774-789, doi:10.1093/hmg/ddp543 (2010).

333 Warner, D. R. *et al.* PRDM16/MEL1: a novel Smad binding protein expressed in murine embryonic orofacial tissue. *Biochim Biophys Acta* **1773**, 814-820, doi:10.1016/j.bbamcr.2007.03.016 (2007).

334 Liu, F. *et al.* A genome-wide association study identifies five loci influencing facial morphology in Europeans. *PLoS Genet* **8**, e1002932, doi:10.1371/journal.pgen.1002932 (2012).

335 Nishikata, I. *et al.* A novel EVI1 gene family, MEL1, lacking a PR domain (MEL1S) is expressed mainly in t(1;3)(p36;q21)-positive AML and blocks G-CSF-induced myeloid differentiation. *Blood* **102**, 3323-3332, doi:10.1182/blood-2002-12-3944 (2003).

336 Suzukawa, K. *et al.* Identification of a breakpoint cluster region 3' of the ribophorin I gene at 3q21 associated with the transcriptional activation of the EVI1 gene in acute myelogenous leukemias with inv(3)(q21q26). *Blood* **84**, 2681-2688 (1994).

337 Fears, S. *et al.* Intergenic splicing of MDS1 and EVI1 occurs in normal tissues as well as in myeloid leukemia and produces a new member of the PR domain family. *Proc Natl Acad Sci U S A* **93**, 1642-1647 (1996).

338 Sakai, I. *et al.* Novel RUNX1-PRDM16 fusion transcripts in a patient with acute myeloid leukemia showing t(1;21)(p36;q22). *Genes Chromosomes Cancer* **44**, 265-270, doi:10.1002/gcc.20241 (2005).

339 Nucifora, G. *et al.* Consistent intergenic splicing and production of multiple transcripts between AML1 at 21q22 and unrelated genes at 3q26 in (3;21)(q26;q22) translocations. *Proc Natl Acad Sci U S A* **91**, 4004-4008 (1994).

340 Duhoux, F. P. *et al.* PRDM16 (1p36) translocations define a distinct entity of myeloid malignancies with poor prognosis but may also occur in lymphoid malignancies. *Br J Haematol* **156**, 76-88, doi:10.1111/j.1365-2141.2011.08918.x (2012).

341 Masetti, R. *et al.* Whole transcriptome sequencing of a paediatric case of de novo acute myeloid leukaemia with del(5q) reveals RUNX1-USP42 and PRDM16-SKI fusion transcripts. *Br J Haematol* **166**, 449-452, doi:10.1111/bjh.12855 (2014).

342 Poiesz, B. J. *et al.* Detection and isolation of type C retrovirus particles from fresh and cultured lymphocytes of a patient with cutaneous T-cell lymphoma. *Proc Natl Acad Sci U S A* **77**, 7415-7419 (1980).

343 Yoshida, M. *et al.* Aberrant expression of the MEL1S gene identified in association with hypomethylation in adult T-cell leukemia cells. *Blood* **103**, 2753-2760, doi:10.1182/blood-2003-07-2482 (2004).

344 Shing, D. C. *et al.* Overexpression of sPRDM16 coupled with loss of p53 induces myeloid leukemias in mice. *J Clin Invest* **117**, 3696-3707, doi:10.1172/JCI32390 (2007).

345 Wattel, E. *et al.* p53 mutations are associated with resistance to chemotherapy and short survival in hematologic malignancies. *Blood* **84**, 3148-3157 (1994).

346 Du, Y., Jenkins, N. A. & Copeland, N. G. Insertional mutagenesis identifies genes that promote the immortalization of primary bone marrow progenitor cells. *Blood* **106**, 3932-3939, doi:10.1182/blood-2005-03-1113 (2005).

347 Modlich, U. *et al.* Leukemia induction after a single retroviral vector insertion in Evi1 or Prdm16. *Leukemia* **22**, 1519-1528, doi:10.1038/leu.2008.118 (2008).

348 Lessard, J. & Sauvageau, G. Bmi-1 determines the proliferative capacity of normal and leukaemic stem cells. *Nature* **423**, 255-260, doi:10.1038/nature01572 (2003).

349 Herault, O. *et al.* A role for GPx3 in activity of normal and leukemia stem cells. *J Exp Med* **209**, 895-901, doi:10.1084/jem.20102386 (2012).

350 Ogilvy, S. *et al.* Transcriptional regulation of vav, a gene expressed throughout the hematopoietic compartment. *Blood* **91**, 419-430 (1998).

351 de Boer, J. *et al.* Transgenic mice with hematopoietic and lymphoid specific expression of Cre. *Eur J Immunol* **33**, 314-325, doi:10.1002/immu.200310005 (2003).

352 Mi, H. *et al.* PANTHER version 11: expanded annotation data from Gene Ontology and Reactome pathways, and data analysis tool enhancements. *Nucleic Acids Res* **45**, D183-D189, doi:10.1093/nar/gkw1138 (2017).

353 Mi, H., Muruganujan, A., Casagrande, J. T. & Thomas, P. D. Large-scale gene function analysis with the PANTHER classification system. *Nat Protoc* **8**, 1551-1566, doi:10.1038/nprot.2013.092 (2013).

354 Satoh, T., Fantl, W. J., Escobedo, J. A., Williams, L. T. & Kaziro, Y. Platelet-derived growth factor receptor mediates activation of ras through different signaling pathways in different cell types. *Mol Cell Biol* **13**, 3706-3713 (1993).

355 Nayak, R. C., Chang, K. H., Vaitinadin, N. S. & Cancelas, J. A. Rho GTPases control specific cytoskeleton-dependent functions of hematopoietic stem cells. *Immunol Rev* **256**, 255-268, doi:10.1111/imr.12119 (2013).

356 Kim, I., Saunders, T. L. & Morrison, S. J. Sox17 dependence distinguishes the transcriptional regulation of fetal from adult hematopoietic stem cells. *Cell* **130**, 470-483, doi:10.1016/j.cell.2007.06.011 (2007).

357 Weksberg, D. C., Chambers, S. M., Boles, N. C. & Goodell, M. A. CD150- side population cells represent a functionally distinct population of long-term hematopoietic stem cells. *Blood* **111**, 2444-2451, doi:10.1182/blood-2007-09-115006 (2008).

358 Morishita, K. Leukemogenesis of the EVI1/MEL1 gene family. *Int J Hematol* **85**, 279-286, doi:10.1532/IJH97.06174 (2007).

359 Pasqualucci, L. *et al.* Inactivation of the PRDM1/BLIMP1 gene in diffuse large B cell lymphoma. *J Exp Med* **203**, 311-317, doi:10.1084/jem.20052204 (2006).

360 He, L. *et al.* RIZ1, but not the alternative RIZ2 product of the same gene, is underexpressed in breast cancer, and forced RIZ1 expression causes G2-M cell cycle arrest and/or apoptosis. *Cancer Res* **58**, 4238-4244 (1998).

361 Deng, Q. & Huang, S. PRDM5 is silenced in human cancers and has growth suppressive activities. *Oncogene* **23**, 4903-4910, doi:10.1038/sj.onc.1207615 (2004).

362 Matsuo, H., Goyama, S., Kamikubo, Y. & Adachi, S. The subtype-specific features of EVI1 and PRDM16 in acute myeloid leukemia. *Haematologica* **100**, e116-117, doi:10.3324/haematol.2015.124396 (2015).

363 Eveillard, M. *et al.* The closely related rare and severe acute myeloid leukemias carrying EVI1 or PRDM16 rearrangements share singular biological features. *Haematologica* **100**, e114-115, doi:10.3324/haematol.2014.121079 (2015).

364 Milne, T. A. Mouse models of MLL leukemia: recapitulating the human disease. *Blood* **129**, 2217-2223, doi:10.1182/blood-2016-10-691428 (2017).

365 Moir, D. J. *et al.* A new translocation, t(1;3) (p36;q21), in myelodysplastic disorders. *Blood* **64**, 553-555 (1984).

366 Yamato, G. *et al.* Clinical features and prognostic impact of PRDM16 expression in adult acute myeloid leukemia. *Genes Chromosomes Cancer* **56**, 800-809, doi:10.1002/gcc.22483 (2017).

367 Jo, A. *et al.* High expression of EVI1 and MEL1 is a compelling poor prognostic marker of pediatric AML. *Leukemia* **29**, 1076-1083, doi:10.1038/leu.2015.5 (2015).

368 Ganan-Gomez, I. *et al.* Deregulation of innate immune and inflammatory signaling in myelodysplastic syndromes. *Leukemia* **29**, 1458-1469, doi:10.1038/leu.2015.69 (2015).

369 Somervaille, T. C. & Cleary, M. L. Identification and characterization of leukemia stem cells in murine MLL-AF9 acute myeloid leukemia. *Cancer Cell* **10**, 257-268, doi:10.1016/j.ccr.2006.08.020 (2006).

370 Zambrowicz, B. P. *et al.* Wnk1 kinase deficiency lowers blood pressure in mice: a gene-trap screen to identify potential targets for therapeutic intervention. *Proc Natl Acad Sci U S A* **100**, 14109-14114, doi:10.1073/pnas.2336103100 (2003).

371 Kamezaki, K., Luchsinger, L. L. & Snoeck, H. W. Differential requirement for wild-type Flt3 in leukemia initiation among mouse models of human leukemia. *Exp Hematol* **42**, 192-203 e191, doi:10.1016/j.exphem.2013.11.008 (2014).

372 Chrzanowska-Wodnicka, M. Regulation of angiogenesis by a small GTPase Rap1. *Vascul Pharmacol* **53**, 1-10, doi:10.1016/j.vph.2010.03.003 (2010).

373 Cheng, C. *et al.* Endothelial cell-specific FGD5 involvement in vascular pruning defines neovessel fate in mice. *Circulation* **125**, 3142-3158, doi:10.1161/CIRCULATIONAHA.111.064030 (2012).

374 van Buul, J. D., Geerts, D. & Huveneers, S. Rho GAPs and GEFs: controling switches in endothelial cell adhesion. *Cell Adh Migr* **8**, 108-124 (2014).

375 Bryan, B. A. & D'Amore, P. A. What tangled webs they weave: Rho-GTPase control of angiogenesis. *Cell Mol Life Sci* **64**, 2053-2065, doi:10.1007/s00018-007-7008-z (2007).

376 Yang, F. C. *et al.* Rac and Cdc42 GTPases control hematopoietic stem cell shape, adhesion, migration, and mobilization. *Proc Natl Acad Sci U S A* **98**, 5614-5618, doi:10.1073/pnas.101546898 (2001).

377 Florian, M. C. *et al.* Cdc42 activity regulates hematopoietic stem cell aging and rejuvenation. *Cell Stem Cell* **10**, 520-530, doi:10.1016/j.stem.2012.04.007 (2012).

378 Suzuki-Utsunomiya, K. *et al.* ALS2CL, a novel ALS2-interactor, modulates ALS2-mediated endosome dynamics. *Biochem Biophys Res Commun* **354**, 491-497, doi:10.1016/j.bbrc.2006.12.229 (2007).

379 Shibata, S., Teshima, Y., Niimi, K. & Inagaki, S. Involvement of ARHGEF10, GEF for RhoA, in Rab6/Rab8-mediating membrane traffic. *Small GTPases*, 1-9, doi:10.1080/21541248.2017.1302550 (2017).

380 Wang, J. & Deretic, D. The Arf and Rab11 effector FIP3 acts synergistically with ASAP1 to direct Rabin8 in ciliary receptor targeting. *J Cell Sci* **128**, 1375-1385, doi:10.1242/jcs.162925 (2015).

381 Holmfeldt, P. *et al.* Functional screen identifies regulators of murine hematopoietic stem cell repopulation. *J Exp Med* **213**, 433-449, doi:10.1084/jem.20150806 (2016).

382 Maryanovich, M. *et al.* An MTCH2 pathway repressing mitochondria metabolism regulates haematopoietic stem cell fate. *Nat Commun* **6**, 7901, doi:10.1038/ncomms8901 (2015).

383 Takubo, K. *et al.* Regulation of glycolysis by Pdk functions as a metabolic checkpoint for cell cycle quiescence in hematopoietic stem cells. *Cell Stem Cell* **12**, 49-61, doi:10.1016/j.stem.2012.10.011 (2013).

384 Malek, T. R., Danis, K. M. & Codias, E. K. Tumor necrosis factor synergistically acts with IFN-gamma to regulate Ly-6A/E expression in T lymphocytes, thymocytes and bone marrow cells. *J Immunol* **142**, 1929-1936 (1989).

385 King, K. Y. & Goodell, M. A. Inflammatory modulation of HSCs: viewing the HSC as a foundation for the immune response. *Nat Rev Immunol* **11**, 685-692, doi:10.1038/nri3062 (2011).

386 Cull, A. H. & Rauh, M. J. Success in bone marrow failure? Novel therapeutic directions based on the immune environment of myelodysplastic syndromes. *J Leukoc Biol* **102**, 209-219, doi:10.1189/jlb.5RI0317-083R (2017).

387 Kristinsson, S. Y. *et al.* Chronic immune stimulation might act as a trigger for the development of acute myeloid leukemia or myelodysplastic syndromes. *J Clin Oncol* **29**, 2897-2903, doi:10.1200/JCO.2011.34.8540 (2011).

388 Kornblau, S. M. *et al.* Recurrent expression signatures of cytokines and chemokines are present and are independently prognostic in acute myelogenous leukemia and myelodysplasia. *Blood* **116**, 4251-4261, doi:10.1182/blood-2010-01-262071 (2010).

389 Wang, Y. *et al.* Leukemia cell infiltration causes defective erythropoiesis partially through MIP-1alpha/CCL3. *Leukemia* **30**, 1897-1908, doi:10.1038/leu.2016.81 (2016).

390 Samudio, I., Fiegl, M. & Andreeff, M. Mitochondrial uncoupling and the Warburg effect: molecular basis for the reprogramming of cancer cell metabolism. *Cancer Res* **69**, 2163-2166, doi:10.1158/0008-5472.CAN-08-3722 (2009).

391 Mishra, P. & Chan, D. C. Metabolic regulation of mitochondrial dynamics. *J Cell Biol* **212**, 379-387, doi:10.1083/jcb.201511036 (2016).

392 Testa, U., Labbaye, C., Castelli, G. & Pelosi, E. Oxidative stress and hypoxia in normal and leukemic stem cells. *Exp Hematol* **44**, 540-560, doi:10.1016/j.exphem.2016.04.012 (2016).